

تطوير إنتاج البلاطات الخرسانية (الشتاير)

علاء مهدي الخطيب
قسم هندسة البناء والانشاءات
الجامعة التكنولوجية

طارق صالح آل عطار
قسم هندسة البناء والانشاءات
الجامعة التكنولوجية

شاكر أحمد المشهداني
قسم هندسة البناء والانشاءات
الجامعة التكنولوجية

الخلاصة

تضمن البحث إجراء دراسته شامله لواقع حال وآفاق تطوير منتج بلاطات التسطیح الخرسانية (الشتاير) الشائع الإستخدام والإنتاج في العراق. تَبَيَّنَ إن أغلب , إن لم يكن كل , المنتج يفشل في تحقيق متطلبات المواصفه القياسية العراقية 1107 لسنة 1988. تم إعداد نماذج تتضمن مكعبات وإسطوانات ومواسير ومن ثم قطع شتاير لمحاكاة الأساليب المتبعه محلياً وجرى فحصها لمعرفة مقاومتها للانضغاط والإنشطار والإنشاء ومن ثم تحملها للحمل المستعرض وقياس قابليتها للإمتصاص , وقد إتضح من خلال الفحص بأنها دون المستوى القياسي المطلوب. من خلال معرفة قوة التحمل المستعرض المطلوبه تم حساب مقاومة الإنشاء الدنيا المستهدفه ومن ثم جرى تصميم خلطه خرسانية تُلَبِّي ذلك وقد أُطلق عليها إسم الخلطه الجديده. تم تكرار إعداد النماذج (التي بلغ مجموع عيناتها الكلي 60 عينه) ولكن بإستخدام الخلطه الجديده مع الإهتمام بتدرج الركام وإسلوب المعالجه. أثبتت الفحوصات بأن نماذج الشتاير تفوق متطلبات المواصفه.

رغم نجاح النماذج الجديده مختبرياً , لازال الاعتقاد قائماً بوجود إمكانيه لفشل بعض النماذج عندما يستمر الإنتاج النمطي وتضعف المراقبه والسيطره النوعيه, وعليه تم تجريب طريقه جديده لتعزيز بلاطات الخلطة الجديده بمشبكات سلكيه. أدت هذه الطريقه الى زيادة قوة التحمل المستعرض بمقدار 21%.

كلمات رئيسية

بلاطات التسطیح, مقاومة الانضغاط, مقاومة الشد بالانشطار, مقاومة الانشاء, مشبك سلكي.

ABSTRACT

A case study had been made to investigate the reasons of the repetitive failure during concrete tiles testing. Cubes, cylinders, and prisms in addition to full-scale concrete tiles had been prepared. Half of these samples were made using the same popular concrete mix. Test results indicated that, these samples were below standard requirements. The second half of the test samples was prepared using a newly designed concrete mix. Based upon the recommended breaking load, the required flexural strength of the tiles was calculated. This mix was designed to comply a flexural strength that was recommended by specifications. Care had been also concentrated on aggregate grading and concrete curing. Tests showed positive results.

In spite of this success it is still believed that there is a possibility of some failures may be due to mass production or due to bad quality control. A new proposed model had been prepared and tested. Finally these newly proposed tiles had shown that it was more resistant to breaking loads by +21% in comparison with the previous samples. This result might insure the production of safe concrete tiles.

Building & Construction Engineering Department, University of Technology.

المقدمة

تتسجم فكرة هذا البحث التطبيقي مع التطلعات الخاصة بتطوير المواد الإنشائية عن طريق الإستخدام الأمثل للموارد والإمكانيات المتاحة في القطر. لوحظ بأن البلاطات الخرسانية (المستخدمة للتسطيح والمعروفة تجارياً بالشتاير) المنتجة في شركات القطاع العام ومعامل القطاع الخاص تعاني بإستمرار من فشلها في الفحوصات المختبرية ولا تُلبي متطلبات المواصفه القياسية العراقية المُعتمَده (م ق ع 1107 – 1988). إن تَردي نوعية الشتاير المُنتج وإنخفاض جودته عن الحدود القياسية المطلوبه يُعَرِّضُه للتلف إثناء الخزن والمناقله ويكون سَهْل الكسر إثناء تنفيذه في موقعه النهائي. كل ذلك يُشكّل هدرًا إقتصاديًا كبيرًا , خصوصاً إن هذا المنتج شائع الإستخدام في العراق.

من خلال التشخيص الدقيق للمشكلة وبعد إجراء العديد من أَلقاءات مع المُنتجين تأكَّد لنا بأن هناك عدم عناية في كافة خطوات سير العملية الإنتاجية إبتداءً من إنتقاء المواد الأولية وفحوصاتها وإنتهاءً بإسلوب الخزن والمداولة. كل ذلك يؤدي إلى تَردي نوعية المنتج وفشله في فحوصات السيطره النوعيه خصوصاً في فحص قوة التحمل المُستعرَض.

إن تحسين خواص منتج الشتاير من خلال تحسين خواص الخلطة الخرسانية امر بديهي , حيث ان زيادة محتوى الإسمنت او استخدام ركام خشن مكسر او مقاس اقصى للركام غير كبير وتخفيض نسبة الماء/الاسمنت واستخدام المضافات والرص الجيد إثناء العمل والمعالجه المستمره , سينعكس إيجابياً على كافة خواص الخرسانه المنتجه وبالتالي تأمين متطلبات المواصفات (Neville and Brooks – 1987),

(Neville – 1995). إن سبب الإخفاق في هذا المجال بالنسبة للخرسانة المسبقة الصب قد اشار إليه أحد الباحثين حيث أكد على ضرورة توحيد الغايات والأهداف بين المصممين والعاملين في معامل الصب المسبق وخصوصاً أن فحوصات السيطرة النوعية في هذه المعامل تجرى على نماذج بمقاساتها الفعلية ويتم إختيارها بشكل عشوائي من أكداست متراكمة من المنتج (Newman and Choa – 2003).

إن قلة مهارة العاملين وعدم إكترائهم بالعديد من المتطلبات إثناء عملية الإنتاج يؤدي دائماً إلى إخفاقهم في الوصول إلى الهدف المنشود ألا وهو إنتاج شتاكر ذو مواصفات عالية ، ويكون هذا أكثر وضوحاً في مقاومة الشتاكر للتحمل المستعرض بالرغم من التوصيات النظرية العديدة في هذا المجال. لذلك فقد تم التركيز في هذا البحث على تحسين خواص منتج الشتاكر من خلال تصميم خلطه خرسانيه مناسبه إضافة إلى إقتراح إستخدام مشبكات سلكيه لضمان الحصول على شتاكر مقبول بالرغم من بعض هفوات العمال إثناء عملية الإنتاج والخزن والمناقله والتفذيذ في الموقع النهائي .

تشير بعض البحوث السابقة (Shah and Key – 1972, Netlon Ltd. – 1988, Engel and Bakis – 2001) إلى أن هناك إمكانية لتحسين خواص البلاطات الخرسانيه المسبقة الصب وخاصةً مقاومتها للإثناء والصدم من خلال إستخدام المشبكات سواء كانت من البوليمر أو الحديد أو الياف أخرى ، حيث أن هذه المشبكات ستساهم في:

- أ. تحسين متانة وديمومة البلاطات.

- ب. تحسين الخواص الميكانيكيه العامه للبلاطات.

- ج. زيادة قابلية البلاطات على إمتصاص الصدمات.

- د. تقليل نسبة التلف إثناء المناقله أو الإرتطامات المفاجئه.

- هـ. تقليل كمية التشققات الشعريه المتوقع حدوثها إثناء الصب والمعالجه.

كما توصل باحثون آخرون (Brooks and Kenai – 1995, Mathews et al. – 1981, Shah and Key – 1972) إلى أن نوع المشبك وعدد الطبقات المستخدمه وشكل الفتحات وأبعادها يؤثر على سلوك البلاطات الخرسانيه المسبقة الصب من حيث مقاومته ودرجة التشقق ومسار التشققات وعرض وعمق التشقق وكيفية إنتشار وتشظي الضرر. ما يهمننا في هذا البحث هو إتخاذ إجراءات بسيطه وغير مكلفه لتلافي إخفاقات شائعته في منتج الشتاكر العراقي ، وهذا ما سنتطرق له إثناء خطة البحث العمليه.

الجانب العملي:

المواد المستخدمة:

لجعل البحث قابل للتطبيق ، تم استخدام نفس المواد المحلية الشائعة الاستخدام من قبل معامل إنتاج الشتاير، الا أنه تم التأكيد على مطابقتها للمواصفات (وهذا ما لاتعتمده أغلب معامل إنتاج الشتاير) . وعموماً تم استخدام المواد التالية :-

أ. الإسمنت: تم استخدام الإسمنت البورتلاندي الإعتيادي المنتج في معمل إسمنت القائم ووجد بأنه مطابق للمواصفه العراقيه (م ق ع 5 - 1984) .

ب. الركام الناعم : تم استخدام الركام الناعم المُجهز من منطقة الأخيضر وكان مطابق للمواصفه العراقيه (م ق ع 45 - 1980)، تدرجه ضمن المنطقه الثانيه (zone-2) ، ووزنه النوعي يبلغ 2.65 ، في حين بلغت نسبة الأملاح الكبريتيه 0.2 في المائه. وكان نظيفاً وخالياً من الشوائب العضويه.

ج- الركام الخشن :- تم استخدام الحصى المكسر ، المُجهز من مقالع النباعي، ذو مقاس أقصى (14) ملم. وكان تدرجه مطابق للمواصفه العراقيه (م ق ع 45 - 1980)، ووزنه النوعي يبلغ 2.6 ، أما النسبة المئويه للأملح الكبريتيه فتساوي 0.02 في المائه، وإن كثافته المرصوصه الجافه كانت بمقدار 1640 كغم/م³. وكان نظيفاً وخالياً من الشوائب العضويه المنظوره.

إستخدام الماء الصالح للشرب لخلط ومعالجه الخرسانه في كافة أعمال البحث.

هـ. المشبك السلكي: تم استخدام مشبك سلكي حديدي ذو فتحات سداسيه ذات مقاس 19ملم من النوع المنسوج، وكان قطر السلك المستخدم في هذا النسيج يبلغ 0.80 ملم ، وذو مقاومة شد قصوى مقدارها 275 نت/ملم² .

و. القوالب: تم إنتقاء قوالب غير متضرره ذات أبعاد قياسيه دقيقه لضمان إنتاج بلاطات بقياس (800×800×3 ± ملم. وروعي طلاء القوالب بالزيت لتسهيل عملية نزع الشتاير بعد تصلبه منها.

الخلطات الخرسانية:

لضمان الحصول على خرسانه ذات مقاومه تؤدي إلى إكساب قطع الشتاير قوة تحمل مستعرض أعلى من المطلوب في المواصفه العراقيه القياسيه رقم 1107 لسنة 1988 تم إعتداد الطريقه البريطانيه (Neville - 1995) لتصميم خلطه خرسانيه بحيث تؤمن مقاومه إنضغاط دنيا لاتقل عن 30 نت/ملم² بعمر 28 يوم ومقاومه إنشاء لاتقل عن 4 نت/ملم² بعمر 28 يوم . هذا بحد ذاته سيكون كافياً لزيادة الحمل المستعرض المطلوب لكسر قطعة الشتاير إنشاء الفحص عن القيمه القياسيه البالغه 5.4 كيلونيوتن حيث ان:

$$f_r = \frac{Mc}{I} \quad (1)$$

أو:

$$f_r = \frac{\left(\frac{Pl}{4}\right)\left(\frac{h}{2}\right)}{\left(\frac{bh^3}{12}\right)} = 4N/mm^2$$

$$\therefore P = 5.4kN$$

بناءً على ذلك وبعد إجراء خلطات تجريبية موقعيه مُصَغَرَه لمراعاة نوعية وظروف الركام المستعمل فعلياً في الخلط , وتصحيح النسب فقد كانت الخلطة الخرسانية المقترحة ذات نسب خلط وزنيه بمقدار 1: 1.5 : 2.85 ونسبة ماء / إسمنت مقدارها 0.5 بذلك يكون محتوى الإسمنت المستخدم في هذه الخلطة يساوي 410 كغم/ م³ (وهذا أول جانب من الاختلاف بين التصميم والواقع إذ أن المعامل لا تستعمل هذه الكميات من الإسمنت لعوامل إقتصادية معروفة لديهم). وقد تم تسمية هذه الخلطة بالخلطة الجديد M_{new} .

لإغراض المقارنه تم استخدام نفس الخلطة الشائع المستخدمه من قبل معامل إنتاج الشتاير دون أي تدخل حيث كانت الخرسانه تُحضر بمقادير حجميه وقد تم تحويلها إلى نسبة خلط وزنيه تقريبيه تساوي 1 : 1.75 : 3.25 ونسبة ماء / أسمنت مقدارها 0.65 بذلك يكون محتوى الإسمنت المستخدم في هذه الخلطة حوالي 360 كغم/ م³ تقريباً. وكان غالبية الركام الخشن المستعمل غير مكسر وبمقاس أقصى يبلغ 25 ملم تقريباً (على أي حال لم نلاحظ سيطره نوعيه معتمده على المواد الداخلة في صناعة الخرسانه أصلاً). و تم تسمية هذه الخلطة بالخلطة القديمه M_{old} .

النماذج وفحوصاتها:

لغرض إستكمال جوانب البحث فقد تم تهيئة نماذج لإجراء فحوصات مرجعيه إضافةً إلى إنتاج نماذج شتاير بالقياس الكامل ، و تم تحضير النماذج التاليه لإجراء الفحوصات المؤشره إزائها:

أ. مكعبات $150 \times 150 \times 150$ ملم لفحص مقاومة الإنضغاط بعمر (7, 28, 60) يوم وبمعدل ثلاثة مكعبات لكل عمر.

ب. إسطوانات 300×150 ملم لفحص مقاومة الشد بالإنشطار بعمر (7, 28, 60) يوم وبمعدل ثلاثة إسطوانات لكل عمر.

ج. مواشير بأبعاد $500 \times 100 \times 100$ ملم لفحص مقاومة الإنثناء بنفس الأعمار آنفة الذكر وبتسليط حملين مُركّزين يؤثران على نقاط تثليث الفضاء البالغ 450 ملم. وتم إعداد موشوران لكل عمر.

د. شتاير بأبعاد $\{ 42 \pm 3 \times 800 \times 800 \}$ ملم. لإجراء الفحوصات القياسية بعمر 28 يوم. و تم إعداد ثلاثة عينات لكل نموذج.

هـ. شتاير حاوي على مشبك سلكي موضوع بالطريقة الموضحة تفصيلها في الشكل (1). لإجراء الفحوصات القياسية بعمر 28 يوم. و تم إعداد ثلاثة عينات لكل نموذج.

لإستكمال متطلبات المقارنه والإستنتاج الدقيق تم تهيئة كافة النماذج أعلاه بإستخدام الخلطة القديمه M_{old} وجرى تكرارها بإستعمال الخلطة الجديده M_{new} .

إعداد نماذج الشتاير:

لإنتاج نماذج فحص الشتاير بالقياس الكامل, وفق النسبه المصممه للخلط وإستخدام نفس المواد الأوليه والمكائن والمهارات المتيسره , تم إجراء الآتي:-

أ. إستخدام الحصى المكسر الموجود موقِعياً بعد غربلته بإستخدام غربال قياس 14ملم لإستبعاد الحصى ذو المقاسات الكبيره. أي بعباره أخرى تم إستعمال حصى مكسر ذو مقاس إسمي أقصى مقداره (14) ملم. جرى غسل الحصى على أرضيه نظيفه لمنع إختلاطه بالأطيان. إن عملية الغسيل تزيل ذرات الغبار الملتصقه على سطوح حُبَبَات الحصى وتساعد على زيادة ترابطها مع المونه الإسمنتيه. إن ترطيب الحصى بالماء قبل الخلط يجعله مُشَبَّعاً بالماء فعندما يُخَلَط مع بقيه مكونات الخلطة الخرسانيه لايمتص أي كميّه من الماء الضروري لتفاعل الإسمنت, وإنما يُسهم في فرز الماء في اليوم الأول من الصب بإتجاه المونه الإسمنتيه بطريقه تشبه المعالجه الداخليه للخرسانه مما يزيد من ترابطها وبالتالي مقاومتها .

ب. تمت غربلة الرمل الموجود في الموقع باستخدام غربال قياس 5 ملم على أرضيه نظيفه لتلافي إختلاطه بأتربه الأرضيه. بذلك تم إستبعاد كُتَل الرمل المتوقع وجودها في الرمل , التي لا تتفتت خلال الخلط , والتي يُعتَقَد بأنها تُشكِل نقاط ضعف في المنتج النهائي.

ج. تم إختيار القوالب بأبعاد 800×800 ملم والتي لا يقل إرتفاعها عن 40 ملم للحصول على السُمك القياسي المطلوب.

د. تم خلط الخرسانه وفقاً للنسبه التجريبيه الوزنيه التي جرى تصميمها والبالغه 1 : 1.5 : 2.85 مع نسبه ماء/إسمنت بمقدار 0.5.

هـ. تم إستخدام الخلطه الجديده M_{new} لإنتاج نوعين من النماذج A و B . كل نموذج يتألف من ثلاثة عَيِّنَات بِالْقِيَاس الكامل ($42 \times 800 \times 800$) ملم. النموذج الأول A يُمَثِّل حاله الإعتياديه بدون مشبك سلكي . أما النموذج B فَقَدْ جرى إنتاجه بإستخدام الإسلوب المُبتَكِر التالي:

وُضِعَ خليط خرساني يُعادل ثلاثة أرباع الكميهِ المطلوبه لإنتاج قطعة شتاير واحد في قالب الصب. بعد الإهتزاز والتسويه أوقف الإهتزاز لوضع التَّعْزِيز المُولَف من قطعة نسيج سلكي مُشَبَّك مُرَبَّعَه بأبعاد (50×50) سم , كما موضح في الشكل (1), بطريقه تكون أضلاعها متعامده على أقطار قالب الصب . هذه الطريقه تضمن الحصول على أكبر مساحة تعزير (تسليح) في المقاطع الوسطيه لقطعة الشتاير بإستخدام أقل ما يمكن من المشبك السلكي. ثم أُضيفت الكميهِ المتبقيه من الخليط الخرساني البالغه حوالي ربع الكميهِ المطلوبه لإنتاج قطعة شتاير واحد لتغطيه المشبك السلكي بسُمك مقداره حوالي سنتمتر واحد . بعد ذلك جرى تسليط إهتزاز وعمل تسويه للسطح.

كما تم تكرار العمل ذاته بإستخدام الخلطه القديمه M_{old} لإنتاج نموذجين من الشتاير. يتألف كل نموذج من ثلاثة عَيِّنَات , هما النموذج C الإعتيادي ونموذج D الحاوي على مشبك سلكي.

تهيئة النماذج ومعالجتها:

تم إعتِمال الآتي في تهيئة ومعالجة النماذج لغاية تاريخ الفحص:

أ. النماذج المرجعيه: تم معالجة العينات المرجعيه (المكعبات , الأسطوانات، المواشير) بالماء حيث تم الخزن في أحواض ماء لغاية تاريخ الفحص.

ب. نماذج الشتاير M_{new} : تمت معامله النماذج وفق الإسلوب التالي:

بعد مرور ساعتين من بدء الصب جرى الإستمرار بالترطيب وذلك برش العينات بالماء لمدة 20 ساعه وهي داخل القوالب . بعد ذلك فُتِحَت القوالب وأُخْرِجَت كافه العَيِّنَات وَوُضِعَت بصوره شبه عموديه. بَعْدَ 10

ساعات من فتح القوالب جرى غمر العينات في حوض خرساني مملوء بالماء لمدة 27 يوماً , حيث أُخرجت قبل يوم واحد من تاريخ الفحص المختبري بعمر 28 يوم.

ج. نماذج الشتاكر M_{old} : تمت معاملة العينات وفقاً للطريقة الشائعة في المعامل العراقيه لغاية تاريخ الفحص.

النتائج ومناقشتها:

يوضح الجدول (1) معدل نتائج الفحوصات المرجعية للخلطة الخرسانية القديمه المعتمده من قبل المعامل M_{old} والخلطة الخرسانية الجديده المقترحه إنشاء البحث M_{new} . كما توضح الاشكال (2, 3, 4) مسار تطور المقامات المختلفه مع الزمن.

بينما يوضح الجدول (2) نتائج فحوصات الشتاكر المنتج من الخلطتين وكذلك بإستخدام المشبكات السلقيه مع كل منهما. هذا ومن الجدير بالذكر بأنه تمت الإستعانه بالمركز القومي للمختبرات الإنشائيه لإجراء الفحوصات القياسيه لكافه نماذج الشتاكر.

تشير النتائج الموضحه في الجدول (1) إلى أن الخواص الميكانيكيه للخلطه الجديده M_{new} هي أعلى مما في الخلطه القديمه M_{old} , حيث إن نسبة الزياده في مقاومة الإنضغاط بعمر 28 يوم تبلغ (45 %) , وإن نسبة الزياده في مقاومة الشد بالإنشطار تساوي (46 %) , وكذلك الحال بالنسبه إلى مقاومة الإنثناء فقد كانت (3.30) نت/ملم² في الخلطه القديمه وأصبحت (5.11) نت/ملم² في الخلطه الجديده.

يتضح من الشكل (2) بأن هناك تطور جيد في مقاومة الإنضغاط لكلا الخلطتين , إلا أن معدل التطور في الخلطه M_{new} أفضل مما هو في الخلطه M_{old} , ففي عمر 7 أيام كانت مقاومة الإنضغاط للخلطتين M_{new} , M_{old} هي (23.5) نت/ملم² و (16.8) نت/ملم² على التوالي. وقد إزدادت قيمتها بعمر 28 يوم إلى (38.4) نت/ملم² و (26.5) نت/ملم² , وأصبحتا بعمر 60 يوم (45.9) نت/ملم² و (30.7) نت/ملم².

يوضح الشكل (3) معدل زيادة مقاومة الشد بالإنشطار مع الزمن للخلطتين ويتبين بأن المقاومة للخلطه M_{new} قد إزدادت بنسبة (53%) و (80%) بعمر 28 يوم و 60 يوم على التوالي بالمقارنه مع المقاومه بعمر 7 أيام. في حين أن تلك الزياده قد كانت بنسبة (30%) و (48%) للخلطه M_{old} .

كذلك الحال بالنسبه لمقاومة الإنثناء وكما مبين في الشكل (4). فقد إزدادت مقاومة الإنثناء للخلطه M_{new} بمقدار (1.36) نت/ملم² و (2.5) نت/ملم² بعمر 28 يوم و 60 يوم على التوالي بالمقارنه مع المقاومه بعمر 7 أيام. في

حين أن الخلطة M_{old} قد إزدادت مقاومتها للإنتشاء بمقدار (0.93) نت/ملم² و (1.8) نت/ملم² بعمر 28 يوم و 60 يوم على التوالي عند مقارنتها بمقاومة الإنتشاء بعمر 7 أيام.

ومن الجدير بالذكر أن نسبة مقاومتي الشد بالإنتشار والإنتشاء من مقاومة الإنضغاط هي الأخرى قد تحسنت في الخلطة M_{new} بالمقارنة مع نتائج الخلطة M_{old} . إن نسبة مقاومة الشد بالإنتشار من مقاومة الإنضغاط قد كانت (8.4%) في الخلطة M_{old} في حين (8.5%) في الخلطة M_{new} وبعمر 28 يوم. وأن نسبة مقاومة الإنتشاء من مقاومة الإنضغاط قد كانت (12.5%) في الخلطة M_{old} وقد تحسنت إلى (13.3%) في الخلطة M_{new} وبعمر 28 يوم أيضاً.

إن تحسن جميع خواص الخلطة الخرسانية المقترحة M_{new} بالمقارنة مع الخلطة الخرسانية التقليدية M_{old} الشائعة الإستخدام في معامل إنتاج الشتاير له أسباب عديدة ومشخصه مسبقاً ولكن كان لابد لنا من إجراء الفحوصات لمعرفة النتائج بشكل دقيق. إن زيادة محتوى الإسمنت وتقليل نسبة الماء/الإسمنت واختيار ركام خشن مكسر ذو مقاس أقصى 14 ملم وإجراءات السيطرة النوعية على المواد الداخلة في صناعة الخرسانة كل تلك العوامل قد ساهمت في تحسين خواص الخلطة الخرسانية ، وكذلك أدت إلى زيادة نسبة مقاومتي الشد بالإنتشار والإنتشاء كنسبه من مقاومة الإنضغاط وذلك لتحسن الترابط بين عجينة الإسمنت والركام الخشن في الخلطة الجديدة.

كل ما ورد آنفاً من نتائج يشير إلى أن الشتاير المنتج من الخلطة المقترحة الجديدة M_{new} سيكون قطعاً أفضل بكثير من الشتاير المنتج من الخلطة التقليدية القديمة M_{old} ، وهذا ما يبينه الجدول (2) حيث توضح النتائج بأن الشتاير المنتج من الخلطة القديمة غير مطابق للمواصفات من ناحية المقاومة (الحمل المستعرض) والإمتصاص ، حيث كان معدل مقاومته للحمل المستعرض بمقدار (3.3) كيلو نيوتن ونسبة الإمتصاص (3.94%) خلال 30 دقيقة و (7.90%) خلال 24 ساعة ، في حين أن تلك الخواص قد تحسنت في الشتاير المنتج من الخلطة الجديدة وأصبحت مقاومته للحمل المستعرض بمقدار (6.2) كيلونيوتن ونسبة إمتصاص ذات معدل (3.10%) خلال 30 دقيقة و (4.20%) خلال 24 ساعة.

إن إضافة المشبك السلبي بالطريقة التي تم ذكرها بالتفصيل في متن هذا البحث قد تدارك جزء من خلل الشتاير المنتج من الخلطة القديمة حيث أصبح معدل مقاومة نماذج الشتاير للحمل المستعرض بمقدار (4.40) كيلونيوتن أي إنها تحسنت بنسبة (33%) وإقتربت من الحد الأدنى المطلوب في المواصفه ، كذلك فقد تحسنت خواص الإمتصاص حين أصبحت ذات معدل (3.10%) خلال 30 دقيقة و (7.50%) خلال 24 ساعة بدلاً من (3.94%) خلال 30 دقيقة و (7.90%) خلال 24 ساعة.

أما إستخدام المشبك السلبي في إنتاج الشتاير من الخلطة الجديدة فقد حسن مرةً أخرى من المنتج وأصبحت مقاومته للحمل المستعرض بمقدار (7.5) كيلونيوتن بدلاً من (6.2) كيلونيوتن ومعدل نسبة الإمتصاص (2.65%) خلال 30 دقيقة و (3.60%) خلال 24 ساعة بدلاً من (3.10%) خلال 30 دقيقة و (4.20%) خلال 24 ساعة.

وهذا يعني أننا أصبحنا في مأمن بالمقارنة مع المواصفه القياسية وهذا هو ما نتوخاه لملاقات أي إخفاقات تنتج إنشاء العمل من قبل كادر غير ماهر أحياناً أو بسبب عدم المراقبه الجيده والمستمره للمنتوج أو حدوث إخفاقات إنشاء الخزن والمناقله.

الإستنتاجات:

من خلال النتائج التي تم الحصول عليها من هذا البحث وضمن المحددات المتعلقة به يمكن إستنتاج الآتي :

أ. لايمكن الحصول على شتاكر جيد ومقبول وفقاً للمواصفات بإتباع الأساليب الحاليه الشائعة الإستخدام في معظم المعامل المحليه التي لا تهتم بنوعية المواد الأوليه الداخله في صناعة الشتاكر ولا بدقه نسب خلطها ومن ثم معالجتها.

ب. إن إستخدام الخلطه الخرسانيه الوزنيه المقترحه البالغه 1 : 1.5 : 2.85 مع نسبة ماء /أسمنت مقدارها 0.5 مع ركام خشن مكسر ذو مقاس أقصى مقداره 14 ملم ، وإتباع السيطره النوعيه في العمل، بما فيها إجراء خلطات موقعيه تجريبيه عند حصول تغيير في مصدر تجهيز الركام او تغير محتواه الرطوبي خلال فصول السنه، سيؤدي إلى إنتاج شتاكر مستوفي لشروط المواصفه القياسيه العراقيه رقم 1107 لسنة 1988.

ج. إن إستخدام المشبكات السلكيه لتعزيز الشتاكر يؤدي إلى زيادة مقاومته لحمل الكسر بمقدار 21%+ مقارنة مع الشتاكر الذي لا يحتوي على مشبكات سلكيه.

المراجع:

- Brooks, J.J. and Kenai, S.,” Impact Properties of Polymer-grid Reinforced Cement Mortar.” The International Journal of Cement Composites and Lightweight Concrete, Vol.11, No.3, 1995.
- Engel, R. S. and Bakis, C.E.,” Fiber Reinforced Polymer-grids for Reinforced Concrete.” National Science Foundation Center, June, 2001.
- Mathews, M.S., Rao, P.S., and Srinuasan. P., “Impact Studies on Ferrocement Slabs.” International Symposium on Ferrocement, RILEM, 1981.
- Netlon Ltd.,” Tensor Grids in Concrete Applications.” The Civil Engineering Division, Blackburn, December, 1988.
- Neville, A.M., “ Properties of Concrete. “ Long man Group Ltd., 4th edition, 1995.

Neville, A.M., and Brooks, J.J., "Concrete Technology." Wiley & Sons Inc., New York, 1987.

Newman, J. and Choa, B. "Advanced Concrete Technology." Butterworth-Heine Main, First Published, 2003.

Shah, S.P. and Key, W. H. "Impact Resistance of Ferrocement." ASCE Proceedings, Journal of Structural Division, January 1972.

المواصفه القياسيه العراقيه رقم 5 , " السمنت البورتلاندي " , وزارة التخطيط , الجهاز المركزي للتقييس والسيطره النوعيه , بغداد , 1984 .

المواصفه القياسيه العراقيه رقم 45 , " ركام المصادر الطبيعيه المستعمل في الخرسانه والبناء " , وزارة التخطيط , الجهاز المركزي للتقييس والسيطره النوعيه , بغداد , 1984 .

المواصفه القياسيه العراقيه رقم 1107 , " البلاطات الخرسانيه السابقيه الصب " , وزارة التخطيط , الجهاز المركزي للتقييس والسيطره النوعيه , بغداد , 1988 .

الرموز:

f_r : مقاومة إنثناء الخرسانه (N/mm^2) .

M : العزم المطلوب لكسر النموذج بالإنثناء ($kN.m$) .

c : نصف سُمك النموذج (mm) .

P : قوة التحمل المستعرض (kN) .

l : المسافه بين نقاط إسناد النموذج (mm) .

I : عزم القصور الذاتي للمقطع العرضي للنموذج (mm^4) .

b : عرض النموذج (mm) .

h : إرتفاع النموذج (mm) .

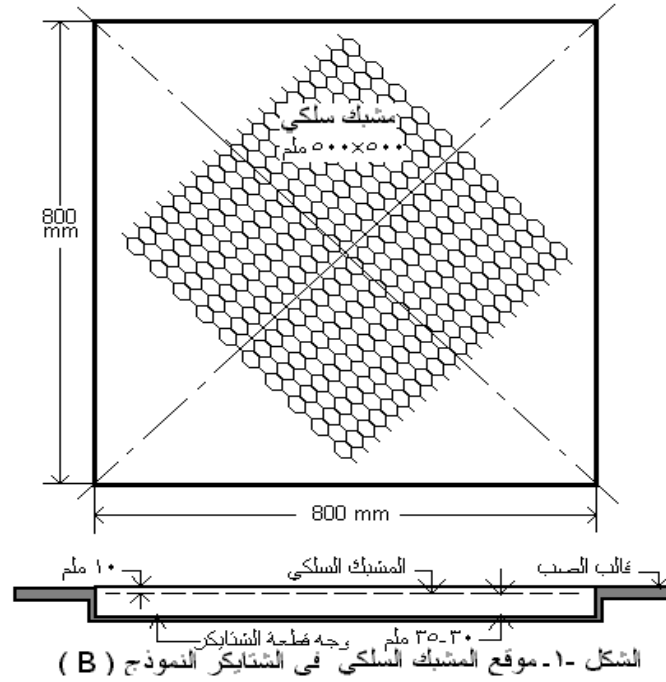
جدول (1): نتائج الفحوصات المرجعية للخلطات الخرسانية.

نوع الخلطة	معدل مقاومة الإنضغاط N/mm^2	معدل مقاومة الشد بالإنشطار N/mm^2	معدل مقاومة الإنثناء N/mm^2
------------	----------------------------------	---	----------------------------------

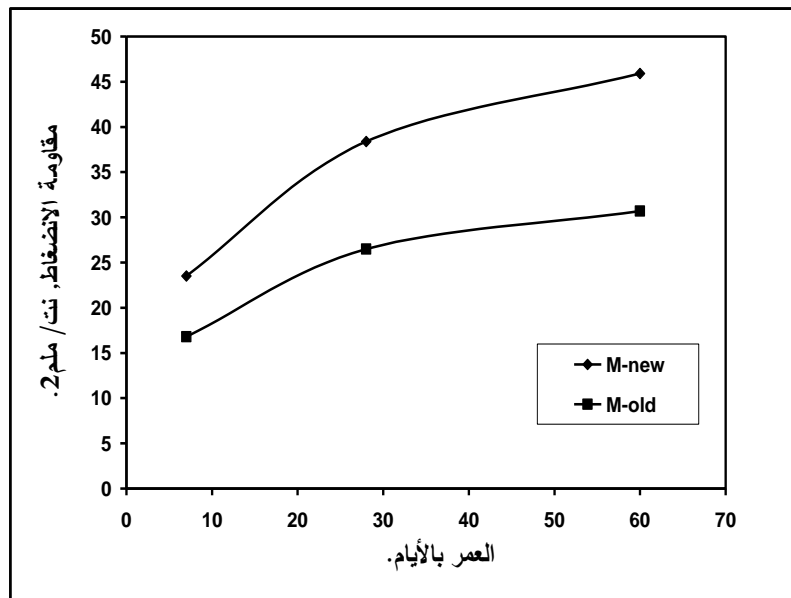
60	28	7	60	28	7	60	28	7	
يوم	يوم	يوم	يوم	يوم	يوم	يوم	يوم	يوم	
6.25	5.11	3.75	3.82	3.25	2.12	45.9	38.4	23.5	M _{new}
4.16	3.30	2.37	2.55	2.23	1.72	30.7	26.5	16.8	M _{old}

جدول (2): نتائج فحص البلاطات الخرسانية.

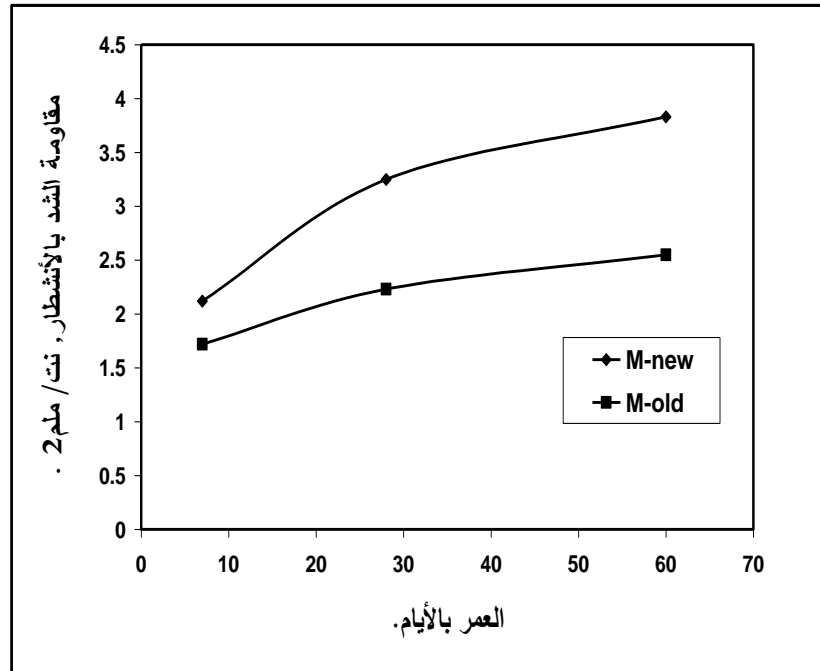
الإمتصاص %				قوة التحمل المستعرض kN			نوع الخلطه		
حدود المواصفه		نتيجة الفحص		حدود المواصفه	المعدل	نتيجة الفحص			
24 ساعه	30 دقيقه	24 ساعه	30 دقيقه						
10 حد أعلى	4 حد أعلى	4.30 4.05 4.20	3.20 3.00 3.10	5.4	6.2	5.6 6.4 6.6	M _{new} بدون مشبك		
كذلك	كذلك	3.80 3.40 3.60	2.85 2.50 2.60	كذلك	7.5	8.5 7.2 7.0	M _{new} مع المشبك		
		9.50 6.00 8.20	4.33 3.67 3.82			كذلك	3.3	3.7 3.3 2.8	M _{old} بدون مشبك
		7.20 7.50 7.80	3.50 3.00 2.80					كذلك	4.4



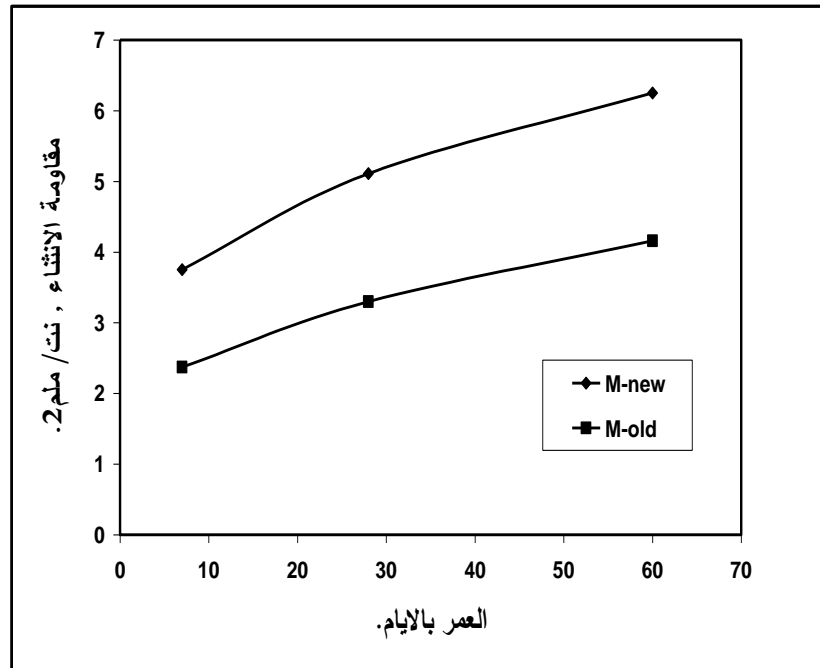
الشكل (1): موقع المشبك السلبي في بلاطات النموذج B.



الشكل (2): تطور مقاومة الانضغاط مع العمر للخلطات الخرسانية.



الشكل (3): تطور مقاومة الشد بالانشطار مع العمر للخلطات الخرسانية.



الشكل (4): تطور مقاومة الانثناء مع العمر للخلطات الخرسانية.

الجامعة و الاحساس بالانتماء المكاني البنيوي " دور الفعل التصميمي للفضاءات الخارجية في تحقيق بنية الاتصال السيميائية للجامعة "

هديل ثامر الخزاعي
ماجستير هندسة معمارية
جامعة القادسية

هدى عبد الصاحب العلوان
مدرس / كلية الهندسة
جامعة بغداد

مستخلص البحث

يتقصى البحث دور الفعل التصميمي للفضاءات الخارجية للبيئة الحضرية للجامعة في تحقيق بنية اتصال سيميائية متكاملة تخلق حواراً مستمراً بين المتلقي والهيئة المادية للبيئة الحضرية (من خلال الاستحضار اللاواعي للمعاني و الدلالات السيميائية الكامنة فيها) وتحقيق احساس الأفراد بالانتماء المكاني اليها , معززة بذلك الدور الانساني والاجتماعي والثقافي للجامعة ومساهمتها الفعالة في بناء الانسان الكامل .

لقد شكّل غياب الاطار النظري الشامل لدور الفعل التصميمي للفضاءات الخارجية في تحقيق البنية السيميائية المتكاملة للبيئة الحضرية للجامعة , مشكلة البحث الرئيسية . وقد نجم ذلك عن قصور المعرفة في الادبيات المعمارية السابقة في تقديم اطار نظري واضح ومتكامل لذلك الدور (نتيجة تركيز غالبية الطروحات على مفردات و مؤشرات مجزأة) , فضلاً عن غياب الربط الجدلي و المنطقي بين النظريات المعمارية والنظريات العلمية في مجالي البنيوية Structuralism والسيميائية Semiotics والذي يمكّن من تشكيل الاطار النظري ذي الاحاطة الشمولية . وعلى ضوء المشكلة البحثية تحدد هدف البحث في التوصل الى بناء انموذج نظري تتحدد من خلاله الاسس والآليات الرئيسية للفعل التصميمي للفضاءات الخارجية في تحقيق البنية السيميائية المتكاملة للبيئة الحضرية الجامعية . لقد تطلب تحقيق الهدف بناء الاطار النظري على ضوء فرضية البحث المطروحة , و من ثم استخلاص الاستنتاجات والتوصيات الخاصة بالبحث . وقد افرزت النتائج التي خلص اليها البحث آلية واضحة لدور الفعل التصميمي للفضاءات الخارجية في تحقيق البنية السيميائية المتكاملة للبيئة الحضرية للجامعة تتحدد من خلال تفاعل وتزامن آليات المركبات الاساسية الثلاث للبنية المكانية (الادراكية والفضائية والسلوكية) . ان هذه الآلية تمكن المصمم من خلق بيئات حضرية أكثر دلالة ومعنى وتحقيق احساس افرادها بالانتماء المكاني اليها .

The Campus and the Sense of Belonging to Place and Structure

ABSTRACT

The research investigates the role of the Campus Landscape Design in achieving a complete semio-communicational structure that creates a continuous dialogue between the perceiver and the physical entity of the urban environment

(through the unconscious recall of meanings and semiotic indexes implicit therein) and achieves individuals' sense of belonging to place , thereby emphasizing the human ,social and cultural role of the university and its vital contribution in building up the Whole Man .The absence of a comprehensive theoretical framework for the role of the Landscape Design in achieving a semio-communicational structure for the campus urban environment ,constitutes the main research problem.This problem arises from the lack of knowledge in the previous architectural literature in providing clear theoretical frame-work concerning the above mentioned role (as a result of literature concentration on fragmented and separate attributes) , as well as the absence of a dialectic and reasonable interrelation between architectural theories and scientific theories in the fields of Structuralism and Semiotics . In view of the problem under investigation , the aim of the present research is defined as arriving at the establishment of a comprehensive theoretical model , by which are determined the principles and mechanisms of the role of the Landscape Design in achieving a semio-communicational structure for the campus urban environment . Arriving at this aim requires the building of the theoretical framework in the light of the main research hypothesis, and eventually the extraction of the research conclusions and recommendations . The result of the research , led to clear mechanism for the role of landscape design in achieving a semio- communicational structure for the campus urban environment . This mechanism is formed by the reaction and simultaneity of the components of the three basic characteristics of place structure (cognitive , spatial and behavioral). By applying this mechanism , the designer will be able to create meaningful environments that achieve people's sense of belonging to place .

المقدمة

يتناول البحث بالدراسة و التحليل دور الفعل التصميمي للفضاءات الخارجية للجامعة في تحقيق بنية اتصال سيميائية للبيئة الحضرية تنتج عن تفاعل وتراكب ظواهر متعددة مادية ومعنوية وحسية تعمل بمجموعها على تكوين بنية بيئية متماسكة ذات خصائص محددة وهوية معرفة تخلق حوارا مستمرا بين المتلقي و الهيئة المادية للبيئة الحضرية يسهم بدوره في فهم بنيتها وتمييز عناصرها وادراك وتفسير رموزها وعلاماتها والاحساس بالتوجه المكاني والزمني فيها ، فضلا عن الاحساس بالاطمئنان والامان والارضاء العاطفي والمعنوي مولدة بذلك الاحساس بالانتماء المكاني اليها .وعليه يتناول البحث دراسة العلاقة السيميائية بين الانسان و التنظيم البصري والفضائي لبنية البيئة الحضرية للجامعة من خلال الفعل التصميمي للفضاءات الخارجية في تنظيم عناصر ومكونات البيئة و فضاءاتها و اظهار المعاني الكامنة فيها واحضارها في العالم الملموس من خلال التشكيل البصري و الفضائي للمتغيرات الفيزيائية لكي تكون بنية البيئة المصممة أكثر دلالة و معنى و أكثر انسجاما و تجاوبا مع الحاجات والمتطلبات الانسانية والسايكولوجية والاجتماعية والثقافية منتجة بذلك بنية مادية تعكس البنية الفكرية المتكاملة للجامعة . فأهمية هذه الدراسة تأتي من امكانية الفهم العلمي و النفسي للعلاقة السيميائية بين الانسان و التنظيم البصري و الفضائي لبنية البيئة الحضرية و امكانية استخلاص مفرداتها بما يمكننا من استعمالها مستقبلا في عملية التصميم بطريقة منطقية وعلمية مدروسة وصولا الى تحقيق بيئة معمارية ذات بنية سيميائية تحقق تألف الافراد معها وتولد الاحساس بالانتماء المكاني اليها .

مشكلة البحث

بالرغم من الطروحات التي تناولت طبيعة العلاقة بين مفهوم البنية و البيئة الحضرية للجامعة ودور الفعل التصميمي للفضاءات الخارجية في تحقيق هذه العلاقة , فقد ظهر جليا غياب الفهم الواضح لدور الفعل التصميمي للفضاءات الخارجية للجامعة في تحقيق بنية اتصال سيميائية تخلق حوارا مستمرا بين المتلقي و الهيئة المادية للبيئة الحضرية و تحقق الاحساس بالانتماء المكاني اليها . و قد نتجت هذه المشكلة عن :

أولا : غياب الاطار النظري الشامل لذلك الدور نتيجة تركيز غالبية الطروحات على مفردات ومؤشرات مجزأة .

ثانيا : غياب الربط الجدلي و المنطقي بين النظريات المعمارية و النظريات العلمية في مجالي البنيوية Structuralism و السيميائية Semiotics و الذي يمكن من تشكيل الاطار النظري بشكله المتكامل . و عليه فقد تبلورت مشكلة البحث بالشكل الآتي :

عدم وجود اطار نظري واضح و متكامل لدور الفعل التصميمي للفضاءات الخارجية في تحقيق بنية اتصال سيميائية للبيئة الحضرية للجامعة .

هدف البحث

تبعاً للمشكلة البحثية تحدد هدف البحث بالآتي :

التوصل الى بناء انموذج نظري يتحدد من خلاله الاسس و الآليات الرئيسية للفعل التصميمي للفضاءات الخارجية في تحقيق بنية اتصال سيميائية للبيئة الحضرية للجامعة .

فرضية البحث

[ان للفعل التصميمي للفضاءات الخارجية دورا اساسيا في تحقيق بنية الاتصال السيميائية المتكاملة للبيئة الحضرية للجامعة(والتي تحقق الاحساس بالانتماء المكاني) من خلال تفاعل وتزامن آليات الفعل التصميمي للمركبات الاساسية الثلاث للبيئة المكانية والتي تتمثل بالبنية السيميائية الادراكية و البنية السيميائية الفضائية و البنية السيميائية السلوكية] .

مشكلة البحث و الخلفية النظرية

معنى الجامعة

الجامعة- كما عرفت اليونسكو- مؤسسة للتعليم العالي , يكون المجال فيها مفتوحا لمن أكمل الدراسة الثانوية , وتعطي مدة تدريب لا تقل عن ثلاث سنوات (كقاعدة عامة من 4-6 سنوات) [Unesco ,p.128] . و من جهة اخرى ينظر للجامعة على انها هيكل من الاشخاص مجتمعين في مكان معين لنشر و استيعاب المعرفة في حقول دراسية متقدمة [Birks ,p.6] . أما تعريف الجامعة على ضوء الاسم التقليدي لها Universita , فيحمل معنا مزدوجا و هو : اتمام المعرفة والمساهمة العامة في تطويرها [Unesco,p.10] . فضلا عن ذلك تعرف الجامعة على أنها النموذج الاساس للتعليم Educational Prototype لمؤسساتنا الحديثة , عليه فأن مظهرها الفيزيائي لا بد ان يكون تجسيدا لوصفها و هدفها المتمثل بجمع الناس لاغراض تربوية واجتماعية [Neuman ,p.84] . من جهة اخرى يؤكد (Pearce) ان الجامعة تعد جزءا مكمل للمدينة المصممة فيها , كون الجامعات تنمو داخل المدن [Pearce ,p.10] . ومن وجهة نظر اخرى يجدها(Keith) مقرا للبحث عن المعرفة Knowledge و هذا ما يجعل من جودة تصميمها حافزا مشجعا على التعلم[Neuman ,p.79] . أما مصطلح Campus فيعني حرم

الجامعة وارضها ومرجها [Dober, p.12] , كما يعني تلك المنطقة من الارض حيث تقع الابنية الجامعية المعروفة بالكليات أو الاقسام وكل ما تتطلبه من خدمات و مكملات. كما تمثل كلمة Campus النموذج المثالي للحرم الجامعي و الذي لا يكتمل معناه الا بوجود الفضاءات الخارجية المصممة بما يخدم الاشكال الفيزيائية لمؤسسات التعليم العالي [Ibid, p.xi] . ونظرا لما يتمتع به مصطلح Campus من مفهوم يعد الاعم والاكثر شمولية فيما يخص تصميم البيئة الحضرية للجامعة , سيتم اعتماده كأساس للبحث الحالي ووهذا ما سيتم توضيحه في المحاور اللاحقة من البحث .

قيم الجامعة و دورها في المجتمع

في دراسته الموسومة (الحضارة والشخصية) يبحث (النوري) دلالة القيمة على خصائص الشيء و فاعليته النسبية لان يكون هدفا خيرا او شرا يسعى الانسان الى بلوغه او تجنبه وبحسب ناحيتي الارضاء النفسي و المنفعة المرتبطة بالغاية لذا فان قيمة مجتمع او حضارة ما تعد "تركيز انفعالي و ذهني حول اهداف محددة , تكون بشكل مبادئ يحتضنها افراد المجتمع " او هي " استنتاجات مستخلصة عن دراسات عميقة تقضي الى تشخيص نماذج منطقية متناهية الانتظام " [النوري، ص: 40-41]. ومن الجدير بالذكر ان القيمة تتضمن الوعي بمظاهره الثلاثة الوجدانية , النزوعية و الادراكية [Schulz, p.10] . فالمظهر الوجداني للوعي بالقيمة يظهر بالشعور العاطفي او الانفعالي و بدرجات مختلفة . والمظهر النزوعي هو المجهود الظاهر حركيا لبلوغ هدف معين او معيار سلوكي معين , أما المظهر الادراكي فيتضح في عملية ادراك الشيء موضوع القيمة وتمييزه , وما يتصل به من عمليات عقلية ذهنية فكرية كالنذكر والتصور . وعليه و بالعودة الى موضوع البحث الاساس نجد ان قيمة الجامعة استنادا الى ما جاء اعلاه تتمثل بكونها وعيا وجدانيا و نزوعيا و ادراكيا في آن واحد وفقا للقيم الانسانية لجوانب الحياة المختلفة . وهذا ما يؤكده تعريف (Newman) للجامعة على انها مكان لتعليم المعرفة العامة Universal Knowledge. وفي الوقت ذاته هي مؤسسة انسانية تنمّر عن شخص واسع المعرفة Broad Knowledged بفكر انتقادي Critical Intelligence و لياقة خلقية Moral Decency وحس اجتماعي Social Sensitivity [6,p:xv] . وهذا ما يأتي منسجما مع رأي (Ikeeda) في ان الجامعة تعكس نوع التعليم الذي يعزز مفهوم حب الانسانية Love for Humankind وينمي الشخصية Character ويوفر اساس Basis لادراك معنى السلام بما يسهم بتطوير المجتمع [Neuman, p.14] و يتوافق مع ذلك مفهوم (Erskine) للجامعة بأنها نموذج انساني Human Model لمؤسسات التعليم العالي [Erskine, PP.42-43] . ويمكن اجمال القيم الانسانية للجامعة بالقيم السايكولوجية المكانية منها والجمالية , والاجتماعية فضلا عن الثقافية وكالاتي :

الجامعة قيمة سايكولوجية مكانية - جمالية

تتجلى القيمة السايكولوجية للجامعة من خلال دورها في اثارة الذكريات reminiscence ويعزى ذلك الى جانبين الاول سايكولوجي- مكاني و الاخر سايكولوجي - جمالي . في كتابه (سايكولوجية- مكانية) كونه يمثل هدفا حساسا ضمن المحيط يتمثل بأثارة الذكريات لدى الطلبة نتيجة لاستجابة تفاعلهم للمكان الذي يسهم بتغذية نموهم الفكري [Gaines, p:11]. و هذا ما يتفق واهداف الجامعة بوصفها مؤسسة تعليمية تحدث و تولد الاحساس بالمكان Sense of Place والشعور بالطمأنينة و هنا يكمن مركز القوة في تصميم الجامعات [Neuman, p:2] . كما يجدها (Neuman) مفتاحا لتجسيد تلك المبادئ المعتمدة في كافة قرارات تخطيط الجامعة على انها وسيلة للاحساس بالمكان بما يعرف بمفهومية الجامعة ووضوحيتها وذلك من خلال القدرة على فهم بنيتها و تمييز عناصرها و ادراك و تفسير رموزها و علاماتها والاحساس بالتوجيه

المكاني والزمني فيه [Ibid,p.4] ومن جانب آخر نجدها قيمة (سايكولوجية – جمالية) إذ إن المرحلة الجامعية تعد حقبة مهمة جدا في حياة الفرد , لذا فإن تجربة الانتماء اليها و لو لسنوات محددة يجب ان تكون بالاهمية والقيمة المرجوة منها وهذا ما يستوجب اعطاء ذلك المكان نوعا متميزا من التنظيم والجمال الذي يغني مفهوم التجربة الفكرية و لا يتعارض معها لغرض خلق شخصية متميزة للجامعة و بيئة حضرية بارزة جديرة بالذكرى Memorable Environment تبهر الزائر، وتطبع لغة بصرية في ذاكرة الطالب كمفتاح لسنين دراسته [Ibid,p.103] . كما يؤكد (Dober) على ان ذاكرة المكان تعد واحدة من المعايير الاساسية في تصميم الجامعات .

"Memory of place has significance for all campuses" [Doper,p.36]

الجامعة قيمة اجتماعية

في كتابه *The Idea of a University* يجد (Neuman) ان الجامعة قيمة اجتماعية كونها مؤسسة تمثل نوعا متميزا من التعليم بما يحقق الكفاءة و المقدرة على خلق شخصية اجتماعية متفاعلة مع اجمالي المجتمع . ويعرّف (Neuman) الجامعة و تصميم البيئة الجامعية عموما على انه تعبير استثنائي عن المستقبل المتوقع الذي يسهم في تعبيرية العقل وبنية الفكر والقدرة على التفاعل المدني والاجتماعي [Neuman,p:xv] . وهذا ما يعزز مفهوم (Mumford) للجامعة بأنها مؤسسة ذات اعتبارات اجتماعية كونها اساسا لفعالية التعليم ووسيلة لتعلم و طلب المعرفة بأماكنيات متنوعة و بطرق متميزة فضلا عن كونها اسلوبا لادراك خصوصية المجتمع , إذ أن بإمكان كل شخص ان يتحصن اجتماعيا من خلال ممارسة تجربة التعليم الجامعي . لذلك تعد الجامعة واحدة من اهم السبل المؤدية الى تحقيق مبدأ المثالية في كل من مفهوم المواطنة والاعتبارات الاجتماعية [Mumford,p:42] .

الجامعة قيمة ثقافية

ومما لا شك فيه أن الجامعة تشكّل قيمة ثقافية حتمية إذ يجدها (Stefanos) بداية واستمرار للجزور الثقافية "The campus refers to the beginning and continuity of cultural roots" كما تعبر عن الايمان بمستقبل روح الريادة "The campus refers to the belief in the future of the pioneering spirit" [Neuman,p:2] ومن الجدير بالذكر أن المبدأ الوظيفي للجامعة وفقا لمفهوم (Woods) يكمن في تشجيع عملية التبادل الثقافي والتوليد الفكري بين الناس لغرض زيادة حقول المعرفة الانسانية و التحكم في سيطرة الانسان على فعالياته الثقافية، الجماعية منها والفردية [Woods,p:83] 0 كما أكدت منظمة اليونسكو على القيمة الثقافية للجامعة بناءا على وظائفها والتي يمكن تلخيصها بالتعليم العالي , البحث العلمي , التعليم المستمر فضلا عن تعزيز الدور الثقافي والاجتماعي الذي يمهد الطريق لبناء الانسان الكامل "The Whole Man" [Uneseco ,p.12] .

اهمية تصميم البيئة الحضرية للجامعة

ان الاستعراض السابق لدور الجامعة وما تعنيه من قيم في جوانب الحياة المختلفة و ما لذلك من تأثير واضح في بناء انسان كامل يسهم و بشكل فعال في بناء وتطور المجتمع , يحتم علينا الاخذ بنظر الاعتبار اهمية تصميم البيئة الحضرية للجامعة لتبدو ملائمة لتحقيق الهدف المبتغى منها و تفعيل الجامعة لتكون مؤهلة لاداء وظائفها . وفي هذا المجال يرى (Neuman) في كتابه *College and University Facilities* ان تصميم البيئة الحضرية للجامعة يمثل توازنا بين ثلاث عوامل أساسية تتمثل بالتخطيط الفيزياوي Physical Planning والنشوء التاريخي Historical Evolution والتقدم التكنولوجي Technological Progress [Neuman,p.26] . و من جهة اخرى يرى (Neuman) ان البيئة الحضرية للجامعة يجب ان تصمم

وفقا لمعايير تمتاز بمدى الاستجابة الفيزيائية لوظائفها المتنوعة و تكون نموذجا للترابط بما يشجع على الثقة المتبادلة ما بين الطلبة والاساتذة و الزائرين , من خلال دقة التعبير عن وظائفها , وبما يعزز مفهوم الانسانية بكل مقاييسها و الانسجام الفيزيائي الذي يشير الى ما تعنيه هذه المؤسسة التعليمية من قيم مختلفة . كما يجد ان الحضور الفيزيائي الكلي للمؤسسة الجامعية يأتي من كونها تمثل محيطا مترابطا من الابنية و الفراغات , وان هذا المحيط المتماسك ينتج عن هيكلية التخطيط الثابت والفضاءات الخارجية المتميزة اضافة الى قوة نسيج العمارة. في حين يجد (Dober) ان تصميم البيئة الحضرية للجامعة يمثل وسيلة فيزيائية للتعبير عن التصميم الحالي والتوسع المستقبلي للموقع . ان نظرية (Dober) للتصميم تقع ضمن ثلاثة محاور اساسية تتمثل بالطوبوغرافية Topography , تصميم الفضاءات الخارجية Landscape Design و الكتل البنائية Building Masses , و بما يحقق الوظيفة الامثل ويثير الاحساس الاجمل [Dober,p.xviii] . و في كتابه *University Builders* يؤكد (Pearce) ان الاهتمام بتصميم البيئة الحضرية للجامعة وفقا لافكار فلسفية متميزة يعزز تصورنا للتعليم العالي المعاصر.

"Design of universities environment according to philosophical ideas will underpin our conception of contemporary higher education"

[Pearce,p.7]

مفهوم الفضاءات الخارجية للجامعة

وفقا لمفهوم (Fairtrother) نجد أن الفضاء الخارجي ببساطة ليس مجرد منطقة من سطح الارض او مجرد ساحة ضمن الخارطة و انما نظرنا اليه و كما تتركه حواسنا البصرية تعبر عن مفهوم التوافقية Harmony والتوحيد Unity و يكمن دور الانسان هنا في كونه وسيلة لخلق الفضاء الخارجي بما يحمله من مفاهيم وظيفية Functional وجمالية Aesthetical [Neuman,p:35]. ويعرف البعض الفضاء الخارجي على انه نظام Order و هذا ما نجده في رأي (Stanley) اذ يرى ان مبدأ عمارة الفضاءات الخارجية هو عملية تصميم لانظمة معينة متوافقة مع بعضها ذات انسجام و تألف بالعلاقات و بما يحقق مفهوم النظام [Stanley ,www]. و في كتابه *Ecological Design Handbook* يعبر (Stitt) عن مصطلح الفضاء الخارجي على انه وسيلة لتجسيد الاعتبارات الاجتماعية و الطبيعية [Stitt,p:66]. اما في الكتاب *Introduction to the Interpretation of Ordinary Landscape* فقد عبر (Meinig) عن الفضاءات الخارجية على أنها وسيلة لتجسيد الاعتبارات الثقافية وهذا ما نلمسه بوضوح في قوله (ان البيئة تدعمنا كمخلوقات و الفضاءات الخارجية تبرزنا كثقافات).

"An environment sustains us as creatures;landscape displays us as cultures" [Meinig,www.].

و هذا ما يتفق مع وجهة نظر (Prigogine&Isabelle) و التي تؤكد على أن الثقافة نتاج صناعي Artifact و ان الفضاءات الخارجية تعد مركز نشاط ملائم لتعزيز مفهوم تلك الثقافة كونها نتاج التداخل بين كل من استعمالات الارض Landuse و البيئة الثقافية Cultural Environment [Prigogine,www.]. اما الفضاءات الخارجية للجامعة تحديدا , فوفقا لتعريف (Reuter) نجدها ليست بقايا فضاءات Leftover-Spaces بين أبنية الجامعة فحسب, بل هي سلسلة من الاماكن المصممة مشكّلة محيطا مركبا من الفضاءات الخارجية و التي يفترض ان تضفي الاحساس بالامان وتشجع على المشاركة مع الجماعة بما يعزز مفهوم التفاعل الاجتماعي و تروق للجميع وبمختلف المستويات [Reuter ,P.35]. و في كتابه *Campus Landscape* يشير (Dober) الى اهمية دور الفضاءات الخارجية بالنسبة لاجمالي البيئة الحضرية للجامعة كونها تعكس و بدقة متناهية الافكار المبتغاة من عملية التخطيط والتصميم للبيئة الخضراء و بما يرمز لمؤسسة التعليم العالي [Dober ,p:xv]. كما تمثل الفضاءات الخارجية

للجامعة النقطة الفاصلة بين الداخل و الخارج و هذا ما يتطلب اظهارها بمظهر متجدد Fresh Look ومن خلالها يتم تحويل الافكار الى خيال ملموس اي ترجمتها لتبدو حقيقة واضحة قابلة للتقييم و ذات نتائج جديرة بالقبول والرضا , وهذا ما يلعب دورا متميزا في تفعيل الخيال ويعزز مكانة مؤسسة التعليم العالي بالمقارنة بالمؤسسات الاخرى و بالتالي يميز كل من الجامعات بشكل عام و كلياتها بشكل خاص لتحثل الصدارة كمواقع لجذب الطلبة وكل من يرتادها و يشجع على اعتماد افكار متميزة فيما يخص التصميم البيئي للجامعة ويثبت حضورها الجمالي الفني ويبيدي الحرم الجامعي كمحيط اجتماعي ثمين Community Asset . فضلا عن ذلك تعرف الفضاءات الخارجية للجامعة على أنها فضاءات منظمة لموقع الجامعة ليبود متناسقا كما تمثل العلاقة الرابطة بين الكتل الحضرية Urban Blocks والفضاءات الحضرية Urban Spaces المحيطة بها ووسيلة لتحقيق وظيفة الاحساس بالامان Safety و ما يترتب عليه من الاحساس بالانتماء للمكان Sense of Belonging to Place . وهذا ما يكسبها سمة وظيفية تضاف الى سابقتها من السمات آنفة الذكر .

دور الفعل التصميمي للفضاءات الخارجية للجامعة

في كتابها Campus Landscape Concept Plan نلمس تأكيدا واضحا لـ (Barbra) مفاده أهمية تطوير الفضاءات الخارجية للجامعة لتبلغ الاهداف التالية [Dober ,p.47] :-

- الصورة الذهنية للجامعة Campus Image :- اذ لا بد للفضاءات الخارجية للجامعة ان تخلق هوية بصرية متميزة توحد البيئة المبنية لتلك الجامعة كما ان تلك الفضاءات يجب ان تعكس التأثيرات الخاصة بالفضاءات المحلية و المتمثلة بمحيط الموقع و تاريخ استعمال الموقع اضافة للاستعمال الحالي للموقع.
- التعريف الفضائي – الحيزي :- Spatial Definition :- اذ ان الفضاءات الخارجية للجامعة يجب ان تعرف كل من مناطق الجامعة, الفضاءات, طرق الحركة و المداخل بما يساعد على التوجيه المكاني Spatial Orientation و ايجاد الطريق Way Finding ضمن بيئة الجامعة .
- نوع الحياة :- Quality of Life :- اذ تمنح الفضاءات الخارجية للجامعة من يرتادها القدرة الكافية على تحسس بيئة خارجية مريحة تعكس الرضا و القبول لدى مستخدميها .
- الاستعمال التربوي :- Educational Use :- فالفضاءات الخارجية للجامعة يجب ان توظف على انها موضع تزرع فيه الاشجار لاغراض علمية و بيدي للعيان اصناف النباتات من المجاميع المتنوعة باعتبارها مصدر تربوي للجامعة والمجتمع في آن واحد .
- صيانة الموارد و البيئة :- Resource Conservation & Environment :- و ذلك بالاستجابة للطبيعة المحلية من خلال الحفاظ على الاماكن الطبيعية النادرة الموجودة فيها اساسا .

يخلص البحث هنا الى أن دور الفعل التصميمي للفضاءات الخارجية للجامعة يتحقق من خلال تشكيلها لتكون حلقة وصل بين مكونات اجزاء الجامعة وسبيلا لربط ابنية الجامعة مع مجاوراتها من الكتل و الفضاءات الحضرية , كما أن وظائف الفضاءات الخارجية المصممة تشكل تواسلا مع وظائف فضاءاتها الداخلية , فضلا عن دورها الفعال في اغناء المتطلبات الوظيفية منها و الجمالية و الحسية .

بناء على ذلك يعد دور الفعل التصميمي للفضاءات الخارجية للجامعة الاساس في تشكيل البنية المادية لاجمالي بيئتها الحضرية و سببا لخلق نسيج مترابط ضمن نسيج المدينة المصممة فيها تلك الجامعة بما يجعل تشكيل الاولى يبدو كمدينة صغيرة ضمن مدينة أكبر. لذا سيركز البحث

الحالي على هذا النوع من الفضاءات لما لها من دور أساسي في ابراز البيئة الحضرية للجامعة كبنية مادية ظاهرة تعد انعكاسا للبيئة الفكرية الكامنة في مضمونها .

الطروحات النظرية السابقة

دراسة 2003 /David J. Neuman

في كتابه *College and University Facilities* نظم (Neuman) وسيلة لسهولة الاستعمال لمرافق الجامعة المختلفة وتحديد ما يخص فضاءاتها الخارجية من خلال تحديد هيكلية لبيان نمط التصميم بالاعتماد على كل من البرنامج , تخطيط الموقع, دليل تصميم الجامعة, سبل ايجاد الطريق, اذ يؤكد (Neuman) على ان الفضاءات الخارجية و الساحات تعد حلقة وصل ما بين اجزاء ومكونات الجامعة المختلفة و هذا ما يجعل البيئة الجامعية تبدو كتلة متلاحمة و يثير رغبة البقاء فيها لمدة اطول , وهنا يتجسد دور تصميم الفضاءات الخارجية للجامعة اعتمادا على وظائفها المتنوعة لتكون امتدادا لوظائف الفضاءات الداخلية فيها , موفرا بذلك القاعدة المعلوماتية اللازم اتباعها في عملية تخطيط و تصميم البيئة الحضرية للجامعة وصولا الى انجاح الهدف الوظيفي لتلك الفضاءات بما يليق بالجامعة كمؤسسة مرموقة للتعليم العالي .

- دراسة 2000/Richard P. Dober

في كتابه *Campus Landscape* سلط المعمار (Dober) الضوء على المحددات والتصنيفات الخاصة بالفضاءات الخارجية للجامعة , من خلال تحديد دليل عملي للفضاءات المفتوحة بالاعتماد على دراسة كل من المواقع , المخططات و اسس التصميم الخاصة بتلك الفضاءات والتوصل الى بناء الاطار الفكري الخاص بكل مظاهر التصميم للفضاءات المفتوحة معتمدا على امثلة لحقب زمنية متنوعة القديمة منها و المعاصرة .

دراسة 1991/Thomas A. Gaines

في كتابه *The Campus as a Work of Art* اشار المعمار (Gaines) الى ان افضل الجامعات هي تلك التي تمتاز بدقة التخطيط و التصميم على حد سواء لكل من عمارة الجامعة وفضاءاتها الخارجية معتمدا في تصميمه للفضاءات الخارجية للجامعة على تحقيق مبدأ الجمالية بما يعالج تصميم ابنيته و يسهم في تنظيمها الحضري و يحقق الهدف المراد منها في الحفاظ على الانجاز البصري (المنظور العام) و الاحساس بالتوجيه و ما يترتب على ذلك من تأثيرات سايكولوجية على شاغلي البيئة الجامعية , ومن جملة ما اشار اليه (Gaines) هو ان فقدان التوجيه يعد احدى المؤشرات المؤدية الى فشل العملية التصميمية للجامعات , وما يترتب على ذلك من سلبات سايكولوجية على شاغلي تلك البيئة .

- دراسة 2003 /Franklin, Durkin

في بحثهم الموسوم *The Role of Landscape in Creating Sustainable Campuses* يشير كل من (Franklin, Durkin) الى ان الكليات و الجامعات تأخذ عادة بالتوسع بنسب مختلفة في تخطيطها بالاعتماد على المحددات الطبيعية منها والتاريخية والثقافية وما ينتج عن اجتماع تلك المحددات من تأثير ملموس على تصميم البيئة الخارجية بغية الارتقاء لتحقيق المساعي الرامية لخدمة الجماعة وبما يشجع على التواصل الاجتماعي و بالشكل الذي يتلائم وطبيعة المجتمع المعني وما ينتج عن ذلك من رغبة في الانتماء للجماعة و تبادل الصلات الاجتماعية ضمنها بهدف ضمان دور تصميم البيئة الخارجية للجامعة في الالمام بكل ما يتطلبه بناء المجتمع المتحضر [Franklin ,www.] .

دراسة 1997/Ann Arbor

في كتابها *Special Planning for Special Places* تؤكد (Ann) على دور الفعل الناتج عن تشكيل الفضاءات الخارجية الخاصة بالبيئة الجامعية وربطها مع بعضها بأسلوب تهيمن فيه صفة التفاعل بين اجزاء الفضاءات المترابطة مما يسمح بالتداخل غير المباشر بين الكليات المختلفة وفقا لنمط يتيح فرصا أكبر لاجتماع الطلبة وما لذلك من تأثير مباشر على التبادل الفكري بين طلبة الاقسام المختلفة، فيظهر الهدف هنا اجتماعي ثقافي. كما أشارت في الكتاب ذاته الى الاثر الفعال لتصميم الفضاءات الخارجية في تعزيز الفعاليات الثقافية الفردية منها والجماعية فضلا عن توسيع الآفاق الخاصة بحقول المعرفة بمختلف أنماطها بين شاغلي ذلك النوع من فضاءات الجامعة.

دراسة 2002 /Fides , Louise , Helen

في بحثهم الموسوم *The Impact of Facilities on Students Choice of University* اعتمد (Fides,Louise,Helen) على الاثر السايكولوجي المترتب على اتقان فن تصميم الفضاءات الخارجية للجامعات , مؤكدين على فعل مستوى التسهيلات Level المتبعة في تخطيط اجمالي البيئة الخارجية على كيفية الاحساس بعلاقة الكتلة بالفراغ ضمن تلك البيئة , واهمية تشكيل الفضاءات الخارجية و تداخلها بأسلوب يعد العامل المحفز Stimulus Factor على استمرارية بقاء الطلبة ضمن ذلك المحيط وتفاعلهم النفسي مع اجمالي البيئة البصرية Visual Environment وكيفية اظهارها كمذكر بصري Visual Reminder ومراعاة التفاعل الناتج عن الدقة المعتمدة في تصميم الفضاءات الخارجية .

- نقد الطروحات النظرية السابقة

نستخلص من مراجعة الطروحات المتنوعة التي تناولت موضوع (الفعل التصميمي للفضاءات الخارجية للجامعة) الملاحظات الآتية :-

* ناقشت الطروحات دور الفعل التصميمي للفضاءات الخارجية للجامعة بشكل مجزأ . وركزت غالبيتها على مؤشرات تصميمية متفرقة تحقق النواحي الوظيفية أو السايكولوجية أو الاجتماعية أو غيرها . ولم توضح الطروحات دور الفعل التصميمي لهذه الفضاءات في تحقيق النسق والتآلف بين مكونات البنية المادية للبيئة الحضرية للجامعة ، و بما يعكس البنية الفكرية الشاملة لها .

* تميزت الدراسات السابقة بتوفيرها معلومات حول كيفية ادراك الفرد للبيئة من حوله وتفاعله معها . الا انها لم توضح ابعاد العلاقة التعبيرية بين الفرد والتنظيم البصري والفضائي لبنية البيئة الحضرية والتي تحدد ابعاد الطبيعة التفاعلية وتولد احساسه بالانتماء المكاني اليها .

- استخلاص المشكلة البحثية

ويتضح لنا من خلاصة مناقشة الطروحات السابقة ارتباط المشاكل المعرفية بمحورين أساسيين

• المحور الاول :
مشكلة غياب الاطار النظري الواضح لدور الفعل التصميمي للفضاءات الخارجية في تحقيق بنية مادية متكاملة تعكس البنية الفكرية الشاملة للجامعة .

• المحور الثاني :
مشكلة غياب الاطار النظري لدور الفعل التصميمي في تحقيق علاقة اتصال سيميائية بين الفرد والتنظيم البصري والفضائي لبنية البيئة الحضرية تحقق الاحساس بالانتماء المكاني اليها .

وفي ضوء المشاكل المعرفية أعلاه ، تبلورت مشكلة البحث وتحدد هدفه بالشكل الآتي :

مشكلة البحث :

عدم وجود اطار نظري واضح لدور الفعل التصميمي للفضاءات الخارجية في تحقيق بنية اتصال سيميائية للبيئة الحضرية للجامعة تولد الاحساس بالانتماء المكاني اليها .

هدف البحث :

التوصل الى بناء انموذج نظري تتحدد من خلاله الاسس والآليات الرئيسية للفعل التصميمي للفضاءات الخارجية في تحقيق بنية اتصال سيميائية للبيئة الحضرية للجامعة.

بنية البيئة الحضرية و الانتماء المكاني

- ماهية البنية في المنظور الفلسفي

ان مفهوم كلمة البنيوية يأتي من البنية "Structure" او التركيب بما ينطوي عليه من دلائل تخطيطية معمارية معبرا عنها بالنظام المؤلف من الظواهر المتماسكة التي يتوقف كل منها على الآخر، و لا يمكن ان يكون ما هو عليه الا بفضل علاقته معها [خليل، ص42]. ويعتبر (Lynch) نظام البنية احد أهم المعايير التي تجسد مدى وضوحية البيئة المبنية ، اذ يعرف البيئة الواضحة بأنها "تلك البيئة التي تدرك بنيتها كنظام متقن التكوين من العناصر والمكونات المرتبطة مع بعضها" [Lynch, p.7]. كما يرى الكثير من المفكرين ان البنية منظومة تعبيرية ، من هذا المعنى انطلق المفكر اللغوي (Vico) في مناداته بفكرة البنيوية لأول مرة بكونها طريقة لادراك العالم المحيط من خلال بنى ادراكية يقيمها الانسان مستندا على معتقداته و مفاهيمه حيث يشير الى وجود لغة ذهنية مشتركة في طبيعة الانظمة البنيوية لدى جميع المجتمعات التي تدرك جوهر الاشياء الموجودة في الحياة الاجتماعية و تكشف ذاتها بتركيب البنى و اخضاع طبيعتها لمتطلبات البناء [هوكز، ص19]. و قد سميت البنيوية ايضا بالتركيبية كمحاولة لتطبيق اساليب مؤسس عالم اللغة التركيبي (Ferdinand de Saussure) الذي يعد اللغة نظام اشارات يجب ان يدرك بصورة تزامنية اي يدرك كنظام متكامل في نقطة زمنية معينة من خلال تحليل تراكيبها وعلاقاتها مع بعضها البعض في ذلك النظام . عليه يخلص البحث الى تعريف بنية البيئة الحضرية على انها : نظام من الاشارات الكامنة بين فضاءات البيئة الحضرية والمتلقي شاغلها، والسبب في ذلك يعزى الى تشكّل البنية من عناصر متجانسة بما يجعل اجمالي تجانسها باعثا لمؤشرات تطلق بهدف اصال معلومات معينة للجهة المستلمة (الأشخاص شاغلها) .

- ماهية السيميائية

من الممكن تصوّر قيام علم يدرس حياة الاشارات في المجتمع وفقا لمفهوم (Saussure) وسيكون جزءا من علم النفس الاجتماعي ، و بالنتيجة جزءا من علم النفس يطلق عليه بالسيميولوجي Semiology أي علم الاشارة (و هي لفظة مشتقة من اللفظة الاغريقية Semeion بمعنى اشارة او علامة) [هوكز، ص114] . كما يعد علم الاشارات من أثمر المفاهيم النابعة من الفكرة البنيوية العامة للخمسينات والستينيات و من غير اليسير التمييز بينهما ، اذ ان حدود علم الاشارة مشتركة مع البنيوية : ذلك ان اهتمامات الحقلين ليست منفصلة جوهريا و على المدى البعيد يتوجب ضم كلا الحقلين في حقل ثالث يجمعهما و يسمى ببساطة (الاتصال) . في هذا السياق تظهر البنيوية نفسها بصفاتها طريقة للتحليل تربط حقول اللسانيات و علم الاجناس والعلاماتية [المصدر نفسه، ص114] كما يمكن اعتبار علم الاشارة وفقا لمفهوم (Barthes) حقلا يتعلق بطبيعة الرموز Nature of Symbols ، و ان ما يهتم به هذا الحقل يمكن اجماله بالمثلث الاشاراتي الاساسي و الذي يمثل بدوره العلاقة الرابطة بين كل من الرمز Symbol ، الفكر

Thought , و المدلول Referent [Lang, p.205]. ان ما هو اساسي في علم الاشارة يتضح في ظهور الفكرة Concept كدليل و هذا ما يولد نسق الاشارات Signs Context [Eco, www.].
ويجد آخرون ان دراسة علم الاشارات يقودنا الى دراسة ثقافة مجتمع ما ويوسع المصادر الخاصة بالنقد و المناقشات الخاصة بالنصوص المؤلفة للمعاني , وفي هذا المجال وجد (Genette) ان البنيوية تعد (دراسة لتركييب الثقافة من خلال تطابق المعاني وفقا للعلاقات بين الاشارات و التي تشكل المعنى وتظهره كسلسلة تعكس مدى التتابع الثقافي). ويرى البحث هنا أن أهمية السيميائية تكمن ضمن مستلزمات ادراك بنية البيئة الحضرية , جاعلا من مدى ادراك المتلقي لشكل الفضاءات المكونة للبيئة الحضرية ومعناها هدفا يحمل في جميع ابعاده صورا مختلفة عن كيفية توافق العلاقات بين الفضاءات من جهة ومعززة لوظيفته من جهة اخرى , من خلال انعكاس الاشارات الكامنة فيه .

البيئة الحضرية بوصفها بنية اتصال سيميائية

ان علم الاشارات يميز بين المعنى الثابت و المعنى الايحائي , بين الانظمة والرسائل المنقولة بواسطتها , بين الاصناف الكاملة من الاشارات و التي تعد بدائل لبعضها الاخر وتلك العلاقات الافقية المباشرة , حيث ترتبط الاشارات معا في هيئة سلسلة [بارت, ص13]. كما ان فهمنا للتركييب المعمارية للنسيج يقود ادراكنا لمعانيها بما يسمح بالتنبؤ به الى درجة كبيرة ليقاطعه فيها نظاما آخر ليمنحه حيوية جديدة , و اذا ما ارتبط تركيبان معا لتتشابه صورهما او موقعهما فأن هذه الظاهرة تخلق احساسا ادق بتشابههما أو اختلافهما والذي بدوره يغني العمل ويحول بصورة مستمرة الصور الذهنية و يخلق صورة جديدة بتصادم مستوياته المختلفة وتكثيفها. و ان كل ما ندركه في المشهد الحضري ندركه بالمقارنة و التباين فقط , فالعنصر الذي لا يملك علاقة متباينة بالعناصر الاخرى يكون غير مرئي و أن غياب بعض الوسائل قد يكون ذا معنى [Pechoux, p.85].
لقد برزت البنيوية كمحاولة للحصول على تفسيرات جديدة , حيث تنظر الى النسيج على انه نظام من الاشارات التي يجب أن تدرس تزامنيا , و أن المعنى ليس عنصرا كامنا في الاشارة و لكنه وظيفي ينتج عن اختلاف الاشارة عن الاشارات الاخرى و يركز على الاهتمام بالتركييب الموضوعي للاشارات و التي تجعل النسيج معبرا . يخلص البحث هنا الى تعريف بنية البيئة الحضرية على انها : نتاج لمنظومة من العناصر المكونة لنسيج من الفضاءات المكملة لبعضها الاخر , و التي تستند اساسا على نظام الاتصال القائم بين الانطباعات التي يحملها المتلقي عن تلك العناصر والمعالم المشكّلة لذلك المكان و (الدلالات و المعاني) الكامنة في تلك الفضاءات و ملامحها المميزة التي تتضح من خلال التطابق الواضح بين (المفردات الفكرية للبنية) و (البنى المادية). عليه تعد البيئة الحضرية بنية اتصال سيميائية . و هذا ما يتطلب تحديد الخصائص المكانية للبنية السيميائية .

2-3- ماهية الانتماء المكاني

تعددت الدراسات و البحوث التي تناولت مفهوم الانتماء المكاني مما ولّد عدة مصطلحات للتعبير عن هذه الظاهرة ففي كتابه Psychology وضع (Mackeackie) ظاهرة الانتماء المكاني كترج ثالث بالنسبة لتسلسل الحاجات الانسانية من الاقوى الى الاضعف , بعد الحاجة النفسية الى الامان Safty و الحماية Protection مما يدل على أن الانسان لا يشعر بالانتماء الى المكان الا بعد شعوره بالحماية و الامان في المكان ذاته [Mackeackie, p.161]. ووفقا لآراء علماء النفس فقد عرّف البعض الانتماء على انه حاجة مكتسبة ذات دافع اجتماعي تنشأ اساسا من تفاعل الانسان مع بيئة معينة ذات تقاليد و معايير اجتماعية محددة و التي تسمح باحداث التعديل في نوع و شكل بعض الدوافع . وفي كتابه Road Form and Townspace ينظر (Moclusky) الى الانتماء المكاني كحاجة ذات مكونات فسيولوجية تتحرف وفقا لما هو

سائد اجتماعيا و ثقافيا وحضاريا [Moclusky, p.40]. و من الجدير بالذكر اشارة الادبيات السابقة الى ثلاثة مصطلحات تشير كل منها الى سمات خاصة مميزة للانتماء المكاني اعتمدت الاولى منها على مفهوم السلوكية Behaviorism, في حين اتخذت الثانية من مفهوم الظاهراتية Phenomenology أساسا لها, أما الثالثة فقد استندت على مفهوم البنيوية- التركيبية- Structuralism. و سيتم التركيز على الاخيرة لارتباطها المباشر بمحور البحث حيث نجد أن البنيوية جاءت استنادا الى فكرة مفادها أن مفهوم الانتماء المكاني يعتمد على أهمية النسق والنظام, وأهمية الكل ضمن هذا النظام و هذا ما يأتي كنتيجة لعلاقة الانسان مع المكان بوصفه جزءا من بنية ذلك المكان, ولا كيان له الا ضمن هذه البنية المترابطة. و كون الاحساس بالانتماء للبيئة الحضرية لا يمكن أن يكون بعزل الامكنة المكونة لها عن مقترناتها و ارتباطها المتمثلة بفكر وتجارب الاسلاف و عاداتهم و تقاليدهم وكل ما هو مثير للذكريات و الناتج عن الذاكرة الجمعية المتركمة بفعل تأثير المكان على شاغله, وهذا ما يعزى الى صلة المكان بمحيطه المجاور و المتمثلة بعلاقة (الكل والجزء). وكون البحث الحالي يعنى بمفهوم بنية البيئة الحضرية, سيسلط الجزء اللاحق منه الضوء على البنيوية بوصفها أساسا لتحقيق الاحساس بالانتماء المكاني للبيئة الحضرية من قبل شاغليها وذلك من خلال دراسة الانطباعات التي يحملها المتلقي عن تلك البيئة و المنعكسة عن (المعاني والدلالات) الكامنة فيها. و يتطلب ذلك الاخذ بنظر الاعتبار أهم خصائص البنية السيميائية - المكانية للبيئة الحضرية وكالاتي :-

- البنية السيميائية - الادراكية للبيئة الحضرية

يركز مفهوم الادراك اهتمامه على انواع التفكير الكامنة في ذهن الانسان, والتي تولد ردود الافعال و التصرفات لشخص ما تجاه البيئة الفيزيائية بما فيه تنظيمها الفضائي وتشير الدراسات الى ان سلوك الاشخاص يعتمد بشكل كبير على الصور التي يحملونها عن هيكل وهيئة البيئة الحضرية, فالطريقة التي يتم من خلالها هيكلية البيئة الحضرية في الازدهان, تؤثر في ادراك و تحسس الفرد و سهولة الاستدلال و ايجاد المسار ضمنها وصولا الى هدفه ضمن فضاءات البيئة الحضرية, و هذا ما يولد اعتقادا بوجود صلة قوية بين التكوين الحضري والمجتمع ووجود بيئة معينة يمكن ان يكون نتيجة لتعاقب تجسيد تصورات و قيم معينة يحملها المجتمع قد تكون أكثر أهمية من تأثير الاقتصاد و المناخ والقوى الاخرى, اذ يمتلك المكان حدودا نفسية و معنوية ترتبط بكيان الانسان و حضارته وتأثيرها يعود الى القوة التي يمتلكها ذلك المكان في تحقيق مواقع جذب و تذكّر مولدة مجموعة من المعاني Meanings و المفاهيم Themes تضيف للمكان قيما انسانية ويحاول من خلالها الانسان الحصول على الاستقرار مما يجعلها تلعب دورا اساسيا في تشكيل المحيط البيئي و السلوكي للانسان و تعريفه و تؤثر بشكل فعال في تشكيل الهيئة الحضرية [Rapoport, p.221]. وهذا ما يدعونا لتسليط الضوء على مفاهيم ادراك البيئة الحضرية عموما من خلال تقسيمها الى مفهومين وكالاتي :-

المفهوم الاول : وضع من قبل (Hillier&Hanson-1984) حيث اعتمد على فكرة العلاقة بين الخصائص الموضعية و الخصائص الشمولية للنظام الفضائي الذي يكون واضحا الى درجة أن اي عنصر فيزيائي يمكن رؤيته و موجود حول شخص ما يعطي دليلا لموقعه بالنسبة للنظام الفضائي الكلي, فمن خلال حركة الشخص و انتقاله ضمن المدينة, فأن كل ما يراه موضعيا هو دائما متغير, و كل ما يراه شموليا يكون غير متغير, و من خلال هذه الديناميكية, يستطيع الشخص ان يميز موقعه الشمولي من خلال المعلومات الموضعية الموجودة حوله, و هذا يحصل عندما تمتلك البيئة الحضرية بمجملها درجة عالية من التماسك و الوضوحية على المستوى الكلي لها [Ibid,p.13].

المفهوم الثاني : و الذي وضعه الباحث الرائد (Lynch) والذي ينص على أن اي بيئة تترك عند زائرها او شاغلها انطبعا خاصا تتداخل في تكوينه ملاحظات عديدة أو ذكريات معينة مما تعرضه البيئة من مشاهد و علاقات يختار منها ما يدركه و يتحسسه مشكلا ما يسمى بالخرائط الادراكية التي تختلف باختلاف الافراد و المجتمعات و طبيعة تحسسه للبيئة من حولهم [Lynch,p.7] . و لذا جرت عدة دراسات لتصنيف مكونات البنية الادراكية - المكانية و التي تم من خلالها تحديد عناصر البيئة التي تعطيها (معنى) و ما لذلك المعنى من تأثير في امكانية التصور Imageability , و قد استندت معظمها على دراسة (Lynch) , ففي كتابه *The Image of The City* اثبت أن المدينة أو أية بيئة حضرية تكون قادرة على توليد صور ذهنية قوية و متماسكة لدى المتلقي , اذا كان من الممكن فهمها بصيغة انماط شكلية Formal Patterns ذات استمرارية و حضور عالين مع وجود مجموعة من الاجزاء المتميزة عن بعضها و المتمفصلة بشكل واضح و مقروء . و توصل (Lynch) الى ان صورة المدينة City Image مبنية حول سلسلة من العناصر النمطية التي تعد مهمة لهيمنتها البصرية كتلميحات للتوجيه و بوصفها علامات Signs لخصائص اجتماعية او تاريخية او وظيفية للمدينة , و تبعا لهذه الدراسة تم تحديد خمسة اصناف من عناصر البناء الفيزيائي لهيكل المدينة و التي يستخدمها الناس عادة لبناء مخططاتهم الذهنية Mental Schemata عن المكان و هي : المسارات Paths و الحافات Edges و القطاعات Districts و العقد Nodes و المعالم Landmarks . وهنا يظهر دور الاتصال الذي يتضح جليا عبر وجود مستوى معين من التوافق ما بين (معاني الاشكال) و (المضامين التعبيرية) للبيئة الحضرية ضمن المستوى الادراكي , وهذا ما يولد بنية سيميائية ملموسة ما بين الانسان شاغل البيئة الحضرية و المكان المتمثل بالبيئة الحضرية نفسها تعمد من خلاله تلك البنية الى نقل المعاني الكامنة وراء تلك الفضاءات من خلال منظومة تعبيرية تمتاز بأمكانية ادراكها من قبل كل من الباعث (بيئة البيئة الحضرية) و المستلم (المتلقي المتمثل بشاغل البيئة) على حد سواء محفزا لديه الشعور بالانتماء لتلك البيئة نظرا لدقة تعبيريتها عن المعنى المكنون فيها .

- البنية - السيميائية - الفضائية - للبيئة الحضرية

اذ تتكون البيئة الحضرية بشكل اساسي من مجاميع من الكتل المتصلة و المترابط بعضها مع البعض الاخر , و يتخلل هذه المجاميع من الكتل هيكل مترابط من الفراغات و التي تعمل بشكل كفوء على خلق منظومة فضائية حضرية فعالة و حيوية يمكن تحسسه من خلال خصائصها التشكيلية مما يضيف على المكان نمطا معيناً من الترابطات بين الكتل الحضرية و الفضاءات الحضرية و يكسبها خصائصا وظيفية و فضائية متميزة [Rapoport,p.53] . و توافقا مع ما جاء و بالرجوع الى مفهوم (Rapoport) نجد ان البنية الفضائية للمكان تمثل القاعدة الاساس لتعريف المكان و اعطاء خصائصه و ابعاده الفضائية المختلفة , و تظهر من طريقة تجمع المكونات الفضائية لمختلف النظم الفضائية , و علاقتها مع بعضها البعض , ومعانيها التي تختلف من مكان لآخر مما يميز بيئة حضرية عن اخرى تبعا للعلاقة البصرية بين الاجزاء و بين الجزء و الكل في توقيع المكونات الحضرية على اختلاف مستويات التعريف و التفاعل بين قطبي تكوين الهيئة الحضرية الفضاء و الكتلة [Ibid,p.14-15] . يخلص البحث في هذا الجزء الى ان الفضاءات الخارجية تعمل كارتباطات links ضمن اجمالي البيئة الحضرية , و في الوقت نفسه تعمل كأماكن places لاحتواء الفعاليات الاجتماعية . كما تعد مورفولوجية البيئة الحضرية , بما فيها فضاءاتها الخارجية , عاملا اساسيا في تحسس الانسان و ادراكه و انتمائه لتلك البيئة , وهذا ما يولد تحفيزه لاستعمال فضاءاتها , اذ يكون الشكل العام للبيئة الحضرية نابعا من خصائص التنظيم الشمولي لهيكل فضاءاتها و ليس من التنظيم الفضائي الموضوعي , ويعزى ذلك

الى طبيعة البنية الفضائية السيميائية للهيكل الحضري و التي ترسل الى المتلقي بطبيعة تشكيلها مجموعة من المعاني و الدلالات تتميز بالتنوع المشهدي و التغيرات المستمرة و المتعددة في المحاور البصرية .

- البنية- السيميائية- السلوكية للبيئة الحضرية

أن تحديد العلاقة بين التنظيم الفضائي والسلوك الانساني يستوجب دراسة السلوك الفضائي الملموس كناتج نهائي للعمليات الاساسية التي تمت مناقشتها آنفا . و قد اختلفت الدراسات و التوجهات البحثية و التي اتخذت من العلاقة بين خصائص التنظيم الفضائي والسلوك البشري موضوعا لدراساتها باعتبار أن الاول هو متغير مستقل و أن الثاني يمثل متغيرا معتمدا , ومن أهم التوجهات التي تناولت الموضوع :

التوجه السلوكي : اذ يشير هذا التوجه الى أن سلوك الاشخاص دالة لدوافعهم من خلال الفرص المتاحة في البيئة الحضرية [Lang,p.97] . وتؤكد أن الدور الاساسي في تقييم الانماط السلوكية واكتسابها يكون من خلال التجربة .

التوجه الايثولوجي : وهو اتجاه نظري يفترض أن السلوك عند الانسان متواجد بشكل مماثل له عند الحيوانات الاخرى , وأن سلوك الانسان فطري يمكن تفويمه بفعل الحضارة , و أهم النظريات التي تمثل هذا الاتجاه هي فكرة محيطات السلوك التي تم ذكرها آنفا ونظرية التقارب والنظرية الحيزية .

التوجه الاجتماعي في كتابه *Against Enclosure* يشير (Hillier) الى اعتماد هذا التوجه على دراسة المفاهيم الاجتماعية للتوصل الى مبادئ تنظيم الفضاء و احتوائه للفاعليات الاجتماعية منها والسلوكية باتجاه عزل المجاميع الاجتماعية ضمن احتواءات موضعية وبتكرارها يتكون الهيكل الشمولي للنظام الفضائي [Hillier,p.63] . وأهم المبادئ التصميمية لهذا التوجه :

الاحتواء : اذ يعد الاحتواء من أهم المبادئ التصميمية اللازم اعتمادها في عملية تكوين العناصر الفضائية الموضعية و يمكن تعريفه عمرانيا من خلال استمرارية السطوح المحيطة به واجتماعيا من خلال العلاقات الخاصة بين المجاميع الفضائية . **التكرار :** وهو مبدأ تنظيمي لتكوين الهيكل الشمولي من خلال تكرار الاحتواءات الموضعية كفضاءات خاصة لتكوين الهيكل الشمولي . **التدرج :** وهو مبدأ لتنظيم الاحتواءات الموضعية اذ بتكرارها نحصل على احتواءات أكبر ذات تدرج هرمي من الخاص الى العام . كما أكد (Hillier) على أن الفشل في كيفية استخدام هذه المبادئ يقود و بدون ادنى شك الى فشل المخططات تشكيل البيئة الحضرية . يخلص البحث هنا الى أن : اهمية التوجه الاجتماعي في تصميم البيئة الحضرية تكمن في اعتبارها وسيلة للحفاظ على تماسك بنية البيئة الحضرية و منعها من التجزئة , و هذا ما يكسب فضاءاتها نوعا من الحيوية و كفاءة في مدى الاشغال و التي تعد من اهم السمات الواجب توفرها لتحقيق مبدأ الانتماء لتلك الفضاءات .

دور الفعل التصميمي للفضاءات الخارجية في تحقيق بنية الاتصال السيميائية للجامعة

- الفعل التصميمي للفضاءات الخارجية ضمن بنية البيئة الحضرية للجامعة

تتمثل المكونات الاساسية لبنية البيئة الحضرية بعنصرين أساسيين هما الكتلة Mass والفضاء Space . و يتداخل هذان العنصران مع بعضهما في تكوين البنية بالشكل الذي يجعل من الصعب الفصل بينهما و اعطاء اولوية لاحدهما . و يتمثل جوهر تصميم البيئة الحضرية في

طبيعة تنظيم العلاقة المتبادلة بين هذين العنصرين من جانب , و ارتباطهما بالانسان من جانب آخر. و تصبح البنية الشكلية للبيئة الحضرية حصيداً لتفاعل ادراك الانسان و فهمه للعلاقة الجدلية بين الكتلة والفضاء و امكانية تعبير هذه العلاقة عن الابعاد الوجودية للانسان و عن أفكاره و حضارة عصره من خلال الصفات المادية و المعنوية للبيئة الناتجة و العلاقة بين مكوناتها الاساسية. و يشير (Norberg-Schulz) الى أن الهوية المميزة للتكوين البيئي (البنية) تعتمد بشكل أساسي على طبيعة الشخصية الشكلية للنسيج الحضري و علاقته بمحيطه الوجودي Existential Environment [Schulz,p.78]. و يمكن أن تتكون هذه الشخصية بطرق و أنماط مختلفة تبعاً لاسلوب التنظيم المكاني للفضاءات و الكتل في اطار التكوين الحضري الشامل و اعتماداً على المبادئ الادراكية الاساسية (مثل الوحدة و الاستمرارية , الاستقرار و الاتجاهية , الاحتواء و الانفتاحية .. وغير ذلك) منتجة بذلك بنية مكانية Place Structures مادية مختلفة ذات طبيعة تجميعية Clustered أو خطية Linear أو حلقة احتوائية Ring Enclosure.

- تصنيف العناصر الاساسية لبيئة البنية الحضرية للجامعة

وفقاً لتصنيف الرائد (Lynch), فإن مكونات بنية البيئة المبنية تشتمل على العناصر الاساسية الخمسة و المتمثلة بـ (المسارات , المعالم , القطاعات , العقد و الحافات). أن التناسق الكلي لتلك العناصر هو الذي يحبك صورة مكثفة و حيوية , كما أن توافق عناصر البنية يتبع مبدأ (Von Meiss) في التماثل Articulation و التكامل Integration , فالتماثل يؤكد استقلالية العناصر في حين يحقق التكامل تداخل العناصر ضمن كل واحد [Von Meiss,p.80]. فعناصر البنية على الرغم من استقلاليتها و حضورها المتميز , لا تظهر منفصلة و إنما تترتب معاً بشكل بنية مكانية قابلة للتصور و الاستيعاب Imageable Structure . بناءً على ذلك فقد صنف (Dober) عناصر بنية البيئة الحضرية للجامعة كما يأتي : طرق و ممشي الجامعة , المعالم (الشواخص , البوابات و الفضاءات الرمزية للجامعة) , فضاءات الوصل (الفضاءات الرئيسية , الفضاءات الثانوية , الفضاءات الرطبة و الفضاءات الجافة) , نطاقات الجامعة و أخيراً حدود و محيط الجامعة. وقد أشار (Dober) الى أن (كل جامعة بمكوناتها و عناصرها تمثل مكاناً متميزاً).

لقد توصل البحث , في المحور الثاني , الى تعريف الانتماء المكاني بوصفه نتاجاً لاجمالي خصائص البنية السيميائية المكانية للبيئة الحضرية (الادراكية , الفضائية و السلوكية). و على ضوء ذلك ستخصص الفقرات الآتية لاستخلاص دور الفعل التصميمي للفضاءات الخارجية للبيئة الحضرية لـ (الجامعة) في تحقيق بنية الاتصال السيميائية المتكاملة , و ذلك من خلال :

- استخلاص دور الفعل التصميمي في تحقيق البنية السيميائية - الادراكية -
- استخلاص دور الفعل التصميمي في تحقيق البنية السيميائية - الفضائية -
- استخلاص دور الفعل التصميمي في تحقيق البنية السيميائية - السلوكية -

- دور الفعل التصميمي في تحقيق البنية السيميائية الادراكية

ان تحقيق بنية الاتصال السيميائية - الادراكية - للبيئة الحضرية (الجامعة) هو نتاج لدور الفعل التصميمي لمكوناتها و المتمثلة بـ (الطرق و الممشي , المعالم , فضاءات الوصل , النطاقات , الحدود و المحيط). من خلال التأكيد على الحضور الفيزيائي لهذه العناصر و توافقها و انسجامها مع بعضها ضمن بنية البيئة الحضرية , و كما يأتي :-

طرق ومماشي الجامعة

يعرّف (Dober) طرق الجامعة على أنها (مدخل مهم لتصميم فضاءاتها الخارجية). ويشير (Michael) في كتابه *Campus Master Plan* الى أن نظام الحركة داخل الجامعة يعد مسببا مهما في تشكيل المكونات المكملة لفضاءاتها الخارجية لما تحمله من تعبيرية عن الجمال، الوظيفة، الامان، الوضوح فضلا عن تعبيريتها الواضحة عن سبل ايجاد الطريق. الشكل (1). كما تعد طرق الجامعة من المكونات الاساسية في عملية هيكلية مخطط الجامعة الاساس، والتي يجب مراعاة سبل توزيعها لتكون خدمية، ولا يحذب تصميمها بنمط يبيدها بهيئة مهيمنة على بانوراما المشهد العام للبيئة الحضرية للجامعة. ويفترض تصميمها بمنتهى الدقة بما لا يتعارض و التسلسل البصري المبتغى من التصميم الاساس في حالة توفر هذه الشروط ستسهل عملية ادراك طرق الجامعة كعناصر ايجابية تخدم التصميم الكامل لفضاءات الجامعة الخارجية. أما الفعل التصميمي لمماشي الجامعة يفترض أن يحقق هدفين أساسيين: يتمثل الهدف الاول بتجربة تحسس المتلقي في استكشاف الحدث اثناء تجواله من مكان الى آخر ضمن ارجاء الجامعة المختلفة من حيث الوظيفة، الملائمة، الامان، الجمالية، فضلا عن مبدأ النهوض بتلقي ما هو مفاجئ. في حين يتمثل الهدف الثاني بأكتساب المماشي سمة لتكون اداة مباشرة للوصول، تحقيق خاصية الربط، الاستمرارية والعزلية في آن واحد، بعيدا عن التقاطع مع الطرق المخصصة للسيارات، الشكل (2).

معالم الجامعة

يمكن تصنيف المعالم الى نوعين: يتمثل النوع الاول بـ (المعالم العمودية). أما الثاني فيتمثل بـ (المعالم الافقية). تعد الشواخص العمودية Vertical Features من العناصر المهمة والتي تلعب دورا فعالا في تشكيل بنية البيئة الحضرية للجامعة و تقسم الى نوعين: يتمثل النوع الاول بـ (الابنية المركزية) Central Buildings و التي تصمم وفقا لنمط يحقق حضورا فيزياليا يتجسد بما يبعثه شكل المبنى المصمم من اشارات Signs يترجمها المتلقي وفقا لطبيعة الاشارة المرسله الى معاني نابغة من أساس الشكل المادي لذلك المبنى الشكل (3). أما النوع الثاني من الشواخص العمودية فيتمثل بـ (الشواخص النحتية) Sculptural Features والتي تلعب دورا مهما في اغناء الجانب التعبيري للبيئة الحضرية للجامعة وتعكس حضورا فنيا بين ارجاء فضاءاتها الخارجية، و يطلق عليها بـ (العناصر الطوبولوجية) Topological Elements، أي الهندسة اللاكمية و التي تتضمن اعمالا لمنحوتات فنية يتم تصميمها وتحديد مواقعها لتكون مرئية من مختلف ارجاء محيط الفضاءات الخارجية للجامعة مما يبيدها كجزء من مجموع الفضاءات، الشكل (4). و تعد البوابات الرئيسية من العناصر المهمة للتعبير عن سيميائية المؤسسات المختلفة، كما يعد تصميمها تعبيراً فيزيائياً واضحاً عن مبدئي الترحيب و التوديع فضلا عن اضافة سمة الوضوحية Imageability على اجمالي البيئة الحضرية للجامعة من خلال التعريف باتجاهية المحاور Axes المؤدية لاجزائها المختلفة الرئيسية منها و الثانوية (5). اضافة الى وظيفتها المتمثلة بربط الفضاءات ما بين المسارات داخل و خارج البيئة الحضرية للجامعة مع مجاورات موقعها الاساس، الشكل (6). فضلا عن ذلك تعرف بوابة الجامعة على أنها سبيل لتحقيق ظاهرة التتابع البصري Visual Progression لكل ما هو واقع أمام بوابة الجامعة من المسارات والابنية ووسيلة لسحب المتلقي (شغل البيئة الجامعية) وبشكل متسلسل عبر فضاءاتها الخارجية و ما يترتب على ذلك من امكانية لاستكشاف طبيعة الفضاءات اثناء التجول بين أركانها بناء على المعاني المكونة فيها و المتجسدة في اشكال فضاءاتها. اما المعالم الافقية فقد تمثلت بالفضاءات الرمزية للجامعة Campus Symbolic Spaces وتمثل الخلفية الاساسية للبيئة الثقافية المصممة فيها الجامعة كما تسهم بصورة ملحوظة في تفعيل الحياة الجامعية، كونها تهدف الى التذكير بتجارب الاسلاف في البيئة المبنية، الشكل (7).

فضاءات الوصل

وهي مشابهة للعقد Nodes التي صنفها (Lynch) , على أنها (الاماكن التي تحتوي على فعاليات معينة و تمثل نقاط الاصل و الغاية التي يتم التردد عليها بشكل منتظم ضمن البيئة الحضرية) [Lynch,p.83] . وتقسم فضاءات الوصل الرابطة بين بقية الفضاءات الخارجية للبيئة الحضرية للجامعة الى أربعة أنواع رئيسية هي : الفضاءات الرئيسية ، الشكل (8) . والفضاءات الثانوية ، الشكل (9) . والفضاءات الرطبة ، الشكل (10) . والفضاءات الجافة ، الشكل (11) .

نطاقات الجامعة

وهي مشابهة للقطاعات Districts التي صنفها (Lynch) , على أنها (مناطق تحتوي على المسارات و الكتل البنائية والعناصر الحضرية كافة) [Ibid,p.37] . وتعرف نطاقات الجامعة على أنها مواطن لاندماج و تفاعل كل من ابنية الجامعة وفقا للوظيفة المميزة لكل مبنى مع اجمالي الفضاءات الخارجية المحيطة بها , بما يجعل كل من الابنية و مجاوراتها من الفضاءات محتواة ضمن حدود معينة تطوقها و تعرف عائدتها Its Belonging (هويتها) . كما يتصل كل نطاق مع الاخر مشكلا سلسلة مترابطة من النطاقات التي تؤول بدورها الى النطاق الاعم بواسطة روابط رئيسية . والذي يمثل النطاق المركزي للبيئة الحضرية للجامعة حيث تقام الفعاليات المركزية ، الشكل (12) .

حدود و محيط الجامعة

وهي مشابهة للحافات Edges التي صنفها (Lynch) على أنها (عناصر خطية مستمرة أو متقطعة , و تمثل حدودا لاستمرارية الهيكل الحضري) [Ibid,p.35] . في حين يمكن تصنيفها في البيئة الحضرية للجامعة الى نوعين : يطلق على النوع الاول اسم (الحدود) ، الشكل (13) . أما النوع الثاني فيطلق عليه اسم (المحيط) ، الشكل (14) . نستخلص مما ذكر أعلاه أن تحقيق البنية السيميائية الادراكية للبيئة الحضرية للجامعة هو نتاج الفعل التصميمي لمكوناتها (الطرق و المماشي ، المعالم ، فضاءات الوصل ، النطاقات ، الحدود و المحيط) . ومن خلال آلية تصميمية تؤكد على الحضور الفيزيائي لهذه العناصر وتوافقها و انسجامها مع بعضها ضمن بنية البيئة الحضرية .

- دور الفعل التصميمي في تحقيق البنية السيميائية الفضائية

ان تحقيق بنية الاتصال السيميائية - الفضائية - للبيئة الحضرية للجامعة هو نتاج لدور الفعل التصميمي في خلق النظام داخل و خارج البنية الحضرية ، من خلال تحقيق (التنظيم الفضائي) و (الاحاطة الفضائية) . و كما يأتي :-

التنظيم الفضائي

يقصد بالمبدأ التنظيمي Organization Principle النظام الذي يؤسس علاقة متماسكة بين عناصر البنية . فكل عنصر يمتلك نوعا من الاستقلال , ولكنه في الوقت نفسه يكون جزءا من محيط أكبر يرتبط معه وفقا لمبدأ تنظيمي واضح . و عليه فإن البنية النظامية Ordered Structure هي تلك التي تتميز بوجود مبدأ تنظيمي أساسي , يملئ تنظيم أجزاء تكوينها البيئي ويمكن قراءته و استيعابه بسهولة . أما البنية غير النظامية Disordered Structure فهي البنية التي تكون علاقة الاجزاء مع بعضها عشوائية لا يحكمها مبدأ تنظيمي عام . كما يمكن ان

نشير الى المبدأ التنظيمي بأنه ذلك المبدأ الذي يضمن الانتظام المنطقي والشمولي بين العناصر المستقلة لمكان ما و الذي يمكن قراءة الكل من الاجزاء ، الشكل (15) .

الاحاطة الفضائية

يؤكد (Von Meiss) في كتابه *Elements of Architecture* على أن غياب حدود واضحة للمكان تمنعنا من تكوين صور مدركة للبيئة الحضرية المبنية ، و كلما تكون الاحاطة الفضائية معرفة الحدود تكون الصور الذهنية المنعكسة عنها أكثر ادراكا [Von Meiss, p.26] . بناء على ذلك تعد الاحاطة الفضائية عاملا فعالا في ادراك البنية الكلية ، الشكل (14) . كما أن أهميتها لا تقل عن أهمية التنظيم الفضائي ، فكلاهما يسهمان في توضيح البنية ذهنيا . فاذا كان التنظيم الفضائي يوطد النظام داخل البنية ، فإن الاحاطة الفضائية توطده من الخارج . عليه يخلص البحث في جزئه الحالي الى تعريف (البنية الفضائية للبيئة الحضرية للجامعة) على أنها : بنية سيميائية ناتجة عن الدورالاتصال السيميائي للفعل التصميمي لفضاءاتها الخارجية في تحقيق التنظيم الفضائي داخل و خارج بنيتها . من خلال التعبير وبصورة جلية عن شخصية البنية الفضائية للجامعة بالانتقال بفضاءاتها الخارجية من حالتها الوجودية كفكر الى وجود مادي يتمثل بهيئتها الفيزيائية المنعكسة عن ما يحتويه جوهرها من رموز.

- دور الفعل التصميمي في تحقيق البنية السيميائية السلوكية

والذي يتحقق من خلال خلق تجربة بصرية متميزة نتيجة تحسس و استيعاب الخصائص الفضائية و كالآتي :

- المقياس : ويقصد به تنظيم العلاقة بين حجم الفضاء و شكله مع حجم الانسان وتحدد على اساس قدرة المشاهد الاستيعابية و ادراكه للصورة الحضرية ، و هي من اساسيات تكوين الاحساس بالمكان . و المقياس " هو الانطباع الجمالي تجاه الحجم الفيزيائي لكل من الكتلة والفضاء " ، بناء على ذلك يتضمن المقياس وجود قوتين نسبيتين ، الاولى هي الهيئة الفيزيائية ، و التي ترتبط بالحجم ، و الثانية الهيئة الفلسفية و الحسية المتأتبة من تصور الانسان المسبق وما يحمله من دلالات خاصة بقياس الشيء . ووفقا لما تم طرحه فإن بنية البيئة الحضرية تتشكل عادة من سلسلة من الفضاءات الحضرية بما فيها الفضاءات الخارجية و التي يجب أن تشترك بنفس الخواص والمواد المقياس واللغة المعمارية ليكون مظهرها مألوفاً و يسهل ادراك معانيها من قبل المتلقي بما يحقق احساسه بالانتماء المكاني لتلك البيئة . و تتراوح مقاييس الفضاءات بين المقياس الانساني Human Scale و بين المقاييس النصبية Monumental Scales ، و يعبر المقياس عن البعد الانساني و يؤثر في تحسس الانسان ضمن هذا الفضاء وشعوره بالضيق أو الامان أو الطمأنينة ، والتواضع أو التسلط أو النفور و حسب الانتماء المكاني .

- التناسب : ويمثل العلاقة بين ابعاد الفضاء و العلاقة بين الجزء و الكل التي ينجم عنها معاني يفترض ان تصل الى الانسان و أن يتحسسها ، حيث يفترض أن تحقق مستويات الراحة البصرية والنفسية التي لا بد ان ترتبط بالقيم الجمالية للنسب المستعملة .

- الاحتواء : يعد الاحتواء مبدأ اساسي في تكوين العناصر الفضائية الحضرية الموضوعية Spatial Elements فالاحتواء من الناحية الفضائية يعني أن الفضاء المحدب يكون متميزا عن غيره بكونه محاطا بأسطح الابنية . و من الناحية الاجتماعية يعني ان هذه الابنية وشاغلها تتمتع بعلاقة خاصة مع ذلك الفضاء ، و هذه العلاقة تمنح شاغلي البيئة الحضرية هوية Identity مشتركة . وتعني درجة التحديد بالعناصر الفيزيائية للفضاء مع بعضها البعض والتي قد تكون حواجز فعلية تمنع الحركة و الاختراق بين الداخل والخارج أو قد لا تعد كونها

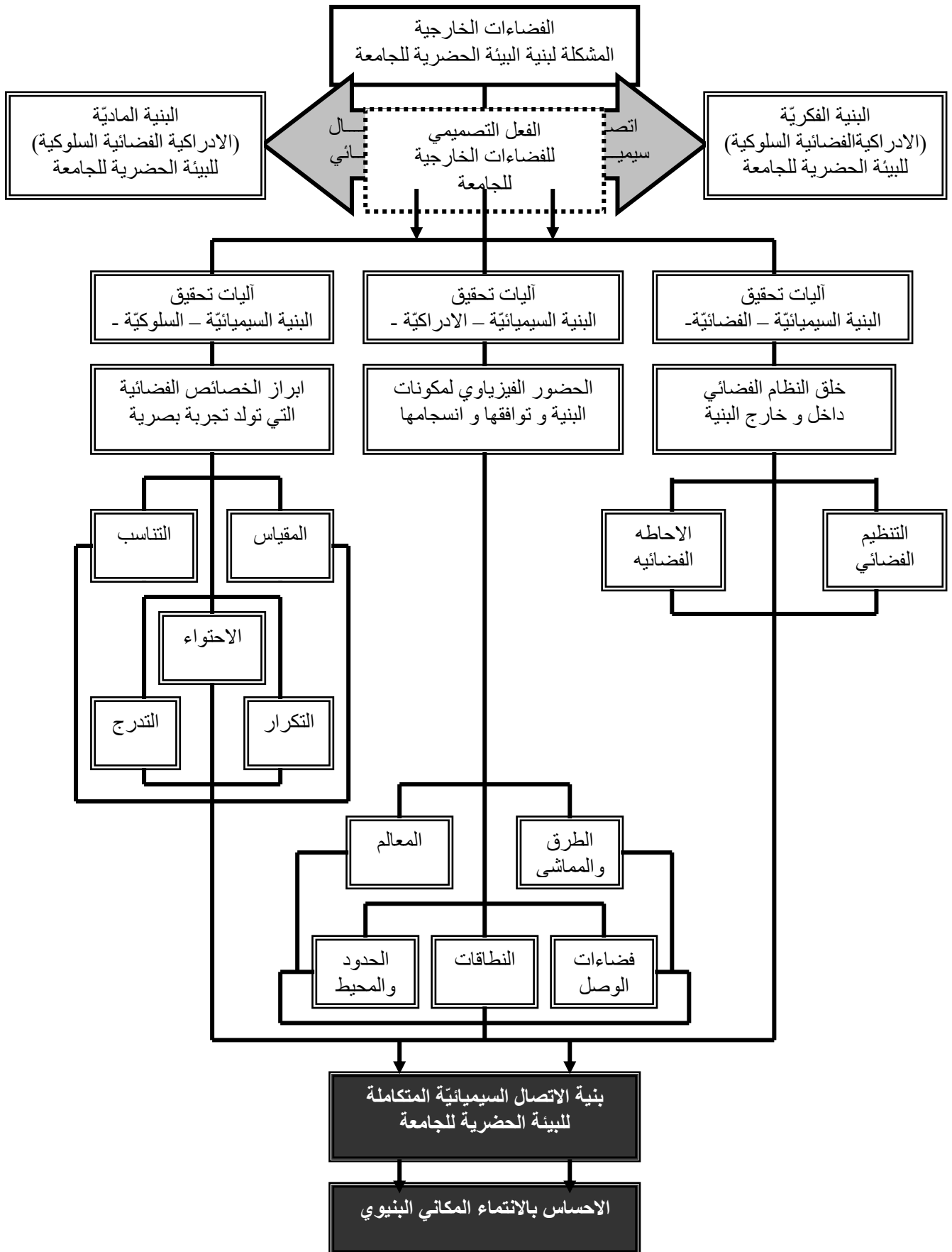
وسائل تحديد رمزية توفر تداخلا بصريا بين الداخل و الخارج , وتحدد الاغراض والخصائص الاجتماعية درجة الترابط الموجودة و المطلوبة عبر هذه الحواجز – اي درجة الانغلاقية - مما يتطلب توفير عزل و خصوصية معينة بين الداخل و الخارج أو درجة من الاجتماعية ولغرض الاختلاط بين شاغلي المكان . كما أن الفضاء المحاط و المحدد من قبل الابنية و بصورة نظامية يعد أحد مقومات تحقيق مفهوم الوحدة البصرية للمشهد الحضري والذي يميز هويتها Identification من خلال تنظيم خط السماء الذي يعطي تأثيرا قويا وكافيا لتحديد هيئة الفضاء , و بالتالي تحفيز الشعور بالانتماء المكاني لذلك الفضاء بالنسبة لمتلقيه .

- التكرار: وهو مبدأ تنظيمي لتكوين الهيكل الشمولي من خلال تكرار الاحتواءات الموضعية كفضاءات خاصة لتكوين الهيكل الشمولي . كما يمثل مفهوم التكرار المبدأ التنظيمي الذي يظهر فيه النظام الحضري الشمولي بوصفه نتاج لتجميع الاجزاء الموضعية و التي يغلب عليها طابع الهندسية Geometry في المخططات و التصاميم . اذ ان هذا المفهوم يتضمن دلالة المجتمع المجزأ ، و هو مجتمع يتألف من وحدات ثانوية منفصلة لكنها متماثلة و تماثلها في مجتمع اكبر يكون من خلال التمثيلات الرمزية اكثر من ان يكون من خلال التكامل الفضائي .

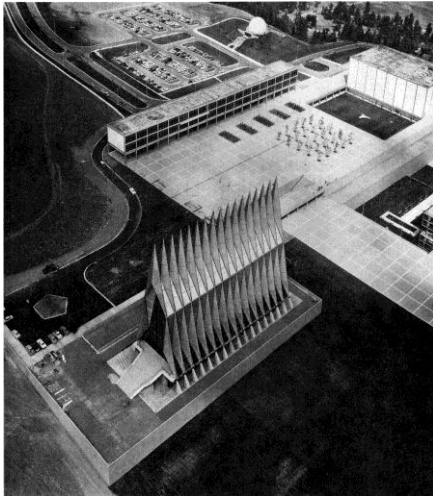
- التدرج: هو مبدأ لتجميع الوحدات الاجتماعية الموضعية في تدرج فضائي على المستوى الشمولي . و يؤكد على هيمنة الشكل الهندسي للفضاءات ، مما يخلق سطحا حضريا يمتلك وضوحا يمكن ادراكه عن بعد ، الا انه يؤثر و بشكل ملموس على الوضوح الفضائي من الموضعي الى الشمولي . كما يمثل التدرج مبدأ لتنظيم الاحتواءات الموضعية اذ بتكرارها نحصل على احتواءات أكبر ذات تدرج هرمي من الخاص الى العام .

و عليه فان البنية السلوكية للبيئة الحضرية للجامعة هي بنية سيميائية ناتجة عن الدور الاتصالي السيميائي للفعل التصميمي لفضاءاتها الخارجية في خلق نوع من الحوار بين (هينتها الحضرية) المنعكسة عن ما يحتويه جوهرها من رموز و (السلوك الفضائي لمتلقيها) , نظرا لاستدعاء ذاكرة المكان المتحققة من التجربة البصرية الناتجة عن استيعاب المتلقي للخصائص الفضائية الاساسية المتمثلة بـ (المقياس , التناسب , الاحتواء , التكرار و التدرج) . ومالها من دور فعال في نظرتة الشمولية لاجمالي الفضاءات الخارجية للجامعة و بالتالي احساسه بالانتماء اليها .

لقد توضح على ضوء الاطار النظري المطروح في البحث ان للفعل التصميمي للفضاءات الخارجية دورا اساسيا في تحقيق بنية الاتصال السيميائية المتكاملة للبيئة الحضرية للجامعة (والتي تحقق الاحساس بالانتماء المكاني) من خلال تفاعل و تزامن آليات الفعل التصميمي للمركبات الاساسية الثلاث للبيئة المكانية التي تتمثل بالبنية السيميائية الادراكية و البنية السيميائية الفضائية و البنية السيميائية السلوكية .



استخلاص الاطار النظري لدور الفعل التصميمي في تحقيق بنية الاتصال السيميائية للجامعة



الشكل (3)

United States Air Force Academy

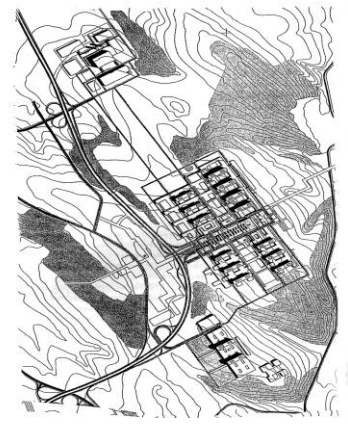
تصميم المبنى المركزي ليتخذ (مقياسا صرحيا) مميزا , يعلن عن هوية الجامعة عن بعد ليكون دليلا على موقعها نسبة الى مجاوراتها من المؤسسات



الشكل (2)

Rochester University

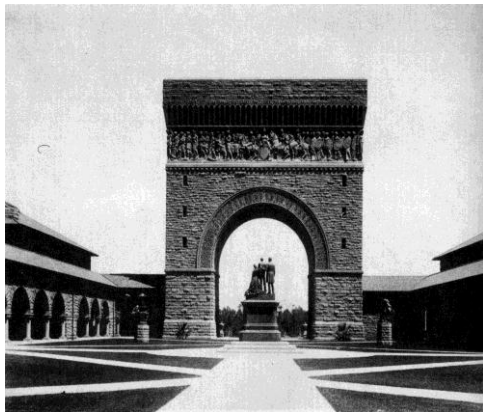
تصميم ممشي الجامعة الرئيسي ابتداءا من المدخل الرئيسي مما ساعد على تفعيل وظيفة الفضاءات الخارجية المجاورة له ، فضلا عن وظيفته الرئيسية المتمثلة بتقوية الهيكلة اللازمة لتعريف الحافات الداخلية و ضواحيها .



الشكل (1)

Bocum University

تصميم الهيكل الضخم للجامعة جاء ليتلائم مع سعة فضاءاتها الخارجية و متداخلا مع الحدائق و الغابات المجاورة لموقع الجامعة الأساس بما يجعلها متضامة و محكمة فضلا عن كونها كفوءة في اداء الوظيفة المبتغاة منها .



الشكل (5)

Stanford University

تصميم البوابة الرئيسية للجامعة يتسم بالفخامة والامكانيات التصميمية الجريئة مما يندبها كنصب سيميائي يستدعي الذاكرة للتأمل قليلا لاستخلاص معناها و الدلالات المتجسدة في شكلها الفيزيائي .

المصدر : (Safdie,1999)

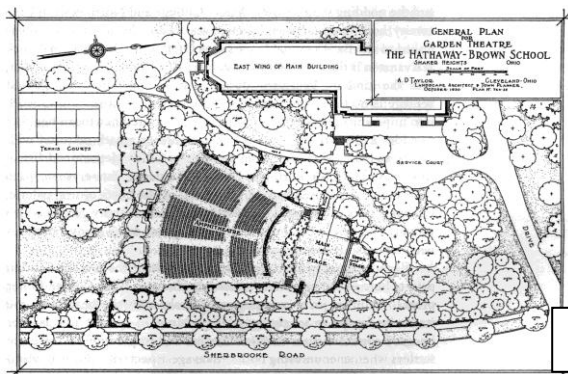


الشكل (4)

Ohio State University.

U. S. A

تصميم المنحوتات لتتخذ أشكال الارقام و بارتفاعات مختلفة بالقرب من مدخل الكلية المتخصصة بعلم الرياضيات اعتمادا على الفن المعاصر Contemporary Art مشكلا دلالة مميزة و ملفتة للانتباه مما يعزز البيئة الخارجية للجامعة من خلال الإشارة الى خصوصية اجزاءها (الكليات) ضمن نسجها الكلي (البيئة الحضرية للجامعة) .

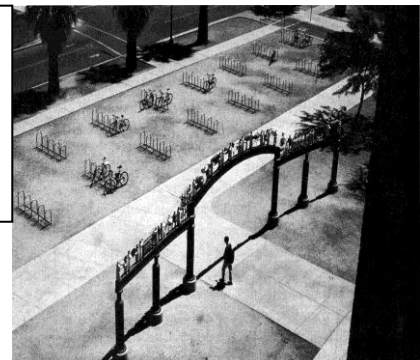


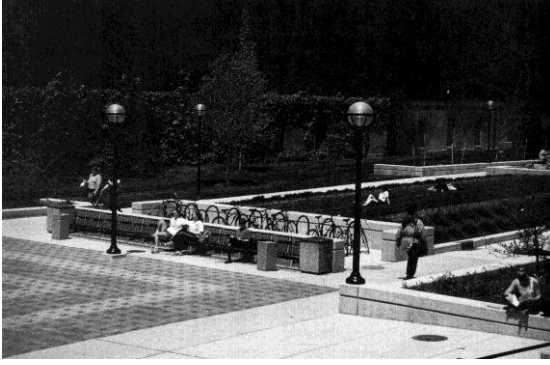
الشكل (6)

University of Arizona

يسمى هذا النوع من البوابات ب (البوابة الثانوية) كونها خاصة بكلية معينة و هنا تمثل بوابة لكلية الفنون , و تعد من المعالم ذات الدلالات على وضوح المكان و أحيانا تحمل تعبيرية نحوية مما يكسب تصميمها سمة النتائج الفني .

الشكل (7)





الشكل (9)

University of Michigan

تصميم الفضاءات الثانوية لتشكل نقاط للاستراحة و الجلوس و تكون وظيفية بحثة , و معزولة عن الابنية الاكاديمية و متداخلة مع الفضاءات الخارجية في آن واحد .



الشكل (8)

Claremont-McKenna College

تصميم الفضاءات الرئيسية للجامعة اعتمادا على اسس و أفكار تعبيرية محلية مما يمنحها معاني تعكس هوية البنية المصممة فيها الجامعة



الشكل (11)

College of Santa Fe

تصميم فضاءات الوصل بين المماشي بأضفاء سمة الجسادة عليها لتعمل بالضد من بعض مجاوراتها من الابنية التي قد تنسم بالشفافية



الشكل (10)

University of Miami, U.S.A.

تصميم فضاءات الوصل بين المماشي بأسلوب يضفي البهجة على اجمالي البنية الخارجية للجامعة من خلال توظيف عنصر الماء في العقد الرابطة بين المماشي المؤدية الى قطاعات الجامعة المختلفة .



الشكل (13)

Harvard University

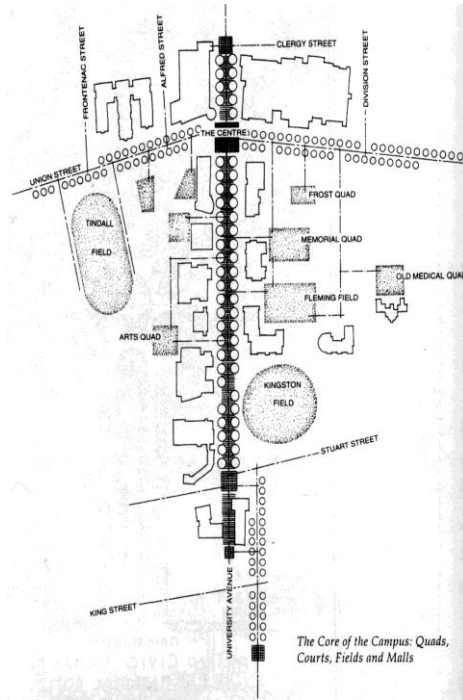
تصميم الاسيجة و الجدران بأسلوب مصمت لتعمل كمحدد لنطاقات الجامعة كل على حدة و اكسابها هيئة تعكس خصوصية النطاق الواحد الذي يعمل كجزء من الهيئة الاجمالية لحدود النطاقات المشكلة لاجمالي النسيج الحضري للجامعة .



الشكل (12)

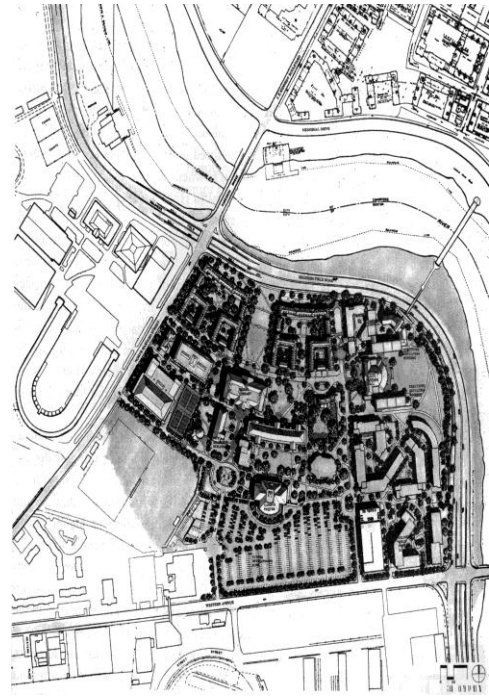
University of California

تصميم نطاقات الجامعة وفقا لنمط يعمل ضمنه النطاق الواحد كجزء من مجموع النطاقات المجاورة له و تؤول جميعها الى النطاق المركزي لبيئة الجامعة .



الشكل (15)

تصميم العلاقات الرابطة بين الفضاءات الخارجية للجامعة وفقا
لنمط تنظمي يلعب دورا مهما في اظهار البيئة الحضرية
كمجاميع متجانسة من الابنية و الفضاءات الخارجية المتلاحمة
ا ضمن محيطها الحصري



الشكل (14)

Harvard University

تصميم محيط البيئة الحضرية للجامعة جاء ليكمل فكرة تصميم
البيئة الخارجية لها من حيث التسلسل البصري بالانتقال من فضاء
الى آخر ضمن بيئة الجامعة وصولا الى محيطها و الذي يمتاز
بسمه ادراكه و تحسسه الفيزياوي من خارج موقعها و من داخله في
ان واحد .

الاستنتاجات و التوصيات

- الاستنتاجات

- ان للفعل التصميمي دورا اساسيا في تحقيق بنية الاتصال السيميائية المتكاملة للبيئة الحضرية للجامعة والتي تحقق الاحساس بالانتماء المكاني من خلال تحديد آليات مركباتها الاساسية الثلاث المتمثلة بالبنية السيميائية الادراكية والبنية السيميائية الفضائية والبنية السيميائية السلوكية .
- ان تحقيق بنية الاتصال السيميائية الادراكية للبيئة الحضرية للجامعة هو نتاج لدور الفعل التصميمي لمكوناتها (الطرق و المماشي- المعالم – الفضاءات الوصل – النطاقات – الحدود والمحيط) .
- وعليه فان آليات الفعل التصميمي لتحقيق بنية الاتصال السيميائية الادراكية تتحدد من خلال التأكيد على الحضور الفيزياوي لهذه المكونات وتوافقها وانسجامها مع بعضها ضمن بيئة البيئة الحضرية .
- ان تحقيق بنية الاتصال السيميائية الفضائية للبيئة الحضرية للجامعة هو نتاج لدور الفعل التصميمي في خلق النظام الفضائي داخل و خارج بنية البيئة .
- وعليه فان آليات الفعل التصميمي لتحقيق بنية الاتصال السيميائية الفضائية تتحدد من خلال تحقيق (التنظيم الفضائي) من جانب ، و الذي يهدف الى تنظيم العلاقات الرابطة بين

- الفضاءات الخارجية للبيئة الحضرية مما يحقق النظام الفضائي داخل بنيتها . و تحقيق (الاحاطة الفضائية) من جانب آخر والتي تهدف الى التنظيم الشمولي لاجمالي البيئة الحضرية و احتواء فضاءاتها و ابراز حدودها مما يحقق النظام الفضائي خارج بنيتها .
- ان تحقيق بنية الاتصال السيميائية السلوكية للبيئة الحضرية للجامعة هو نتاج لدور الفعل التصميمي في تحقيق شخصية بصرية متميزة تضيف على المتلقي ميزة ادراك بنيتها الاجمالية حسيا و ذهنيا و تحقق الاحساس بالانتماء للمكان.
- و عليه فان آليات الفعل التصميمي لتحقيق بنية الاتصال السيميائية السلوكية تتحدد من خلال ابراز اهم الخصائص الفضائية التي تؤثر في استيعاب المتلقي و نظرته للفضاء و تولد تجربة مميزة . و تتمثل هذه الخصائص بـ (المقياس ، التناسب، الاحتواء ، التكرار، التدرج البصري ... الخ) .
- ان تفاعل و تزامن آليات المركبات الاساسية الثلاث للبيئة المكانية (الادراكية والفضائية والسلوكية) يحقق بنية اتصال سيميائية للبيئة الحضرية للجامعة تخلق حوارا مستمرا مع متلقيها و تحقق احساسه بالانتماء المكاني اليها .

- التوصيات

- بعد أن توضحت فاعلية الاطار النظري المطروح في البحث في رصد دور الفعل التصميمي للفضاءات الخارجية في تحقيق بنية سيميائية متكاملة للبيئة الحضرية للجامعة ، والوصول الى آلية واضحة تجسد هذا الدور على الصعيد الادراكي والفضائي والسلوكي يوصي البحث بالآتي :
- على الصعيد التطبيقي : اعتماد الاطار النظري بوصفه وسيلة تحليلية يتم بموجبها تقييم سيميائية بنية البيئة الحضرية ، ووسيلة تصحيحية يتم من خلالها اعداد التصاميم الجديدة أو تقييم بدائل التصاميم البيئية غير المنفذة بهدف الوصول الى بيئة معمارية أكثر دلالة ومعنى تتحقق فيها الدرجات المطلوبة من التفاعل البيئي والمتعة الحسية .
- على الصعيد النظري : استثمار المفاهيم والنظريات المطروحة في حقول البنيوية والسيميائية لاغناء مجالات الفكر المعماري و الاهتمام بالدراسات الادراكية و البصرية التي تعد مصادرا ومراجعا اساسية مهمة في تخطيط و تصميم البيئات المبنية و صياغة فضاءاتها الحضرية لتحقيق مفهوم الاحساس بالانتماء المكاني اليها.

المصادر و المراجع العربية والاجنبية و شبكة المعلومات الدولية

- بارت , رولان (1986) , "درس السيميولوجيا" , ترجمة : بن عبد العال , عبد السلام , دار توبقال , المغرب
- خليل , خليل أحمد (1996) , "موسوعة لالاند الفلسفية" , منشورات عويدات – بيروت , باريس
- النوري , قيس (1988) , " بيئة الانسان من منظور الثقافة و المجتمع " , عمارة البحث العلمي , جامعة اليرموك , الاردن .
- هوكز, ترنس , (1986) , " البنيوية و علم الاشارة " , الطبعة الاولى , بغداد .

- Birks, T. (1972) "*Building the New Universities*", Copyright Note – Tony Birks & Michael Holford .
- Dober, P. (2000) "*Campus Landscape*", John Wiley & Sons Ltd., USA .
- Eco, J. (2000) "Symbols & Semiology", from :[http://www. Campus.com](http://www.Campus.com).
- Pecheux, M. (1981) "*Language , Semiotics and Idiology* ", London .
- Erskine, S. (2002), Comment : Education and Architecture, in Journal of "*The Architectural Review*", May, Volume ccix, No.1248, Printed in UK.
- Fides,S. ,Louis,A. ,Helen, M. (2003) "*The Impact of Facilities on Students Choice of University*", from : <http://www.shu.ac.uk>
- Franklin,C. ,Durkin,T. (2003) "*The Role of The Landscape in Creating Sustainable Campuses* " , from : <http://www.university business.com>
- Gaines, A. (1991) "*The Campus as a Work of Art*",Greenwood Publishing Group, Inc., USA.
- Hillier, B. & Hanson ,J. (1984) " *The Social Logic of Space* ", Cambridge University Press, Cambridge.
- Hillier, B. (1988) "*Against Enclosure*", in "Rehumanising Housing", London, ButterWorths
- Lang , John. (1987) " *Creating Architectural Theory_* ", Van Nostrand Reinhold , New York .
- Lynch, K. (1960) "*The Image of The City*", The MIT Press, Cambridge, Massachusettes
- Mackeachie, E . (1970) "*Psychology*", Six Edition, John Wisley & Sons, Publishing Company, Massachusetts.
- Meinig, R.(1993) "*Introduction to the Interpretation of Ordinary Landscape*", from : <http://www.university business.com>
- Moclusky, J. (1979) "*Road Form and Townspace*", The Architectural Press, London .
- Mumford, W. (. (2002), Comment : Education and Architecture, in Journal of "*The Architectural Review*", May, Volume ccix, No.1248, Printed in UK.
- Neuman, J. (2003) "*College and University Facilities*", John Wiley & Sons ll Inc., Canada.
- Newman, J. (1996) "*The Idea of a University*",Yale University Press,London .
- Norberg-Schulz , C. (1971) "*Existence ,Space and Architecture* ", Van Nostrand Reinhold Company, New York
- Pearce, M. (2001) "*University Builders,Great Britain*",John Wiley & Sons Ltd.,London .
- Pecheux, M. (1981) "*Language , Semiotics and Idiology* ", London .
- Prigogine, F. , Isabelle, A. (1995) "*Landscape Architecture*", from : <http://www.university culture.uk.com>
- Rapoport, A.(1977) "*Human Aspects of Urban Form*", John Wisley & Sons, New York
- Reuter, A. (1999) "*The Land Use*", from : <http://www.university culture.uk.com>.
- Schulez, R. (1974) "*Structuralism in Literature*", Yale University Press.

- Stanley, R. (1997) "*The Correspondance Orders of Campus Landscape*", from :
<http://www.campus hub.com>
- Stitt, A. (1999) "*Ecological Design Hand Book*", McGraw-Hill Publishing
 Co.,Institute of Architecture, University of San Francisco Press, U.S.A.
- Unesco, (1970) "*Planning The Development of Universities-I-*", International
 Institute for Educational Planning, Paris
- Unesco, (1976) "*Planning Buildings and Facilities for Higher Education*",
 Architectural Press Ltd., Paris.
- Unesco, (1982) "*Higher Education and the New International Order*", A;collection
 of Papers, Edited by Bikas C. Sanyal.
- University of York,(1972),"*University of York Development Plan*"
 England,(1962-1972) .
- Von Meiss, P. (1991) "*Elements of Architecture*" : *From Form to Place*", E
 &Fnspon, London, U.K.
- Woods, S. (1965) "*Free University:The Architecture of Universities_*", McGraw
 Hill, New York .
- .

التآزيرية في منشآت قوى الشد

انس حميد
جامعة بغداد - كلية الهندسة

عاطف السهيري
جامعة بغداد - كلية الهندسة

الخلاصة

يشهد العالم في هذه الحقبة من الزمن ظهور العديد من المفاهيم التي ساعدت بتطور التكنولوجيا وغيرها من العوامل على بروز أشكال متعددة من العمارة. تتصف الكثير من هذه الأشكال بصفات التكنولوجيا من كفاءة باستعمال مواد ملائمة لفعل الشد، معظم هذه الأشكال ذات منشآت قائمة على قوى الشد.

وعلى الرغم من أن منشآت هذه القوى لايزال يكتنفها التردد والشك، إلا أن بواورها بدأت تظهر واضحة في البلدان العربية والأقاليم المجاورة بعد تأثرها بمنجزات الدول المتقدمة تكنولوجياً والعمل على تطبيق بعض من تلك المنشآت في واقعهم المحلي، ولاسيما إذا ما توفرت العوامل التي تساهم في نشوء مثل هذه المنشآت على أراضيها وإستيعاب المفاهيم المرتبطة بمثل هذه القوى. وكانت حقول المعرفة العلمية بمجالاتها المختلفة قد كشفت الكثير من جوانب نواتج هذه القوى، إلا أن هناك بعض القصور في التغطية الكاملة لماهية هذه النواتج. ليقود ما سبق الى طرح مشكلة البحث بعدم وجود تصور نظري شامل للمبادئ والمفاهيم المرتبطة بهذا النوع من القوى نتيجة لضعف القاعدة المعرفية المعمارية المتعلقة بها والمتعاملة معها، وبالتالي عدم وضوح دور وأهمية هذه القوى في العمارة.

وعليه تم تناول الموضوع وفق منهج وصفي تحليلي من خلال طرح إحدى المفاهيم الأساسية ذات العلاقة بالبحث وهو مبدأ التآزيرية وإبراز دوره في مبادئ العلوم الحياتية بهدف إعطاء تصور حول موضوع التآزيرية لمنشآت قوى الشد ودوره في إبراز عمارة مواكبة لعجلة التطور والحدثة، على أساس علمي مفهوم قابل للإدراك من قبل جمهور المثقفين، وبوجود أسس معرفية للنظم المنشئية الموجودة تساعد في ملء الفجوات التخصصية. ويصل البحث في نهايته الى الإستنتاجات التي تلقى بعض الضوء على موضوع تآزيرية منشآت قوى الشد.

Tensegrity in Tensile Forces Structures

ABSTRACT

The world witnesses in this period of time the appearance of various structural concepts. Technology and other factors helped in the development of many architectural forms that carried technological character manifested through efficiency, lightness, most of these forms are tensile structures.

In spite of the fact that the use of tensile structures is still in doubt and suspicion, they started to appear in Arab countries and neighbouring regions, after they had been affected by the technological achievements of the technologically developed countries, and started to use such structures in their local buildings, especially if the factors needed to adapt such kind of structures are present on their lands, also the minds that can deal with such structures with special forces. The scientific fields had discovered a lot of in this field, but there is a gap in dealing with principles and concepts of this force and its products. This had formed our research problem.

So, the study depends on descriptive-analytical method in dealing with one of the basic concepts and thier biological bases which aim to give an imagination about tensile forces related to this subject -this is tensigrity concept- and its role in achieving architecture modern.

The research concluded many points that throw some light on the subject of tensigrity of tensile forces stryucture.

المقدمة

تظهر منشآت قوى الشد في الغالب بأشكال نحيفة قليلة السمك بأسلوب رشيق خفيف الوزن تبعاً لظروف القوى السارية ضمن عناصرها. تتوفر وبنفس مبدأ هذه القوى العديد من الأمثلة الحياتية بأشكال مختلفة وبسمات خفة مقاربة، لذا فسيتم التطرق لبعض هذه الأمثلة المتفاعلة مع هذه القوى وكيفية إنعكاسها على أشكالها من خلال مبدأ التأزيرية الذي يمثل النمط الذي ينتج عن قوى دفع وسحب لهما علاقة مترابطة مع بعضها البعض، تكون فيه قوى السحب مستمرة وقوى الدفع متقطعة وبصورة متوازنة لتنتج عنها نقاوة الشد والإنضغاط.

تعريف التأزيرية Tensegrity (1)

قبل التطرق لتعريف التأزيرية لابد من تعريف القوى بشكل عام على أنها حالة دفع أو سحب مؤدية الى تغيير حركة أو شكل جسم، حيث يمكن أن تظهر معايير تأثيرها على المنشأ من خلال مقدارها وإتجاهها وموقع تأثيرها على الجسم. تمثل القوى إحدى الحالات التي يمكن أن يتعرض لها المنشأ أو أي جزء من أجزائه وفقاً لطبيعة القوى وما تحمله من خواص وسمات تحاول أن تترك تأثيراتها على ذلك المنشأ وضمن ظواهر السكون والثبات والاستقرار والموازنة وغيرها من العوامل التي تعد عوامل حتمية للمنشأ الصحيح. (م/14 ؛ ص/28)

(1) جاء هذا المصطلح من علم synergy والذي يدل على معنى التأزر أو التعاون.

- إن سبل تعامل المنشأ مع القوى المسلطة تساعد المنشأ على الصمود بوجه مثل هذه القوى لغرض إزالة التخوف وتحقيق مبدأ الموازنة, ومن هذه السبل:-
- توزيع القوى والأحمال: حيث يفضل في أن يكون جزءاً واحداً من المنشأ هو المسؤول عن حمل جميع الأحمال المسلطة.
 - توجيه القوى والأحمال: ويفضل توجيهها على طول المركبات ذوات الزوايا.
 - إعطاء المنشأ شكلاً مناسباً: والذي يعمل على مقاومة قوى معينة كقوى الشد والمؤثرة في المنشأ.
- (م/4 ؛ ص/5)

تعريف قوى الشد

هي حالة من الإجهاد تكون فيها جزيئات المادة ذات قابلية لفعل السحب نحو خارج مركز الجسم أو العنصر. تمثل الإستطالة حالة مثالية لفعل الشد, إن مقدار وحدة إستطالة القابلو تدعى بـ "إنفعال الشد **tensile strain**" والذي يتناسب مع الحمل المحمول من قبل كل وحدة مساحة لمقطع العنصر. فالإستطالة هي التشويه المهم المصاحب لقوى الشد. فالقياسات الدقيقة والعامّة تبين بأنه كلما ازداد الحمل على عنصر ما خاضع لقوى الشد استطال ذلك العنصر مع إختزال لمساحة مقطعه. فالتغيير الحاصل لقطر العنصر يعرف بـ "نسبة **Poisson**" نسبةً الى الفيزيائي الفرنسي **Poisson** في بدايات القرن التاسع عشر, حيث تمثل النسبة ما بين التغير في قطر العنصر وإنفعاله الطولي **longitudinal strain**. (م/9 ؛ ص/82)

ليتبين هنا أهمية الإجهاد المسبق للعناصر تجاه القوى غير المرغوب بها, أي أن من خلال فعل الإجهاد المسبق يمكن تجنب الإزاحة الكبرى الممكن حصولها نتيجة عملية السحب. لذا فالتأزيرية هي النمط الذي ينتج عن قوى دفع وسحب لهما علاقة مترابطة مع بعضها البعض, حيث قوى السحب مستمرة وقوى الدفع متقطعة وبصورة متوازنة لتنتج عنها نقاوة الشد والإنضغاط. ان هذا النمط يعمل على إبداع نظام إستقرار ذاتي جاسئ. (م/12 ؛ ص/1)

قوى الشد تصاحب في الغالب عملية مط **stretch**, إستطالة **elongate** وأحياناً تمزيق **tear**; حيث تمثل هذه القوى حالة الفعل ورد الفعل في الوقت ذاته. قوى الشد تمتد وتسحب المادة من نهايتها بعيداً عن المركز, وتقاس متانة المادة لقوى الشد من خلال أعظم قوى شد يمكن للمادة تحملها ومقاومتها قبل بلوغ الفشل. (م/8 ؛ ص/11)

أما **قوى الإنضغاط** فتصاحب عملية تقصير **shorten** وتحطيم **crush** للمادة بعمليتي الكسر والعصر, حيث تمثل قوى الإنضغاط حالة الفعل ورد الفعل في ذات الوقت شأنها شأن قوى الشد. تقاس متانة قوى الإنضغاط من خلال أعظم قوى إنضغاط يمكن للمادة مقاومتها قبل فقدانها لشكلها وبالتالي

فشلها. وكما يصاحب تعبير حالة السحب **pull state** لقوى الشد يصاحب تعبير الدفع **push** والضغط **pressure** قوى الإنضغاط. (م/8 ؛ ص/14)

كان مبدأ التآزرية قد ظهر لأول مرة من خلال نحت فيزيائي للفنان **Kenneth Snelson** وهو أحد طلاب **R. Buckminster Fuller**⁽¹⁾. جاء هذا النحت تعبيراً تجريبياً للإنسان والذي كان قد دعاه بـ "قطعة س **X-piece**" في عام 1949، هذا النحت مكون من أسلاك ودعائم. أدرك **Fuller** بأن هذا النحت كان مثلاً لنمط قوي من التنظيم الموجود في الطبيعة.

توجد المتآزرات في جميع أنحاء الطبيعة بإنتظار مكتشفها. فعلى سبيل المثال يمثل إطار السيارة الهوائي احد تطبيقات مبدأ التآزرية والذي وجد قبل فترة طويلة من نحت **Snelson** ولكنه لم يعرف كنوع تآزري. (م/12 ؛ ص/2)

تتصرف قوانين قوى الرفع والدفع في هذه المنشآت والتراكيب بشكل مختلف عند تطبيقها ضمن النظام التآزري، حيث تجبر النشئت المتولد على تقوية المنشأ من خلال عناصر الشد المجهدة كأسلاك الشد في الخرسانة المسلحة مسبقة الاجهاد، يكون الغرض منها هو تقوية الأجزاء الضعيفة.

مبدأ التآزرية في الكيمياء الحياتية

تلعب الكيمياء الحياتية ولاسيما الخلوية دوراً مهماً في عالم الأنظمة الهيكلية الحياتية والتي يمكن الاستفادة منها في مجال عمارة الشد، فشعيرات الهيكل الخلوي **cytoskeletal filaments**⁽¹⁾ تعمل على توليد ومقاومة أحمال ميكانيكية وبالتالي تكون مسؤولة وبشكل كبير عن قدرة الخلية على مقاومة تشويه شكلها. تشغل هذه الشعيرات كمسارات حركة للأعضاء من خلال توجيه الإنزيمات لإنتاج ردود أفعال كيميائية حيوية تسهم في الوظائف الخلوية. (م/12 ؛ ص/6)

يمكن تمثيل الخلية على إنها غشاء مطاطي يحيط بالساييتوبلازم بصورة لزجة وذات مطاطية. وجهة النظر هذه للخلية هي محاولة بسيطة لفهم كيفية تنظيم القوى الميكانيكية سلوك خلية.

وعلى هذا الأساس، يمكن اعتبار الخلية ضمن الهيكل الخلوي عبارة عن إطار مشدود تآزري متكون من الدعامات الجزيئية ومن حبال وقابلات. وينطبق الأمر على الجزيئات المكونة من الخلايا التي تمثل تراكيب مترتبة بصورة معقدة لتكون النتيجة أنظمة ضمن أنظمة (كما هو الحال في الخلايا والجزيئات والأنسجة والأعضاء). (م/6 ؛ ص/1)

فعلى سبيل المثال، يتم التحكم بالتركيب الهندسي للأعصاب في الدماغ وكذلك شبكية العين بواسطة قوى النسيج الداخلية، هذه القوى كانت قد تولدت ضمن الهيكل الخلوي للخلايا المؤسسة لها.

(1) معماري ألماني من مواليد 1895 تلقى تعليمه في **Milton Academy**، تأثر بنظرية أنشتاين النسبية وأنعكس ذلك على العمارة بصورة واضحة. اعتمد على الرياضيات والهندسة المجسمة لشرح منشأ نواة الخلية. كان له إهتمامات بالبحر والسفن السارية فيه أشكالاً ومنشآت كما تأثر بجماليات الماكينة وأنعكست على أعماله التي امتازت بصفة الجيوديسية كمشروع **Marine Corps Dome 1954**.

(1) الهيكل الخلوي هو الهيكل المسؤول عن شكل الخلية وعادةً ما يتكون من شعيرات **filaments** ونبيبات **tublets** دقيقة.

وعليه، فإن وجود الاجهاد المسبق الموجود في كلّ عنصر أو نسيج يعمل على تصليب (إعطائه الصلابة المناسبة) عناصر الشد الداخلية التي ستقاوم الضغط المتولد في الخلايا الملتصقة لتعمل على تثبيت شكل الخلية.

تعمل الآلية التآزرية الخلوية كالآتي:- (على المستوى الجزيئي، يتكون الهيكل الخلوي من تركيب تآزري يقبع تحت غشاء. هذا التركيب مكون من شبكة منفصلة من جزيئات بروتينية⁽²⁾). هذه الشبكة تكون في العادة مسبقة الاجهاد نتيجة للصفة التنافذية لأغشية هذه الشبكة والتي تكون منتظمة بصورة شبكة جيوديسية).

يمكن أن تتصرّف هذه المنشآت التآزرية للخلايا بشكل مستقر، وعند تزواجها مع بعضها تعمل كنظام تآزري واحد متكامل مكونة الجزيئات. (م/6 ؛ ص/13)

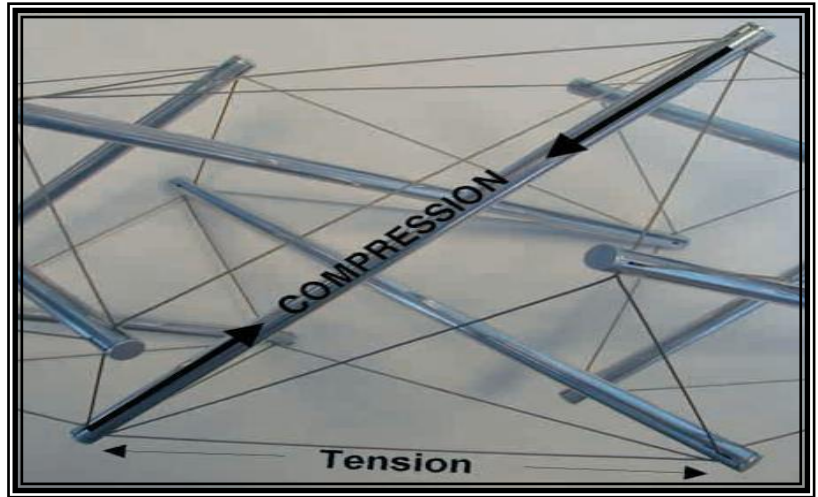
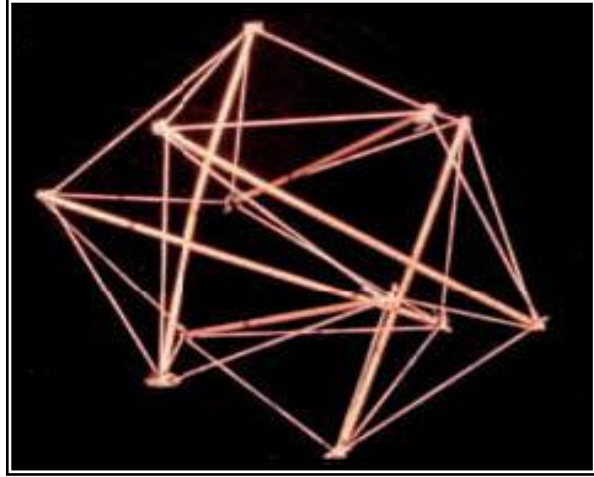
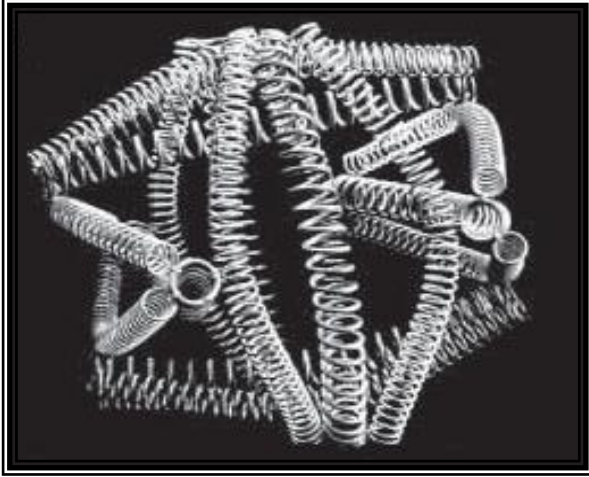
التآزرية الخلوية هي مبدأ يتكون من أنظمة تركيبية تحافظ على أشكالها بالشد المستمر لا بالضغط المستمر. فنحت Snelson طبق الى نموذج أكبر متكوّن من قضبان فولاذية معزولة مقاومة للصدأ ومعلّقة في الهواء بقابلوات شد عالية، [الشكل: 1] مثال سلس وواضح و يرمز الى البساطة المميزة التي أدت إلى وصف هندسة هذا النحت كشبكة مشدودة للعناصر الهيكلية المقاومة لتشويه الشكل والثبات الذاتي من خلال دمج عناصر الدعم والأسناد التي تكون مقاومة للانضغاط.



يصوّر النحت المماثل لهذا المنشأ والمتكون من اوتاد خشبية وخيوط مطاطية [الشكل: 2] توازن القوى المستندة على الضغط الموقعي المتقطع والشد المستمر والمسؤول عن إستقرار الشكل. وفيه تم استبدال العناصر الصلدة غير الضرورية بنوابض مرنة تختلف في مطاطيتها [الشكل: 3]. [الشكل: 4] يبين توازن القوى المستندة على الضغط المتقطع والشد المستمر. تطبيقاً لمقولة Fuller حول تعريف التآزرية "تتضمن التآزرية صنفين منشئيين هما الاجهاد المسبق والجيوديسية، والذان يفشلان في

⁽²⁾ مكونات الجزيئات البروتينية spectrin , ankryin , actin والتي تتواجد بشكل شبكة ضمن الهيكل الخلوي.

حالة تصرفهما ككيان واحد مستقل عن الآخر عند خضوعهما لقوى الشد بصورة ميكانيكية بدون إرسال مستمر من قوى الشد، وذلك من خلال عناصرها الهيكلية المقسمة على شكل مثلثات **geodesics** لإعاقه الحركة بشكل هندسي". (م/7 ؛ ص/2)



يمثل نحت Snelson تركيب - منشأ - الخلية، فنحته المتكوّن من الدعائم المعدنية الكبيرة والحبال المطاطية مماثل لما تحتويه نواة الخلية من الأعواد والخيوط المطاطية. فخلال هذا التماثل الخلوي، تمثل الدعائم الكبيرة النبيبات المجهرية؛ وتقابل الحبال المطاطية الشعيرات المجهرية التي تحمل قوى الشد في الهيكل الخلوي. (م/6 ؛ ص/2)

مبدأ التآزرية في العلوم الحياتية وتطبيقها في العمارة

واحدة من الجدالات التي تحوم حول مسألة كون الهيكل الخلوي مثل شبكة العضلات والأوتار والعضل والأربطة ولكن دون عظام، لذا فأين ستكون عناصر الضغط؟ كثيرة هي التفسيرات والشروحات ولكن أبسطها هي ما تكون مرتبطة بمثال شبكة العنكبوت التي يتعذر علينا وصفها دون الإعتبار لفروع الشجرة المرتبطة بها وخلالها. (م/6 ؛ ص/7)

إن مبدأ التآزرية في الكيمياء الحياتية الخلوية يمكن تطبيقه عملياً في العمارة. فعلى سبيل المثال يكون غشاء السطح للخيمة مستقراً من خلال وضعه تحت الشد، حيث يمكن إنجاز هذا الأمر بوسائل مختلفة كدفع أعمدة الخيمة الى الاعلى عكس اتجاه غشاء السطح، أو سحب الغشاء عكس اتجاه أوتاد الخيمة الثابتة في الأرض مع ربط الغشاء إلى فرع الشجرة. تزود أعمدة الخيمة الداخلية والحبال الخارجية بوظائف حمل لأن كلاهما تقاوم القوى الداخلية الموجهة الى غشاء الخيمة. من خلال هذا التوازن للقوى التآزرية والذي يولد الشد مسبق الاجهاد يتولد الشكل الثابت للخيمة. (م/6 ؛ ص/7)

الجهاز العضلي للإنسان وعلاقته بمبدأ قوى الشد

إن نفس مبادئ الإنشاء التي تحمل سمة الواقعية لمنشأ الأبنية يمكن أن تطبق على جسم الإنسان لأن كلاهما يمثلان نظاماً منشئياً، فجسم الإنسان والتوزيع المنشئي يحدد من خلال الوزن وتركيب مواد الجسم. (م/14 ؛ ص/20)

عادةً ما تكون أجسامنا مزودة بمثال مألوف للمنشأ التآزري مسبق الإجهاد، فعظامنا تتصرف كدعائم مقاومة لفعل سحب العضلات والأوتار والأربطة التي تعمل على استقرار الشكل من خلال التصلب والمتغير عادة اعتماداً على الإجهاد المسبق للعضلات. (م/6 ؛ ص/8)

سيتم مناقشة الجهاز العضلي للإنسان وفقاً لمبدأ قوى الشد اعتماداً على مرتكزين:-

* **المرتکز الأول:** دراسة مكونات الجهاز العضلي لغرض معرفة آلية عملها عند خضوعها لفعل الشد.

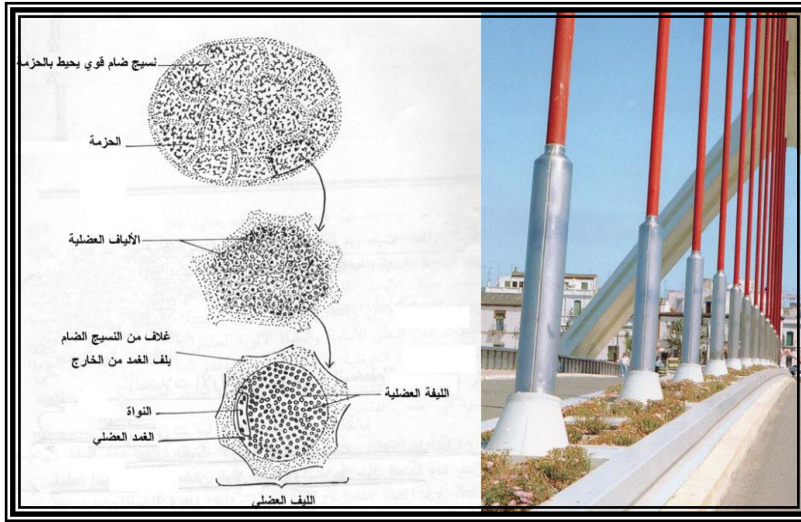
* **المرتکز الثاني:** دراسة أشكال بعض مكونات الجهاز العضلي من أوتار وعضل لغرض المقارنة مع أشكال لمنشآت قوى الشد والإستفادة منها لإشتقاق أشكال جديدة.

تركيب العضلة⁽¹⁾

إن الوحدة البنائية للعضلة هي الليف العضلي، فهي خلية واحدة متعددة النوى تكون بصورة طولية ممتدة على طول العضلة المرتكزة على نقطتين أو أكثر من الهيكل العظمي الذي يمثل المساند والدعائم الصلبة الحاملة للأغشية والتي تنقل أحمالها الى الأرض. (م/2 ؛ ص/215)

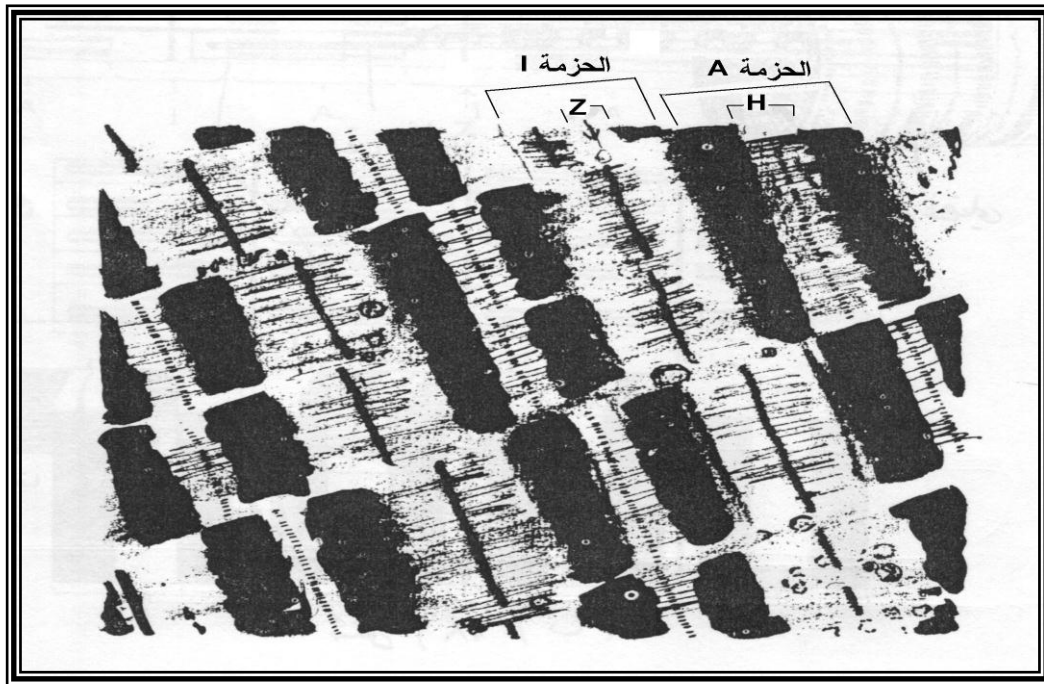
(1) يوجد في الجسم ثلاث أنواع من العضلات تختلف من ناحية الشكل و التركيب: 1. العضلات الإرادية (والتي تكون مسؤولة عن حركة و انتصاب الجسم معتمدة على شد العضلات). 2. العضلات اللاإرادية. 3. العضلات القلبية.

يحيط بالليف العضلي غلاف يسمى "الغمد العضلي **sarcolemma**" والذي يكون بشكل انبوب يسهل عملية التقلص والانبساط للليف العضلي بداخله. هذا التركيب مماثل للغلاف المحيط بالنوابض المرنة تحت فعل الشد والذي يعمل على الحفاظ عليها من الظروف الخارجية مع سهولة في الصيانة والإدانة، حيث أن واحدة من المآخذ والنقاط السلبية لمنشآت قوى الشد هي عمليات الصيانة الصعبة للقابلات والنوابض وغيرها من عناصر الشد. يشابه الليف العضلي النوابض المعدنية المرنة والمغلقة بغطاء حماية [الشكل: 5]. (م/2 ؛ ص/215)



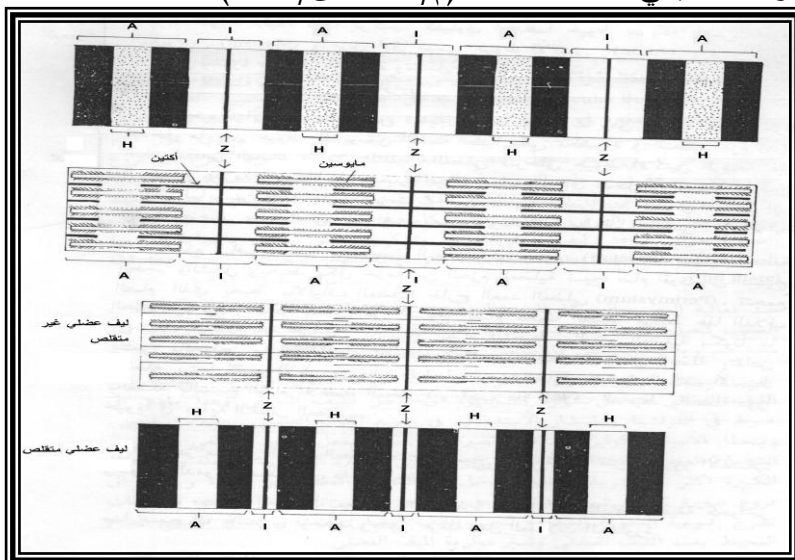
يكون هيولي الخلية العضلية cytoplasm على شكل خيوط طويلة رفيعة رقيقة كل خيط يسمى بـ "الليف العضلية **myofibril**". تقطع اللييف العضلي على امتداده حزم مستعرضة غامقة اللون تتناوب بانتظام مع حزم فاتحة اللون أوسع من الحزم الغامقة. يطلق على الحزم الغامقة (**حزم A**) والحزم الفاتحة (**حزم I**). تقطع حزم **A** بخط رفيع شاحب يسمى (**حزمة H**) وحزم **I** تقطع بخط غامق يسمى (**حزمة Z**).

لقد أظهر المجهر الإلكتروني أن اللييف العضلي منظم بشكل خيوط طويلة دقيقة أحدهما خيوط سمكية تسمى "خيوط المايوسين **myosin**" وأخرى خيوط أدق تسمى "خيوط الأكتين **actin**" [الشكل: 6], وتقسّم خيوط الأكتين بصورة عرضية بحزم **Z** لتشكل المنطقة المحصورة بين حزمتي **Z** الوحدة التقلصية والإنبساطية للعضلة والمسماة بـ "الساركومير **sarcomere**". (م/2 ؛ ص/220)



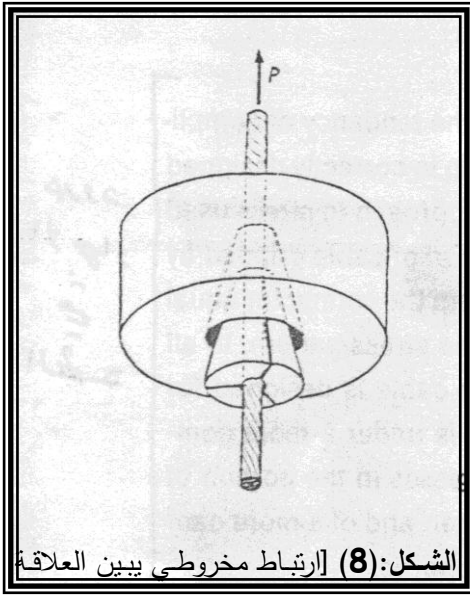
آلية عمل العضلة

تتصل خيوط الأكتين من نهاية واحدة بحزمة Z ومن النهاية الأخرى تكون حرة لتدخل بين خيوط المايوسين الثابتة نسبياً والمحصورة في منطقة حزم A أثناء عملية التقلص العضلي. حيث تتحرك خيوط الأكتين الرفيعة غير المرتبطة بحزمة Z وتتداخل ما بين خيوط المايوسين لتدخل في الفسحة، لتقترب بذلك حزمنا Z من بعضهما عند التقلص العضلي وتبتعد عند الإنبساط العضلي. أي تقلص حزم I لتبقى حزم A غير متغيرة ومحفوظة بطولها الطبيعي [الشكل: 7]. (م/2 ؛ ص/220)



الأوتار tendon

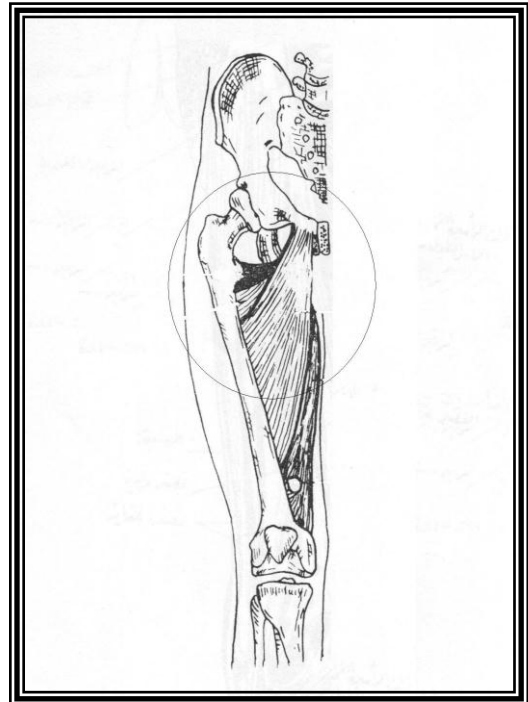
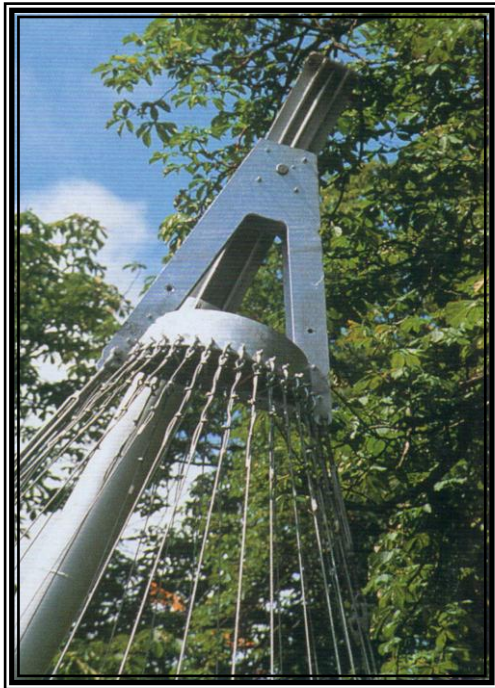
يتكون الوتر من مجموعة حزم ذات خلايا نجمية كثيفة صلبة وقوية جداً وأكثر قوة من الألياف العضلية. الوتر أملس ذو لون أبيض لفة الأوعية الدموية فيه لحاجته القليلة إلى الغذاء. تقدر قوة الوتر بتحمل قطر السنتمتر الواحد منه وزن يتراوح ما بين 600-1000 كغم ذو مقاومة للتمدد وقابلية للانحناء لتغيير الاتجاه نحو المغرز (نقطة الارتباط بالعظم) ليستطيع تغيير اتجاه سحب العضلة مع صلابته لمقاومة الاحتكاك لذا يحل محل الألياف العضلية في المناطق المعرضة للإحتكاك من خلال اتصالاتها بالعظام. (م/2 ؛ ص/222)



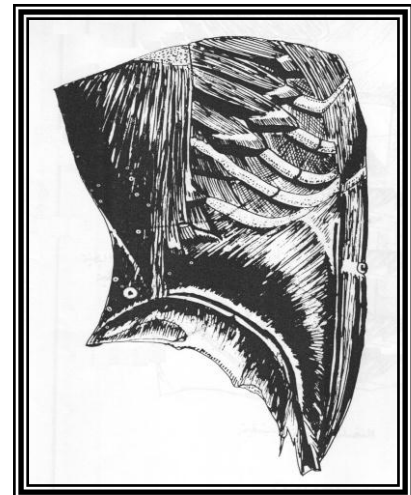
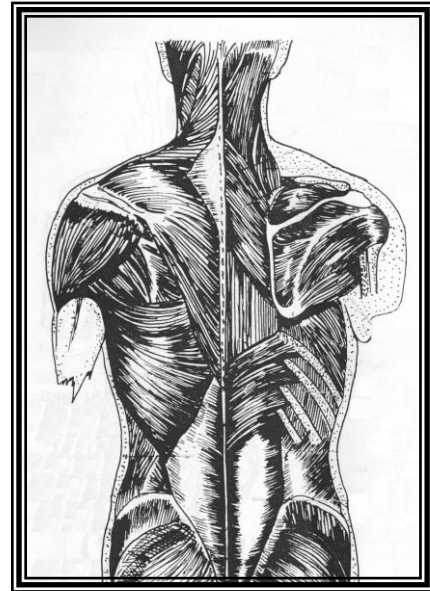
ما بين عناصر الشد وعناصر الضغط السائدة

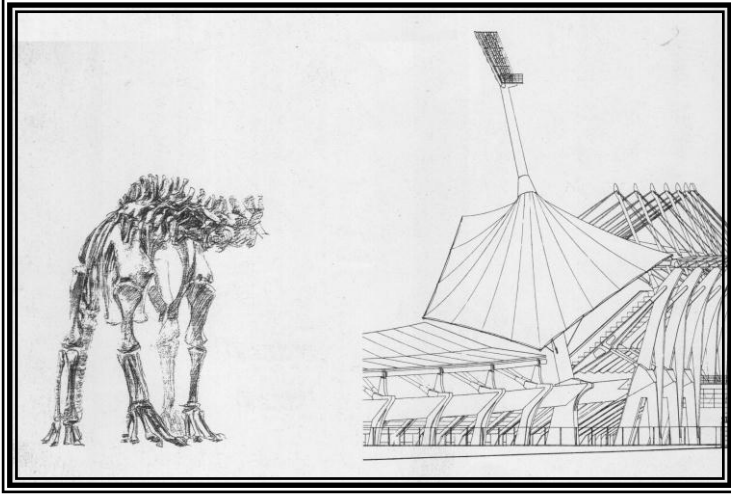
لها. (م/9 ؛ ص/219)

مثلاً تلعب الأوتار دوراً مهماً بين كل من العظم والعضل وطريقة ارتباطهما معاً من خلاله، يمكنه لعب نفس الدور في المنشآت الغشائية وغيرها من منشآت الشد. حيث يمكنها أن تكون حلقة الوصل بين الدعائم والركائز (وبغيرها من عناصر الضغط المماثلة في عملها لعمل العظام) وبين الأغشية والسطوح المقوسة وأغلفة الخيم والأشكال المشرومية (وبغيرها من عناصر الشد المماثلة في عملها لعمل العضلات). [الشكل: 8] - [الشكل: 15]



الشكل: (9) [ارتباط عضلي مع العظم عن طريق الأوتار في عظم الفخذ (م/2 ؛ ص/355)، وتطبيق هذا الارتباط الحيوي بنفس المبدأ في منشآت قوى الشد كما في الشكل: (10). حيث يمكنها أن تكون حلقة الوصل بين عناصر الضغط المماثلة في عملها لعمل العظام وبين عناصر الشد المماثلة في عملها لعمل العضلات]. (م/11 ؛ ص/81)

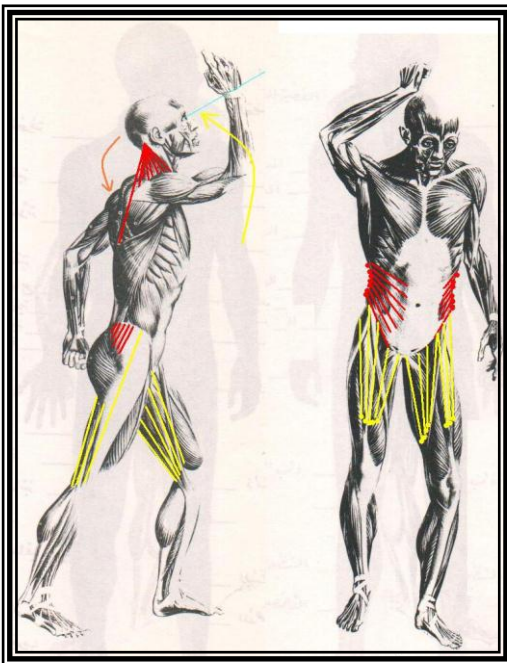




آلية الوقوف في جسم الإنسان

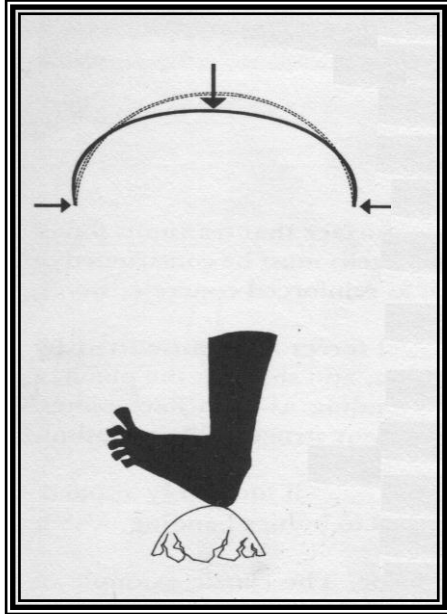
أن نظام الدعم والإسناد في الإنسان يمثل واحداً من الأشكال العليا في الحياة والذي من خلاله يمكن فحص واختبار فصاحة الأشكال النحتية ونقاوتها. نظام الدعم هذا هو نظام مشدود مدعم بتكوين عضلي يشابك العمود الفقري والصدر ممثلاً نظام دعم مشدود. فلوح الكتف -على سبيل المثال- لا يضغط على الصدر وعظم الترقوة تعمل كدعامة ضغط وغيرها من الأمثلة التي تعد صوراً واقعية لمبدأ التآزرية. (م/12 ؛ ص/11)

في حالة الوقوف على الطرفين السفليين يستند الجسم ويتوازن على قاعدة صغيرة نسبياً هي أخمص القدمين، فهذه القاعدة الصغيرة لا تتناسب من حيث أبعادها مع أبعاد الجسم طويلاً وعرضياً ولكن آلية التوازن تتم من خلال فعل العضلات مع عوامل أخرى. (م/2 ؛ ص/482)



فالرأس يتوازن على الفقرات العنقية مع حاجته إلى شد بسيط بالعضلات لبقاءه متوازناً في موضعه والعينين في اتجاه أمامي. عضلات الرقبة والظهر الخلفية تكون على شكل شبكة من الحزم العضلية التي تعمل على إسناد وتوازن الرأس على العمود الفقري مع قيام بعض العضلات المتخصصة بربط الفقرات وإسناد وموازنة العمود الفقري على الحوض. يسند الحوض من الأمام بعضلات البطن الأمامية من الأعلى وعضلات الفخذ الأمامية من الأسفل، ويسند الحوض من الخلف عضلات الفخذ الخلفية مع عضلات أخرى، إضافة إلى وجود عضلات أولية وسطى من جانب الحوض تمنعه من التمايل إلى الجانب. [الشكل:

قشرة البيض وعلاقتها بمبدأ التآزرية



تعد قشرة البيضة المثال الأكثر وضوحاً للمنشآت القشرية shells. يمكن تعريفها بأنها غلاف رقيق غير سميك مع سطح مقوس يعمل على نقل وأرسال القوى على طول تقوسها إنتهاءً بالدعائم. غالباً ما تشيّد المنشآت القشرية من مواد قابلة للتقوس والإعوجاج كالخرسانة المسلحة والخشب والمواد المعدنية الفلزية وغيرها من المواد اللدائنية. (م/13 ؛ ص/67)

إن آلية نقل القوى في هذه القشرة بسيطة ومذهلة في ذات الوقت. فبسبب التقوس تنتقل القوى الداخلية من خلال الإجهادات المباشرة للشد والإنضغاط والقوى في مستوي سطح القشرة أكثر من الإنحناء كما في المستويات أو السطوح المستوية. [الشكل: 17]

إن أوائل التطبيقات العملية للقشريات من صنع الإنسان كانت القبة. ومن أجل إستيعاب القوى المتولدة في القبة يمكن الأستعانة بنصف قشرة بيضة، فإذا ما دفعت الى الأسفل من خلال قمته وبشكل تكون فيه موضوعة على سطح مستو، يمكن ملاحظة أن قوى الإنضغاط المسلطة ستصبح قوى شد عند حافات القشرة. وبالتالي سيؤدي ذلك الى زيادة في عرض قاعدتها المرتبطة بالسطح المستوي مع تمزقها بعيداً عن المركز. (م/14 ؛ ص/68)

في حالة إنشاء القبة فإن هذا التوضيح والشرح يمكن ترجمته وتطبيقه عملياً من خلال إستعمال حلقات شد عند عنق القشرة كوضع قابلوات حول الحافات السفلية من أجل إعادة إنفعال re-strain قوى الشد. إذا ما وضعت فتحة في قمة القبة، فإن حلقات ضغط ستكون ضرورية جداً. [الشكل: 18]

(م/2 ؛ ص/68)



مبدأ الكفاءة ضمن مبدأ التآزرية

يعد مبدأ الكفاءة واحداً من الأمور الواجب مراعاتها عند تصميم أي عمارة. حيث يرى بأن القوى المفترضة في تصميم المنشآت التي تسري في المبنى يجب إرسالها بصورة مباشرة وبشكل كفوء ومنطقي. في الفقرات التالية سيتم مناقشة بعض الصعوبات والأمور العالقة بهذا المفهوم. (م/5 ؛ ص/208)

المبادئ الأساسية للكفاءة المنشئية لمنشآت الشد المتآزرة

(1) إن واحدة من الخطوط العريضة العامة لمبدأ الكفاءة تبين بأن الأشكال المنشئية تفضل أن تكون مشابهة لتلك الأشكال الموجودة في الطبيعة والعمل على تحليلها ودراستها وإستنباط النظم منها، لا سيما نظم نقل أحمالها وأوزانها الى الأرض. يرى جمهور الدارسين في مجال تطور الطبيعة هو أن التطور كان ومازال يخص الأشكال التي تمتلك سمة التطور لإمتلاكها صفة الكفاءة لأجل البقاء. ومن أجل إنجاز بعض الأشكال المنشئية بدرجة مماثلة من الكفاءة يحبذ الإقتباس والإستلهام من بعض الأشكال الطبيعية. (م/5 ؛ ص/208)

فعلى سبيل المثال، يمكن ملاحظة هذا المبدأ بأبسط أشكاله بالمقارنة مع منشأ قصر العمل Labour في Turin للمهندس الإنشائي Nervi [الشكل: 19]، الشكل مقارب لأغصان الشجرة التي تعمل على جمع الأحمال وتوجيهها نحو الدعام كالجذع الذي يعمل عمل الأعمدة. ومن ثم تنتقل الأحمال بصورة طبيعية للأسفل باتجاه الجذور التي تعكس صورة الأسس [الشكل: 20].



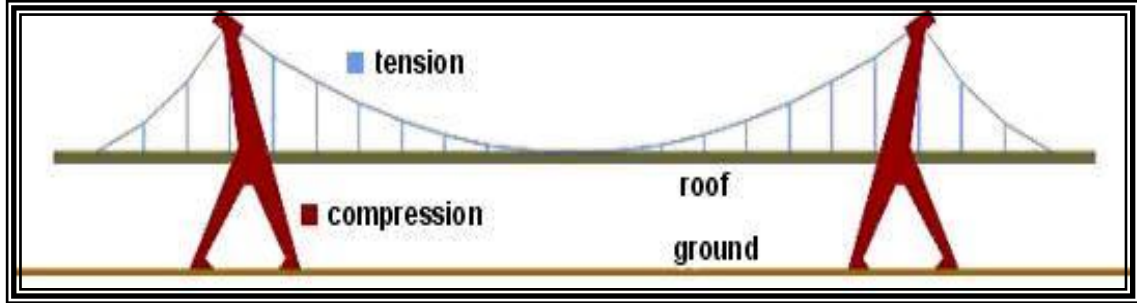


وبالنسبة لمبدأ قوى الشد ومبدأ الكفاءة، فإن صفة الطبيعة تمثل حلقة الوصل بين كلا المبدئين. يمكن ملاحظة ذلك من خلال ما تم شرحه -اعتماداً على الكفاءة المنشئية للأمتلة الطبيعية- في المحور الذي تناول النظام العضلي للأنسان والبيضة وغيرها من الأمتلة التي تكون فيها قوى الشد أساسية. (2) الأمر الآخر والمتعلق بمبدأ الكفاءة هو تدرج كفاءة المنشأ تبعاً للقوى الأساسية التي يعتمد عليها المنشأ. ففي المنشآت أو العناصر المنشئية المعتمدة على فعل الإنحناء تكون جزيئات المادة القريبة من المحور المركزي المحايد تحت الإجهاد؛ في الواقع فإن جزيئات المادة في قمة وقعر العنصر معرضة بالكامل للإجهاد. (م/5؛ ص/209)

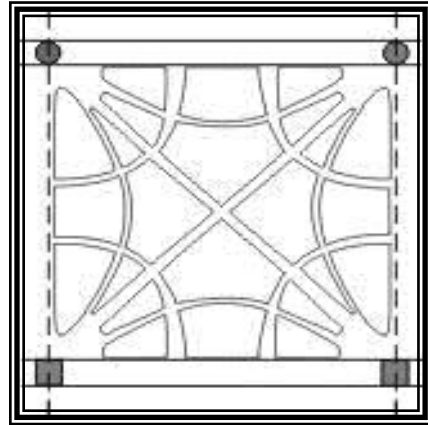
وفي منشآت الشد أو الضغط البسيط، فإن جميع جزيئات المادة في المقطع العرضي يجب أن تعمل بقدرتها الكاملة. عند عناصر الضغط تكون معرضة للانبعاج كعامل محدّد للمدى الذي يمكن للمادة بأن تستغل قبل الفشل. لذا فإن عناصر ومنشآت الشد هي أكثر الوسائل سهولة وكفاءة لنقل الأحمال، ثم يلي ذلك عناصر ومنشآت قوى الإنضغاط، لتأتي أخيراً منشآت الإنحناء.

بالنسبة للإعتبار للمهمة المعمارية، فإن منشآت قوى الشد لابد أن تضم عناصر شد مشدودة بعناصر مجاورة مغروسة في الأرض كالركائز والدعائم والرواسي أو معلقة بالقمم. إضافة الى ذلك، فإن ردود الأفعال المساهمة في ميل العناصر (الداعية للميل) في الكثير من العناصر المنشئية كالقبة (ردود أفعالها تسعى لزيادة عنقها الى الخارج) والقبولوات (ردود أفعالها تسعى لزيادة هطولها نحو الأرض) لابد من جعلها تقاوم تلك الردود للأفعال بواسطة حلقات شد أو إنضغاط بشكل روابط أو أسس ثقيلة. وعلى

النقيض من ذلك فمن السهل ضمان ردود الأفعال من جسر عمودي تماماً حيث يكون مقاوماً بسهولة أكثر في مستوى الأسس. (م/5 ؛ ص/210) [الشكل: 21]



شكل عنصر أو منشأ ما لابد أن يعكس المسار والجريان الطبيعي للقوى والأحمال خلاله. فعلى سبيل المثال يتضمن المقطع العرضي للجسور المعلقة على إختلافات في أحجامها بموجب مخطط حمل الإنحناء، كما إن تثخين الأعمدة في منتصف إرتفاعها يعمل على زيادة مقاومتها للإنبعاج. [الشكل: 22]



بفية تطبيق مبدأ الكفاءة المنشئية

وبإختصار وكطبيعة تطبيقية لما ورد أعلاه، يمكن القول بأنّ القوى لابد أن تجمع سوية وتتدفّق وتسري طبيعياً الى الأرض بأكثر الطرق مباشرة وإختصاراً خلال الأشكال والعناصر المنشئية ليكون حلاً منطقياً. وبصورة أقرب الى أن تكون صيغة، يمكن تحقيق ذلك من خلال:-

- (1) يجب إستعمال كلّ المواد المنشئية أو الإنشائية قريباً من خواصها وقدرتها،
 - (2) تحقيق أدنى حد من وزن المادة (تقليل الوزن الميت قدر الإمكان)،
 - (3) يجب إن يكون الفعل المنشئي، تحسناً وإدراكاً، واضحاً للشخص غير المتخصص قبل كل شيء.
- (م/5 ؛ ص/211)

فيما يخص موضوع المواد وإستعمالاتها، فلا بد أن تكون المواد المستعملة مستخدمة بموجب خواصها الطبيعية. حيث تنص الفكرة الصحيحة والسليمة بأنّ الشكل الناتج الصحيح والسليم يمثل نتيجة حتمية لخواص المادة عند شيوع إستخدامها. (م/5 ؛ ص/211)

الإستنتاجات العامة

- هنالك أسس معرفية للمنشآت التي تعتمد على قوى الشد والتي تتصف بخفتها وإستهلاكها الشحيح للطاقة مع موضوعية إختزال كلفة موادها وتصنيعها وتلازمهما مع الوزن والحجم المنتقل إضافة الى وقت الإنجاز والطاقة المخزونة في هكذا منشآت، وتمثل التآزيرية إحدى هذه الأسس.
- يحتاج التصميم المعماري لمنشآت قوى الشد الى متطلبات خاصة ومنها التصميم الإنشائي. يستند هذا التصميم على مفاهيم وتعريف أولية تعد أساسية بدءاً من معرفة سلوك القوى وإنتهاءً بالمادة.
- التطرق الى أنماط منشئية بمستويات متباينة ومختلفة يزيل جزءاً من اللبس والتخوف الذي يحوم حول منشآت قوى الشد كما هو الحال في نمط التآزيرية وعضلات الإنسان وسلوك الخلايا الحية، والتي تساهم في إنشاء عمارة تعتمد على مبادئ مماثلة لقوى الشد.
- أنماط التآزيرية مختلفة الأشكال سواء أكانت من القضبان المعدنية والخيوط المطاطية أم من النواضج المرنة فهي مماثلة لغشاء الخلية إذ يعتمد شكلها على فعاليات الخلية الميكانيكية وسبل ثبات أشكالها ضمن مستويات الكيمياء الحياتية.
- تبعاً لمبدأ التآزيرية فإن منشآت قوى الشد تتطلب متانة على مستوى عال. ويمكن الحصول على هذه المتانة من خلال الأشكال الملائمة والمدروسة، بالإضافة الى أن الشكل يتبع القوى.
- تصنف منشآت قوى الشد المستندة الى التآزيرية ضمن منشآت العمارة العضوية لما لها من سمة التغيير والحركة والأشكال المنحنية التي يمتاز بها الكائن العضوي عن الكائنات الساكنة والجامدة. كما يمكن تقليل التخوف لعمارة قوى الشد بربط منشآتها بالأشكال الهندسية الأساسية المرتبطة بمفاهيم الإستقرار والثبات، تطبيقاً لتعبير "الشكل يتبع القوى".

المصادر والمراجع

- الجبوري، أنس حميد، **قوى الشد في العمارة-دراسة تحليلية لواقع العمارة المعاصرة**، إطروحة ماجستير، كلية الهندسة/ قسم الهندسة المعمارية- جامعة بغداد، 2006.
- الدوري، قيس إبراهيم، **علم التشريح**، مخصص لطلبة كلية التربية الرياضية، وزارة التعليم العالي والبحث العلمي/ جامعة بغداد، مديرية دار الكتب للطباعة والنشر - جامعة الموصل، 1988.
- Calatrava, Santiago, **Galinsky**. GNU Free Documentation License, 2006.
[http://www.galinsky.com/Santiago Calatrava.htm]
- Essien, Victoria, **Structures and Forces**. External and Internal Forces acting on structures, McGraw-Hill Book Company, Inc. 2006.
[http://www.edquest.ca/pdf/sia74-2notes.pdf]
- Holgate, Alan, **The art in Structural Design**. Oxford University Press, London, 1986.
- Ingber, Donald E., **Tensegrity Cell Structures and Hierarchical System Biology**. Journal of Cell Science 116, 1157-1173 © The Company of Biologists Ltd, 2005.
[http://www.booklounge.com/books/architecture/materials-form-and-architecture]
- Internet Article/ Google searching images/ **skeleton structure building**, 1998.
[http://images.google.com/images?svnum=10&hl=en&lr=&rls=GGLR%2CGGLR%3A2006-36%2CGGLR%3Aen&q=skeleton+structures+building&btnG=Search]
- Lisborg, Niels, **Principles of Structural Design**. B.T. Batsford Ltd., London, 1961.
- Salvadori and Heller, **Structure in Architecture: The Building of Buildings**. Prentice-Hall Inc. Englewood Cliffs, New Jersey, 1975.
- Sturzebecher and Ulrich, Peter and Sigrid, **Architecture for sport**. Wiley Academy, a division of John Wiley & Sons Ltd, Great Britain, 2002.
- Vandenberg, Martiz, **Cable Nets, Detail in building**. Academy Editions, London, 1998.
- Wikipedia, the free encyclopedia, **Tensegrity**. GNU Free Documentation License, 2005.
[http://en.wikipedia.org/wiki/tesigritiy]
- Wikipedia, the free encyclopedia, **Tensile Architecture**. GNU Free Documentation License, 2003.
[http://en.wikipedia.org/wiki/tensile_architecture]
- Wilson, Forrest, **Structure: the Essence of Architecture**. Studio Vista Van Nostrand Reinhold Company, New York, 1971.

الاختيار الأمثل لمواقع المدارس الابتدائية الجديدة في منطقة بغداد الجديدة باستخدام التحسس النائي ونظم المعلومات الجغرافية

لمى حنا

جامعة بغداد كلية الهندسة

بشار سليم

جامعة بغداد كلية الهندسة

خلاصة البحث

يقدم البحث كيفية استخدام نظم المعلومات الجغرافية في بناء الموديل التحليلي لأختيار أفضل المواقع لإنشاء مدارس جديدة ضمن منطقة الدراسة الواقعة في الجزء الجنوبي الشرقي من مركز مدينة بغداد. و باستثمار معطيات التحسس النائي والاعتماد على مرئية فضائية ملتقطة لمدينة بغداد أعدت خرائط رقمية متعددة الطبقات (Layers) لمنطقة الدراسة. وهذه يمكن الاستفادة منها والرجوع إليها في أي وقت و تحديث أي بيانات فيها باستخدام برامج نظم المعلومات الجغرافية. وبعد استكمال عملية بناء قاعدة البيانات الجغرافية لتلك الخرائط تم استخدام برنامج البناء النماذجي للتحليل المكاني model builder of spatial analysis وتم أعداد نموذج تحليلي لاستنباط أفضل المواقع المحتملة للمدارس الابتدائية الجديدة بالأعتماد على معايير ومواصفات فنية وعلمية. ومن ثم أعداد مرسمات layouts ذات مواصفات هندسية وجغرافية لهذه المواقع المقترحة.

Selecting the Best Locations of New Primary Schools in New Baghdad by Using Remote Sensing and Geographic Information Systems

ABSTRACT

This paper deals with the using of Geographic Information Systems to build up analytical model to choose the best locations of new schools within the study area. This has been done by using satellite image of Baghdad city. Then multi themes digital maps were prepared to the study area. These can be used to update their data

by using Geographic Information Systems software. Then, an analytical had been prepared to create the best probable locations, for new primary schools, depending on criteria, scientific technical specifications. Finally, we prepared layouts with geographical geometrical specifications for these proposed locations.

هدف البحث

يهدف البحث الى أنشاء نموذج لأختيار أفضل المواقع لإنشاء مدارس جديدة ضمن الأحياء السكنية بالاعتماد على عدة عوامل تؤثر في نوع الاختيار. وقد تم استخدام نظم المعلومات الجغرافية وتكنولوجيا التحسس النائي كوسيلة لبناء قاعدة بيانات متكاملة لمنطقة الدراسة بالاستعانة بمرئية فضائية تغطي منطقة الدراسة بالإضافة إلى بيانات إحصائية وبيانات تفصيلية عن واقع حال المنطقة، والذي سيؤمن الاختيار الأمثل لهذه المواقع. آخذين بنظر الاعتبار كافة المتغيرات المطلوبة باستخدام كافة البرمجيات المتيسرة مما يضمن تقليل الكلفة والوقت وبالتالي المساعدة على أتخاذ القرارات.

منطقة الدراسة

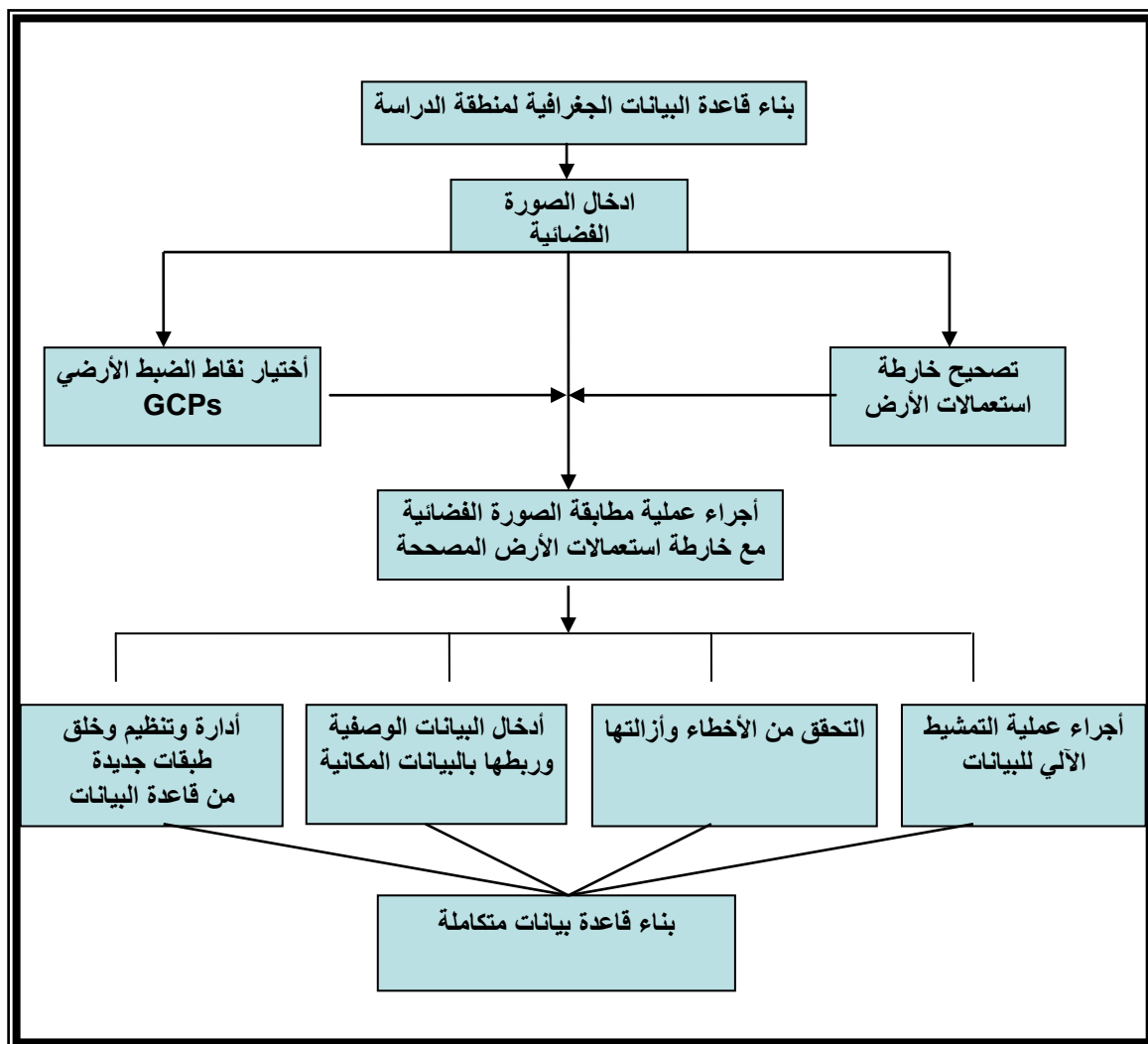
تقع منطقة الدراسة شكل رقم (1) في الجزء الجنوبي الشرقي من مركز مدينة بغداد وبالتحديد ضمن منطقة بغداد الجديدة (حي الخليج) والتي تتألف من اثنتا عشر محلة سكنية وتتحصر بين خطي طول $44^{\circ}30'20''$ ، $44^{\circ}28'00''$ ودائرتي عرض $33^{\circ}19'15''$ ، $33^{\circ}18'20''$ ، وقد اختيرت هذه المنطقة بسبب الزيادة السكانية. كما وأن أغلب المدارس الموجودة مدارس مزدوجة حيث تشترك اكثر من مدرسة واحدة في نفس البناية والتي لاتلبي معايير الأبنية المدرسية التي تعد لكل مدرسة بناية مستقلة بها أضافة الى أنها تؤثر على المستوى العلمي لطلبة هذه المدارس.



شكل رقم (1)، منطقة الدراسة في صورة القمر الصناعي IKONOS

مراحل بناء قاعدة بيانات منطقة الدراسة:

تم الاعتماد على صورة فضائية لمدينة بغداد للقمر الصناعي Quikbird بالإضافة الى خارطة أستعمالات الأرض لجزء من مدينة بغداد في بناء قاعدة البيانات الجغرافية لمنطقة الدراسة. وبصورة عامة، يمكن أنجاز أي مشروع لنظم المعلومات الجغرافية عن طريق سلسلة من الخطوات المنطقية حيث أن كل خطوة تبنى على أساس الخطوة التي تسبقها، أن الخطوات المنطقية التي استخدمت في هذا البحث جاءت كما في الشكل (2).



شكل (2)، الخطوات المنطقية لبناء قاعدة بيانات نظم المعلومات الجغرافية لأختيار أفضل موقع مدرسة

المعايير المكانية الخاصة باختيار مواقع المدارس :

أن اختيار مواقع المؤسسات التعليمية من العوامل المهمة التي يجب أن تؤخذ بنظر الاعتبار في عملية التخطيط التعليمي. وأن أهم الأسباب التي دعت إلى الاهتمام بمجال التخطيط التعليمي هو التزايد الكبير في عدد طلاب المدارس نتيجة لتزايد عدد السكان إضافة إلى قلة أعداد الابنية المدرسية نسبة الى عدد المدارس المتوفرة حالياً" وبالتالي أدى الى اشتراك عدد من المدارس في نفس الابنية. بالإضافة إلى افتقار عدد من المحلات السكنية للمدارس، وسوء توزيعها بشكل مناسب.

نستطيع أن نخلص من خلال الدراسات المعنية بالخدمات التعليمية بأن هنالك عدة معايير في اختيار مواقع المؤسسات التعليمية وهي:

أمكانية الوصول وحوض الخدمة التعليمية.

- توفر الفضاءات الأرضية ومساحاتها التي يمكن إقامة المدارس عليها ضمن الحدود النموذجية.

- بعد المواقع المختارة عن المناطق الصناعية.

- بعد المواقع المختارة عن طرق النقل.

. أماكن الوصول وحوض الخدمة التعليمية:

يعد عامل المسافة عاملاً مهماً يجب اعتماده معياراً أساسياً في عملية التوزيع المكاني للخدمات التعليمية حيث أن مراكز الخدمات هذه يفترض أن يكون الوصول إليها سهلاً ومن المفضل أن تكون مراكز الخدمات في المحلة أو الحي مشيدة في موقع يسهل الوصول إليه سيراً، أي على طريق المماشي التي لا تتقاطع مع طرق النقل والمرور لغرض توافر الأمان للسابلة. أما مراكز الخدمات العليا التي تخدم أكثر من محلة سكنية كالحي والقطاع والمدينة، فإنه لا بأس من توقيعهما بالقرب من خطوط المرور والنقل العام وعلى هذا الأساس نشأ مفهوم (حوض الخدمة للمؤسسة التعليمية) الذي يعني مساحة جغرافية تخدمها مؤسسة تعليمية واحدة. ويحدد هذا الحوض بما تقدمه المؤسسة من خدمة لمجموعة من السكان والجدول رقم(1) يوضح حوض الخدمة نسبة الى نوع الخدمة التعليمية التي تقدمها. [1],[2].

نوع الخدمة التعليمية	توزيعها	الفترة الزمنية التي يحتاجها الطالب للانتقال من المسكن الى المدرسة مشياً (دقيقة)	حوض الخدمة (نصف قطر الدائرة) متر	السبب المباشر لسعة الحوض
التعليم الابتدائي	ضمن المحلة السكنية	10-5	800-400	القابلية الجسمية للتلميذ
التعليم الثانوي	منطقة وسطى بين عدة أحياء سكنية	20-10	1600-800	تخدم أكثر من حي سكني

جدول رقم(1) يوضح حوض الخدمة للمؤسسة التعليمية

توفر الفضاءات الأرضية ومساحاتها:

إن توفر الفضاءات الأرضية ومساحاتها من المعايير الأساسية عند دراسة توقييع المدارس للمناطق الحضرية حيث هناك أسس ومعايير لأبنية الخدمات التعليمية ومساحتها المطلوبة ضمن المعايير الخاصة والتي تتراوح مساحتها النموذجية ما بين 6000 م² لمدرسة عدد صفوفها 12 صف الى 12000 م² لمدرسة عدد صفوفها 24 صف. [3],[4].

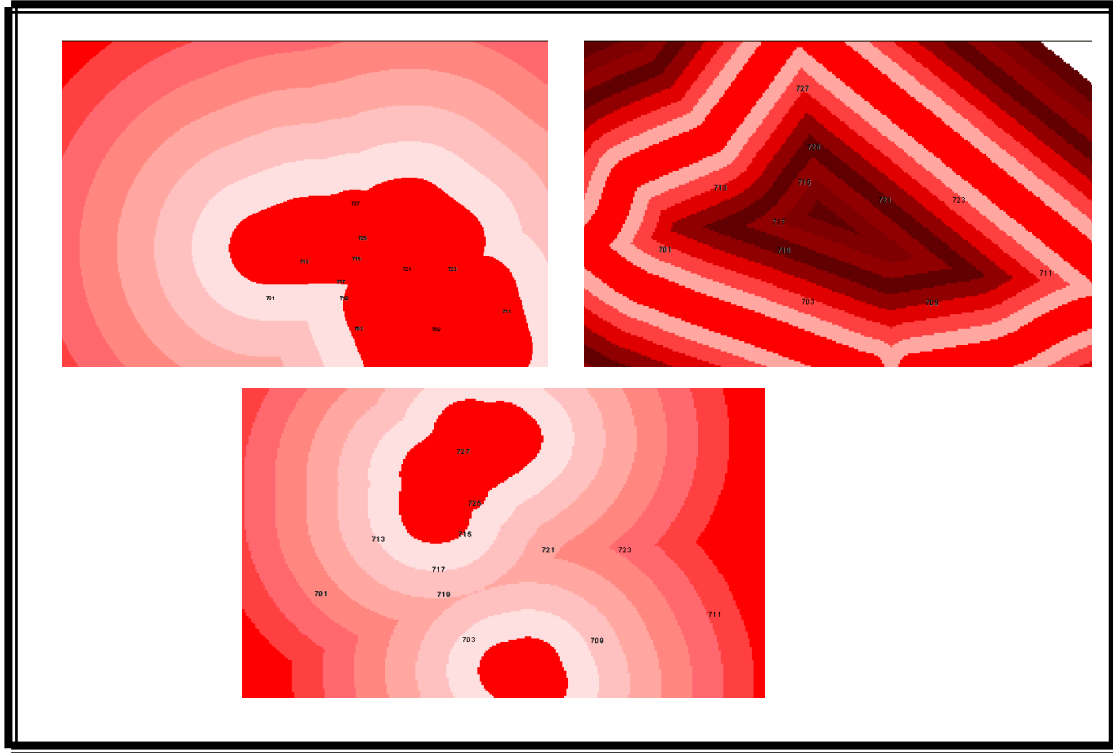
بعد المواقع المختارة عن المناطق الصناعية:

يعتبر هذا المعيار من المعايير المهمة عند عملية التوقيع المكاني للمدارس حيث يفضل توقييعها بعيدة عن المناطق الصناعية لما تسببه من ضوضاء واعتبارات بيئية سلبية. وكلما كان الموقع المختار للمدرسة بعيداً عن هذه المناطق كلما كان الاختيار أفضل.

بناء النموذج التحليلي المكاني:

تم استخدام برنامج المحلل المكاني كملحق لبرنامج Arcview والذي يتضمن تقنية model builder يتم من خلاله بناء نموذج تحليلي لاختيار أفضل موقع مدرسة ابتدائية. يتم فتح نافذة model builder من واجهة المشروع برنامج Arc view حيث تم تفعيل كلا من spatial analyst , model builder من أيقونة الامتدادات extensions للبرنامج. يبدأ العمل بالنموذج بفتح واجهة البرنامج من برنامج Arcview وبعدها يتم استدعاء الطبقات اللازم إدخالها ضمن المعايير المكانية لاختيار أفضل موقع مدرسة. أن البناء النماذجي model builder لا يتعامل مع الطبقات الاتجاهية vector themes وإنما مع الطبقات المتسامته raster(grid) themes لذا يجب في بادئ الأمر تحويل كل الطبقات المدخلة ضمن المعايير المكانية إلى طبقات متسامته عن طريق تطبيق عملية تحويل صيغة البيانات المتجهة. بعد عملية تحويل البيانات تتم عدد من المعالجات processes اللازم إجراؤها على البيانات المدخلة لانتخاب أفضل موقع مثل عملية النطاق buffer كما في الشكل (3)، حيث سيتم ادخال جميع نواتج العمليات التي أجريت على البيانات المدخلة الى عملية التراكب الموزون Weighted Overlay وتستدعى كل طبقة من تلك الطبقات حتى يتم استكمالها واعطاء كل منها وزن خاص حسب اهمية وأفضلية تلك الطبقة بالإضافة الى أعطاء كل الطبقات مقياس موحد (evaluation scale). أعطي ضمن عملنا مقياس من خمسة درجات (1-5) وزعت على كل خلية في كل طبقة من الطبقات المدخلة. يوضح الشكل رقم (4) النموذج النهائي لاختيار

أفضل موقع مدرسة ابتدائية والذي يتألف من مجموعة من الخلايا تمثل البيانات المدخلة Input themes والعمليات التي تجرى عليها Functions وناتج هذه العمليات Output themes.

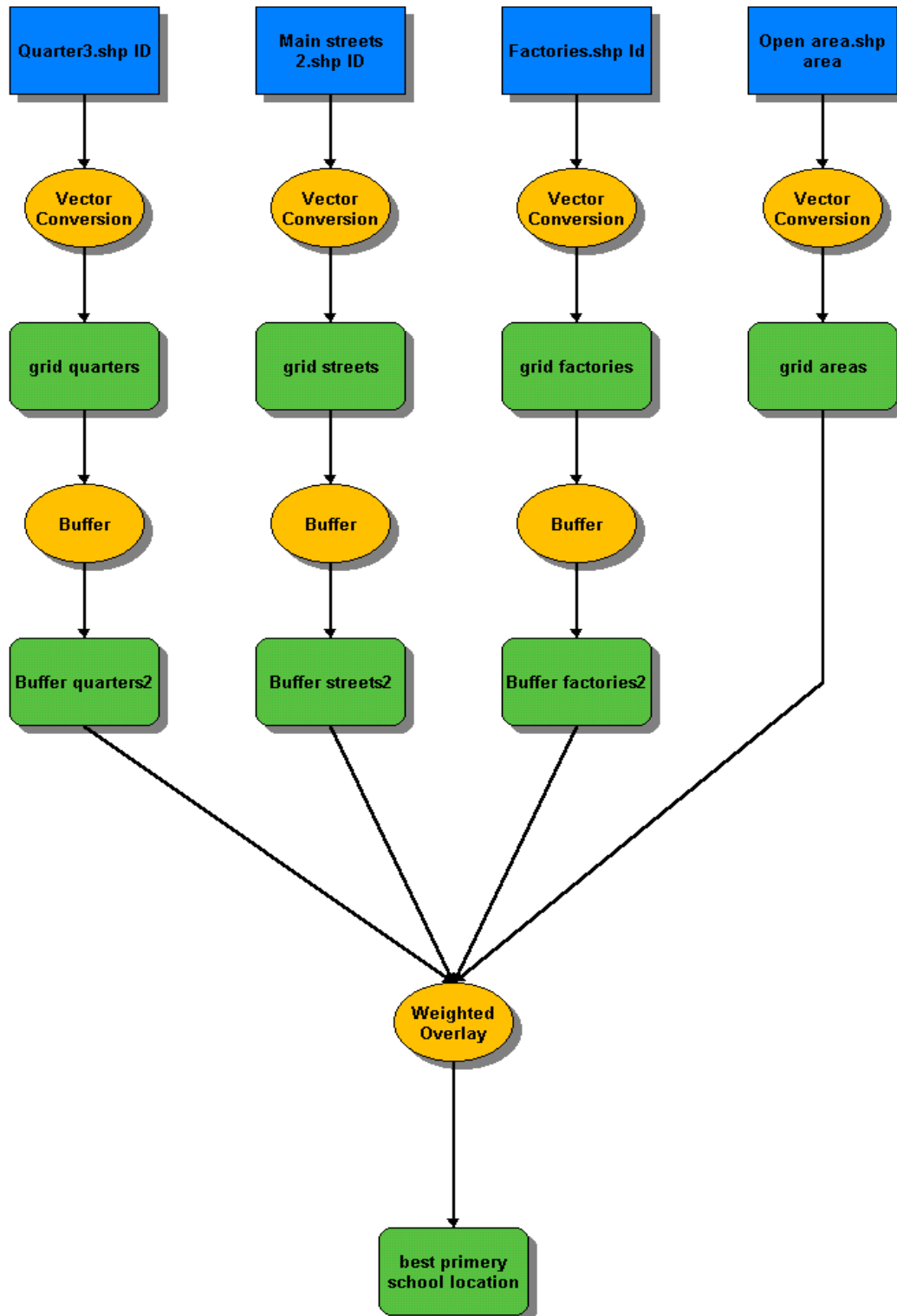


شكل (3)، عمليات الأنطقة

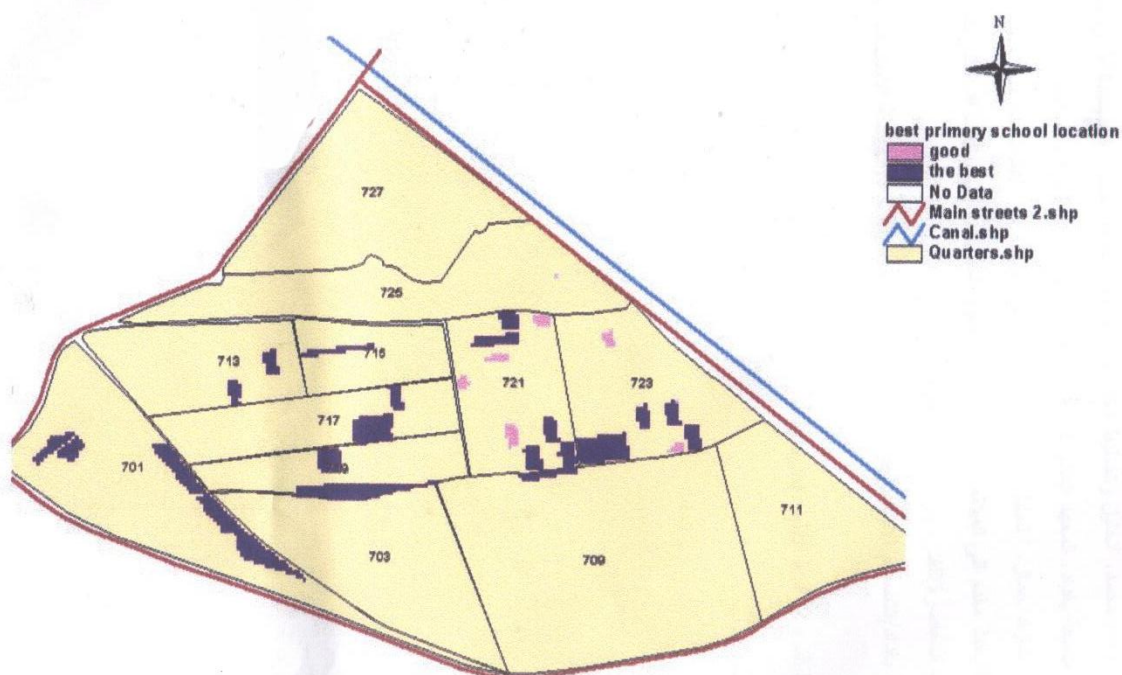
بعد إدخال كل طبقة من قاعدة البيانات المعدة ، تبدأ سلسلة من العمليات المكانية ضمن برنامج البناء النماذجي للتحليل المكاني منها عملية التحويل الاتجاهية الى الصيغة المتسامته حيث يلاحظ في النموذج أن كل الطبقات المدخلة تم تحويلها الى الصيغة المتسامته للبدأ بعمليات أخرى منها عملية خلق الأنطقة Buffering Process.

تم عمل أنطقة حول المحلات التي لوحظ فيها زيادة بعدد المدارس الابتدائية وأختير عرض النطاق 400 متر والذي يمثل المسافة المطلوبة لحوض الخدمة للمدارس الابتدائية كما تم عمل أنطقة حول الشوارع الرئيسية عرض النطاق 200 متر وكذلك الحال بالنسبة للمناطق الصناعية وبعد أكمال عمل الأنطقة وتسمية البيانات الناتجة من هذه العملية تتم عملية أخرى، وهي عملية التراكب الموزون Weighted Overlay Process. لاختيار أفضل موقع مدرسة ابتدائية تم فتح النافذة الخاصة بعملية التراكب واختيار مقياس موحد لخلايا الطبقات المدخلة Evaluation scale، والذي تراوح ما بين (1-5) وبعدها تتم عملية استدعاء الطبقات وفيلاتها المطلوبة. تم ادخال طبقة أنطقة المحلات (buffer quarter1) وأعطائها وزن قدره 35% وأعطاه كل خلية من خلايا الطبقة مقياس من (1-5) حيث يعطى للخلية القليلة الأهمية رقم 1 بالمقارنة مع الخلية

التي لها أهمية ضمن عملية التحليل والتي تعطى رقم 5. وبعدها يتم ادخال الطبقة الثانية وهي طبقة أنطقة الشوارع الرئيسية ((buffer streets وأعطاؤها وزن قدره 15% وادخال مقياس لكل خلية من خلايا الطبقة، أما الطبقة الثالثة المدخلة فهي طبقة المساحات الفارغة ذات الصيغة المتسامته (grid open area) وكذلك اعطاؤها وزن قدره 35% وادخال مقياس لكل خلية واخيرا" الطبقة الرابعة وهي طبقة أنطقة المناطق الصناعية (buffer factories) والتي اعطي لها وزن قدره 15%. وبالتالي يجب أن يكون مجموع الأوزان 100% وهكذا سوف يكون النموذج جاهز للتنفيذ كما في الشكل (4) والشكل (5) التي توضح المواقع المتلى للمدارس الابتدائية بعد عملية التحليل.



شكل (4)، النموذج النهائي لاختيار أفضل موقع مدرسة ابتدائية



شكل (5)، المخطط النهائي الذي يوضح أفضل المواقع الممكنة لاختيار مدرسة ابتدائية

الاستنتاجات

لقد أظهرت الدراسة فاعلية استخدام نظام المعلومات الجغرافية GIS في حل المسائل المتعلقة باختيار أفضل المواقع location analysis من خلال إجراء عمليات التحليل الحيزي الملائمة لطبيعة المسألة موضوع البحث.

وفر برنامج البناء النمذجي model builder تقنية سريعة وقابلة للتحديث والإضافة في إجراء الحل وفق المعايير القياسية المتبعة في اختيار المواقع وإمكانية تغيير أوزان العوامل المؤثرة في الاختيار حسب المعطيات والمستجدات.

يتضح مما تقدم إن نظم المعلومات الجغرافية أصبحت الوسيلة الفعالة والحديثة التي يتم إتباعها في تحديد سياسات المؤسسات الحكومية واتخاذ القرارات.

المصادر

1. أحمد، وفاء محمد، "تحليل وتخطيط الخدمات التعليمية لمنطقة بغداد الجديدة" أطروحة ماجستير، جامعة بغداد، المعهد العالي للتخطيط الحضري والإقليمي للدراسات العليا، 1997.
2. جلال، شازاد جمال، "تحليل سهولة الوصول الى المدارس الابتدائية في مدينة السليمانية" بحث مقدم الى المؤتمر العلمي الرابع (التطور المكاني في العراق في ظل الاتجاهات المعاصرة) للفترة من 7/31 ولغاية 2005/8/1.
3. أمانة بغداد/التصميم الأساسي/دراسة حول تخطيط مدينة بغداد (الهيئة الاستشارية اليابانية).
4. وزارة التربية/دائرة الأبنية المدرسية.

ANTISEIZURE CHARACTERISTICS OF LEADED ALUMINUM ALLOYS UNDER DRY SLIDING CONDITIONS

Dr. Akeel D. Subhi

Department of Production Engineering and Metallurgy
University of Technology
Baghdad-Iraq

ABSTRACT

Aluminum-Silicon alloys, with soft lubricant metal, are considered to be one of the important tribological alloys which resist seizure. The effect of different lead percentages (1-20%Pb) that added to the modified eutectic Al-12%Si alloy on the wear rate and resistance was studied by sliding these alloys under dry sliding conditions on a carbon steel disc at different sliding distances (2.24-40.37 km). The results showed that the wear rate was decreased and wear resistance increased with increasing lead percentage of Al-12%Si alloy. Furthermore, wear rate was increased linearly with increasing sliding distance.

الخلاصة

تعد سبائك الالمنيوم-سليكون المحتوية على معدن مزيت من السبائك الترابيولوجية المهمة المقاومة للالتصاق. يهدف هذا البحث الى دراسة تاثير اضافة الرصاص بنسب مختلفة (1-20%Pb) على معدل ومقاومة البلى لسبيكة Al-12%Si الايوتكتيكية المحورة تحت تاثير الانزلاق الجاف على قرص من الفولاذ الكربوني عند مسافات انزلاقية مختلفة (2.24-40.37 km). اوضحت النتائج انخفاض معدل البلى وزيادة مقاومة البلى مع زيادة نسبة الرصاص لسبيكة Al-12%Si. علاوة على ذلك فان معدل البلى يزداد بصورة خطية مع زيادة مسافة الانزلاق.

KEYWORDS:

Aluminum Alloys, Antiseizure Characteristics, Sliding Conditions

INTRODUCTION

Aluminum based alloys; especially eutectic aluminum-silicon alloys are regarded to be one of the most important tribological alloys due mainly to the presence of silicon (Lee 1998 and Yasmin 2004). Silicon is the second most abundant impurity of aluminum. It imparts fluidity in casting, weldability and high mechanical properties (Mondolfo 1976). These properties incited many researchers in order to approach the convenient application. Therefore, replacement of cast iron by

aluminum based alloys in manufacturing automobile pistons is the start point in the early ninetieth century (**Sarkar 1980**). Lead is technically and economically the best qualified metal for use as a soft phase alloying addition to aluminum based alloys. Leaded aluminum alloys are characterized by low wear rate, antifriction and antiseizure characteristics suitable for a variety of bearing applications (**Tiwari 1987**). (**Rudrakshi et al. 2004**) found that the wear properties of spray formed Al-Si-Pb alloy were improved to be greater than that of Al-Si alloy as a result of microstructural features of spray formed alloy and the nature of the worn out surfaces. (**While Hao et al. 2005**) showed that the main reason of decreasing wear in the hot extruded Al-4Si-20Pb alloy attributed to the constituents of lubricating film that created between the mating surfaces. They indicated that this film is composed of mixture of Fe_2O_3 , Pb_4SiO_6 and a small amount of Fe_2O_3 at room temperature, and $\text{Pb}_4\text{Al}_{12}(\text{SiO}_3)_7$, SiO_2 , Al_2O_3 and a small amount of Fe_2O_3 at high temperature. The same result is concluded by (**An et al. 2006**) when irradiated Al-Si-Pb alloys with high current pulsed electron beam in which the different constituents of lubricating film is the main reason of decreasing wear.

In this work, some light will be thrown to study the effect of lead addition on wear rate and resistance of modified eutectic Al-12%Si alloy.

MATERIALS AND METHODS

Leaded aluminum alloys were prepared using commercial high purity aluminum, lead and Al-18%Si master alloy as starting materials. The master alloy of Al-18%Si was previously prepared by adding high purity silicon as chunks to the molten of commercial high purity aluminum using gas fired furnace under the pressure effect via graphite block in a graphite crucible to prevent any floatation of silicon on the molten surface of aluminum. The molten of Al-18%Si alloy was casted in a metallic mould to produce ingot of Al-18%Si master alloy. A specified amount of commercial high purity aluminum was added to the molten of Al-18%Si master alloy to obtain Al-12%Si alloy. Lead was added separately in different amounts, that corresponding to 1-20%Pb, to the diluted Al-18%Si master alloy with aluminum to produce different types of leaded Al-12%Si alloys. The addition of lead was carried out using vortex method as a result of no solubility and miscibility between lead and eutectic Al-12%Si alloy. In this method, lead was added as chips to the molten of diluted Al-18%Si master alloy with aluminum in a graphite crucible using graphite fan to prevent any reaction. The inclination angle of vortex mixing and speed of mixer rotation were 30° and 1256 rpm respectively. All leaded alloys were mixed at 650°C for 10 min individually to obtain homogenous distribution of lead inside the molten of Al-12%Si alloy. The pouring temperature for each alloy was fixed at the same temperature of vortex mixing in which each alloy was poured into a cooled carbon steel mould to obtain chilled ingots of Al-Si-Pb alloys. All casted ingots have the dimensions of 100 mm length and 15 mm diameter. Chemical composition of pure aluminum, master alloy and prepared Al-Si-Pb alloys is tabulated in table I. The ingots of Al-Si-Pb alloys were cut and turned to produce specimens suitable for microstructural and wear study. For microstructural study, each alloy specimen was cold mounted and then ground using different SiC emery papers. Primary polishing was carried out using slurry of alumina while final polishing was achieved using diamond paste. All microstructural study specimens were etched using 1% Vol. HF etching solution.

Pin on disc type wear testing apparatus with 450 Hv carbon steel disc was used in this work in order to determine antiseizure characteristics of Al-Si-Pb alloys. Wear test specimens that previously prepared have the dimensions of 10 mm length and 5 mm diameter. The sliding circle diameter and bearing pressure were fixed at 14 cm and 63.6 kPa respectively. A wide range of running periods was used ranging from 10 min to 3 hr in order to produce different sliding distances (2.24-40.37 km).

RESULTS AND DISCUSSION

Fig. 1 shows the microstructure of modified eutectic Al-Si alloys. It is clear from this figure that two phases are presented in the matrix of Al-Si-Pb alloys. These phases are eutectic and lead, while one phase presented in the matrix of Al-12%Si alloy which is eutectic. **Fig. 1** also shows the potent effect of chilling on producing modification of eutectic silicon in the matrix of leaded alloys, in which fibrous eutectic silicon associated with aluminum dendrites can be recognized in the matrix for each alloy. This modification in eutectic silicon morphology from angular and flake as in ordinary conditions to the fibrous as in this work has a crucial role on increasing the mechanical and tribological properties of eutectic Al-Si alloys as mentioned elsewhere (**Subramanian 1991, Fatahalla 1999 and Liao 2002**). It is explicit to know that lead decreasing the hardness of Al-Si alloys in a magnitude dependent on its percentage in the matrix. This decreasing in hardness value does not mean decreasing in wear properties of Al-Si alloys. This can be demonstrated by showing the relationship between sliding distance and wear rate as shown in **Fig. 2**. It is clear from this figure that the wear rate was increased linearly with increasing sliding distance for each alloy. In the other side, the wear rate was decreased with increasing lead percentage at any sliding distance. Plastic deformation always associated with wear in the subsurface region of the base matrix of Al-Si alloys. The deformation of aluminum phase results in fragmentation of silicon phase into fine particles distributed in the subsurface region (**Pramila Bai 1984**). In this work, no fragmentation was occurred as a result of potent effect of modification that occurred in eutectic silicon morphology as explained above. The aluminum and silicon phases in the eutectic of Al-Si alloys behave independently on each other during dry sliding in which the silicon phase resists the applied bearing pressure while the aluminum phase accommodates the plastic deformation in the matrix. The presence of lead in the matrix of modified Al-12%Si alloy results in decreasing the wear rate as explained above. This is because the lead acts as a lubricant and reduces wear between mating surfaces as a result of its extrusion during dry sliding of leaded aluminum alloys on carbon steel disc and forming a trib-layer of low shear strength spreads over modified eutectic Al-12%Si alloy substrate. The smearing of lead prevents adhesion between the mating surfaces in areas dependent on lead location in the matrix of modified eutectic Al-12%Si alloy. Therefore, wear rate will be decreased and in the same time seizure resistance will be increased. This result can be demonstrated precisely from the relationship between lead percentage and wear resistance, as shown in **Fig. 3**, in which the wear resistance increases with increasing lead percentage. From curve fitting programme, the wear resistance (W_R) changes with lead percentage (L_p) according to the following formula:

$$W_R = -0.021L_p^2 + 1.267L_p + 35.83 \quad (1)$$

This illuminates the importance of lead addition; especially the adhesive compatibility of slid metals (**Norton 1998**) indicated clearly the low metallurgical compatibility between lead and iron where iron can be considered as a counterface material. This makes Al-Si-Pb alloys a suitable choice for bearing applications. The relationship between wear rate (W_r) and hardness (H_v) is shown in **Fig. 4** in which the wear rate decreases with decreasing hardness, i.e. increasing lead percentage, according to the following formula obtained from curve fitting programme

$$W_r = 0.002H_v^2 - 0.2H_v + 6.250 \quad (2)$$

CONCLUSIONS

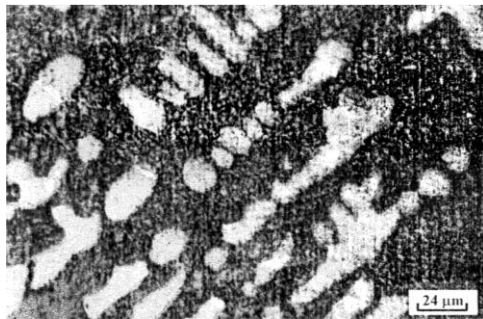
Rapid cooling of leaded eutectic Al-12%Si alloys in a metallic mould could produce modification of eutectic silicon morphology in the matrix of these alloys. The presence of accompanied lead that added using vortex method with modified eutectic silicon led clearly to remarkable changes in the antiseizure characteristics of leaded alloys. These changes can be summarized by decreasing wear rate and increasing wear resistance with increasing lead percentage, i.e. decreasing hardness.

REFERENCES

- An, J., Shen, X.X., Lu, Y., Liu, Y.B., Li, R.G., Chen, C.M. and Zhang, M.J., "Influence of High Current Pulsed Electron Beam Treatment on the Tribological Properties of Al-Si-Pb Alloy", *Surface and Coatings Techno.*, 200 (2006) 5590.
- Fatahalla, N., Hafiz, M. and Abdulkhalek, M., "Effect of Microstructure on the Mechanical Properties and Fracture of Commercial Hypoeutectic Al-Si Alloy Modified with Na, Sb and Sr", *J. Mater. Sci.*, 34 (1999) 3555.
- Hao, S.Z., An, J., Liu, Y.B. and Lu, Y., "Tribological and Structural Properties of Lubricating Films of Al-4Si-20Pb Alloy During Dry Sliding at Different Temperatures", *Mater. & Design*, 26 (2005) 181.
- Lee, J.A., "High-Strength Aluminum Casting Alloy for High-Temperature Applications", NASA, Marshall Space Flight Center, Dec., 1998.
- Liao, H., Sun, Y. and Sun, G., "Correlation Between Mechanical Properties and Amount of Dendritic α -Al Phase in As-Cast Near Eutectic Al-11.6%Si Alloys Modified with Strontium", *Mater. Sci. and Engg. A*, 335 (2002) 62.
- Mondolfo, L.F., "Aluminum Alloys: Structure and Properties", Butterworths (London), 1976.
- Norton, R.L., "Machine Design-An Integrated Approach", Prentice-Hall Inc. (New Jersey), 1998.
- Pramila Bai, B.N. and Biswas, S.K., "Subsurface Deformation in Dry Sliding of Hypo-Eutectic Al-Si Alloys", *J. Mater. Sci.*, 19 (1984) 3588.
- Rudrakshi, G.B., Srivastava, V.C., Pathak, J.P. and Ojha, S.N., "Spray Forming of Al-Si-Pb alloys and Their Wear Characteristics", *Mater. Sci. and Engg. A*, 383 (2004) 30.
- Sarkar, A.D., "Friction and Wear", Academic Press (London), 1980.
- Subramanian, C., "Wear of Al-12.3Wt.%Si Alloy Slid Against Various Counterface Materials", *Scripta Metall.*, 25 (1991) 1369.
- Tiwari, S.N., Pathak, J.P. and Malhotra, S.L., "Lead- A Potential Soft-Phase Alloying Addition to Aluminum Bearing Alloys", *Aluminum*, 63 (1987) 411.
- Yasmin, T., Khalid, A.A. and Haque, M.M., "Tribological (Wear) Properties of Aluminum-Silicon Eutectic Base Alloy Under Dry Sliding Conditions", *J. Mater. Proce. Techno.*, 153-154 (2004) 833.

Elements	Si	Fe	Cu	Pb	Mn	Ti	Al
Al	0.11	0.11	0.008	0.001	0.007	0.005	Rem.
Al-18%Si	18.2	0.31	0.09	0.001	0.02	0.009	Rem.
Al-12%Si	12.4	0.24	0.03	0.001	0.01	0.007	Rem.
Al-12%Si-1%Pb	11.9	0.24	0.03	1	0.01	0.007	Rem.
Al-12%Si-6%Pb	12.7	0.24	0.03	6	0.01	0.007	Rem.
Al-12%Si-12%Pb	12.1	0.24	0.03	12	0.01	0.07	Rem.
Al-12%Si-20%Pb	12.4	0.24	0.03	20	0.01	0.07	Rem.

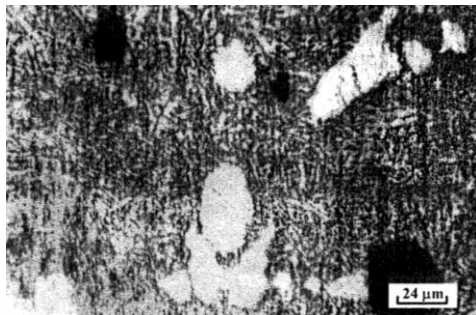
Table I Chemical composition of pure aluminum, master alloy and prepared Al-Si-Pb alloys.



Al-12%Si



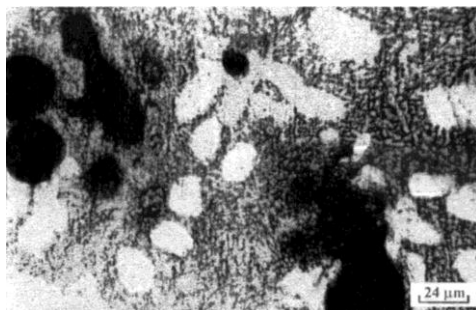
Al-12%Si-1%Pb



Al-12%Si-6%Pb



Al-12%Si-12%Pb



Al-12%Si-20%Pb

Fig. 1 Microstructure of as-cast leaded modified eutectic aluminum-silicon alloys.

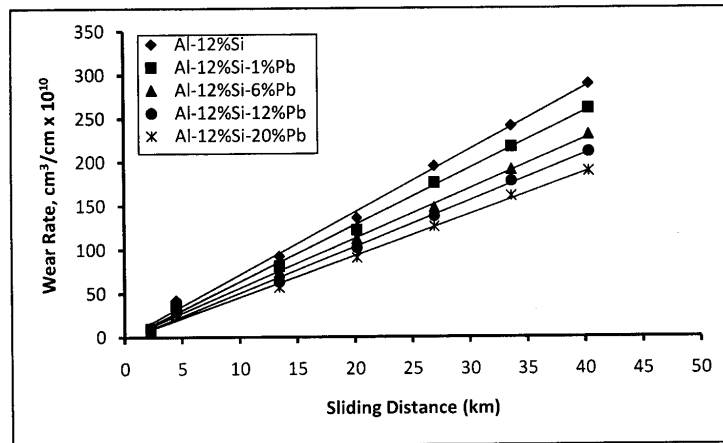


Fig. 2 The relationship between sliding distance and wear rate of Al-Si-Pb alloys.

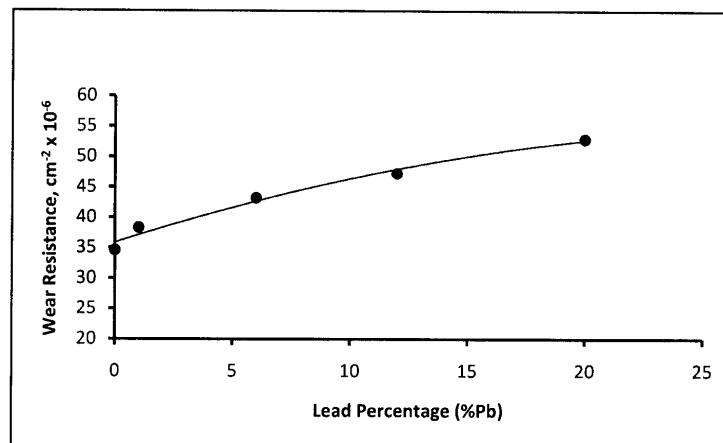


Fig. 3 The relationship between lead percentage and wear resistance of Al-12%Si alloy. Sliding distance, 40.37 km.

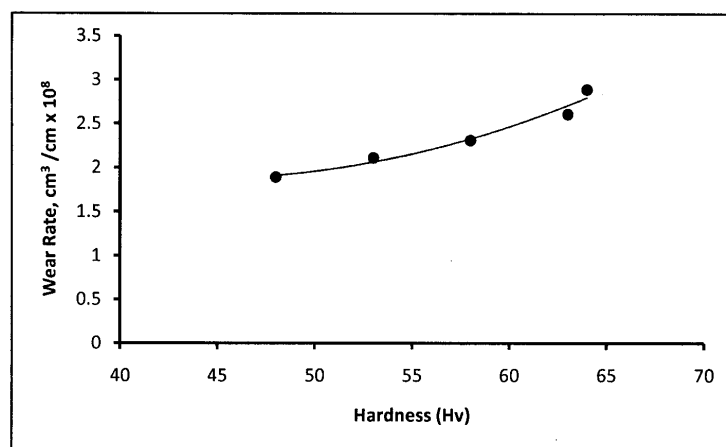


Fig. 4 The relationship between hardness and wear rate of Al-Si-Pb alloys. Sliding distance, 40.37 km.

TWO-DIMENSIONAL CONSOLIDATION ANALYSIS OF PARTIALLY SATURATED EARTH EMBANKMENT UNDER ITS SELF WEIGHT BY USING THE FINITE ELEMENT METHOD

Omar Al-Farouk S. Al-Damluji Yousif J. Al-Shakarchi, and Abdul Kareem E. Zainel

Engineering College - Baghdad University

ABSTRACT

This paper studies the two-dimensional analysis of the consolidation process for partially saturated soils applied to an earth embankment mainly from the theoretical point of view. The method of finite elements is used to find a numerical solution to describe the behavior of soils during consolidation. Moreover, this study was carried for both, isothermal and non-isothermal cases.

The case of two-dimensional, plane strain consolidation is considered, as it is widely needed in the studies of soil mechanics. The parameters studied are displacement in the y-direction, pore water pressure, pore air pressure, and temperature.

The embankment was constructed in Basrah - Iraq, where the temperature is usually high at most days of the year. It is believed that it is more realistic to model the embankment as a partially saturated soil rather than a fully saturated soil as was done before.

The study reveals that: –

- The consolidation process is affected by the degree of saturation. As the paths in the soil that are used by the pore-water and/or the pore-air may transfer from one state (open path) to another state (closed path) and vice versa.
- The pore-water and the pore-air pressures are affected by temperature. The pressure increases when the temperature increases (for a constant volume). This is usually the case inside the partially saturated soil. Temperature can affect indirectly the soil skeleton as a result of the change in pore-air and pore-water pressures.
- The vertical displacement for partially saturated soil consolidation under self weight loading is noticed to have almost regular settlement. Then, there is an accelerated settlement due to the dissipation of the air and water pressures. After a while (after excess pressures dissipation), there will be a classical consolidation form.

KEYWORDS

partially saturated soils, unsaturated soils, soil mechanics, geotechnique, consolidation, non-isothermal consolidation

INTRODUCTION

Soils that are unsaturated form the largest category of materials, which do not adhere in behavior to classical, saturated soil mechanics.

The differentiation between saturated and unsaturated soils becomes necessary due to basic differences in their nature and engineering behavior. An unsaturated soil has more than two phases and the pore–water pressure is negative relative to the pore–air pressure.

Any soil near the ground surface, present in a relatively dry environment, will be subjected to negative pore–water pressures and possible desaturation.

It is the presence of more than two phases that results in a material that is difficult to deal with in engineering practice.

An unsaturated soil is commonly defined as having three phases, namely;

- ♦ solids,
- ♦ water, and
- ♦ air.

It may be more correct to recognize the existence of a fourth phase, namely, that of the air–water interface or *contractile skin*. The presence of even the smallest amount of air makes the soil unsaturated. A small amount of air, may occur as occluded air bubbles, which makes the pore fluid compressible. Generally, it is a larger amount of air, which makes the air phase continuous throughout the soil. At the same time, the pore–air and pore–water pressures begin to differ significantly, with the result that the principles and concepts involved differ from those of classical, saturated soil mechanics.

TYPES OF PROBLEMS :–

The types of problems of interest in unsaturated soil mechanics are similar to those of interest in saturated soil mechanics. Common to all unsaturated soil situations are the negative pressures in the pore–water. The type of problem involving negative pore–water pressures that has received the most attention is that of swelling or expansive clays.

Several typical problems are described to illustrate relevant questions, which might be asked by the geotechnical engineer.

- ♦ **Construction and Operation of a Dam**
- ♦ **Natural Slopes Subjected to Environmental Changes**
- ♦ **Mounding Below Waste Retention Ponds**
- ♦ **Stability of Vertical or Near Vertical Excavations**
- ♦ **Lateral Earth Pressures**
- ♦ **Bearing Capacity for Shallow Foundations**
- ♦ **Ground Movements Involving Expansive Soils**
- ♦ **Collapsing Soils**

CONSTITUTIVE RELATIONS : –

Constitutive relations for an unsaturated soil can be formulated by linking selected deformation state variables to appropriate stress state variables. The deformation state variables must satisfy the continuity requirement. The link of the deformation and stress state variables results in the incorporation of volumetric deformation coefficients. The established constitutive relations can be used to predict volume changes due to changes in the stress state.

Two approaches can be used in establishing the stress versus deformation relationships. These are: the “mathematical” approach and the “semi–empirical” approach. In the mathematical approach, each component of the deformation state variable tensor is expressed as a linear combination of the stress state variables or vice versa. In other words, the relationship between the stress and deformation state variables is expressed by a series of linear equations. The problem with this approach is that it involves the assessment of a large number of soil properties.

The semi-empirical approach involves several assumptions, which are based on experimental evidence from observing the behavior of many materials. These assumptions are that:

- ◆ normal stress does not produce shear strain;
- ◆ shear stress does not cause normal strain; and
- ◆ shear stress component, τ , causes only one shear strain component, (γ) .

In addition, the principle of superposition is assumed to be applicable to cases involving small deformations.

The constitutive relations for an unsaturated soil can be formulated as an extension of the equations used for saturated soil, using the appropriate stress state variables. Assume that the soil behaves as an isotropic, linear elastic material. The following constitutive relations are expressed in terms of the stress state variables, $(\sigma - u_a)$ and $(u_a - u_w)$. The formulation is similar in form to that proposed by Biot in 1941. The soil structure constitutive relations associated with the normal strains in the x-, y-, and z-directions are as follows: –

$$\varepsilon_x = \frac{(\sigma_x - u_a)}{E} - \frac{\mu}{E}(\sigma_y + \sigma_z - 2u_a) + \frac{(u_a - u_w)}{H} \quad (1)$$

$$\varepsilon_y = \frac{(\sigma_y - u_a)}{E} - \frac{\mu}{E}(\sigma_x + \sigma_z - 2u_a) + \frac{(u_a - u_w)}{H} \quad (2)$$

$$\varepsilon_z = \frac{(\sigma_z - u_a)}{E} - \frac{\mu}{E}(\sigma_x + \sigma_y - 2u_a) + \frac{(u_a - u_w)}{H} \quad (3)$$

where

H = modulus of elasticity for the soil structure with respect to a change in matric suction, $(u_a - u_w)$.

The constitutive equations associated with the shear deformations are: –

$$\gamma_{xy} = \frac{\tau_{xy}}{G} \quad (4)$$

$$\gamma_{yz} = \frac{\tau_{yz}}{G} \quad (5)$$

$$\gamma_{zx} = \frac{\tau_{zx}}{G} \quad (6)$$

where

τ_{xy} = shear stress on the x-plane in the y-direction (i.e., $\tau_{xy} = \tau_{yx}$),

τ_{yz} = shear stress on the y-plane in the z-direction (i.e., $\tau_{yz} = \tau_{zy}$),

τ_{zx} = shear stress on the z-plane in the x-direction (i.e., $\tau_{zx} = \tau_{xz}$), and

G = shear modulus.

The modulus of elasticity, E , in the above equations is defined with respect to a change in the net normal stress, $(\sigma - u_a)$.

The above constitutive equations can also be applied to situations where the stress versus strain curves are nonlinear.

Figure 1 shows a typical stress versus strain curve. An incremental procedure using the small increments of stress and

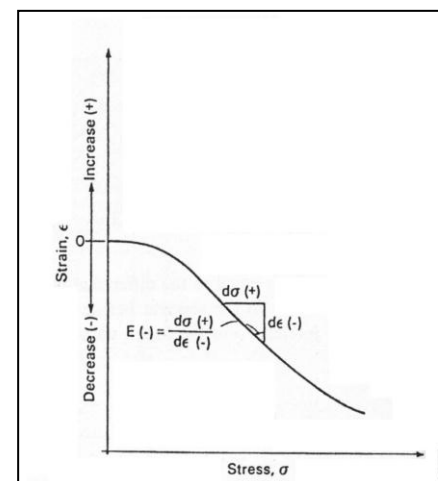


Fig. 1
Nonlinear stress versus strain curve

strain can be used to apply a linear elastic formulation to a nonlinear stress versus strain curve.

The nonlinear stress versus strain curve is assumed to be linear within each stress and strain increment. The elastic moduli, E and H , have negative signs, as indicated in figure 1, and may vary in magnitude from one increment to another.

The soil structure constitutive relations associated with normal strains can be written in an incremental form: –

$$d\varepsilon_x = \frac{d(\sigma_x - u_a)}{E} - \frac{\mu}{E} d(\sigma_y + \sigma_z - 2u_a) + \frac{d(u_a - u_w)}{H} \quad (7)$$

$$d\varepsilon_y = \frac{d(\sigma_y - u_a)}{E} - \frac{\mu}{E} d(\sigma_x + \sigma_z - 2u_a) + \frac{d(u_a - u_w)}{H} \quad (8)$$

$$d\varepsilon_z = \frac{d(\sigma_z - u_a)}{E} - \frac{\mu}{E} d(\sigma_x + \sigma_y - 2u_a) + \frac{d(u_a - u_w)}{H} \quad (9)$$

Equations 7, 8, and 9 represent the general elasticity constitutive relations for the soil structure. The left-hand side of the equations refers to a change in the deformation state variable, while its right-hand side contains changes in the stress state variables. A change in the volumetric strain of the soil for each increment, $d\varepsilon_v$, can be obtained by summing the changes in normal strains in the x-, y-, and z-directions:

$$d\varepsilon_v = d\varepsilon_x + d\varepsilon_y + d\varepsilon_z \quad (10)$$

where

$d\varepsilon_v$ = volumetric strain change for each increment.

Substituting equations 7, 8, and 9 into equation 10 gives: –

$$d\varepsilon_v = 3\left(\frac{1-2\mu}{E}\right)d\left(\frac{\sigma_x + \sigma_y + \sigma_z}{3} - u_a\right) + \frac{3}{H}d(u_a - u_w) \quad (11)$$

Equation 11 can be simplified to the following form:–

$$d\varepsilon_v = 3\left(\frac{1-2\mu}{E}\right)d(\sigma_{mean} - u_a) + \frac{3}{H}d(u_a - u_w) \quad (12)$$

where

σ_{mean} = average total normal stress (i.e., $(\sigma_x + \sigma_y + \sigma_z) / 3$).

The volumetric strain change, $d\varepsilon_v$, is equal to the volume change of the soil element divided by the initial volume of the element:

$$d\varepsilon_v = \frac{dV_v}{V_o} \quad (13)$$

The Initial volume, V_o , refers to the volume of the soil element at the start of the volume change process. Therefore, V_o remains constant for all increments. At the end of each increment, the volumetric strain change, $d\varepsilon_v$, can be computed from equation 12 and the volume change of the soil

element, dV_v , is obtained from equation 13. The summation of the volumetric strain changes for each increment gives the final volumetric strain of the soil: –

$$\epsilon_v = \sum d\epsilon_v \quad (14)$$

Change in the Volume of Water

The soil structure constitutive relationship is not sufficient to completely describe the volume changes in an unsaturated soil. Either an air or water phase constitutive relation must be formulated. It is suggested that the water phase is most suitable for formulating the second constitutive relationship. The water phase constitutive relation describes the change in the volume of water present in the referential soil structure element under various stress conditions. The water itself is assumed to be incompressible, and the equation accounts for the net inflow or outflow from the element. The water phase constitutive relation can be formulated in a semi-empirical manner on the basis of a linear combination of the stress state variables. In an incremental form, the constitutive equation can be written as: –

$$\frac{dV_w}{V_o} = \frac{3}{E_w} d(\sigma_{mean} - u_a) + \frac{d(u_a - u_w)}{H_w} \quad (15)$$

where

E_w = water volumetric modulus associated with a change in $(\sigma - u_a)$, and

H_w = water volumetric modulus associated with a change in $(\sigma - u_w)$.

The summation of water volume changes at each increment gives the final change in the volume of water: –

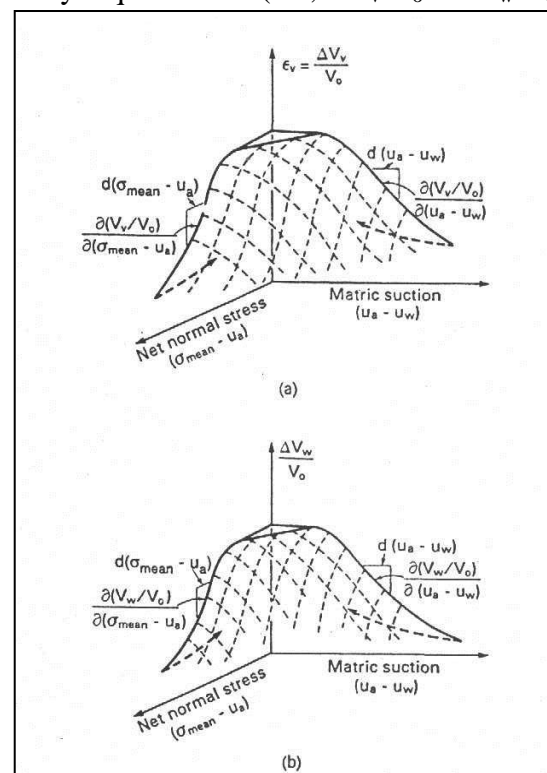
$$\frac{\Delta V_w}{V_o} = \frac{\sum dV_w}{V_o} \quad (16)$$

Change in the Volume of Air

The change in the volume of air in an element can be computed as the difference between the soil structure and water volume changes. The continuity requirements (i.e., $\Delta V_v/V_o = \Delta V_w/V_o + \Delta V_a/V_o$) can also be written in an incremental form using the volumetric strain change, $d\epsilon_v$: –

$$d\epsilon_v = \frac{dV_w}{V_o} + \frac{dV_a}{V_o} \quad (17)$$

The constitutive relationships for an unsaturated soil can be presented graphically in the form of constitutive surfaces (figure 2). The deformation state variable is plotted with respect to the $(\sigma_{mean} - u_a)$ and $(u_a - u_w)$ stress state variables. The coefficients used in the constitutive equations are the slopes of the constitutive surface at a point. The slopes are with respect to both axes. For example, the slopes of the soil structure constitutive surface at a point are equal to $(3(1-2\mu)/E)$ and $(3/H)$ with respect to the $(\sigma_{mean} - u_a)$



and $(u_a - u_w)$ axes, respectively. The coefficients on the constitutive surface are referred to as “volumetric deformation coefficients”. These coefficients vary from one stress state to another for a curved constitutive surface. Similarly, the slopes on the water phase constitutive surface at a point are $(3/E_w)$ and $(1/H_w)$ with respect to the $(\sigma_{\text{mean}} - u_a)$ and $(u_a - u_w)$ axes, respectively.

The above constitutive relations can be formulated for a general, three-dimensional loading in the x-, y-, and z-directions.

Plane Strain Loading

Many geotechnical problems can be simplified into a two-dimensional form using the concept of plane strain or plane stress loading. If an earth structure is significantly long in one direction (e.g., the z-direction) in comparison to the other two directions (e.g., the x- and y-directions) and the loadings are applied only on the x- and y-planes, the structure can be modeled as a plane strain problem. The slope stability, retaining wall, and strip footing are problems commonly analyzed by assuming plane strain loading conditions. For plane strain conditions, the soil deformation in the z-direction is assumed to be negligible ($d\varepsilon_z=0$). Imposing a condition of zero strain in the z-direction in equation 9 gives: –

$$d(\sigma_z - u_a) = \mu d(\sigma_x + \sigma_y - 2u_a) - (E/H)d(u_a - u_w) \quad (18)$$

Volumetric strain during plane strain loading is obtained by substituting equation (18) into equation (11): –

$$d\varepsilon_v = \frac{2(1+\mu)(1-2\mu)}{E} d(\sigma_{\text{ave}} - u_a) + 2\left(\frac{1+\mu}{H}\right) d(u_a - u_w) \quad (19)$$

where

σ_{ave} = average total normal stress for two-dimensional loading (i.e., $(\sigma_x + \sigma_y)/2$).

Equation 19 can be used as the soil structure constitutive relation for plane strain loading.

The water phase constitutive equation is obtained from equation 15 by replacing the $d(\sigma_z - u_a)$ term with equation 18: –

$$\frac{dV_w}{V_o} = 2\left(\frac{1+\mu}{E_w}\right) d(\sigma_{\text{ave}} - u_a) + \left\{ \frac{1}{H} - \frac{(E/H)}{E_w} \right\} d(u_a - u_w) \quad (20)$$

FIELD EQUATIONS AND EQUILIBRIUM ANALYSIS OF AN UNSATURATED SOIL ELEMENT :-

The state of stress at a point in an unsaturated soil can be analyzed using a cubical element of infinitesimal dimensions. Figure 3 illustrates the total normal and shear stresses that act on the boundaries of the soil element. The gravitational force, ρg , (i.e., soil density, ρ , times gravitational acceleration, g) is a body force. The gravitational force acts through the centroid of the element, but is not shown in figure 3 in order to maintain simplicity.

Fig. 2

Three-dimensional constitutive surfaces for an unsaturated soil.

a) soil structure constitutive surface;

b) water phase constitutive surface.

(After Fredlund and Rahardjo, 1993)

The equilibrium analysis of a soil element is based upon the conservation of linear momentum. The conservation of linear momentum can be applied to the soil element in figure 3 by summing forces first in the y-direction.

$$\left(\frac{\partial \tau_{xy}}{\partial x} + \frac{\partial \sigma_y}{\partial y} + \frac{\partial \tau_{zy}}{\partial z} + \rho g \right) dx dy dz = 0 \quad (21)$$

where

- τ_{xy} = shear stress on the x-plane in the y-direction,
- σ_y = total normal stress on the y-plane,
- τ_{zy} = shear stress on the z-plane in the y-direction,
- ρ = total density of the soil,
- g = gravitational acceleration, and
- dx, dy, dz = dimensions of the element in the x-, y-, and z-directions respectively.

Since the soil element does not undergo acceleration, the right hand side of equation (21) becomes zero.

Equation (21) is commonly referred to as the equilibrium equation for the y-direction. Similarly, equilibrium equations can be derived for the x-direction: –

$$\left(\frac{\partial \sigma_x}{\partial x} + \frac{\partial \tau_{yx}}{\partial y} + \frac{\partial \tau_{zx}}{\partial z} \right) dx dy dz = 0 \quad (22)$$

Moreover, for the z-direction: –

$$\left(\frac{\partial \tau_{xz}}{\partial x} + \frac{\partial \tau_{yz}}{\partial y} + \frac{\partial \sigma_z}{\partial z} \right) dx dy dz = 0 \quad (23)$$

Total or Overall Equilibrium

Total equilibrium refers to the force equilibrium of a complete soil element with its four phases (i.e., air, water, contractile skin, and soil particles). The total stress fields of an unsaturated soil element in the x-, y- and z-directions are presented in figure 4 with the exception that no body forces are shown (i.e., gravitational force, ρg). Only the equilibrium in the y-direction will be analyzed and presented. However, the same principles apply to equilibrium in the x- and z-directions. Figure 4 depicts the total stress fields in the y-direction. The force equilibrium equation associated with figure 4 is given in equation (21).

The water phase equilibrium in the y-direction is obtained by summing forces in the y-direction which gives the equilibrium equation for the water phase.

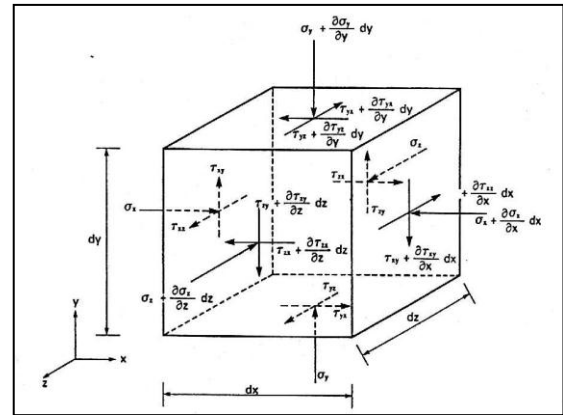


Fig. 3
Normal and shear stresses on a cubical soil element of infinitesimal dimensions.

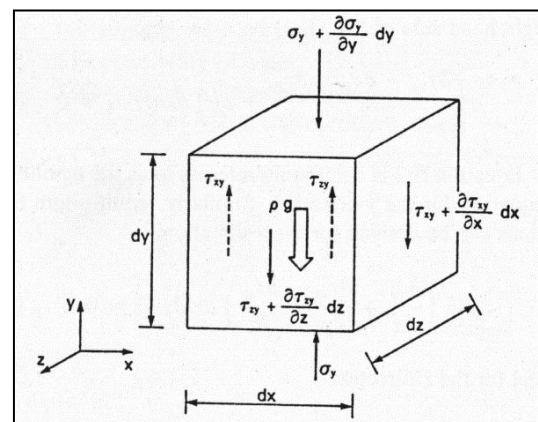


Fig. 4
Components for total equilibrium in the y-direction for an unsaturated soil element

$$\left(n_w \frac{\partial u_w}{\partial y} + n_w \rho_w g + F_{sy}^w + F_{cy}^w \right) dx dy dz = 0 \quad (24)$$

where

u_w = pore-water pressure,

F_{sy}^w = interaction force (i.e., body force) between the water phase and the soil particles in the y-direction, and

F_{cy}^w = interaction force (i.e., body force) between the water phase and the contractile skin in the y-direction.

The air phase equilibrium in the y-direction is obtained by summing the forces in the y-direction which gives the equilibrium equation for the air phase.

$$\left(n_a \frac{\partial u_a}{\partial y} + n_a \rho_a g + F_{sy}^a + F_{cy}^a \right) dx dy dz = 0 \quad (25)$$

where

u_a = pore-air pressure,

F_{sy}^a = interaction force (i.e., body force) between the air phase and the soil particles in the y-direction, and

F_{cy}^a = interaction force (i.e., body force) between the air phase and the contractile skin in the y-direction.

Contractile Skin Equilibrium

The contractile skin is only a few molecular layers in thickness. However, its presence affects the equilibrium conditions in an unsaturated soil. This is due to its ability to exert a surface tension, T_s .

The equilibrium equation for the contractile skin is as follows:

$$\left\{ -n_c \frac{\partial f^*}{\partial y} (u_a - u_w) - n_c f^* \frac{\partial (u_a - u_w)}{\partial y} + n_c \rho_c g - F_{cy}^w - F_{cy}^a \right\} dx dy dz = 0 \quad (26)$$

f^* = final interaction between the contractile skin and the soil structure equilibrium

Final Form of Equilibrium Equation

To obtain the final form of the differential equations, some simplifications and assumptions, need to be made, which are: –

1. For two-dimensional analysis, consider the equilibrium of forces that acts in the x-, and y-directions only, and neglect the equilibrium of forces that acts in the z-direction.
2. The value of contractile skin porosity (n_c) is considered very small and approaches to zero in comparison with other values of porosities (i.e., n_s , n_w , and n_a). So $n_c \approx 0$.

The equilibrium equation will be written as: –

$$\frac{\partial(\sigma_x - u_a)}{\partial x} + n_w \frac{\partial(u_a - u_w)}{\partial x} + \frac{\partial\tau_{yx}}{\partial y} + n_s \frac{\partial u_a}{\partial x} - F_{sx}^w - F_{sx}^a = 0 \quad (27)$$

$$\frac{\partial\tau_{xy}}{\partial x} + \frac{\partial(\sigma_y - u_a)}{\partial y} + n_w \frac{\partial(u_a - u_w)}{\partial y} + n_s \frac{\partial u_a}{\partial y} + n_s \rho_s g - F_{sy}^w - F_{sy}^a = 0 \quad (28)$$

Mass Transfer

The volume of water entering and leaving the element in y-direction is: –

$$\frac{\partial V_w}{\partial t} = \left(v_w + \frac{\partial v_w}{\partial y} dy \right) dx dz - v_w dx dz \quad (29)$$

where

∂V_w = change in the volume of water in the soil element over a specific time dt ,

$\partial V_w / \partial t$ = net flux of water through the soil element,

v_w = water flow rate across a unit area of the soil element in the y-direction, and

dx, dy, dz = infinitesimal dimensions in the x-, y-, and z-directions, respectively.

The water volume change with respect to time could be written as: –

$$\begin{aligned} \frac{\partial(V_w/V_o)}{\partial t} = & -\frac{k_{wy}}{\rho_w g} \frac{\partial^2 u_w}{\partial y^2} - D_{atm} v \alpha \theta_a \frac{\omega_v}{RT} \frac{\partial}{\partial y} \left(\frac{\partial \bar{u}_v}{\partial y} \right) - \frac{\partial}{\partial y} \left(D_{Tliq} \frac{\partial T}{\partial y} \right) \\ & - \frac{1}{\rho_w g} \frac{\partial k_{wy}}{\partial y} \frac{\partial u_w}{\partial y} - \frac{\partial k_{wy}}{\partial y} \end{aligned} \quad (30)$$

where

k_{wy} = coefficient of permeability with respect to water as a function of matrix suction which varies with location in the y-direction [i.e., $k_{wy}(u_a - u_w)$],

ω_i = molecular mass of the diffusing constituent,

R = universal (molar) gas constant,

T = absolute temperature,

D_{atm} = is the molecular diffusivity of water vapor in air, $\text{cm}^2 \text{sec}^{-1}$, D_{atm} could be

obtained by applying the equation $D_{atm} = 5.893 \times 10^{-6} T^{2.3} / u_a$ (31)

α = the tortuosity factor allowing for extra path length (~ 0.66),

v = is the mass flow factor introduced to allow for the mass flow of vapor arising from the difference in boundary conditions governing the air and vapor components of the diffusion system.

$$v = \frac{u_a}{(u_a - u_v)} \quad (32)$$

θ_a = volumetric air content which describes the area available for the vapor to flow, and is equal to $(1-S)$ n.

The water phase constitutive relation for plane strain conditions describes the time derivative of the water volume change as: –

$$\frac{d(V_w/V_o)}{dt} = \left(\frac{1+\mu}{E_w} \right) \frac{d}{dt} (\sigma_x + \sigma_y - 2u_a) + \left\{ \frac{1}{H_w} - \frac{(E/H)}{E_w} \right\} \frac{d}{dt} (u_a - u_w) \quad (33)$$

Equating with equation (30) gives: –

$$\begin{aligned} \left(\frac{1+\mu}{E_w} \right) \frac{d}{dt} (\sigma_x + \sigma_y - 2u_a) + \left\{ \frac{1}{H_w} - \frac{(E/H)}{E_w} \right\} \frac{d}{dt} (u_a - u_w) = & -\frac{k_{wy}}{\rho_w g} \frac{\partial^2 u_w}{\partial y^2} - D_{atm} v \alpha \theta_a \frac{\omega_v}{RT} \frac{\partial}{\partial y} \left(\frac{\partial \bar{u}_v}{\partial y} \right) \\ & - \frac{\partial}{\partial y} \left(D_{Tliq} \frac{\partial T}{\partial y} \right) - \frac{1}{\rho_w g} \frac{\partial k_{wy}}{\partial y} \frac{\partial u_w}{\partial y} - \frac{\partial k_{wy}}{\partial y} \end{aligned} \quad (34)$$

For the case of nearly saturated soils, the second term on the right hand side does not exist, because air will be entrapped as bubbles in the water. Therefore, there is no continuous path for the air phase to move from one place to another. Consequently, there is no vapor movement, as a result, there is no contribution of water vapor to the water mass transfer, so, this term can be omitted for nearly saturated soils. For homogeneous soil, the terms containing $\partial k_{wy}/\partial y$ are equal to zero, so the fourth and fifth terms on the right hand side vanish. In addition to the assumptions mentioned, it is assumed that the water density remains constant (incompressible) and the thermal liquid diffusivity also remains constant. The equation of two-dimensions can be written as:–

$$\begin{aligned} m_1^w \frac{d}{dt} \left(\frac{\sigma_x + \sigma_y}{2} - u_a \right) + m_2^w \frac{d}{dt} (u_a - u_w) = \\ - \frac{1}{\rho_w g} \left[k_{wx} \frac{\partial^2 u_w}{\partial x^2} + k_{wy} \frac{\partial^2 u_w}{\partial y^2} \right] - D_{Tliqx} \frac{\partial^2 T}{\partial x^2} - D_{Tliqy} \frac{\partial^2 T}{\partial y^2} \end{aligned} \quad (35)$$

Air Flow Differential Equation

The air phase is compressible and flows in response to an air pressure gradient and a concentration gradient. Therefore, the flow of air through a referential element of unsaturated soil is computed in terms of mass rate of air flow, J_a . The net mass rate of air flow across the element is obtained as the difference between the mass rate of air entering and leaving the element within a period of time: –

$$\frac{\partial M_a}{\partial t} = \left(J_a + \frac{\partial J_a}{\partial y} dy \right) dx dz - J_a dx dz \quad (36)$$

where

$\partial M_a / \partial t$ = net mass rate of air flowing through the soil element, and

J_a = mass rate of air flowing across a unit area of the soil.

The net mass rate of air flow can be expressed for a unit volume of the soil elements as: –

$$\frac{\partial M_a}{\partial t} = \frac{\partial J_a}{\partial y} dy dx dz \quad (37)$$

or

$$\frac{\partial (M_a/V_o)}{\partial t} = \frac{\partial J_a}{\partial y} \quad (38)$$

where

$\partial (M_a/V_o) / \partial t$ = net mass rate of air flow per unit volume of the element, and

V_o = initial total volume of the element ($dx dy dz$).

According to Fick's law (Hillel, 1971): –

$$J_a = -D_a \frac{\partial C}{\partial y} \quad (39)$$

where

J_a = mass rate of air flowing across a unit area of the soil,

D_a = transmission constant for air flow through a soil,

C = concentration for the air expressed in terms of the mass of air per unit volume of soil, and

$\partial C / \partial y$ = concentration gradient in the y direction.

The negative sign indicates that air flows in the direction of decreasing concentration gradient.

The change of air volume could be described as: –

$$\frac{\partial (V_a/V_o)}{\partial t} = -\frac{1}{\rho_{ao}} D_a^* \nabla^2 u_a - \frac{1}{\rho_{ao}} \left(\frac{\partial u_a}{\partial x} \frac{\partial D_a^*}{\partial x} + \frac{\partial u_a}{\partial y} \frac{\partial D_a^*}{\partial y} \right) - \frac{(1-S)n}{\bar{u}_{ao}} \frac{\partial \bar{u}_a}{\partial t} + \frac{(1-S)n}{T} \frac{\partial T}{\partial t} \quad (40)$$

From the constitutive relation, the change of air volume could be described as: –

$$\frac{dV_a}{V_o} = \frac{d(\sigma_x - u_a)}{E_a} + \frac{d(\sigma_y - u_a)}{E_a} + \frac{d(\sigma_z - u_a)}{E_a} + \frac{d(u_a - u_w)}{H_a} \quad (41)$$

Simplifying yields: –

$$\frac{d(V_a/V_o)}{dt} = (m_1^s - m_1^w) \frac{d}{dt} \left(\frac{\sigma_x + \sigma_y}{2} - u_a \right) + (m_2^s - m_2^w) \frac{d}{dt} (u_a - u_w) \quad (42)$$

Now, equating and simplifying yields: –

$$\begin{aligned} (m_1^s - m_1^w) \frac{d}{dt} \left(\frac{\sigma_x + \sigma_y}{2} - u_a \right) + (m_2^s - m_2^w) \frac{d}{dt} (u_a - u_w) &= -\frac{1}{\rho_{ao}} D_a^* \nabla^2 u_a \\ -\frac{1}{\rho_{ao}} \left(\frac{\partial u_a}{\partial x} \frac{\partial D_a^*}{\partial x} + \frac{\partial u_a}{\partial y} \frac{\partial D_a^*}{\partial y} \right) &- \frac{(1-S)n}{\bar{u}_{ao}} \frac{\partial \bar{u}_a}{\partial t} + \frac{(1-S)n}{T} \frac{\partial T}{\partial t} \end{aligned} \quad (43)$$

The above derivation is valid when the degree of saturation is below about 90%, where continuous paths for the air phase exist to transfer from one place to another.

For the special case of unsaturated soils where the degree of saturation is about >90%, the air phase exists in the form of occluded bubbles and cannot transfer easily, the air transfer takes place by diffusion.

When the air diffuses in the water (as dissolved air in the water phase due to its pressure), the water phase plays a big role in the transport mechanism for the air phase. When the dissolved air reaches a suitable environment (where the air pressure is less), air is freed from the water phase to its original form. The derivation of the continuity equation for this condition is slightly different.

Air Diffusion Through Water

Fick's law can be used to describe the diffusion process. The concentration gradient, which provides the driving potential for the diffusion process is expressed with respect to the soil voids (i.e., air and water phases). In other words, the mass rate of diffusion and the concentration gradient are expressed with respect to a unit area and a unit volume of the soil voids, respectively.

The formulation of Fick's law for diffusion in the y-direction is as follows: –

$$\frac{\partial M}{\partial t} = -D \frac{\partial C}{\partial y} \quad (44)$$

where

$\partial M / \partial t$ = mass rate of the air diffusing across a unit area of the soil voids,

D = coefficient of diffusion,

C = concentration of the diffusing air expressed in terms of mass per unit volume of the soil voids, and

$\partial C / \partial t$ = concentration gradient in the y-direction (or similarly in the x- or z-directions).

The diffusion equation can appear in several forms, similar to the forms presented for the flow of air through a porous medium. The concentration gradient for gases or water vapor (i.e., $\partial C / \partial y$) can be expressed in terms of their partial pressures. Consider a constituent diffusing through the pore-water in a soil. Equation (44) can be rewritten with respect to the partial pressure of the diffusing constituent: –

$$\frac{\partial M}{\partial t} = -D \frac{\partial C}{\partial \bar{u}_i} \frac{\partial \bar{u}_i}{\partial y} \quad (45)$$

where

\bar{u}_i = partial pressure of the diffusing constituent,

$\partial C / \partial \bar{u}_i$ = change in concentration with respect to a change in partial pressure, and

$\partial \bar{u}_i / \partial y$ = partial pressure gradient in the y-direction (or similarly in the x- or z-directions).

Simplifying for two-dimensions will yield: –

$$\frac{\partial (V_a / V_o)}{\partial t} = -\frac{Dh}{\bar{u}_{ao}} \left(\frac{\partial^2 \bar{u}_a}{\partial x^2} + \frac{\partial^2 \bar{u}_a}{\partial y^2} \right) + \frac{Dh}{T_o} \left(\frac{\partial^2 T}{\partial x^2} + \frac{\partial^2 T}{\partial y^2} \right) \quad (46)$$

Equating this expression to the expression in equation 42 yields: –

$$(m_1^s - m_1^w) \frac{d}{dt} \left(\frac{\sigma_x + \sigma_y}{2} - u_a \right) + (m_2^s - m_2^w) \frac{d}{dt} (u_a - u_w) = - \frac{Dh}{\bar{u}_{ao}} \left(\frac{\partial^2 \bar{u}_a}{\partial x^2} + \frac{\partial^2 \bar{u}_a}{\partial y^2} \right) + \frac{Dh}{T_o} \left(\frac{\partial^2 T}{\partial x^2} + \frac{\partial^2 T}{\partial y^2} \right) \quad (47)$$

Heat transfer

The Fourier diffusion equation can be used to describe heat transfer in soils. For one-dimensional flow, the heat flux can be described as: –

$$H = \lambda \frac{\partial T}{\partial y} \quad (48)$$

where

H = heat flux,

λ = thermal conductivity, and

T = temperature.

The heat transfer can be due to conduction, convection, and radiation. In soil, convection and radiation are considered to be negligible (Philip and de Vries, 1957; Lewis and Schrefler, 1987; Edgar et al., 1989; Al-Khaddar, 2000). So the conduction term is considered, in addition to the heat lost due to evaporation of water. This could be described as: –

$$\zeta \frac{\partial T}{\partial t} = \frac{\partial}{\partial y} \left(\lambda \frac{\partial T}{\partial y} \right) - L_v \frac{\partial}{\partial y} \left(D_v \frac{\partial u_v}{\partial y} \right) \quad (49)$$

where

ζ = volumetric specific heat of the soil as a function of water content (J/m³/°C), and

L_v = latent heat of vaporization of water (i.e., 2418000 J/kg).

5. Finite Element Equations :-

Using the method of weighted residuals on equations (27), (28), (35), (47), and (49), a discretized finite element form is reached (Zainal, 2002). The final equations are obtained after simplifying as:-

$$[K] \frac{\partial \mathbf{u}}{\partial t} + [L] \frac{\partial \mathbf{u}_a}{\partial t} + [M] \frac{\partial \mathbf{u}_w}{\partial t} = [\mathbf{f}] \quad \dots(50)$$

$$[W1] \frac{\partial \mathbf{u}}{\partial t} + [W2] \frac{\partial \mathbf{u}_a}{\partial t} + [W3] \frac{\partial \mathbf{u}_w}{\partial t} + [KW] \mathbf{u}_w + [UT] \mathbf{T} = [FW] \quad \dots(51)$$

$$[A1'] \frac{\partial \mathbf{u}}{\partial t} + [A2'] \frac{\partial \mathbf{u}_a}{\partial t} + [A3'] \frac{\partial \mathbf{u}_w}{\partial t} + [KAUa] \mathbf{u}_a = \mathbf{FA}' \quad \dots(52)$$

$$[T1] \frac{\partial \mathbf{T}}{\partial t} + [KH] \mathbf{T} = [\mathbf{FH}] \quad \dots(53)$$

or in matrix form, the equations are represented as:-

$$\begin{bmatrix} K & M & L & 0 \\ W1 & W3 & W2 & 0 \\ A1' & A3' & A2' & 0 \\ 0 & 0 & 0 & T1 \end{bmatrix} \frac{\partial}{\partial t} \begin{Bmatrix} \mathbf{u} \\ \mathbf{u}_w \\ \mathbf{u}_a \\ \mathbf{T} \end{Bmatrix} + \begin{bmatrix} 0 & 0 & 0 & 0 \\ 0 & KW & 0 & UT \\ 0 & 0 & KAUa & 0 \\ 0 & 0 & 0 & KH \end{bmatrix} \begin{Bmatrix} \mathbf{u} \\ \mathbf{u}_w \\ \mathbf{u}_a \\ \mathbf{T} \end{Bmatrix} = \begin{Bmatrix} \mathbf{f} \\ \mathbf{FW} \\ \mathbf{FA}' \\ \mathbf{FH} \end{Bmatrix} \quad \dots(54)$$

After discretization in time domain, the equations are represented as:–

$$\begin{aligned}
 & \begin{bmatrix} [K] & [M] & [L] & 0 \\ [W1] & [W3] + \alpha \Delta t [KW] & [W2] & \alpha \Delta t [UT] \\ [A1'] & [A3'] & [A2'] + \alpha \Delta t [KAUa] & \alpha \Delta t [KAT] \\ 0 & 0 & 0 & [T1] + [KH] \alpha \Delta t \end{bmatrix}_{k,\alpha} \begin{Bmatrix} u \\ u_w \\ u_a \\ T \end{Bmatrix}_{t_k + \Delta t_k} = \\
 & \begin{bmatrix} [K] & [M] & [L] & 0 \\ [W1] & [W3] - (1 - \alpha) \Delta t [KW] & [W2] & -(1 - \alpha) \Delta t [UT] \\ [A1'] & [A3'] & [A2'] - (1 - \alpha) \Delta t [KAUa] & -(1 - \alpha) \Delta t [KAT] \\ 0 & 0 & 0 & [T1] - (1 - \alpha) \Delta t [KH] \end{bmatrix}_{k,\alpha} \begin{Bmatrix} u \\ u_w \\ u_a \\ T \end{Bmatrix}_{t_k} \\
 & + \begin{Bmatrix} [f] \\ [FW] \\ [FA'] \\ [FH] \end{Bmatrix} \Delta t_k \quad \dots(55)
 \end{aligned}$$

Appendix (A) gives the definitions for the matrices encountered in equations 50 to 55. A finite element program is set to deal with solving equation 55 (Zainal, 2002), the results of which are presented in the next section.

Problem Description

The Mdaina trial embankment was constructed in the southern part of Iraq at Al-Basrah province in 1979. The height of the embankment is 5 meters, the width at the top is 12 meters, and the width at the bottom is 37 meters with side slopes of 2.5:1.

Figure 5 shows the cross section that has been adopted for this analysis. For more details, refer to Penman and Burford (1983).

Figure 6 shows the finite element discretization using quadratic quadrilateral of the serendipity type element. This figure shows the right half of the embankment where the height is 5 meters, the top width is 6 meters, and the bottom width is 18.5 meters.

Due to symmetry, the analysis of the left half is assumed to be identical to the analysis of the right half. A one way drainage condition is assumed because of the clayey soil underneath the embankment and the open surface from above.

Material properties shown in table 1 are after Al-Hamrany (1980) and Appendix (B). The thermal degrees are taken depending on the thermal map of Iraq for dry and wet seasons. Temperature is taken for the dry season as 35.8 °C for the upper part of the embankment, and 32 °C for the lower part of the embankment (Zainal, 2002).

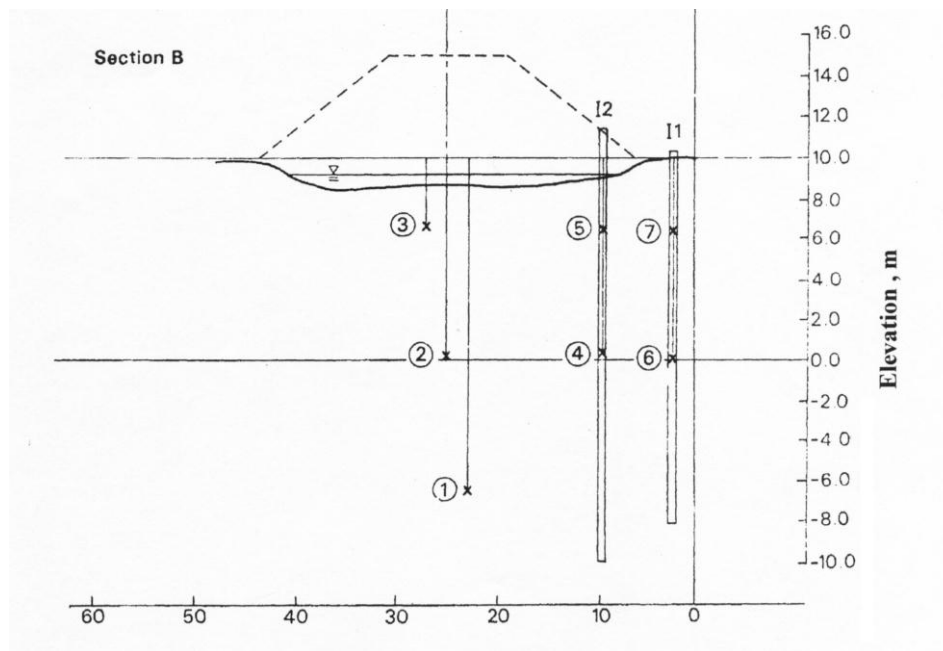


Fig 5
Cross-section of the Mdaina trial embankment

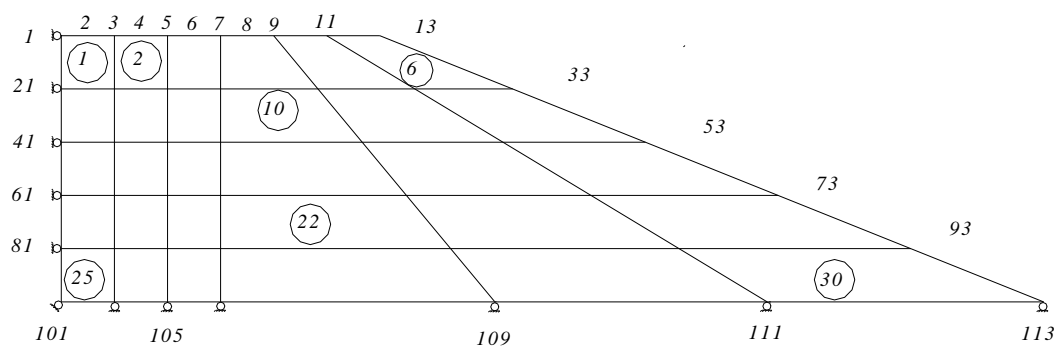


Fig6
Discretized cross section for the finite element
method for half of the Mdaina trial embankment

Soil temperature under 1.0 m depth is considered to be the same as for the 1.0 m depth without a significant loss of accuracy (Al-Khaddar, 2000).

The degree of saturation was assumed 0.95 under the assumption that for clayey soils (like the kind of soils used for this embankment) water may reach a large height due to capillarity. Hence, the soil becomes nearly saturated.

Table 1
Material Properties for the Mdaina Consolidation Problem

Property	Value	Units
Modulus of elasticity E	2870	kN/m ²
Poisson's ratio	0.4	—
Solubility of air in water	0.01708	—
Porosity	50 %	—
Thermal conductivity, λ	72.3168	kJ/°C m day
Degree of saturation, S	90 %	—
Molecular mass of air, ω_a	28.966	kg/kmol
Hydraulic conductivity, k_w	5.76×10^{-8}	cm/sec
Universal gas constant, R	8.31432	J/mol °K
Coefficient of Diffusion, D	1.728×10^{-4}	m ² /day
Volumetric specific heat capacity of the soil solids, ζ_s	2.235×10^6	J/m ³ /°C
Volumetric specific heat capacity of the soil solids, ζ_w	4.154×10^6	J/m ³ /°C
Temperature coefficient of surface tension of water, γ	-2.09×10^{-3}	—

This section is intended to demonstrate the application of the coupled differential equations that were derived previously for two-dimensional consolidation of a saturated soil.

An isoparametric quadrilateral element of the serendipity type is used in solving this problem by the finite element method. An eight-noded element is used for all degrees of freedom, which are: —

1. displacement in the y-direction,
2. pore water pressure u_w ,
3. pore air pressure u_a , and
4. temperature.

A special computer program was designed and implemented to solve this problem. A FORTRAN 90 compiler was used (Power Station) due to its ease when dealing with large matrices and equation solving facilities.

Results

Results of the non-isothermal consolidation of the trial embankment under its self weight are shown in figures 7 to 11.

Figure 7 shows the temperature variation for various nodes at the centerline of the embankment. Figures 8a, b, and c show the temperature distribution inside the embankment after 1, 10, and 100 days, respectively.

Figures 9a, b, and c show the variation of the pore-water pressure at different time factors (for the water phase) $T_{vw} = 0.1$, $T_{vw} = 0.5$, and $T_{vw} = 0.9$.

Figures 10a, b, and c show the variation of the pore-air pressure at different time factors (for the air phase) $T_{va} = 0.1$, $T_{va} = 0.5$, and $T_{va} = 0.9$.

Figure 11 shows the vertical displacement of various nodes at the centerline of the embankment.

The figures mentioned can be used to describe an elementary analysis of the consolidation behavior for the partially saturated embankment under its own self-weight.

Discussion

Figure 7 shows the temperature variation for various nodes at the centerline of the embankment. The difference between the surface of the embankment and its base is already small (less than 4 °C). After about 500 days, the difference is less than 1 °C.

This means that the increase in the water and air pressures inside the embankment due to the increase in temperature can be assumed negligible after 500 days (for this case study). After that, water and air pressure dissipations are continued normally.

Figures 8a, b, and c show the gradual increase of the temperature inside the embankment. The contour lines in figure 8a shows little roughness due to variations in the assumed initial degrees of temperature at some nodes.

Figures 9a, b, and c show the water-pressure inside the embankment in terms of u_w/u_{wmax} (water pressure / maximum water pressure at 0.1 T_{vw}). The dissipation seems to be going smoothly with time (at different time factors for the water phase) as expected for the fully saturated soil.

Figures 10a, b, and c show the air-pressure inside the embankment in terms of u_a/u_{amax} (air pressure / maximum air pressure at 0.1 T_{va}).

The dissipation of the air pressure also seems to be going smoothly with time (at different time factors for the air phase).

At the early stages of consolidation, there is no obvious pattern of sudden increase in the pore-air pressure at specific places (as previously seen in the one-dimensional and two-dimensional problems that were analyzed earlier) (Al-Damluji et al., 2003).

This could be due to the lack of sufficient load that is considered to be the main cause of the increase in the pore-air pressure near the places of applied load. The only load used for this analysis is the self-weight.

Figure 11 shows the vertical displacement for some specified nodes at the centerline of the embankment. The displacement is represented as y/y_{max} (the displacement of the node / maximum displacement of the surface node).

It is noticed from this figure that the difference in the displacement is not constant even when the vertical distances between the nodes under consideration (nodes 1, 21, 41, 61, and 81 in figure 6) are constant (1 m).

This is due to the difference in the vertical load (self-weight) over a specified node (e.g., load over node 21 due to self-weight is much less than the load over node 81 due to self-weight). Obviously, this will make (for example) the difference in settlement between nodes 1 and 21 much less than the difference in settlement between nodes 61 and 81 (as seen in figure 11).

There is still a little initial compression in the air phase as seen by the values of the settlement at the

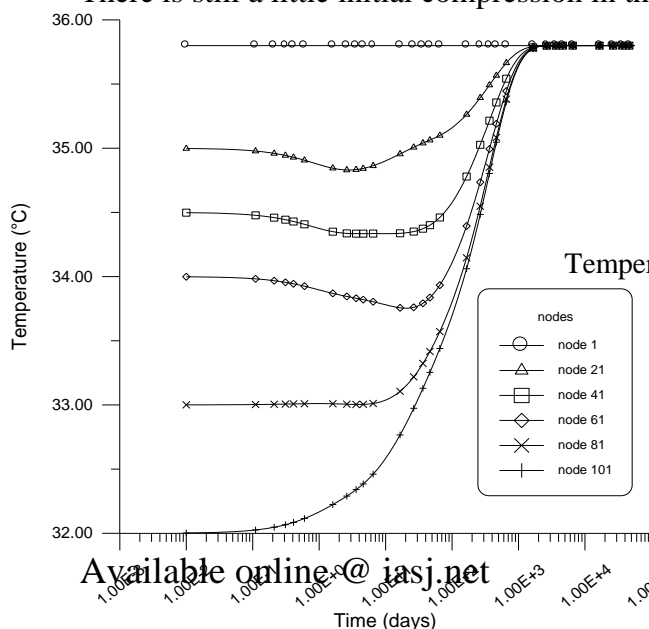


Fig 7

Temperature variation with time for different nodes at the center line

early stages of consolidation. This stage is followed by a descent in the rate of settlement due to air propagation through the soil, then after about 5 to 7 days, there is an increase in the rate of settlement and the consolidation process continues as usual.

The settlement may take longer time than expected due to the lack of enough loads that could accelerate the consolidation process.

Finally, this analysis should not be compared with any other analysis made before where the Mdaina embankment was assumed fully saturated there. This is due to that some of the parameters used in this analysis are assumed for demonstrative purposes.

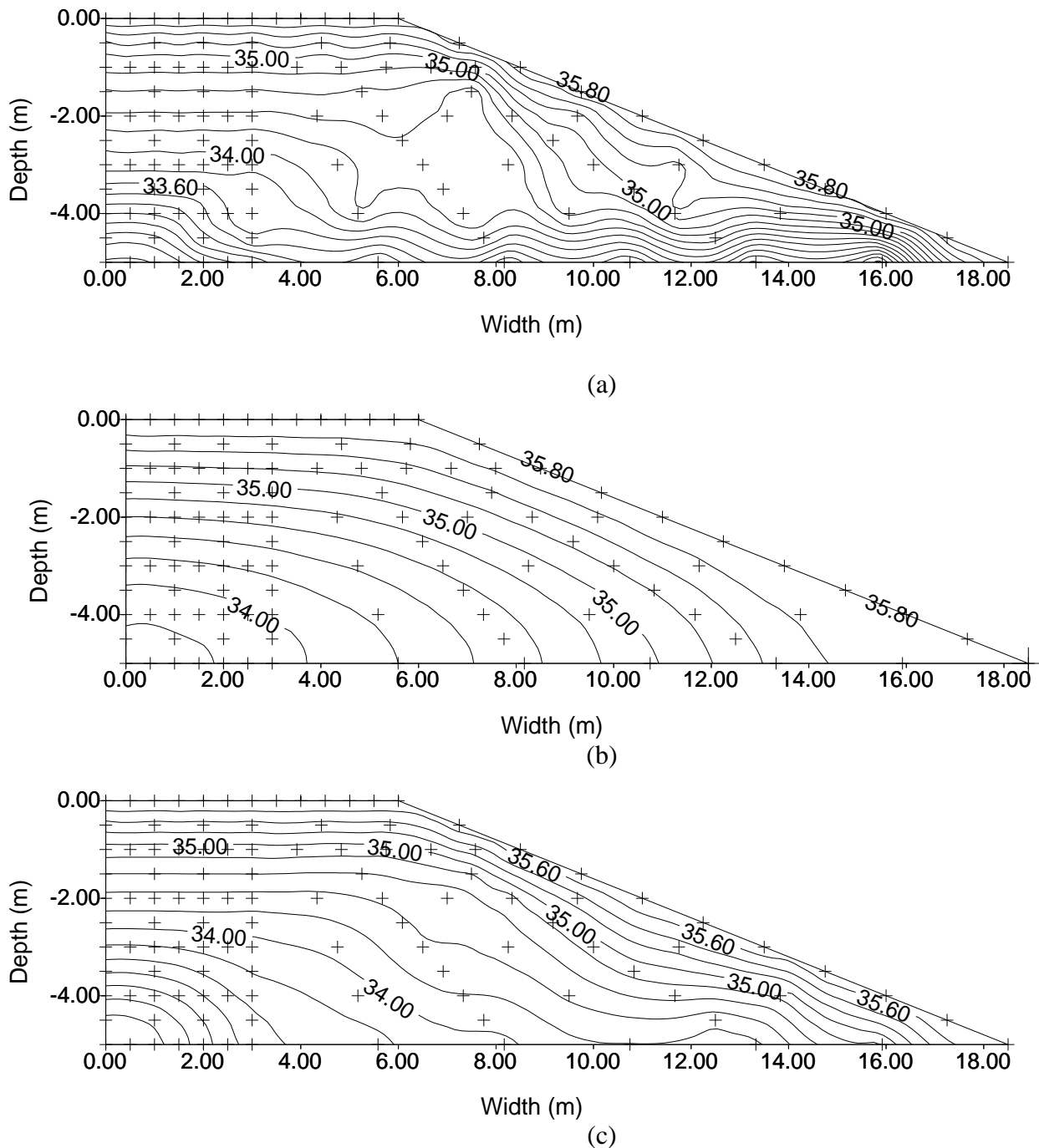
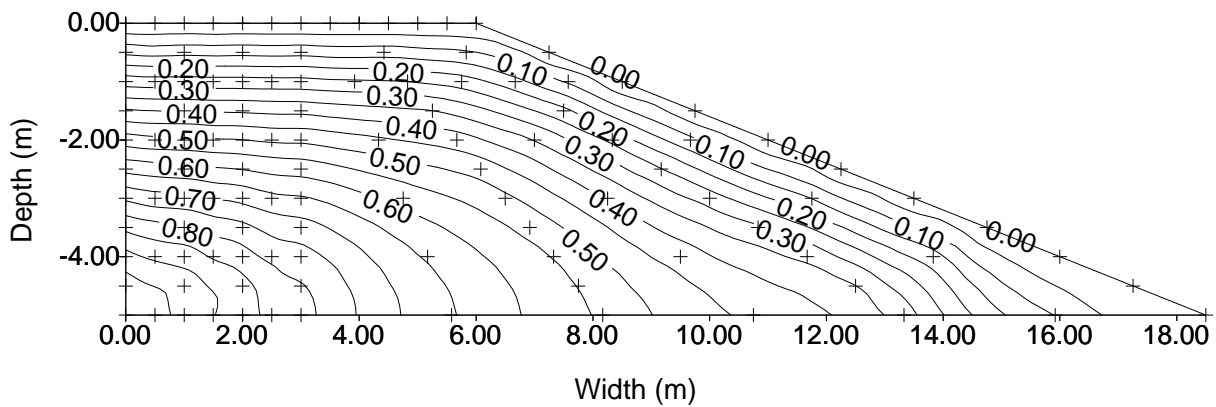
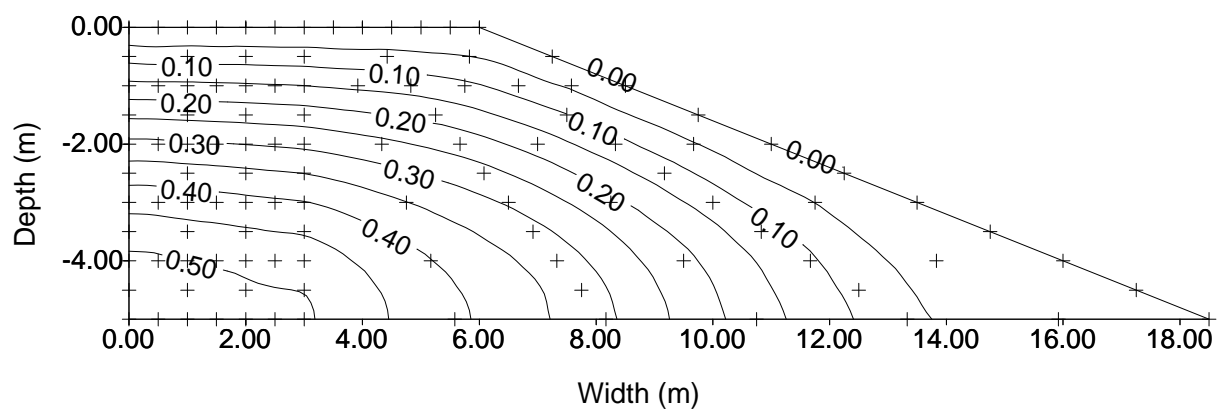


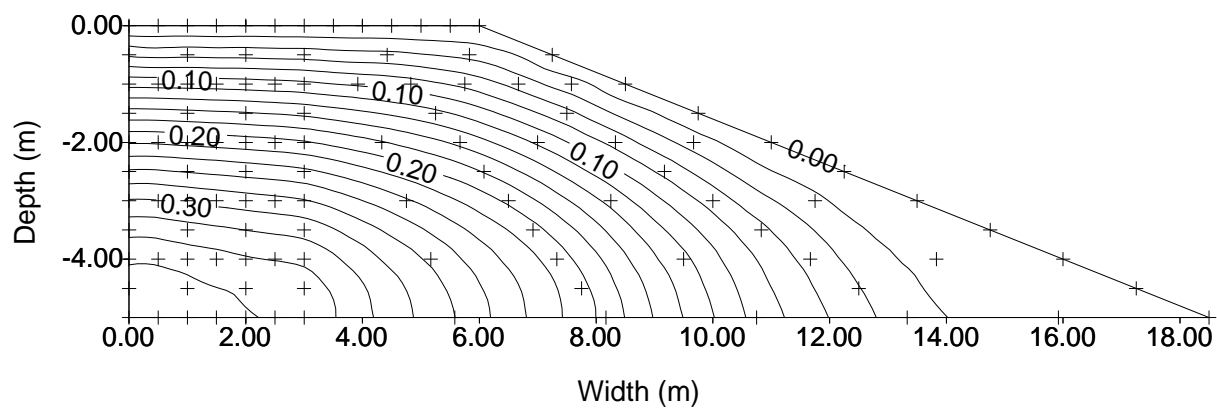
Fig 8
Temperature distribution in the embankment
a) after 1 day ; b) after 10 days; c) after 100 days



(a)



(b)



(c)

Fig 9Water pressure distribution, contour lines represent u_w/u_{wmax} a) at $T_{vw}=0.1$; b) at $T_{vw}=0.5$; c) at $T_{vw}=0.9$

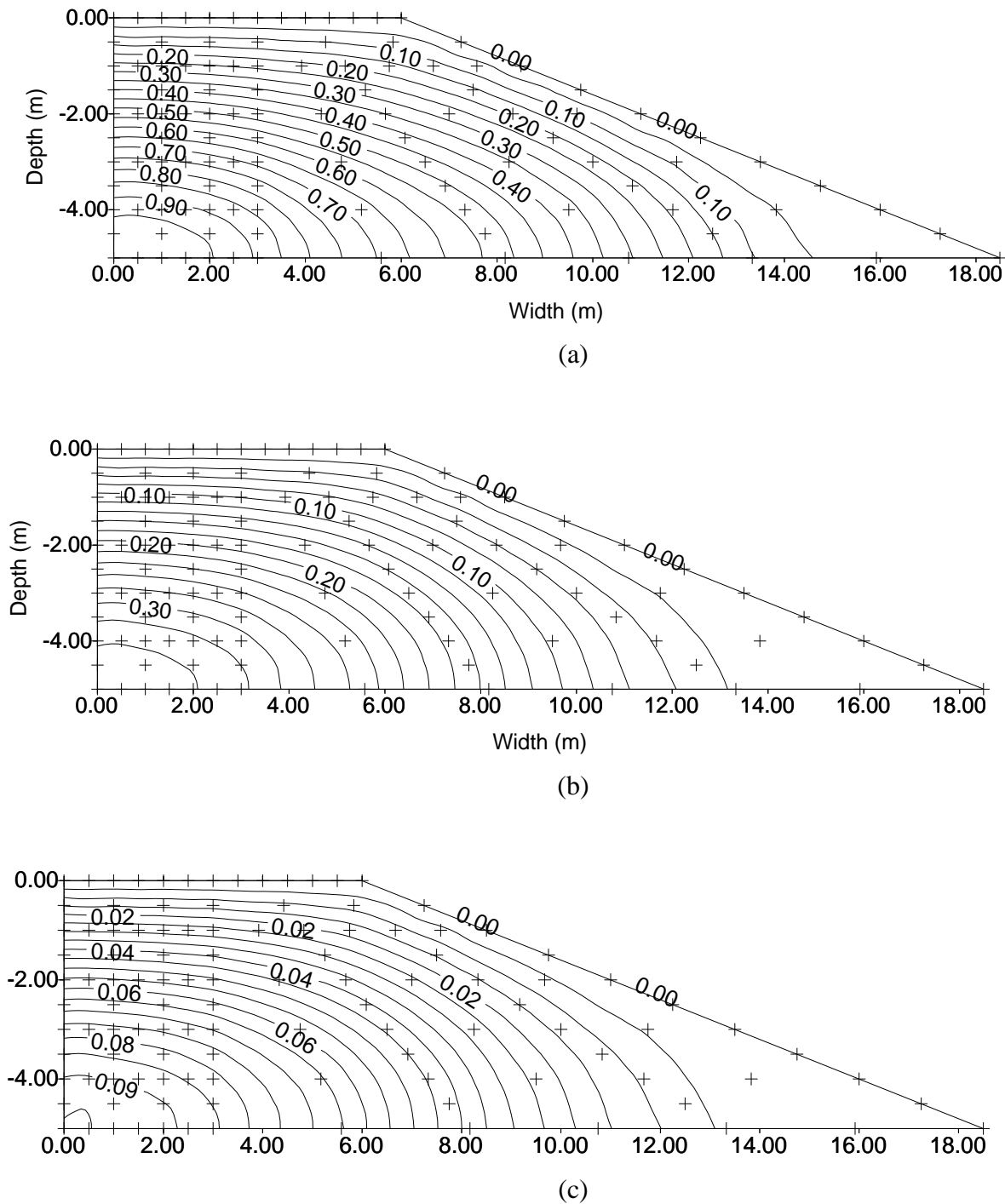
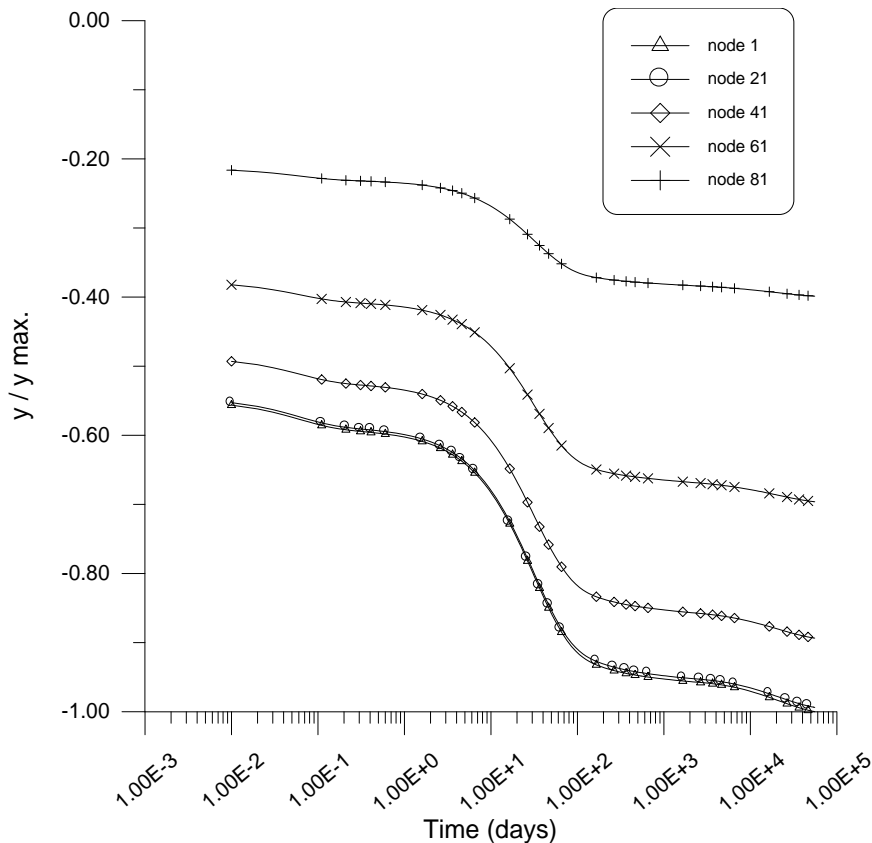


Fig 10

Air pressure distribution, contour lines represent u_a/u_{amax}

a) at $T_{va}=0.1$; b) at $T_{va}=0.5$; c) at $T_{va}=0.9$


Fig11

Vertical displacement for various nodes at the center line of the embankment

CONCLUSIONS

As the subject of modeling of partially saturated soils behavior is considered relatively new, many concluding ideas can be formed in different aspects regarding this regime. From the analysis and discussion of the consolidation problem for the embankment under its self weight, it is concluded that: –

1. The water-phase pressure dissipation behavior is the same as that for the classical consolidation process for ordinary loading.
2. The pore-air pressure dissipation takes the normal shape of the classical consolidation process. This was observed for a degree of saturation about 95%.
3. The vertical displacement for the partially saturated consolidation is nearly similar to the vertical displacement for the fully saturated condition. Except that after the first region (about 1 or 2 days) the vertical displacement begins to accelerate due to pore-air pressure dissipation.
4. Prediction of degree of consolidation is not due to pore-water pressure dissipation only, but pore-air pressure dissipation should be considered also. The degree of consolidation should be calculated separately for the water-phase and the air-phase.

Generally, the increase of temperature causes an increase in the pore-air and pore-water pressures and vice versa. This increase in pressure may cause an expansion in the soil skeleton, and may cause both pressures to take a longer time to dissipate.

The effect of soil skeleton expansion is neglected due to its small effect for many types of soils. If it is taken into consideration, it may affect the soil skeleton and cause more expansion in it.

REFERENCES

- Al-Assady, A. M., 1998, "Effect of Anisotropy on Two-Dimensional Consolidation of Clayey Soil", M.Sc. Dissertation, Department of Civil Engineering, University of Baghdad.
- Al-Damluji, Omar Al-Farouk S., Al-Shakarchi, Yousif J., and Zainel, Abdul Kareem E., 2003, " Two-Dimensional Consolidation Analysis of Partially Saturated Soils By Using The Finite Element Method", The Fifth Scientific Conference, College of Eng., University of Baghdad.
- Al-Hamrany, M. M., 1980, "Trial Embankment Settlement Analysis with Emphasis on Stress Path Method", M.Sc. dissertation, University of Baghdad.
- Al-Khaddar, R. M. A., 2000, "Non-Isothermal Consolidation", Thesis submitted to the College of Engineering of the University of Baghdad in partial fulfillment of the requirements for the degree of Master of Science in Civil Engineering.
- Biot, M. A., 1941, "General Theory of Three-Dimensional Consolidation", Journal of Applied Physics, Vol. 12, No. 2, pp. 155–164.
- Edgar, T. V., J. D. Nelson, and D. B. McWhorter, 1989, "Non Isothermal Consolidation in Unsaturated Soil", Journal of Geotechnical Engineering, Vol. 115, No. 10 Oct. pp 1351-1372.
- Fredlund, D. G., and H. Rahardjo, 1986, "Unsaturated Soil Consolidation Theory and Laboratory Experimental Data" Consolidation of Soils: Testing and Evaluation, ASTM STP 892, R. N. Young and F. C. Townsend, Eds., American Society for Testing and Materials, Philadelphia, pp. 154–169.
- Fredlund, D. G., H. Rahardjo, 1993, "Soil Mechanics for Unsaturated Soils", John Wiley & Sons.
- Hillel, Daniel, 1971, "Soil and Water", Academic Press, Inc.
- Lewis, R.W., and B. A. Schrefler, 1987, "The Finite Element Method in the Deformation and Consolidation of Porous Media", John Wiley & Sons.
- Penman, A. D. M., and Burford, D., 1983, "Construction of the Trial Embankment Near Talha, Iraq", Building Research Establishment.
- Philip, J. R., D. A. de Vries, 1957, "Moisture Movement in Porous Materials Under Temperature Gradients", Transactions, American Geophysical Union, Vol. 38, No. 2, pp. 222–232.
- Zainal, A. E., 2002, "Solution of Some Problems of Partially Saturated Soils Using the Finite Element Method", A Thesis submitted to the College of Engineering of the University of Baghdad in Partial fulfillment of the Requirements for the Degree of Doctor of Philosophy in Civil Engineering.

APPENDIX A

Definitions of matrices

$$[\mathbf{K}] = - \int_{\Omega} [\mathbf{B}]^T [\mathbf{D}] [\mathbf{B}] dx dy \quad \dots(\text{A} - 1)$$

$$[\mathbf{L}] = \left(n_w - \frac{m_2^s}{m_1^s} + n_s \right) \int_{\Omega} \mathbf{B}^T \mathbf{m}^T \mathbf{N} dx dy \quad \dots(\text{A} - 2)$$

$$[\mathbf{M}] = \left(\frac{m_2^s}{m_1^s} - n_w \right) \int_{\Omega} \mathbf{B}^T \mathbf{m}^T \mathbf{N} dx dy \quad \dots(\text{A} - 3)$$

$$\mathbf{f} = \frac{\partial}{\partial t} \left(\int_{\Omega} [\mathbf{N}]^T [\mathbf{B}\mathbf{F}] dx dy - [\mathbf{B}\mathbf{C}] \right) \quad \dots(\text{A} - 4)$$

$$\mathbf{W1} = \frac{m_1^w}{m_1^s} \int_{\Omega} \mathbf{N}^T \mathbf{m} \mathbf{B} dx dy \quad \dots(\text{A} - 5)$$

$$\mathbf{W2} = \left(m_2^w - \frac{m_1^w m_2^s}{m_1^s} \right) \int_{\Omega} \mathbf{N}^T \mathbf{N} dx dy \quad \dots(\text{A} - 6)$$

$$\mathbf{W3} = \left(\frac{m_1^w m_2^s}{m_1^s} - m_2^w \right) \int_{\Omega} \mathbf{N}^T \mathbf{N} dx dy \quad \dots(\text{A} - 7)$$

$$\mathbf{KW} = - \int_{\Omega} \mathbf{R}^T [\mathbf{D}\mathbf{W}] \mathbf{R} dx dy \quad \dots(\text{A} - 8)$$

$$\mathbf{UT} = - \int_{\Omega} \mathbf{R}^T [\mathbf{D}\mathbf{T}] \mathbf{R} dx dy \quad \dots(\text{A} - 9)$$

$$\mathbf{A1}' = \frac{(m_1^s - m_1^w)}{m_1^s} \int_{\Omega} \mathbf{N}^T \mathbf{m} \mathbf{B} dx dy \quad \dots(\text{A} - 10)$$

$$\mathbf{A2}' = \frac{(m_1^w m_2^s - m_1^s m_2^w)}{m_1^s} \int_{\Omega} \mathbf{N}^T \mathbf{N} dx dy \quad \dots(\text{A} - 11)$$

$$\mathbf{A3}' = \frac{(m_1^s m_2^w - m_1^w m_2^s)}{m_1^s} \int_{\Omega} \mathbf{N}^T \mathbf{N} dx dy \quad \dots(\text{A} - 12)$$

$$\mathbf{KAUa} = - \int_{\Omega} \mathbf{R}^T [\mathbf{D}\mathbf{AUa}] \mathbf{R} dx dy \quad \dots(\text{A} - 13)$$

$$\mathbf{KAT} = \int_{\Omega} \mathbf{R}^T [\mathbf{D}\mathbf{AT}] \mathbf{R} dx dy \quad \dots(\text{A} - 14)$$

$$\mathbf{FA}' = - \frac{Dh}{\bar{u}_{ao}} \oint_S N_i \frac{\partial N_i}{\partial n} \mathbf{u}_a dS + \frac{Dh}{T_o} \oint_S N_i \frac{\partial N_i}{\partial n} \mathbf{T} dS \quad \dots(\text{A} - 15)$$

$$[\mathbf{DH}] = \begin{bmatrix} \lambda_x & 0 \\ 0 & \lambda_y \end{bmatrix} \quad \dots(\text{A} - 16)$$

$$[\mathbf{T1}] = \zeta \int_{\Omega} \mathbf{N}^T \mathbf{N} dx dy \quad \dots(\text{A} - 17)$$

$$[\mathbf{KH}] = \int_{\Omega} \mathbf{R}^T [\mathbf{DH}] \mathbf{R} dx dy \quad \dots(\text{A} - 18)$$

$$[\mathbf{FH}] = \int_{\Omega} \left(N_i \frac{\partial N_j}{\partial x} \lambda_x + N_i \frac{\partial N_j}{\partial y} \lambda_y \right) \mathbf{T} dx dy \quad \dots(\text{A} - 19)$$

$$\mathbf{B}^T = \begin{bmatrix} \frac{\partial N_i}{\partial x} & 0 & \frac{\partial N_i}{\partial y} \\ 0 & \frac{\partial N_i}{\partial y} & \frac{\partial N_i}{\partial x} \end{bmatrix} \quad \dots(\text{A} - 20)$$

$$\mathbf{D} = \begin{bmatrix} \frac{2(1-\mu)}{m_1^s} & \frac{2\mu}{m_1^s} & 0 \\ \frac{2\mu}{m_1^s} & \frac{2(1-\mu)}{m_1^s} & 0 \\ 0 & 0 & G \end{bmatrix} \quad \dots(\text{A} - 21)$$

APPENDIX B

Input Data Required for Partially Saturated Soils

In addition to the input data required for the usual case problems, there are some additional parameters that are needed in dealing with partially saturated soil characteristics, which are:–

- **Volumetric Coefficient of Solubility, h :**
which is defined as: –

$$h = (\rho_w / \rho_a) H \quad (B-1)$$

where

H is the coefficient of solubility, and

h for air varies with temperature as shown in figure B-1.

An extrapolation is made to the available data using an exponential function best fit curve obtained by using the computer program Wingraph 1.09 **. The equation obtained has the following form: –

$$y = \exp(-0.0206841 * x) * 0.0285497 \quad (B-2)$$

This equation is included in the computer program to obtain the volumetric coefficient of solubility at each temperature.

- **Coefficient of Diffusion D :**

Its value is taken as $2.0 \times 10^{-9} \text{ m}^2/\text{s}$ (Fredlund and Rahardjo, 1993).

- **Coefficients of Volume Change:**

The values of m_1^s , m_2^s , m_1^w , and m_2^w are taken as $0.006 \times 10^{-4} \text{ kPa}^{-1}$, $0.032 \times 10^{-4} \text{ kPa}^{-1}$, $0.131 \times 10^{-4} \text{ kPa}^{-1}$, and $0.657 \times 10^{-4} \text{ kPa}^{-1}$, respectively (Fredlund and Rahardjo, 1986). These values are taken as results from experimental tests. True data must be obtained from laboratory experiments.

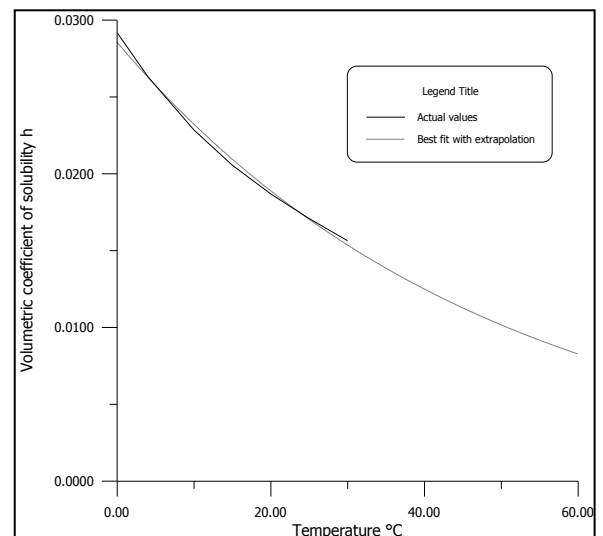


Fig. B - 1
Variation of coefficient of solubility with
temperature showing Data extrapolation (after
Fredlund, and Rahardjo, 1993)

** The computer program Wingraph Ver. 1.09 is a software produced by Golden Software, Inc. 1993 and works under WINDOWS 95/98/2000/Me.

ASSESSING THE RISK AND POTENTIAL OF PERSONAL EXPOSURE TO ROAD GENERATED POLLUTANT EMISSIONS THROUGH URBAN TRANSPORTATION SYSTEM

Saad Issa Sarsam

Assistant Professor - Civil Engineering Department
Engineering College - Baghdad University
Formerly at Mosul University

ABSTRACT

This paper presents a study to assess the degree of personal exposure to traffic generated pollutant emission along urban arterials in Mosul. The traffic flow characteristics (volume, speed, density, and vehicle type) were determined in the field at selected locations on the arterials. The vehicular traffic which includes (drivers, number of passengers in vehicles on the road, and pedestrian) exposed to road generated emissions were obtained through field survey. The vehicle emissions of CO, VOC, and NO_x were calculated using air pollution estimation computer model (Mobile 4.1). It was concluded that the emission of CO, VOC, and NO_x exceeds the standard level requirements. The risk arising from personal exposure to traffic generated emissions of such pollutants was analyzed and the degree of personal exposure of road users (drivers, passengers, and pedestrians) to pollutants emission along urban arterials in Mosul was determined.

الخلاصة

يعرض هذا البحث دراسة لتقدير درجة التعرض الشخصية للملوثات ناتجة عن حركة المرور عبر طرق شريانية في الموصل ان خصائص حركة المرور (الحجم المروري, السرعة, الكثافة, ونوع المركبات) قد تم حسابها في الموقع عند نقاط مختارة على الطرق الشريانية اما حركة المرور والتي تشمل (السائقين, عدد الركاب في المركبات, والمشاة) المعرضين الى انبعاثات الطريق, فقد تم حسابها ايضا من خلال دراسة موقعية

ان انبعاث الملوثات من عوادم المركبات والشاملة (CO, VOC, NO_x) قد تم حساب نسبها باستخدام نمذجة برنامج تقدير ملوثات عوادم المركبات (Mobile 4.1) تم الاستنتاج بان انبعاث هذه الملوثات يتجاوز المستوى المقبول عالميا ان الخطورة الناتجة عن التعرض الشخصي لمستخدمي الطريق لمثل هذه الملوثات قد تم تحليلها وحساب درجة التعرض الشخصي لمختلف انواع مستخدمي الطريق وكذلك للسكان لمثل هذه الملوثات حول وعبر الطرق الشريانية في مدينة الموصل

KEY WORDS

Assessment, Emission, Exposure, Pollutant, Risk

INTRODUCTION

Road generated emissions and public reaction to it have become a major problem in recent years, especially in densely populated areas. The highway planner may be concerned with how pollutants emissions from traffic flow are perceived by persons living or working nearby.

THE PROBLEM AND THE CITY

Mosul is the second largest city in Iraq, it is located at the north with a total area of 32698 km² and an urban area of 220 km². The projected population for the year 2004 is 2.7 million as per 1997 census. The city is surrounded by hills to the south and mountains to the north, such topographical situation may act as a barrier trapping pollutants close to the city. Plastics, chemicals, drugs, wood and portland cement factories are surrounding the major urban area within 15km from the city center. The city continues to grow and is expanding into surrounding agricultural areas. The central part of the city is a mixed commercial and residential area. **Table 1** shows that the vehicles fleets tend to be old and poorly maintained, more than 93% of the passenger car and more than 94% of commercial vehicles are over 15 years old, and of these, most have engines in need of major repairs. It was felt that this will increase the significance of motor vehicle as a pollutant source and the quality of life of urban residents will continue to deteriorate.

Table –1 Classification of vehicles in Mosul by Category of model year as in December- 2004

Vehicle * Model year	Passenger Car	%	Commerical vehicles (pick up,bus,truck)	%
1954-1959	894	0.74	X	0
1960-1971	2972	2.4	8889	10.3
1972-1976	4476	3.7	6728	7.8
1977-1979	3873	3.2	6987	8.1
1980-1984	36472	30.3	35370	41.2
1985-1989	65451	54.5	24728	28.8
1990-1993	4866	4.0	2503	2.9
1994-1996	808	0.67	370	0.4
1997-2004	208	0.17	243	0.3
Total	120020		85818	

* From Traffic Police department - Mosul

FIELD WORK

The current investigation was confined to eleven selected portions of the major arterials lined by 2-3 story buildings on both sides of the road where the traffic pollutants emissions level were expected to be high. Such locations are located at crowded, commercial, residential and open area for comparison. **Plate 1** shows the observation points and the arterial studied.

Determination of traffic flow characteristics

The measurement of traffic volume and composition was conducted using the manual count system by field observer, the number of vehicles of each category was determined during 10 minutes, through each observation point at rush hour.

The time mean speed was recorded for each vehicle category by timing it over a 100m distance. A total of 12 vehicle samples of each category were tested for speed at each observation point. The elevated observation technique was followed so that the observers select typical vehicles at random and record pertinent data regarding their progress through a section of a roadway. Such technique is designed for short-run observations. The speed and volume measurements techniques were as per Pignataro (1973) and Sarsam(1999). Vehicles were assigned to one of two general categories, passenger car (gasoline fuelled) and commercial vehicles (includes pick up, buses and trucks which are mostly diesel fuelled). **Table 2** illustrates the traffic flow characteristics observed. The vehicular traffic which includes (drivers , number of passengers in the vehicle on the road and pedestrian) exposed to road generated emissions were obtained through field survey. An average vehicular occupancy factor of 3 was obtained from direct observation in the field.

Table – 2 Traffic flow characteristics observed along major arterials in Mosul.

Section	volume (vehicle/rus h hour)	% passenger cars	% commerical (pick up, bus,trucks)	Average speed (km/hr.)
1 →	1104	82	18	50.7
←	1206	87.5	12.5	50.3
2 →	1596	80.0	20	57.3
←	1932	83.5	17	55.3
3 →	1692	79.4	20.6	56.5
←	2184	81.3	18.7	49.4
4 →	1128	68.6	31.4	51.5
←	930	74.1	25.9	48.5
5 →	1632	73.8	26.2	32.6
←	1662	74.4	25.3	41.3
6 →	942	67.5	32.5	48.1
←	1092	72.5	27.2	47.8
7 →	276	71.7	28.3	65.5
←	456	72.3	27.7	56
8 →	498	77.1	22.9	54
←	522	86.2	13.8	63
9 →	1932	90.9	9.1	45
←	1116	90.3	9.7	51
10 →	1674	90.6	9.4	63
←	1110	95.1	4.9	46.4
11 →	1368	91.2	8.8	42.8
←	1668	93.5	6.5	39.3

Calculation of pollutants emissions , dose and risk.

The vehicles emissions of CO, VOC and NO_x were calculated using air pollution estimation computer model (mobile 4.1). Essam et al (1997). **Table 3** illustrates the pollutants emissions through rush hour on the arterials. The degree of exposure of road users as a unit life time occupational dose was calculated using the procedure suggested by Beyers et al (1984), and Ortolano (1997), while the risk was calculated using Peirce et al (1998) procedure.

Table – 3 Pollutant emissions through rush hour using ((Mobile 4.1))

Section	CO gm/km	VOC gm/km	NO _x gm/km	CO mg/m ³	VOC mg/m ³	NO _x mg/m ³	Traffic density Veh/km
1 →	7.5	0.95	1.387	2.70	0.343	0.501	21.7
←	7.81	0.968	1.40	3.12	0.387	0.560	24
2 →	6.25	0.875	1.375	2.89	0.405	0.637	27.8
←	6.56	0.887	1.375	3.82	0.517	0.802	35
3 →	6.25	0.875	1.375	3.120	0.437	0.687	30
←	7.18	0.975	1.376	5.280	0.718	1.021	44.2
4 →	7.5	0.937	1.381	2.750	0.343	0.506	22
←	8.1	0.98	1.39	2.592	0.313	0.444	19.2
5 →	13.1	1.42	1.54	10.91	1.183	1.283	50
←	10	1.17	1.43	6.7	0.783	0.958	40.2
6 →	8.12	1.0	1.39	2.652	0.326	0.454	19.6
←	8.43	1.0	1.4	3.203	0.380	0.532	22.8
7 →	5.0	0.78	1.37	0.350	0.054	0.095	4.2
←	6.25	0.87	1.36	0.843	0.117	0.183	8.1
8 →	6.87	0.92	1.37	1.051	0.140	0.209	9.18
←	5.0	0.81	1.36	0.685	0.111	0.187	8.28
9 →	9.25	1.07	1.41	6.582	0.761	1.003	42.7
←	7.5	0.95	0.95	2.725	0.345	0.345	21.8
10 →	5.0	0.81	1.36	2.200	0.356	0.598	26.4
←	8.75	1.05	1.40	3.500	0.420	0.560	24

RISK ASSESSMENT

Risk assessment involves the measurements of the severity of harm inherent in exposure to pollutant emissions, two types of population exposed to risk were identified :

a-The permanent population living and working near the arterial (on both sides and along).

b-pedestrians walking along the road , drivers and passengers of vehicles on the road.

Table 3 shows that the pollutant emissions are likely to represent maximum exposure through rush hour which people probably experienced at the kerb side of the arterial , the dwellers may be exposed to the same as demonstrated by Clench – Ass et al(1989). In measuring the potential health impact of population, it is important to determine the likely population exposure to pollutants. **Table4** shows the unit life time occupational dose of pollutant taken by the road user and dweller and the unit life time occupational risk of cancer per 1000 population for each of road users and dweller . The number of population at risk was also shown in the table, which was calculated using the traffic density and the vehicle occupational

factor. The dwellers are expected to experience a cancer risk five folds larger than road users. The cancer fatalities in Mosul were 1478 at 2004, 893 at 2000 , 830 at 1999, 750 at1998 and 600 at 1996 as obtained from Ministry of health annual report.**Equation 1**, which was obtained from Ortolano (1997) was adopted for calculation of unit life time occupational Dose, and the test conditions and variables were as suggested by Beyers & Dudas (1984).

$$(1) \quad (\text{ULTO Dose}) = \text{Breathing} \times 365 \times 70 \times \text{Dose response} \quad (\text{m}^3 / \text{day}) \quad (\text{days/year}) \quad (\text{year}) \quad \text{information} \quad (\text{gm} / \text{m}^3)$$

The risk analysis was conducted as per the procedure suggested by Peirce (1998) the calculation of unit life time occupational risk of Cancer was adopted using **Equation 2** suggested by WHO (1992).

EPA definition of Unit life time occupational risk implies exposure for 2000 hours per year for 47 years (a working lifetime) . peirce (1998).

$$(2) \quad \text{Unit life time occupational risk of canser/1000} = [\text{Latent canser} \times (10^3 \times 10^3)] / [47 \text{ years} \times (2000/ 8760)]$$

fatality

Table – 4 Degree of exposure to pollutant emissions and risk.

Section	*U.L.O Dose ((gm))						*U.L.O Risk of cancer/1000		
	Road users			Dweller			Road users		Dwellr
	CO	VOc	NOx	CO	VOc	NOx	Risk	Pop. **	
1 ←	115.8	14.7	21.5	347	44	64.5	23.5	56	3.6
	113.9	16.6	24	342	50	72	20.4	72	3.1
2 ←	124	17.3	27.3	372	52	82	21.2	83	3.2
	164	22.2	34.4	492	67	103	16.2	105	2.4
3 ←	133.9	18.7	29.4	402	56	88	19.6	90	3.0
	226.6	30.8	43.8	680	93	132	11.8	133	1.8
4 ←	118.0	14.7	21.7	354	44	65	23.1	66	3.5
	111.2	13.4	19.0	334	40	57	24.8	58	3.8
5 ←	468.5	50.7	55.0	1406	152	165	6.2	150	0.95
	287.6	33.6	41.1	863	101	123	9.8	121	1.5
6 ←	113.8	14.0	19.4	341	42	58	24.2	59	3.7
	137.4	16.3	22.8	412	49	68	20.2	68	3.1
7 ←	15.0	2.31	4.0	45	7	12	167.0	13	25.5
	36.1	5.02	7.8	108	15	23	73	24	11.1
8 ←	45.1	6.0	8.9	135	18	27	59.5	28	9.1
	29.4	4.7	8.0	88	14	24	84.7	25	12.9
9 ←	282.5	32.6	43.0	848	98	129	9.9	128	1.5
	116.9	14.8	14.8	351	44	44	24.4	65	3.7
10 ←	94.4	15.2	25.6	283	46	77	26.4	79	4.0
	150.2	18.0	24.0	451	54	72	18.6	72	2.8
11 ←	221.5	25.8	32.6	665	77	98	12.7	96	1.9
	330.6	37.3	43.9	992	112	132	8.6	127	1.3

	*Unit lifetime occupational **In vehicle population	*low values indicates high risk /1000 population
--	--	---

CONCLUSIONS AND RECOMMENDATIONS:

1- Concentrations of CO, VOC and NO_x and the life time occupational dose of such pollutants exceeds the WHO levels at some observation points. It is expected that air quality will deteriorate in the city.

2- The dwellers are expected to experience a cancer risk five folds larger than road users.

3- The emission per vehicle – km on the arterial in Mosul could be reduced by limiting the speed to a range of 60-65 km/hour.

Its recommended that a stringent control measures for traffic related pollutants should start in the city with direct field measurements of pollutants, collection and processing of vehicle emission data should be repeated periodically.

REFERENCES

Asif Faiz (1996) “Air pollution from motor vehicles :standards and technologies for controlling Emissions” The world Bank.

Beyers M. & Dudas S.(1984) “The clinical practice of medical – surgical Nursing” Little brown and company – Boston 2nd Edition – P.343.

Cini A ; Ditty R. ; Nayaraj B. & prasad v.(1997) “Evaluation of ambient air quality deterioration due to pollution from road traffic in Calicut city” Highway research bulletin No. 56 – I.R.C. Highway research board (p 13 – 30).India.

Clench – AAs , Myher k. , krogne T. Bartonova A.; Johnsrud M. & Neslein Il.(1989) “Carbon monoxide exposure in individuals working along Radhusgata – oslo” Norwegian Institute for Air Research – Lillestrom NILU OR 44/89 – Norway.

Clench –AAs , Larssem S. , Bartonova A. Aarnes M.J. , Myhrek, Christensen C.C., Neslein I.I., Thomassen Y. & Levy F. (1991) “The health effects of traffic pollution as measured in the valerenga area at oslo”.Norwegian Institute for Air Research - Lillestrom NILU OR 7/91- Norway.

Essam S.Sharaf & Garib A.M. (1997) “Incorporation of Environmental impact within highway maintenance decision support system” 1st Jordanian conference on Traffic Engineering and Environment” Amman – Jordan 13-15 may,P 246-258.

Ortolano L.(1997) “Environmental regulation and impact assessment” J.W & Sons Inc. U.S.A.

Peirce J.J, Weiner R.F. & Vesilind P.A (1998) “Environmental pollution and control” Butterworth – Heinemann publication , U.S.A fourth edition. Ch-2.

Pignataro L.J. (1973) “Traffic Engineering – theory and practice”prentice – Hall Inc. . USA.

Sarsam S.I (2000) "Assessing Traffic generated Emissions and Noise impacts along urban arterials in Mosul" Al-Muhandis – scientific Journal of Iraqi Engineers Union- vol.131 No.1 ,Baghdad – IRAQ.

UNEP/W.H.O (1996) "Air Quality Management and Assessment capability in 20 Major cities" Monitoring and Assessment Research centre- London.

W.H.O (1992) "Regional Training course on Air pollution" 4-9 August, Amman – Jordan – CEHA Document No. TLM – 2 – W.H.O

W.H.O / UNEP (1992) "Urban Air pollution in Megacities of the world" W.H.O – U.N.E.P. Black well – oxford.

W.H.O. (1992) "Motor vehicle air pollution – public health impact and control measures"- Division of Environmental health –Geneva - switzerland – W.H.O./PEP-92.4

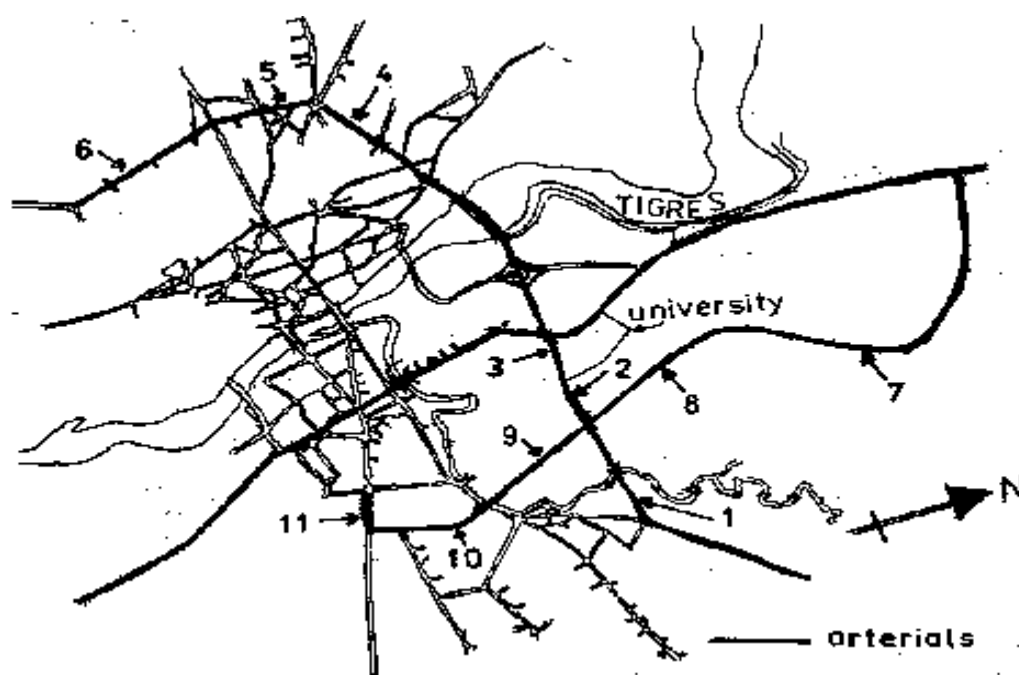


PLATE 1 – Location map, Mosul

DEVELOPMENT OF PAVEMENT CONDITION INDEX MODEL FOR FLEXIBLE PAVEMENT IN BAGHDAD CITY

Namir G. Ahmed

Assistant Prof.(Dep.of H.W.Y. 's

&Transportation Eng. –University
of Al-Mustansiriyah)

Ghassan J. Awda

Consult Eng. (Ministry of
Education)

Suham E. Saleh

Asst Lecturer (Dep.of H.W.Y. 's

&Transportation Eng. –University
of Al-Mustansiriyah)

ABSTRACT

The pavement is one of the basic components of road infrastructure and, therefore, directly influences general levels of transport safety, as well as the quality of transportation services in human and cargo traffic.

Accordingly, the objective of the present study is to develop the prediction model for pavement condition index (PCI) for flexible pavement.

To achieve this objective, (80) selected pavement sections in four sites in the study area and (1100) sample of pavement sections were selected from these sections for the purpose of (PCI) model building. These data include ; longitudinal , transverse, alligator , slippage and block cracking , rutting ,depression , bleeding , polishing , patching and pothole .

The effort to develop a (PCI) model is carried out by using a stepwise regression technique. These statistical processes are carried out with the aid of (STATISTICA – version 5.5) computer package.

The validation process for the developed models shows that, this model is adequate to be used for the prediction of pavement condition for flexible pavements within the range of data.

الخلاصة

التبليط هو أحد المكونات الأساسية لبناء التحتي للطرق ولذا , يؤثر على المستويات العامة مباشرة من أمان النقل و بالإضافة الى نوعية خدمات النقل للإنسان و شحن المرور .

بناء على ذلك فإن أهداف الدراسة الحالية هي تطوير النماذج الخاصة بالتنبؤ على دليل حالة التبليط (PCI) المرن . ولغرض تحقيق هذه الاهداف أختيرت مقاطع التبليط في أربعة مواقع ضمن منطقة الدراسة , لجمع البيانات المطلوبة لبناء النموذج الخاص بال(PCI) وتم فيه اختيار عينة من تلك المقاطع لغرض بناء نموذج. أن هذه البيانات تتضمن: التشقق (Cracking) والمتمثلة ب: الطولي (Longitudinal), العرضي (Transverse), الكلل او التمساحية (Alligator or), الشبكية (Block), والهلالية (Slippage), التحدد (Rutting), التخسف (Depression), النزف (Fatigue), التلميع (Polishing), الترقيع (Patching) والفجوات (Pothole). لقد تم القيام بهذه العمليات لتطوير نموذج (PCI) فقد تم استخدام تقنية الانحدار التدريجي (Stepwise Regression). الاحصائية بمساعدة برنامج الحاسوب (STATISTIC V. 5.5). ان عملية التحقق (Validation) للنماذج المطورة تظهر بأن هذه النماذج ملائمة للاستخدام في التنبؤ عن حالة التبليط المرن ضمن حدود البيانات .

KEY WORDS

Pavement Condition Index, Flexible pavement, ; Longitudinal ,Transverse, Alligator , Slippage and Block cracking , Rutting ,Depression ,Bleeding , Polishing , Patching and Pothole , prediction of pavement condition.

INTROUDECTION

Pavement condition index PCI is one of the most widely used performance measures for pavements, it uses as an indicator of the pavement condition [Susan et. al 2004].

[U.S Army Corps of Engineers 2003] defines the PCI as the default condition index for the PAVER system. A numerical index, ranging from 0 for a failed pavement to 100 for a pavement in perfect condition. Calculation of the PCI is based on the results of a visual condition survey in which distress type, severity, and quantity are identified. It was developed to provide an Index of the pavement structural integrity and surface operation condition.

[Shahin M.Y. (1982)] mentions that, the distress characterization should include three parameters: distress type, severity, and quantity. The lack of any of these parameters will produce an unrepeatable and inconsistent distress characterization.

These points can then be summed and subtracted from some upper limit to give an overall rating of a pavement's structural condition. The equations that describe how to convert from severity and extent of a certain distress type to an index number, or score vary from state to state and can be rather complex [Deighton (1998)] .

STUDY AREA DESCRIPTION

The study area is located on the west of Baghdad in Al-Kharkh side, between latitudes ($33^{\circ} 22' 7.03''$, $33^{\circ} 17' 25.27''$), and Longitudes ($44^{\circ} 17' 55.36''$, $44^{\circ} 19' 59.25''$) respectively.

This area includes: Al- Huriya, Al-Adel, Al- Kadra'a, and Al-Hamra'a districts. **Figure (1)** shows the location of the selected study area. It is important to mention that all the selected roads in the study area are flexible pavements.

The following items are considered in the selection of the study area:-

- 1.The selected sites are close to each other to minimize the travel time between sites.
- 2.The sites are selected are near the residential area in order to minimize the expected effect of congestion or any other effect on this process.
- 3.Same lengths of sections are selected. This will lead the raters to ride over these sections at desired speed and approximately the same travel time has been used.

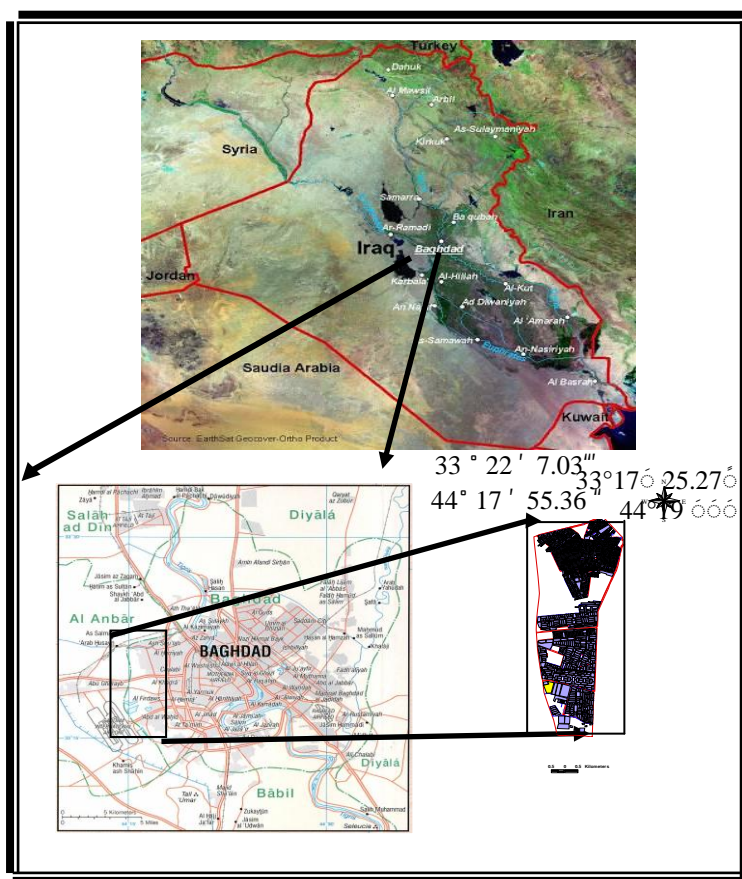


Fig (1) Location of Study Area

DATA COLLECTION PROCESS

The mentioned pavement sections were used to collect the required distresses data for the purpose of model building for the prediction of PCI. The monitoring distresses; types, severity and amount were listed and recorded. The following flexible Pavement distresses were observed in the study area , these distresses includes : Rutting ,alligator, block ,longitude, transverse , slippage cracks, bleeding ,depression ,patching and polishing .

FIELD MEASUREMENTS

The field measurement in the present study consists the following flexible pavement distresses:

Alligator Crack

To measure this type of distress, the distress severity it must be determined. This distress is different in level of severity, such as; low, moderate and high. This type of distress is measured manually by use of tape, in area unit (ft²). **Figure (2)** presents the alligator crack in the study area.



Fig (2) Alligator crack at AL- Huirya City

Bleeding

This type of distress is measured manually by use of cloth tape, in area unit (ft^2), it's observed in most of the selected pavement sections.

This distress is different in level of severity. When the severity is "low", the pavement surface creates a shiny; the pavement surface is glass-like and reflecting surface for the "moderate", and quite sticky for the "high severity". This type of distress can be obvious in the study area as shown in **Figure (3)**.



Fig (3) Bleeding at Al-Hamra'a City

Depression

Depressions are localized in the pavement surface that has elevations slightly lower than those of the surrounding pavement. [ASTM, 2003] starts that the severity level (maximum depth of depression) depends on the range of this depth, "low severity" when the range is "0.5 to 1 inch", "moderate" when the range is "1 to 2 inch" and "high severity" when more than "2 inch". This failure is measured manually by use of tape and straight edge to determine the severity level and is measured in (ft^2) of surface area. **Figure (4)** shows this type of failure in the study area.



Fig (4) High Severity Depression at AL- Adel City

Block Cracking

This distress is measured manually by using tape in " ft^2 ". Block cracks are interconnected cracks that divide the pavement into approximately rectangular pieces. They differ in level of severity, low, moderate and high. **Figure (5)** presents this type of distress in the selected study area.



Fig (5) Block Crack at Al- Huriya City

Longitudinal and Transverse Cracking

These types of distresses are obvious clearly in different severity. Longitudinal cracks are present in parallel to the pavement centerline, and located within the lane (wheel path). This type of crack appears in different severity levels, such as, low, moderate and high level. **Figure (6a)** illustrates this type of failure as appears in the study area.

While the transverse cracks extend perpendicular to the centerline, as shown in **Figure (6b)**, transverse crack severity depends on crack width which is caused by shrinkage of asphalt surface due to low temperature or asphalt hardening or result form reflective cracks caused beneath the asphalt surface.

Many types of these cracks are observed in the selected sections, but in different levels of severity. These distresses are measured manually by use of cloth tape in liner "ft".



a - Longitude



b – Transverse

Fig (6) Longitudinal and Transverse Cracks at Al-Hamra'a

Patch/Patch Deterioration

A patch is an area of pavement that has been replaced with new material to repair the existing pavement. These distresses differ in level of severity, Patch is a good condition and satisfactory, or ride quality is rated as low severity or better [ASTM 2003].

Patch is moderately deteriorated, or ride quality is rated as medium severity, or both. Patch is badly deteriorated, or ride quality is rated as high severity, or both; this type needs replacement soon. It is measured manually by tape in "ft²". **Figure (7)** presents this type of distress as shown in the study area.



Fig (7) Patching at AL-Adel City

Polish Aggregate

This type of failure can be seen in most of the roads in the study area. The polish aggregate is measured manually by use of tape in area unit (ft²). This distress is caused by repeated traffic applications. This type of distress is indicated when the number on a skid resistance test is low or has dropped significantly from a previous rating [Mike and John, 2002]. **Figure (8)** shows this type of distress as a given in the study area.



Fig (8) Polishing at Al-Hamra'a City

Potholes

Potholes are small usually less than (30 inch) in diameter-bowl-shaped depressions in the pavement surface. These distresses differ in level of severity, and the units measured by number. Potholes are measured by counting different types severity; low, when the depth from 13 to ≤ 25 mm and average diameter 100-450mm, medium from 25 to ≤ 50 mm, and average diameter 200-450mm high is > 50 mm and average diameter 450-750mm recording them separately, this type of distress as given by [Mike and John 2002. **Figure (9)** shows this type of distress as seen in the study area.



Fig (9) Pavement Potholes at AL-Huriya city

Rutting

A rut is a surface depression in the wheel paths. These distresses differ in level of severity (Mean Rut Depth), low severity is range ($\frac{1}{4}$ to $\frac{1}{2}$ in.), moderate severity is range ($> \frac{1}{2}$ to 1 in.) and high severity is range (> 1 in) [AASHTO 1986]. Rutting is measured manually in (inch) depth, and its severity is determined by the mean depth of the rut. The mean rut depth is calculated by laying a straightedge across the rut, measuring its depth, then using mean depth in inch. **Figure (10)** presents this type of distress as it appears in the study area.



Fig (10) Rutting at AL- AL-Huriya City

Slippage Cracking

Slippage cracks are crescent or half-moon shaped cracks, usually transverse to the direction of travel. The severity level of this distress is low when the average crack width is ($< \frac{3}{8}$ in.), moderate, the average crack width is ($\geq \frac{3}{8}$ and $< 1 - \frac{1}{2}$ in) or the area around the crack is moderately spalled, or surrounded with secondary cracks, high severity if the width crack is ($1 - \frac{1}{2}$ in) and area around the crack is broken into easily removed pieces. The area associated with a given slippage crack is measured manually by use of tape in (ft²), **Figure (11)** shows this distress as it appears in the study area.



Fig (11) Slippage Crack at AL-Huriya City

REQUIRED DATA FOR PCI AND PCR DETERMINATION

Data Collection

The Data obtained from this procedures is the primary basis for determining requirements of the evaluation process. Pavement condition is related to several factors, including structural integrity, structural capacity, roughness skid resistance, and rate of deterioration.

These factors can be assessed by observing and measuring distresses in the pavement. The PCR is based on the PCI, which is a numerical indicator based on a scale of 0 to 100. Its scale and associated ratings are shown in **Figure (12)**. The following is a description of the procedure used to assess the condition of the pavement;

PAVER system was used in this study as recommended by many U.S agencies [ASTM 2003 , ALswilimi Saleh , 1995, TECHNICAL MANUAL 1995,] The first step in this method procedure involves the identification of a representative area, before a pavement network is inspected, it must be divided into branches, sections, and sample units. A sample unit for asphalt area is approximate (2500 ft²) for roads and parking. This area is selected because the networks of roads range from very poor to very good. The number of sample units to be inspected (n) is determined in **Figure (13)** , as a function of the total number of units in the section (N) and the standard deviation of the PCI (α). For the entire section inspections the inspector walks over each section in each sample unit and records the distresses as shown in **Figure (14)** .

The PCI method uses weighted (deduct) values as a function of distress types ,severities and densities of visible distress .This selected procedure is presented by the U.S. Army Corps of engineering " PCI field Manual ". Each of the various types of pavement distresses was identified and measuring "units are liner feet, , square feet and number ". In addition, for each distress, a level of severity was determined into [low (L), Medium (M), High (H)]. In this study there are various kinds of distresses at different density and severity . For the purpose of pavement evaluation, the pavement condition index (Rating Scale) can be used easily as presented in **Figure (12)**.

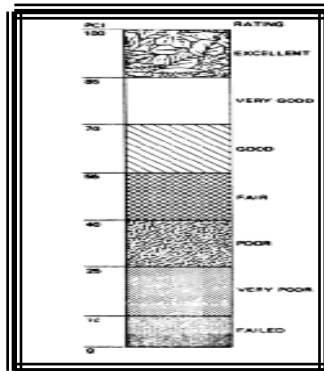


Fig (12) Pavement Condition Index and Rating Scale

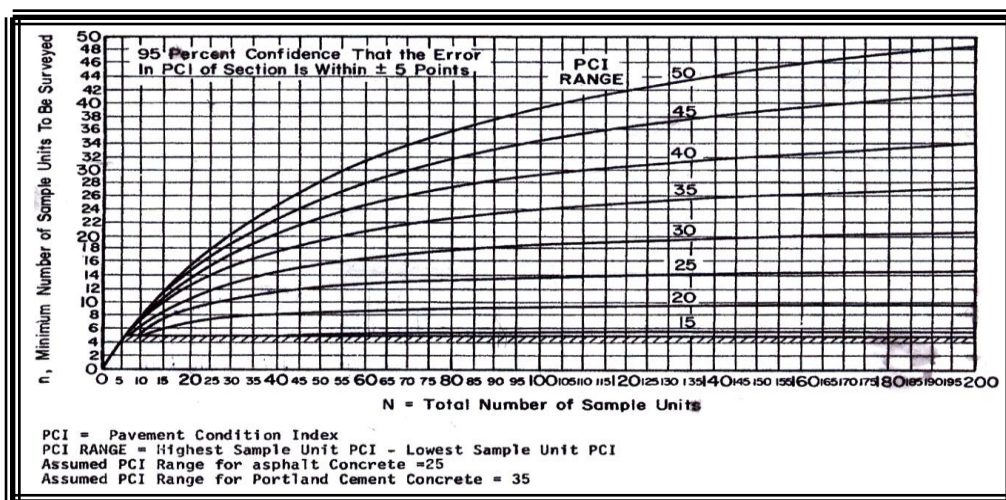


Fig (13) determination of Minimum Number of Sample Units to be Surveyed

Assessment Calculation of PCI

Using the data obtained in the assessment procedure as shown in **Figure (14)**, we performed the following calculations to determine the pavement condition index "PCI". All required information about the following calculations are recorded as given in **Table (A1)** as per **Appendix(A)**.

For each of the different types of distresses, for example a distress density is calculated in **Table (A2)** as per **Appendix (A)**. The formulas from "1 through 3" are used to calculate the distresses density[TECHNICAL MANUAL HEADQUARTERS ,1982]:

$$\text{Density} = \frac{\text{Distresses amount in square feet}}{\text{Sample unit area in square feet}} * 100 \quad (1)$$

$$\text{Density} = \frac{\text{Distresses amount in linear feet}}{\text{Sample unit area in square feet}} * 100 \quad (2)$$

$$\text{Density} = \frac{\text{Number Of pothole}}{\text{Sample unit area in square feet}} * 100 \quad (3)$$

The next step is severity estimation, (i.e. L, M, or H) a deduct value for each distress type is determined. The deduct values are determined through the use of the "deduct value curves". These curves are present in **Figures (15 to 23)**, and represent a part of the [U.S. Army Corps of Engineers Technical Manual 1983], then the deduct values for all distresses are summed to produce "deduct total". To calculate the value of the "correct deduct value", the number of deducts greater than (5) is taken as point "q", from shown in **Figure (24)**, it is used to determine a "correction deduct value" (CDV). These Calculations are recorded in **Table (A3)** as per **Appendix(A)**.

Finally the pavement condition index (PCI) is calculated using the following equ.(4) [TECHNICAL MANUAL HEADQUARTERS ,1982]:

$$\text{Where } \text{PCI} = 100 - \text{CDV} \quad (4)$$

PCI = Pavement Condition Index, and;

CDV = *Correct Deduct Value*.

ASPHALT PAVEMENT INSPECTION SHEET

For use of this form, see TM 5-623; the proponent agency is USACE.

BRANCH _____

DATE _____

SURVEYED BY _____

SECTION _____

SAMPLE UNIT _____

AREA OF SAMPLE _____

Distress Types

<ul style="list-style-type: none"> 1. Alligator Cracking 2. Bleeding 3. Block Cracking *4. Bumps and Sags 5. Corrugation *6. Depression *7. Edge Cracking *8. Jt Reflection Cracking *9. Lane/Shldr Drop Off 	<ul style="list-style-type: none"> *10. Long & Trans Cracking 11. Patching & Util Cut Patching 12. Polished Aggregate *13. Potholes 14. Railroad Crossing 15. Rutting 16. Shoving 17. Slippage Cracking 18. Swell 19. Weathering and Raveling
---	---

SKETCH!

EXISTING DISTRESS TYPE. QUANTITY & SEVERITY

TYPE							
QUANTITY & SEVERITY							
TOTAL SEVERITY	L						
	M						
	H						

PCI CALCULATION

DISTRESS TYPE	DENSITY	SEVERITY	DEDUCT VALUE	
				<div style="text-align: right;"> PCI = 100 - CDV = <div style="border-bottom: 1px solid black; width: 100px; margin: 5px 0;"></div> </div>
q = TOTAL DEDUCT VALUE				<div style="text-align: right;"> RATING = <div style="border-bottom: 1px solid black; width: 100px; margin: 5px 0;"></div> </div>
CORRECTED DEDUCT VALUE (CDV)				

* All Distresses Are Measured In Square Feet Except Distresses 4,7,8,9 and 10 Which Are Measured In Linear Ft; Distress 13 Is Measured In Number of Potholes.

Fig (14) An Sample of a Recorded and Computed of Procedure Data, Asphalt Pavement Inspection Sheet

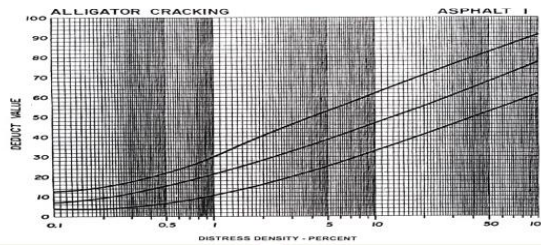


Fig (15) Deduct Value for Alligator Crack

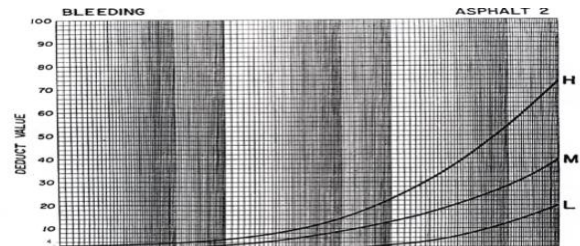


Fig (16) Deduct Value for Bleeding

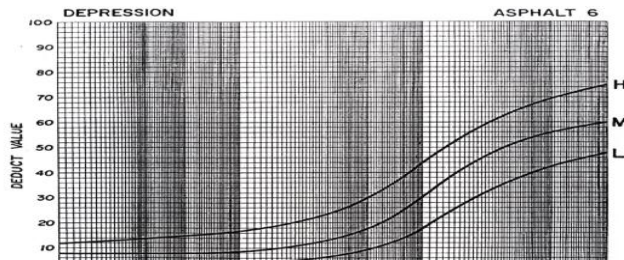


Fig (17) Deduct Value for Depression

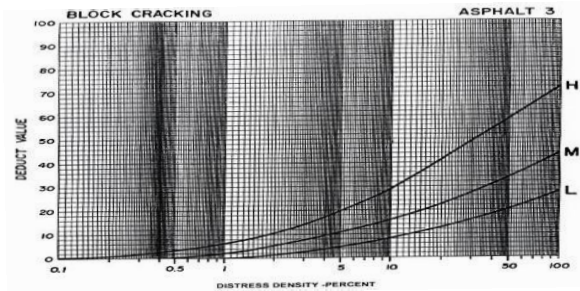


Fig (18) Deduct Value for Block Crack

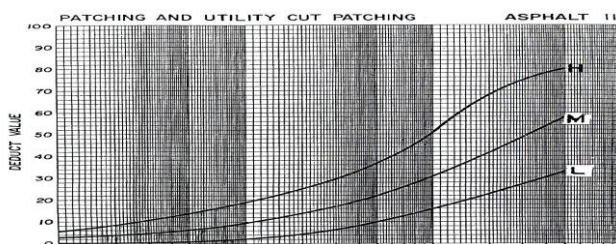


Fig (19) Deduct Value for Patching

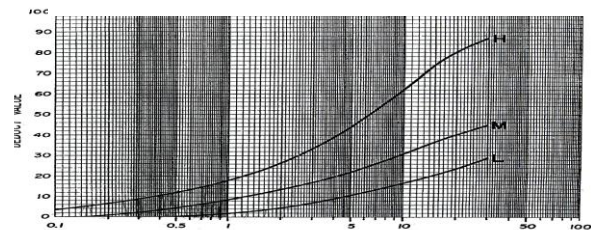


Fig (20) Deduct Value for Long & Tran. Cracking

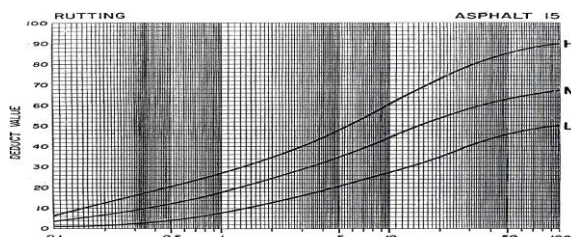


Fig (A-21) Deduct Value for Rutting

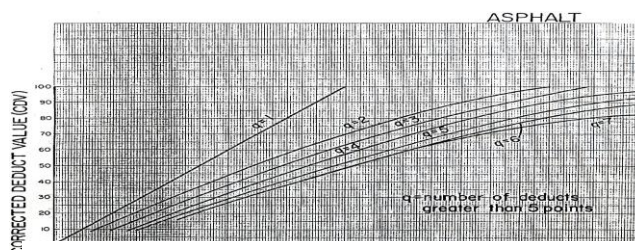


Fig (A-22) Correct Deduct Value Curves for Asphalt - Surfaced Pavements

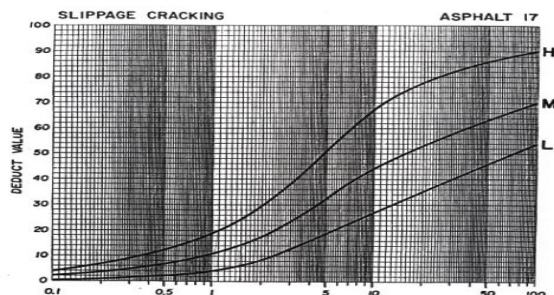


Fig (23) Deduct Value for Slippage Cracking

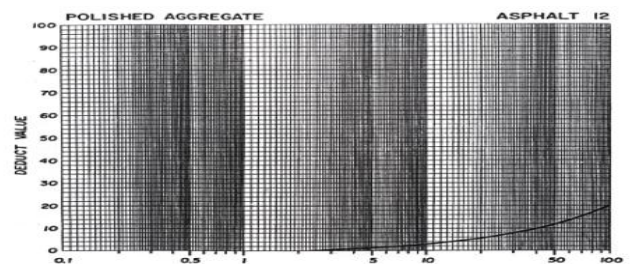


Fig (24) Deduct Value for Polish Aggregate

DEVELOPMENT OF MODEL FOR THE PREDECTION OF PAVEMENT CONDITION INDEX

The statistical techniques used for the models development required for evaluation of the pavement condition indices of the selected roads in the study area.. For the purpose of model development of the pavement condition, these data include: alligator crack, Bleeding ,depression ,block crack, (longitude and transverse) cracks , patching , pothole , polish , rutting and slippage crack .

OUTLIERS

If one or more of observations is different significantly from all others, it is called “outlier “.The cause of a faulty observation may be a mistake .Outliers and influential observations are checked by using Chauvinist's criterion Kennedy and Neville[1975].The results of this test can be found in**Table (5)** .

Table (5): Results of Chauvenet' Test for Outliers of PCI Database

Variable	Mean	Mini m	Maxim	Standard Deviation (s)	$\frac{ xm - \bar{x} }{s}$ X m = min	$\frac{ xm - \bar{x} }{s}$ X m=maxi
PCI	62.746212	8	94	20.796314	2.6324959	1.5028523
Alligator	20.5383	0.00	98.300	26.34316	0.779643324	2.951869932
Bleed	42.8764	2.7	104.8	20.63454	1.9520009	2.9960135
Depression	21.857875	1.3	53.2	10.73053	1.915830812	2.920836156
Block Crac.	238.9614	0.00	1240.00	364.0559	0.65638656	2.749683771
Lon & Tran	31.6042	0.00	105.3	26.99353	1.1708081	2.7496838
Patch	55.662276	0.00	158.2	45.15347	1.2327354	2.27301267
Polish	454.3457	51.5	1098.5	210.1489	1.9169536	3.065228
Pothole	1.8295455	0.00	6.00	1.649207	1.109325734	2.5287633
Rut	0.038346	0.010	0.158	0.039888	0.7106398	2.9997493
Slippage	38.294712	0.00	132.00	35.48959	1.0790408	2.6403602

Sample Size :264 : \bar{X}_m = value of outlier . \bar{x} = sample mean . s = standard deviation .

$\left(\frac{|xm - \bar{x}|}{s} \right)_{\text{tabulated}} = 3.08 >$ all calculated values . Thus the outliers are not rejected

MULTICOLLINEARITY

It is a condition that exists when the independent variables are correlated with another one. By using STATISTICA software the correlation coefficients between all of the variables were calculated and the correlation matrix was setup .This matrix can be seen in **Table (6)** ,the variables having the highest correlation coefficient with the designated dependent variable are selected and calculated, the regression equation is formulated.

Table (6): Correlation Matrix for PCI

STEPWISE REGRESSION PROCEDURE

The procedure begins by computing the simple regression model for each independent variable. STATISTICA software uses the F- statistics and it is usually set at F= 4.0 which is chosen because

Correlations (PCI model .sta- o131.sta)											
	ALIG	BLEED	DEPR	BLOCK	LON_ TRA	PATCH	polish	POTH OLE	RUT	SLIPP	PCI
ALIG	1	-0.054	-0.013	0.201	0.133	0.015	0.007	0.144	0.087	0.196	-0.18
BLEED	-0.054	1	0.0143	0.122	-0.026	-0.003	-0.03	-0.057	0.109	0.034	-0.02
DEPR	-0.013	0.014	1	0.128	-0.004	-0.055	0.03	0.1328	-0.029	0.135	-0.10
BLOCK	0.201	0.122	0.1276	1	0.1588	-0.016	0.061	0.3369	0.095	0.391	-0.39
LO_TRA	0.133	-0.03	-0.0041	0.159	1	0.0193	0.108	0.0425	-0.016	0.118	-0.09
PATCH	0.015	-0	-0.055	-0.016	0.0193	1	0.023	0.0733	0.079	0.015	-0.04
POLISH	0.008	-0.03	0.0298	0.061	0.1084	0.0227	1	0.0650	0.044	-0.002	-0.01
POTHOL	0.144	-0.06	0.1328	0.337	0.0425	0.0733	0.065	1	0.169	0.545	-0.61
RUT	0.087	0.109	-0.0293	0.095	-0.0160	0.0779	0.046	0.1619	1	0.229	-0.27
SLIPPAG	0.196	0.034	0.1351	0.391	0.1177	0.0153	-0.002	0.5449	0.229	1	-0.87
PCI	-0.184	-0.02	-0.1008	-0.38	-0.0864	-0.039	-0.01	-0.607	-0.274	-0.87	1

the significant level is about 5%. The standard is called the F- to – enter for independent variable .

DEVELOPED MODEL

The analysis through the stepwise regression technique is used for the purpose of PCI model development, the following PCI model form results in equ.(5);

$$PCI = 85.3360 - 0.4415 * Slip - 2.3254 * Poth - 37.2875 * RD \quad (5)$$

where:

- PCI* = Pavement Condition Index,
Pot = Pothole in (number),
RD = Rutting in(cm or mm), and;
Slip = Slippage Crack in(m^2).

The regressions summary and stepwise regression, and several possible developed models can be seen in **Tables (7) and (8)**.

Table (7): Regression Summary and Summary of Stepwise Regression for PCI Model.

Regression Summary for Dependent Variable: PCI						
R=0 .88713146 R ² = 0.78700222 Adjusted R ² =0 .7845445						
F(3,260)=320.22 p<0.0000 Std .Error of estimate: 9.6531						
	BETA	St. Err. of BETA	B	St. Err. of B	t(260)	p-level
Intercept			85.33596	1.038846	82.14498	0
SLIPPAGE	-0.75337	0.034637	-0.44146	0.020297	-21.7501	0
POTHOLE	-0.18441	0.034169	-2.32537	0.430868	-5.39693	1.53E-07
RUT	-0.07152	0.029433	-37.2875	15.34546	-2.42987	0.015782

Summary of Stepwise Regression; DV: PCI							
	Step +in/-out	Multiple (R)	Multiple R-square	R-square change	F - to entr /rem	p-level	Variable included
SLIPPAGE	1	0.87020	0.75726	0.757262	817.3521	0	1
POTHOLE	2	0.88440	0.78216	0.024904	29.83831	1.09E-07	2
RUT	3	0.88713	0.78700	0.004837	5.904277	0.015782	3

Models	R ²	SEE
PCI= 85.3360 - 0.4415 *Slip -2.3254 *Po - 37.2875 *RD	0.80	9.6531
PCI=84.31451- 0.44984*Slipp -2.37313 Po	0.78	9.7433

RESULTS OF THE ANALYSIS

The results of the technique that is used to development process of the pavement condition index model, shows that the slippage crack, pothole and rutting have largely affect the pavement condition index.

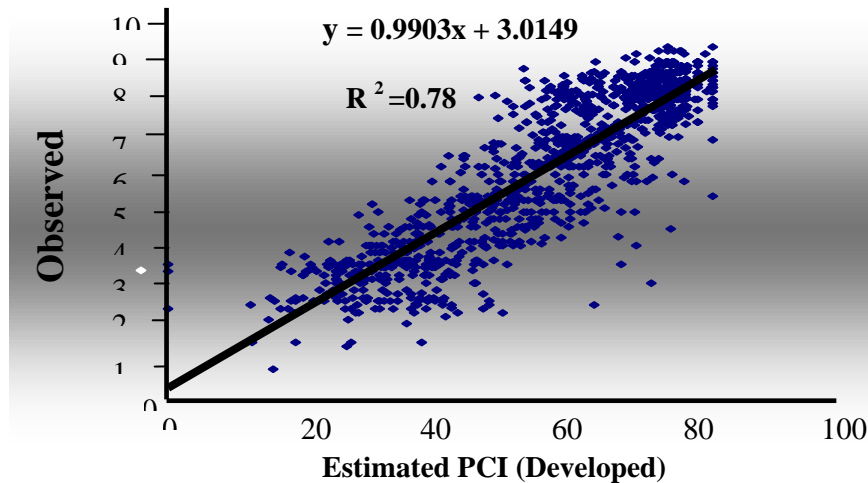


Fig (24) Observed PCI versus New Developed PCI- Model

Pavement condition index can however, be reduced by increasing the distresses in the road pavement. The results show that many variables have little correlation with the PCI and, therefore, little affect PCI, were dropped from the analysis.

It was found that the linear forms of the variables result the best correlation between the independent variables and PCI. The model found shown at previously as a PCI model (equa. 5).

DISCUSSION OF RESULTS

As a result of several different sets of regression models, three variables were found to be common to the general picture of each set to form the PCI model; these are pothole, rutting and slippage crack.

As stated previously the coefficient of determination for PCI model was found to be 0.80, and again that means; 80 percent of the PCI prediction can be explained by this model.

MODEL LIMITATION

As with all regression models, the model is only valid within the ranges of the variables they were developed from .Some additional limitations may be related to the study area. Specific specifications can be listed as follows;

- 1.A uniform pavement sections of a (1200 ft) each is used for the purpose of PCI model development.
- 2.Constant pavement areas of a (2500 ft²) each are used for the purpose of PCI model development.

VALIDATION OF THE DEVELOPED MODEL

The final step in the model building process is validation of the developed models. The objective is to assess the ability of pavement condition index prediction model to accurately predict amount of PCI

in the field. A review of the statistical researches suggested the following methods for validation of a regression model [Ahmed, Namir G 2002].

- check on model predictions and coefficients
- collection new data
- comparison with previously developed Models
- data splitting
- prediction sum of squares

SELECTION OF VALIDATION METHODS

The literature suggests that all available methods of validation could be used. However, in this case, it is not possible to use all the methods of validation. Therefore, the applicability of each method in terms of the validation of the PCI model will be discussed and the most appropriate methods of validation will be selected.

- The fourth method (Data Splitting) recommends that one should not consider data splitting unless $N > 2P + 25$, where N is a sample size and P is number of estimated parameters. For the above mentioned discussion and because of the nature of the available data; the fourth method (Data splitting procedure) was selected to assess the predictive ability of the PCI model. It has been

Variable	Mean	St. division	t	t_c
X= observed	67.60567	19.90337	0.073651	1.645
Y= predicted PCI Model	67.73326			

recommended that one may not consider data splitting unless $N > 2P + 25$.

VALIDATION RESULTS

The half of the observed data (those not used in the development process), is used in the validation process of the PCI_ model. The observed PCI values are plotted against those obtained by using of the developed model. This comparison is presented in **Figure (24)**.

The relation between observed and estimated PCI can be found in the following form in equ.(6);

$$(\text{PCI}) \text{ Observed} = 0.9903 * (\text{Developed PCI}) + 3.0149 \quad (6)$$

These findings seem to be in good agreement with the relation $y = x$. The results of checking the goodness of fit for the relation between observed and estimated PCI model by using Chi-square test and t- test, these testing can be seen in the following paragraphs .

Goodness of Fit

To checking the goodness of fit for the predicted models. t – test and Chi- square test were carried out and the following results are expressed;

t-test : $n = 264$, $df = 525$ confidence level = 95%

There is no reason to reject the null hypothesis. Thus the difference is not significant.

Variable	χ^2 – value	χ^2_c – value
----------	------------------	--------------------

n
d

X= observed	197.1773	233.993
Y= predicted PCI Model		

 $\chi^2_{test} :$
 $=$
264,
 $f =$

263, confidence level = 95%

For $\chi^2 < \chi^2_c$. Thus is no significant difference between the observed and the predicted values

CONCLUSIONS AND RECOMENDATIONS

The main conclusions that can be drawn from this research are summarized as follows:

1- A stepwise regression technique is used in the development process of the following pavement condition index (PCI) Model in Baghdad city:

$$PCI = 85.3360 - 0.4415 * Slip - 2.3254 * Poth - 37.2875 * RD$$

2-The developed (PCI) model is adequate to be used for the prediction of pavement condition index for local flexible pavements within the range of the data.

REFERENCES

- ASTM[2002]: **Standard Terminology Relating to Pavement Distress**; E1778-98, Volume 04- 03.
- ALswilimi, Saleh ,[1995], " **Management of Highway networks Maintenance**", Dar Al-liwa Publishing and Distribution , Riyadh ,(Arabic).
- Deighton [1998] , " **Pavement Condition Rating Systems** " , Transportation Research Record , National Academy of Sciences , Washington . D. C.
- Kennedy , J. B.; & Neville A.M [1975], "**Basic Statistical Methods for Engineers and Scientists** , 2nd Edition, Thomas Y., Crowell Company, In, USA .
- Keller.; & Warrack, B.[1997], "**STATISTICS for Management and Economics** 4th, Edition, USA .
- Susan T.; Mohammad K.; Alan H.; Kevin C.; & Mounir M. [2004], "**An Evaluation of Various Prioritization Methods for Effective Pavement Management : A Canadian Airport Case Study** " , Federal Aviations Administration World Wide Airport Technology Transfer Conference , Atlantic City , New Jersey , USA .
- Shahin A.Y. , [1982] " **Airfield Pavement Distress Measurement and Use in Pavement Management**, "TRB , Annual Meeting, No .893, Washington ,D.C.
- US Army Corps of Engineering [2003], " **User Manual (Micro Paver) 5.1** ," USA.
URL: <http://www.cecer>
- TECHNICAL MANUAL HEADQUARTERS, [1982], "**Pavement Maintenance MANAGEMENT** " , DEPARTMENT OF THE ARMY Council, Washington D .C. No. 5-623 November 1982.

NOMENELATURE

R^2 = Coefficient of Determination

SEE = Standard Estimation Error

$$X^2 = \text{Critical chi-square}$$

APPINDEX (A)

Table (A1) Data base Used For the Pavement Condition

[illegible]

Table (A2) Computed of Density For Distresses in Sample Sections

Site Section	Aluminum Density			Bleeding Density			Deposition Density			Hatched Larva Density			1st & 2nd Trays Density			Patching Density			Pest	Pathologic Density			Hatching Density			Shipping Density		
	T	S	U	T	S	U	T	S	U	T	S	U	T	S	U	T	S	U		T	S	U	T	S	U	T	S	U
1. Shook Tray Stream	0.3574			0.36	0.105								0.0406			0.888		0.1779	0.039									
				0.4	0.1								0.0331					0.0331										
				0.46									0.0331			1.38		0.0331										
				0.384	0.34								0.0331					0.0331								0.23		0.2242
				0.384	0.34								0.0331					0.0331								0.23		0.2242
		0.11		14	0.85			1.35					0.408					2.098		0.0331								0.3125
2. 100 ft. Street	0.6016			0.46	0.1							0.46						0.0331										
				0.384	0.34							0.46						0.0331										
				0.384	0.34							0.46						0.0331										
				0.384	0.34							0.46						0.0331										
				0.384	0.34							0.46						0.0331										
		0.23			0.384	0.34						0.46						0.0331										0.4
3. 100 ft. Street No. 28	0.2374			0.82	0.538	0.11	1.22					0.3062					2.01		0.0331								0.6	
				0.384	0.34							0.3062						0.0331									0.6	
		0.11			0.384	0.34						0.3062						0.0331									0.6	
				0.384	0.34							0.3062						0.0331									0.6	
		0.2374			0.384	0.34						0.3062						0.0331									0.6	
				0.63								0.3062						0.0331									0.6	
3. 0.63 N 30	0.2374			0.384	0.34						0.3062						0.0331										0.6	
				0.384	0.34						0.3062						0.0331										0.6	
		0.11		0.438	0.43		0.43				0.3062						0.0331										0.6	
				0.438	0.43		0.43				0.3062						0.0331										0.6	
				0.438	0.43		0.43				0.3062						0.0331										0.6	
		0.8594		0.83							0.3062						0.0331										0.6	
4. 0.63 N 30	0.6076			1.01	0.339		0.86				0.3062						0.0331										0	
				0.384	0.34						0.3062						0.0331										0	
				0.384	0.34						0.3062						0.0331										0	
				0.384	0.34						0.3062						0.0331										0	
				0.384	0.34						0.3062						0.0331										0	
		0.6676		0.3							0.3062						0.0331										0.68	

Table (A3) Computed of Pavement Condition Rating

[illegible]

EVALUATION OF THE SACRIFICIAL ANODE CATHODIC PROTECTION OF CARBON STEEL IN 0.5M NaCl USING EXPERIMENTAL DESIGN

Aprael Sarkis Yaro

Chemical Engineering Department, College of Engineering, University of Baghdad

ABSTRACT

This study examined the effect of Temperature (T); flow rate(F); and pH ; on the zinc consumption as sacrificial anode in cathodic protection of steel pipe carrying saline solution (i.e., 0.5 M NaCl) using a 2^3 factorial design. Rates of zinc consumption during cathodic protection were measured by weight loss technique and it ranges from 7.5×10^{-3} to 98.9×10^{-3} g/cm².day. For the system under investigation, the cell responsible for cathodic protection is Zn/NaCl/Fe

It was found that both temperature and flow rate increases the zinc consumption while pH decreases it sharply. It was found also that the interaction between the temperature and pH is the dominant term compared with other interactions.

الخلاصة

هذه الدراسة اختبرت تأثير درجة الحرارة، سرعة جريان سائل المحلول الملحي وحامضيته على استهلاك الزنك كمضحي انودي في عملية الحماية الكاثودية لأنبوب حديدي بأستعمال تقنية تصميم التجارب. ان معدلات استهلاك الزنك اثناء عملية الحماية الكاثودية تم قياسها بتقنية فقدان بالوزن و كانت مدياتها تتراوح بين 0.0075 و 0.0989 غم/سم².يوم. الخلية الكهروكيميائية المسؤولة عن الحماية الكاثودية في النظام قيد الدراسة كانت زنك/محلول ملحي/حديد. لوحظ ان درجة الحرارة و سرعة جريان السائل تزيد من استهلاك الزنك كمضحي انودي بينما حامضية السائل تقلل من ذلك بشدة. كذلك لوحظ ان التداخل بين درجة الحرارة و حامضية السائل هي السائدة مقارنة مع بقية التداخلات.

KEY WORD

Sacrificial anode, Cathodic protection, Seawater, Factorial design.

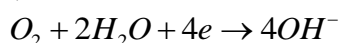
INTRODUCTION

Without some forms of protection, Steel is very susceptible to degradation in chloride- containing environments. To prolong the lifetime and functioning capability of steel, one of the most effective forms of protection is sacrificial anode cathodic protection. Sacrificial anode protection is called "sacrificial" because the anode is

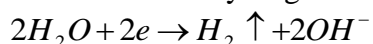
thought of as "sacrificing" itself to protect the structure. This type of protection utilizes a galvanic cell consisting of an anode made from a more active metal than the structure, so this method is also called galvanic anode protection. Sacrificial anodes require no external power. The protection current comes from the electrochemical cell created by the connection of the anode material to the more noble or electrically positive metal of the structure [Ulig, 2000]. In a galvanic couple between dissimilar metals, the galvanic current cathodically protects the more noble metal and preferentially dissolves the more active metal. Electrons flow from the active sacrificial anode to the noble cathode structure. The anodic reaction at the cathode structure, for example:



, is reduced by surplus of electron provided by the sacrificial anode. At the same time, the reduction of dissolved oxygen by reaction:



Or the evolution of hydrogen:



is accelerated. The cathode structure is cathodically protected, and the same electrochemical reactions are present at the cathode as when polarization is provided by impressed current. [Davies, 2003].

The aim of the present work is to study the effect of different operating parameters such as temperature, flow rate and pH on the rate of zinc consumption during cathodic protection of a steel pipe carrying 0.5M NaCl solution adopting 2^3 factorial design. Cathodic protection was carried out by extending a zinc strip along the steel tube to ensure uniform current and potential distribution along the wall tube.

APPARATUS AND PROCEDURE

The apparatus (fig.1) consists of an insulated 6 liters storage reservoir, 210 watt pump of capacity 11.4-54.6 lit/min and a vertical pipeline. The pipeline was made of low carbon steel of chemical composition: C%=0.1648; si%=0.254; Mn%=0.51; s%=0.0062; Cr%=0.0253; Ni%=0.009; Cu%= 0.1511; V%=0.0034; Fe% the remainder.

The tube dimensions were: 13.5 cm length; 2.68cm inside diameter and 0.31 cm thick. A zinc strip of 12.5 cm length and a 1 cm width, 0.6 cm thick was extended along the axis of the low carbon steel tube. The zinc strip was fixed at the inlet and was electrically connected by a wire to the low carbon tube outlet.

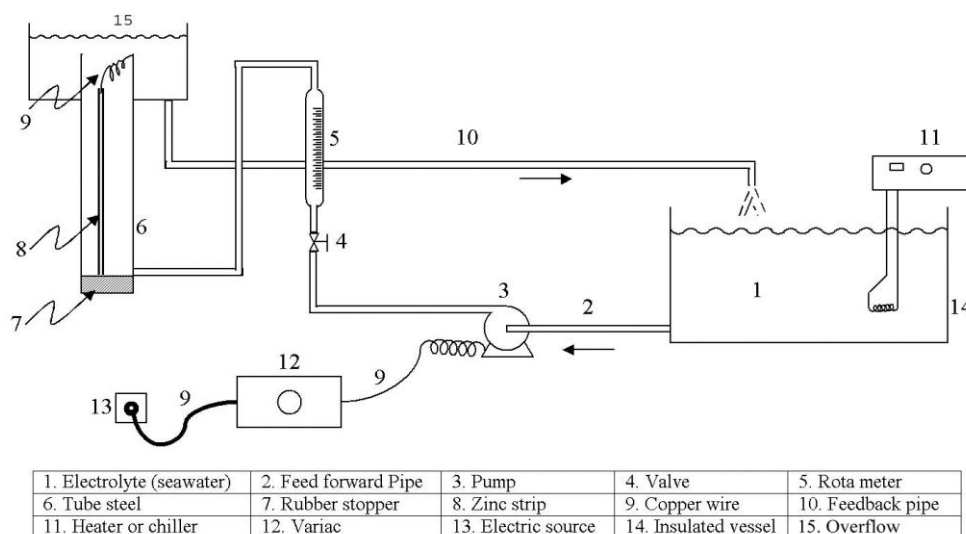


Fig (1): Schematic diagram of apparatus used in sacrificial anode test system

Before each run, a weighed zinc strip was fixed inside a low carbon pipe and 6 liter of 0.5 M NaCl solution after adjusting its pH was placed in the storage tank. The solution was circulated between the pipeline and the storage tank by the pump. Solution flow rate was measured by a rotameter placed after the pump and adjusted by a valve. Temperature was controlled by thermostat heater or chiller, duration of experiments was fixed at 4 h's . After each run, the zinc strip was rinsed in distilled water, dried and reweighed.

Experimental Design and Analysis:

Factorial design [Balton, 1984 and Armstrong, 1990] is an experimental technique by which factors involved in a process can be identified and their relative importance assessed. It is thus a means of separating those factors that are important from those that are not, and identifying the interactions, if any, between the factors chosen. Thus the construction of a factorial design involves the selection of parameters and the choice of responses. A 2^3 factorial design was used to determine the effect of temperature , flow rate and pH, on the zinc consumption used as sacrificial anode in protection of iron pipe carrying seawater (0.5M NaCl solution). To observe a significant weight loss (zinc consumption) for each experiment, duration time was fixed at four hours. The factors and the levels are shown in table (1). The matrix of the factorial design is shown in table (2).

Table (1) Factors and levels used in the 2^3 factorial design.

Factor	Low level	High level
T: temperature, °C	15	45
F: Flow rate ,L/h	300	900
pH: pH of solution	2	8

Table (2) Matrix of the 2^3 factorial design zinc consumption in sacrificial anode used in steel protection *

Exp. No.	Factor T	Factor F	Factor PH	Zinc Consumption (mg/cm ²)
1	-1	-1	-1	7.94
2	+1	-1	-1	13.89
3	-1	+1	-1	11.12
4	+1	+1	-1	16.48
5	-1	-1	+1	2.16
6	+1	-1	+1	3.210
7	-1	+1	+1	2.56
8	+1	+1	+1	3.72

*-1, Low level of the factor; +1, high level of the factor.

Result and Discussion:

The results for the zinc consumption as weight loss in (mg/cm²) during cathodic protection are listed in table (2). Based on the data [Khalid, 2006], the main effects of the factors under study and their interaction were calculated, table (3).

Table (3) Effects and interactions of the selected factors on the zinc consumption used as sacrifice in cathodic protection of steel.*

Factor	Main Effect or interaction
T	3.40
F	1.70
pH	-9.40
TXF	-0.12
TXpH	-2.30
FXpH	-1.22

* T indicates Temperature (°C); F, Flow rate (L/h); pH, acidity of the solution.

Table (3) shows that an increase in the both the temperature of the solution and its flow rate results in an increase in zinc consumption. while the pH of the solution sharply reduces, the zinc consumption within the range studied.

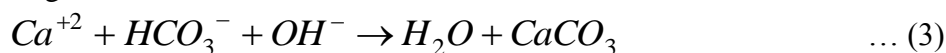
IN other words: The relative importance of main effect coefficients in present investigation indicates that the effect of temperature, flow rate, and pH with coefficient 3.4, 1.7 and -9.4 respectively is not the same (i.e., Temperature and flow rate lead to increase zinc consumption while PH of the solution induces a retarding influence). With factors combined effects, as measured by (TXF),(TXpH) , and (FXpH) are appreciably pronounced in reducing zinc consumption, but still (TXpH) term is the dominant term. According to previous explanation , it can be stated that: The alkaline conditions promoted by cathodic protection in seawater deposit calcareous scales on the surface, while reduce corrosion rates and necessary cathodic protection currents. i.e.,
The reduction reactions:



And



Increase pH at the protected surface by generation of OH^- during cathodic polarization. To some degree this is beneficial, because the ferrous alloys are resistant to mildly alkaline solutions in which a protective oxide film is stable. Also generation of OH^- in seawater deposits calcareous seals by reaction with dissolved calcium and magnesium ions:



Seal deposition causes a continuous decrease in limiting current density for O_2 reduction as scale thickness increases. The current necessary for cathodic protection decreases correspondingly.

To develop a response surface equation to predict the zinc consumption during cathodic protection, the data were analyzed using a commercially available package (statistica). A 2^3 fractional design was used for response surface analysis. The design was chosen because it allows the estimation of complex response functions up to the quadratic order [Box, 1978]. The design of selected experiments as well as the zinc consumption values is shown in table (2). To follow the levels adopted in this design, the factors studied needed to be decoded. The decoding formula was as follows:

$$\text{Coded variable} = \frac{(\text{uncoded value} - 0.5 \times (\text{high value} + \text{low value}))}{0.5 \times (\text{high value} - \text{low value})} \quad \dots (5)$$

The polynomial equation obtained, correlates the temperature (x_1), the flow rate (x_2) and the pH of the seawater (x_3) with the amount of zinc consumption (y) was:

$$Y = 7.64 + 1.7x_1 + 0.86x_2 - 4.7x_3 - 0.06x_1x_2 - 1.15x_1x_3 - 0.61x_2x_3 \quad \dots (6)$$

Where x_1 , x_2 and x_3 are in their coded values.

Equation (6) is statistically acceptable with a correlation coefficient of 0.98.

The effect of solution temperature and pH on zinc consumption for the solution flow rate at its minimum and maximum level (i.e., 300 and 900 L/h) respectively can be seen in figure (2 and 3).

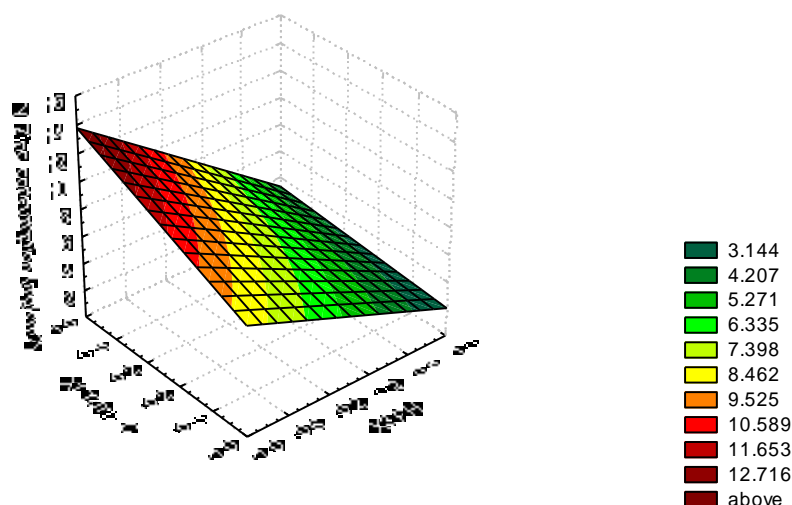


Fig (2) Effect of solution temperature and pH on zinc consumption as sacrificial anode; F= 300 L/h (-1).

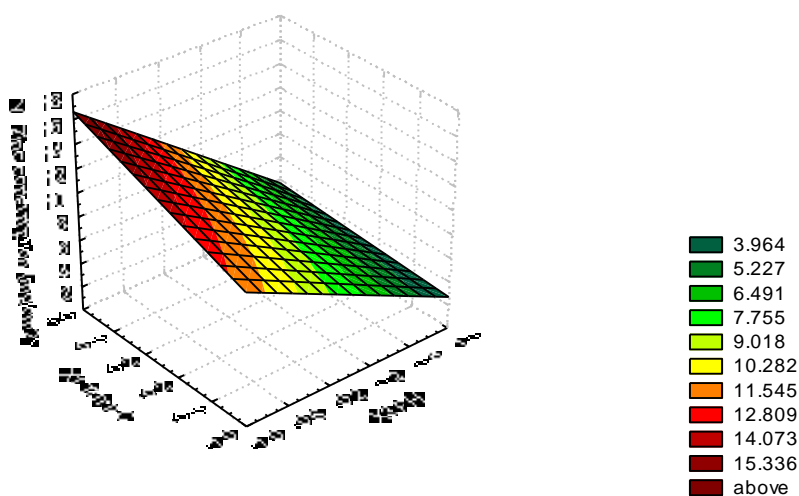


Fig (3) Effect of solution temperature and pH on zinc consumption as sacrificial anode; F= 900 L/h (+1).

It is clear from figure (2) that when the solution pH is at its maximum level, 12 (coded +1), the zinc consumption is about 3.144 mg/cm². This amount increases as the temperature increased and the solution pH shifted toward acidic (i.e. pH=2, coded -1), until it reaches about 13mg/cm² at pH=2 and the temperature is 45°C. This means that the zinc consumption increases about 4 times with pH shifting. Same behavior can be seen in figure (3), but in this case the zinc consumption is more pronounced with flow rate increase to 900 L/h.



Conclusions

Temperature and flow rate of the solution were found to some extent affect the zinc consumption as sacrificial anode in cathodic protection of steel in sea water, but the pH of the solution was found to be significantly the dominant. The correlation of temperature, flow rate, pH of the solution and the amount of zinc consumption as sacrificial anode can be adequately described by equation (6). Finally experimental design techniques such as factorial design proved to be useful for the identification and correlation of the significant factors that affect cathodic protection of steel by zinc consumption.

References

- Armstrong N.A, James K.C., (1990) "Understanding experimental design and interpretation in Pharmaceuticals", England: Ellis Harwood Ltd;:27-54.
- Bolton S., (1984) "Pharmaceutical Statistics: practical and clinical applications,". 3rd ed. Marcel Dekker Ins; New York: 258-280.
- Box. M.J., Hunter W.G, Hunter J.S.. (1978) "Statistics for experimenters : An introduction to design data analysis and model building, New York, : John Wiley and Sons.
- Davies, K.G. (2003), "Cathodic protection in practice", internet site www.npl.co.uk, 25/10/2007.
- Khalid, W.H., (2006) "Cathodic protection of low carbon steel in seawater" Ph.D thesis, university of Baghdad, .
- Myres M.H., (1971) "Response surface methodology", Boston: Allyn and Bacon.
- Ulig, H.H. (2000) , "Corrosion handbook", edited by Winston R.R., 2nd edition, John – Wiley and Sons.



DESIGN AND IMPELMENTATION A PC BASED SYSTEM FOR CIRCUIT TESTING

By :ZAID ALI SALMAN
B.SC. ELECTRONICS & COMMUNICATION ENGINEERING 2002
SUPERVISED BY
Dr. SARKOUT N. ABDULLA
Assistant Professor

ABSTRACT

This thesis deals with design and implementation of PC based control unit for testing systems. The design of the system involves mainly the hardware circuits, and software.

The tester carries out the following types of test Analog circuit test, Digital I.C. test, In-circuit test, and functional test.

The system designed and implemented, the implemented system hardware was built around two parallel ports. The hardware includes four buffers used as I/O channels addressed as Analog input (A\I), Analog output (A\O), Digital input (D\I), and Digital output (D\O). The system also includes Analog to digital converter, Digital to analog converter, and resistor testing circuit. The data to processed can be in digital or in an analog form. In the same time the hardware outputs controlling signals for testing and controlling the equipments. These signals are in digital or analog form.

The implemented system software has two main user interfaces, one for selecting the mode of operation (as read or write), and activates the associated buffer. The other which included the functions of tests.

For the resistor testing, I.C. testing, and circuit testing the system software compares inputs from the unit under test (UUT) with stored upper and lower limits, if the input is a value between them the test is considered successful otherwise the test fails.

The software has been written in "Visual Basic" programming language running under windows® (ME\XP) operating system environment and tested on the already exist hardware.

The system has been tested and it worked successfully for different resistance value and different types of Digital I.C.

INTRODUCTION

The manufactures of the Printed Circuit Board (PCB) face the constant challenge of determining the quality of the product they build. All manufactures have to inspect finished products to insure that they satisfy the required quality standard [1]. Electrical testing has always been an essential tool used in these determinations [2].

A general definition of a test is an experiment done either to confirm or deny a hypotheses or to differentiate between two hypotheses. Testing a device means checking it whether it is operating as expected or not. In any type of testing, needed to know two things. First, which input stimuli should be applied to the device? Inputs should apply only those inputs that activate the fault i.e. the inputs which result in different outputs from the

The need for more effective methods has long been accepted as common place among electronic engineers [3].

The idea of having test equipment, which can check the components in circuit, to determine its performance is an attractive work [4].

Different testing techniques are needed to test the whole board. Automatic testing of electronic devices has been a major factor not only in the overall improvement of product quality and reliability, but also in the dramatic lowering of product costs [3].

Types of Testing Approaches [5].

There are some basic approaches for testing populated circuit boards or modules. These are:

Functional Testing: Using this approach, a board is inserted into an actual system and its behavior is observed while the system performs its regular functions. This approach has several major shortcomings. First, it is extremely difficult to diagnose a failure. Second, it is difficult to develop complete test suites, or even measure how good a given test suite is. In general, it is extremely difficult to develop quantification of faults (or defects) that are covered by a given functional test. This is because no algebra that defines and links functional activity to physical defects such as shorts or opens among the nets. Ones tests are developed; there isn't any mathematical method for determining fault coverage. Only "guesstimates" are available. Finally, functional test set up may be very costly since it is unique to each different board and may also require ancillary functions (e.g. disk unit, etc.) to be available functioning in order for Unit Under Test (UUT) board to be tested.

Card-edge Testing: This is different Testing approach when compared to one above. In this case, a "card-edge"(i.e. edge connector) tester is used to insert UUT board in order to apply signals sequence/combination of signals (and observe responses at all times) at the card-edge. Thus, whereas the card-edge tester can be programmed to mimic the exact behavior of the target system for the UUT board it can also be programmed to control and observe the signal values along the edge-connector at a fine resolution. This improves the testability of the UUT but, like the Functional Testing approach, difficulties in test generation and coverage assessment remain very high. It also suffers from limited-access since complex boards, nets and components on the "interior" of the PCB are difficult to test due to limited access from just the edge connector.

In-Circuit Testing: ICT was developed in response to difficulties in creating card-edge and functional tests in the late '70' and early 80's. This technique represents a major departure from the Functional Testing (and card-edge testing) approach, in that it tests one component on a PCB at a time. As the PCB's functional complexity grew, it became difficult for engineers to understand the entire PCB functionality and test generating tools had difficulty in crating tests for the entire PCB. The 'one IC' at a time became a convenient divide-and-conquer approach to minimize test development time by breaking down the PCB into small MSI (at that time) circuits such as an AND gate that tests could easily and automatically developed. To achieve its goal, In-circuit Testing (ICT) uses a bed-of-nails fixture to contact the board-level nets in order to apply electrical stimulus and observe the response. The bed-of-nails fixture provides an array of spring-loaded test pins that come into contact with the UUT board at specifically designed points, called test points, whose locations must be planned during board layout so that there is sufficient surface area and clearance for paper contact to be made at each pin position. Each test point may be used to inject a signal value into the corresponding net or to observe its present value.

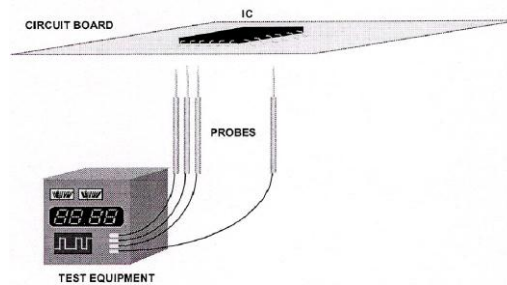


Fig1. Illustration of In-circuit Testing

1.2 Related Works

In 1979 Schreiber made the first Automatic Test Generation Technique classification. But it was in 1979 when P.Duhamel and J.C.Rault published a more exhaustive categorization of known analog circuit testing methods. The types of tests and faults to diagnose were given and classified. The methods were grouped into estimation techniques, topological methods, taxonomical methods and methods for linear circuits [10].

In 1985 J.W. Bandler and A.E. Salama reported another excellent classification, including methods that had just appeared and improvements obtained from them. This is one of the most referenced reviews for analog electronic circuit testing. They classify the methods into two main groups: techniques that need a simulation before the test, and the ones that need the simulation after the test [7].

In 1987 Mohammad Baha Al-Deen used a microcomputer as a based system for circuit testing. The project used the microcomputer as a part of an automatic test system used for Analog In-circuit PCB testing. Testing operation were achieved by comparing voltage taken from UUT with data stored in the microcomputer and the results were displayed by using monitor or a printer to printed out the results [4].

In 1999 Malathe AL-Qezweeny used also a microcomputer in design and implementation a telephone tester. The project used a computer (NEC6001) as a dedicated computer based automatic telephone tester suitable for testing push button and rotary telephone sets [9].

In 2002 Waseem AL-Haidari used a personal computer to build a data acquisition and monitoring system for (Automated Test Equipments) ATE. The system used Industry Standard Architecture (ISA) bus to interface with testing circuit [9].

2. BASIC CONCEPTES OF TESTING SYSTEMS.

The problems associated with testing have increased with introduction of each new generation of equipment. An important contribution towards solving these problems has been made by the introduction of automatic test methods [3].

2.1 Type of Faults: Test Capabilities and Selection

The process of testing or diagnosing circuits consists in applying certain types of excitation to a circuit and then analyzing the responses obtained in order to derive a possible failure. A fault could be defined as any variation of a component value from the nominal. This could produce an abnormal behavior of the global circuit [8]. A typical Automatic Test Equipment (ATE) environment is the one shown in Figure 2

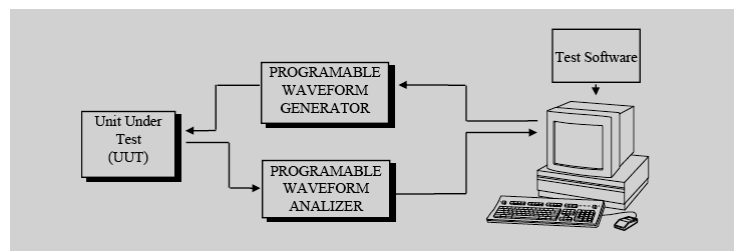


Fig2. : Basic structure of an ATE system

According to the figure, an ATE system should carry out the following basic actions: [10]

. Signal generation, using an external device such as an acquisition card DSP board, waveform generator operated via a GPIB bus, etc. It is necessary to have a set of stored input signals that produce particular circuit responses that are useful for fault detection and isolation. These input stimuli could be sine waves, square waves, DC-signals, ramps, etc.

Take measures from the circuit and obtain signatures. The output response can be interpreted in time or frequency domains. Once the measures are taken, some features can be extracted, for example a tuple [overshoot, rise time] or a particular sequence corresponding to the signal shape. The set of parameters that characterized a signal is known as a signature.

3. Interpretation of the obtained signatures. These signatures can be compared with the ones previously stored, or used to derive possible parameter values. These tasks require an appropriate diagnosis strategy.

There are many researches in the bibliography concerning the testing or diagnosing of electronic circuits. The objective of these two disciplines is almost the same but, although they have a lot in common, there is an important difference between them. In general, the purpose of the test, as it is known in the industrial domain, is to detect a fault in a circuit, while fault diagnosis is not only to detect but also locate the fault or fault identify the incorrect parameter values [10]. Both domains are described in the following paragraphs.

2.2 Functional testing and In-circuit testing

Printed circuit board testing can be divided into two different approaches, namely In-circuit testing and functional testing. Each has a specific job and solves a specific problem.[4]

In-circuit testing can be considered as a diagnostic tool, While functional testing tests the characteristics of parts, electronic performance of the circuit and determines whether a PCB is a fault-free or not. [11]

2.3 The concept of in-circuit tester operation

The testing theory of an in-circuit tester is based on comparison With known good unit. Good master unit (such as: component, circuit, IC, etc) are measured in predetermined sequence and the obtained data are stored in the memory of the computer. The unit to be tested is measured in the same sequence to see if the measured values lie in the certain range centered around the stored data samples. The unit under test is judged to be good if the measured values are the same as the data samples or lie in the certain range centered around them, Therefore the accuracy of the samples is an important point in deciding the performance of the tester.

2.4 Guarding Technique

As mentioned previously, in-circuit testing involves tests of individual components mounted on a PCB, hence the major task of an in-circuit tester is to exclude the influence of other components surrounding the component under test, and this can be achieved using guarding technique.

Guarding is a technique to eliminate as much as possible the effect of impedances surrounding the component under test in order to measure the actual value of the component.

Without guarding, the percentage of components showing a value almost equal with the actual value is 50 to 60 percent for analogue boards and about 80 percent for digital boards [12]. However, these rates do vary according to the kind of the circuit.

The guarding technique uses the characteristics of an op-amp for isolating the component under test from the effect of parallel impedance caused by other components. A typical situation is shown in a Fig. (3) with R_f is a known feedback resistance and R_x is the resistance to be measured, when the measuring voltage V_i is applied, V_o is generated as determined by:

$$V_o = - (R_f / R_x) V_i$$

Since the non-inverting input of the op-amp in fig. (3.) is grounded; hence, it is at zero potential because of the virtual short. As a result of both ends of R_2 comes to zero and current would flow through it. The current through R_1 flows to ground and return to the input voltage source V_i , hence the output voltage of op-amp will be proportional to the value of R_x only (since V_i and R_f are constants).

Generally speaking, when impedance Z_x on a circuit is under the influence of parallel impedance caused by several other components, it is possible to eliminate the influence of other components and measure Z_x , with one end of all other components grounded.

It should be noted that the guarding technique is not applicable to cases where there are two or more individual components completely in parallel. In such instances, the in-circuit tester views these parallel components as a single component with an impedance value equivalent to the impedance formed from the parallel combination. This is a limitation of all in-circuit testers.

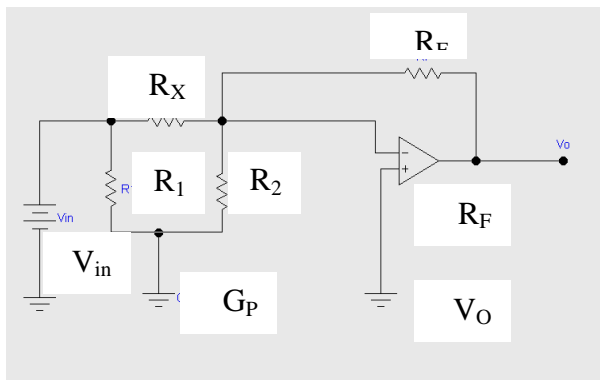


Fig 3. Testing guarded resistor

Digital IC. Testing

The evaluation of the reliability and quality of a digital IC is commonly called "testing", yet it is comprised of distinct phases which are mostly kept separate both in the research community and in industrial practice.

Verification [13]

This is the initial phase in which the first prototype chips are "tested" to ensure that they match their functional specification, that is, to verify the correctness of the design. Verification checks that all design rules are adhered to, from layout to electrical parameters; more generally, this type of functional testing checks that the circuit: (a) implements what it is supposed to do and (b) does not do what it is not supposed to do. Both conditions are necessary. This type of evaluation is done at the design stage and uses a variety of techniques, including logic verification with the use of

hardware description languages, full functional simulation, and generation of functional test vectors. Figure (4) shows the principles of testing digital IC.[14]

Testing Principle

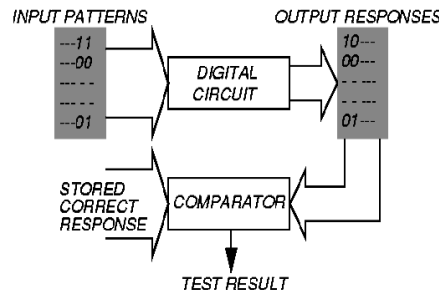


Fig 4. Testing Digital IC. Scheme.

Test Pattern Generation [13]

Test pattern generation is the process of generating a (minimal) set of input patterns to stimulate the inputs of a circuit, such that detectable faults can be exercised (if present). The process can be divided in two distinct phases: (a) derivation of a test, (b) application of a test. For (a), one must first select appropriate models for the circuit (gate or transistor level) and for faults; one must construct the test such that the output signal from a faulty circuit is different from that of a good circuit. This can be computationally very expensive, but one must remember that the process is done only once at the end of the design stage. The generation of a test set can be obtained either by manual methods, or by algorithmic methods (with or without heuristics), or by pseudo random methods. On the other hand, for (b), a test is subsequently applied many times to each integrated circuit and thus must be efficient both in space (storage requirements for the patterns) and in time. Often such a set is not minimal,

3. HARDWARE IMPLEMENTATION

The implemented system is used to test analog passive components (resistors), analog voltages, Digital IC and resistance potential divider. The system is based on using a computer. The test results are displayed on the screen of the RGB monitor.

The block diagram of the testing system is shown in the figure (5) the system consists of several connected units, and consists of the following main units.

Input/output interface unit.

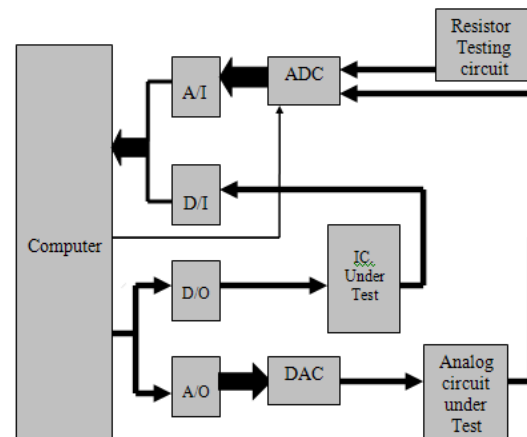
Analog to digital conversion unit.

Resistor testing unit.

Digital IC testing unit.

Digital to analog conversion unit.

Functional testing unit.



Each of these units will be described in details.

Fig(5). Block diagram of the Testing System.

3.1 Input/output interface unit

Interfacing is a term that is applied across a broad range of electronic implementations. It relates to systems as well as to individual components. Interfacing usually involves effectively traversing a boundary one entity to another. In the field of electronics, the entities can be viewed in a hierarchical fashion from a system, subsystem, components.

The tester is interfaced to the computer system via a parallel port. The tester uses the four 74245 octal buffer line drivers (bi-directional buffer) to interface to the computer system. This device is used for several good reasons; it buffers the computer port during the communication with external hardware.

A more important function of these devices is that of computer protection. The devices help to isolate the computer bus from outside problems. If the external hardware were tied directly to the computer bus, this protection would be missing.

The 74245 has the DIR pin to select the direction of data transfer, so this pin is put logic 1 or 0 depending on the direction selected from side A to side B, or from side B to side A respectively.

The four buffers can be used as follows depending on the DIR pin. Analog input (A/I), Analog output (A/O), Digital input (D/I) and Digital output (D/O).

In the proposed system two parallel ports can be used as LPT1 and LPT2,

Figure (6) represents the circuit diagram of the input/output interface unit. The 8-bit data group of the LPT1 is connected to the A data port of the four 74245. While 4-bit of the data group of LPT2 are connected to the Output Enable OE pin of the four buffers respectively.

The aim of this connection is to switch between the buffers by sending an appropriate set of word that activate one of the buffers and isolate the others.

There are another 3-bit from the data group of the LPT2 are connected to the status group of the LPT1 to indicate it to set the 8-bit data group in read or write state to match with the active buffer.

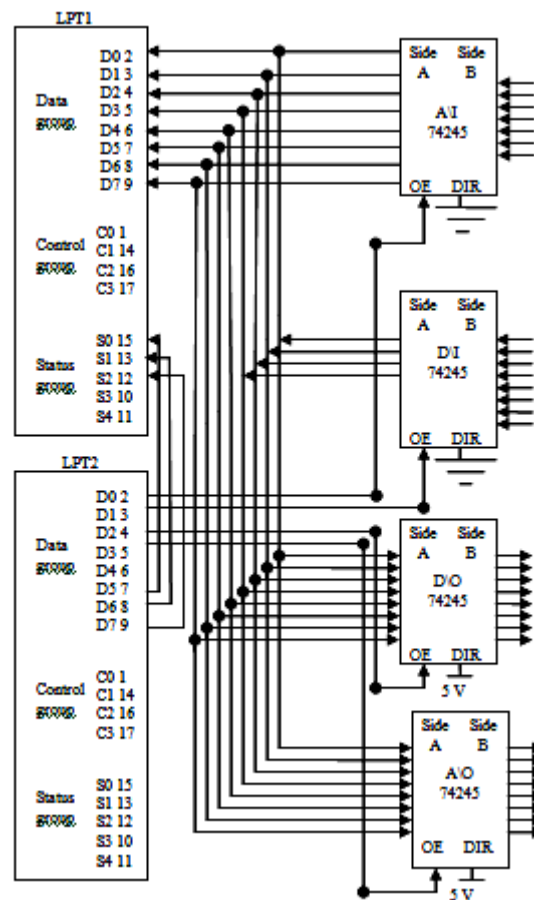


Fig 6. Circuit Diagram of I/O Interface unit

3.2 Single chip data acquisition system (Analog Multiplexer/ADC)

An analog multiplexer is simply a switching unit having a number of analog input channels and a single output channel, which is connected in turn to each of the individual input channels. So the output is one of the inputs and the selection of which one of the inputs will appear at the output is under digital control like a simple decoder. The input to the decoder represents the address of analog input channel and the number of the line inputs to the decoder depends on the number of analog inputs to the multiplexer. In the proposed system three lines from LPT1 are input to the decoder to select one of the 8-channels.

The analog Mux is used to couple the output of the test circuits to the ADC in a preset sequence, while the ADC is used to convert these output analog signals to their digital equivalent by comparing it against a reference signal. In the proposed system the ADC0816 is uses a Successive-approximation technique, which is a feedback system operates on a trial and error technique to approximate an analog input with the corresponding digital code. figure (7) shows the circuit diagram of ADC chip interfaced to the A/I buffer

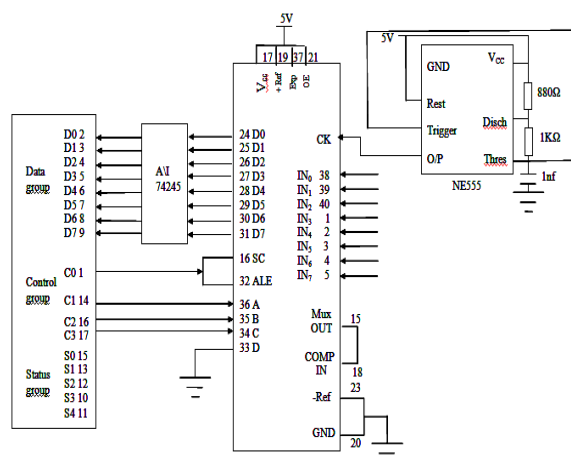


Fig 7. Circuit Diagram of ADC

- Test Circuit for resistors

The test circuits use an op-amp type (LM 358, App.A-3) as the basic building block.

Constant voltage technique is used to test the resistors. The range values of resistor testing circuit covered are between 100 Ω to 15 k Ω , these values are divided into two ranges:

Low range resistors (100 Ω to 1 k Ω).

High range resistors (2.2 K Ω to 15 k Ω).

Each range has a separate test circuit. Figure (8), shows the resistors test circuit. The difference between the low range test circuit and the high range test circuit is the feedback resistor (R_f).

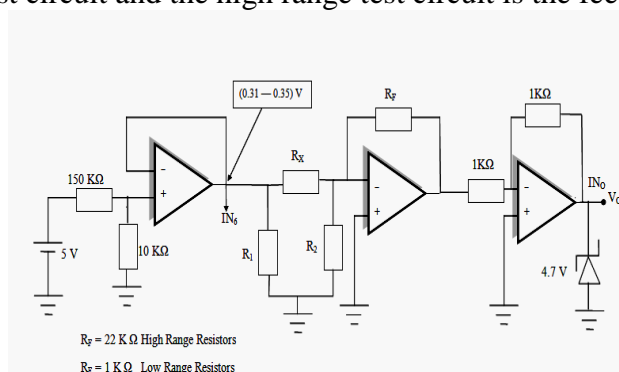


Fig 8. Test circuit for Resistors.

- Digital I.C. Test

One of the main functions that test system does is digital I.C. test. This system tests three types of digital I.C. 74LS00, 74LS08, and 74LS32. The test procedure can be described by three phases. Generation of an appropriate test bit pattern that produces a desired output, that will be done by software which writes the test bit pattern to parallel port (LPT1). This test pattern is applied to the I.C. under test through the D\O buffer which connected to Latch (74LS373, App.A-4). The purpose of using latch is to capture the test bit pattern and apply it to the I.C. under test when the D\O is off and D\I activated. The Enable of the latch and the Output Enable (OE) of the D\I are connected together. So at the beginning of the test D\O is active, D\I is off, and latch behaves as a buffer i.e. the output of the latch follow the input. The next step is to change the status of D\I to be active, in the same time the latch latched the last output. Finally the D\O is set in off mode. The last phase of the test procedure is reading the output response that's come from I.C. under test through D\I and parallel port (LPT1), and compares the output with truth table of the specific I.C. and display the result. Figure (9) shows the circuit diagram of the I.C. tester.

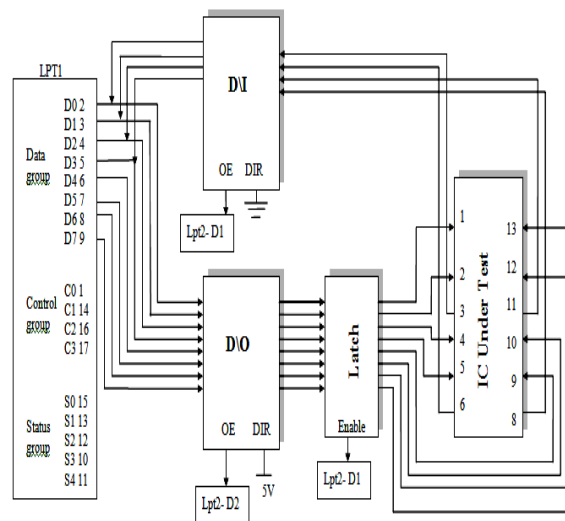


Fig 9. Circuit Diagram of I.C. Tester Circuit

- Testing Circuit Response

This type of test can be called Functional test. It depends on applying certain input on the circuit under test and compare the result obtained by the expected one. In this system an input signal generated from PC is applied through A/O buffer and is converted it into analog form by using digital to analog converter (DAC). The type of DAC used in this project is called R2R DAC, Figure (3.8) shows the circuit diagram of the DAC. The output of the DAC is connected to a buffering circuit to prevent any change in the value of the output of DAC because of load balancing. The output of the DAC is connected to ADC through channel three to check the value of voltages applied to circuit under test. The output obtained from the circuit (Attenuation circuit used in this project) is applied back to ADC through channel two. Figure (10) shows the circuit diagram of attenuation circuit.

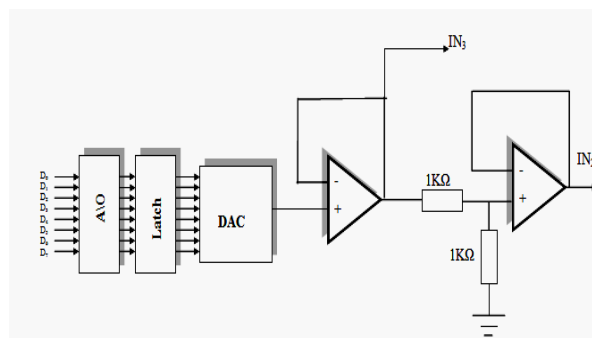


Fig 10. Circuit Diagram of Attenuation circuit

- RESULTS

4.1 User interface

The software of the system consists of two main user interfaces, one is used for choosing the type of operation as Digital input test, Digital output test, Digital I.C. test, and Analog test. Figure (11) shows the user interface according to parallel port 2

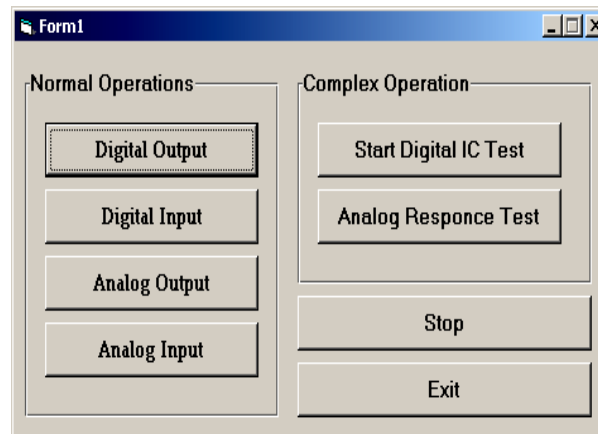


Fig11. User interface according to parallel port 2

The second one receives the order and displays the type of operation and contains the testing program function as receiving the settings and displays the results. Figure (12) shows the user interface according to parallel port 1.

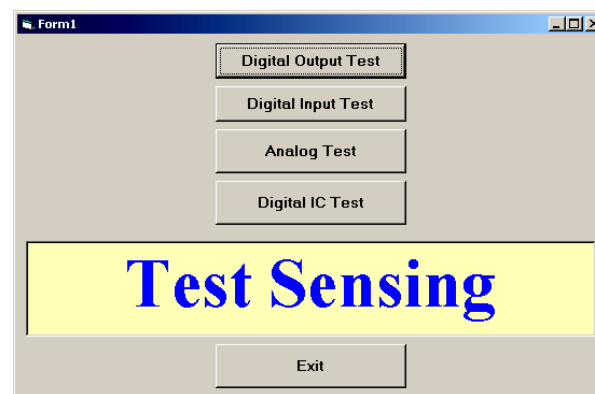


Fig 12. User interface according to parallel port 1

As mentioned previously when the operator clicks one of the button in Fig (11), the type of the clicked button immediately appeared in the text box in Fig (12). The message that appears in Figure (12) presents at the start of the program, which mean that LPT1 senses which mode of test sent to it from LPT2.

Digital I.C. test results

The first two steps is the same in each operation of any type of test, the choice of type and clicking the test button as shown in **Fig (13)**.

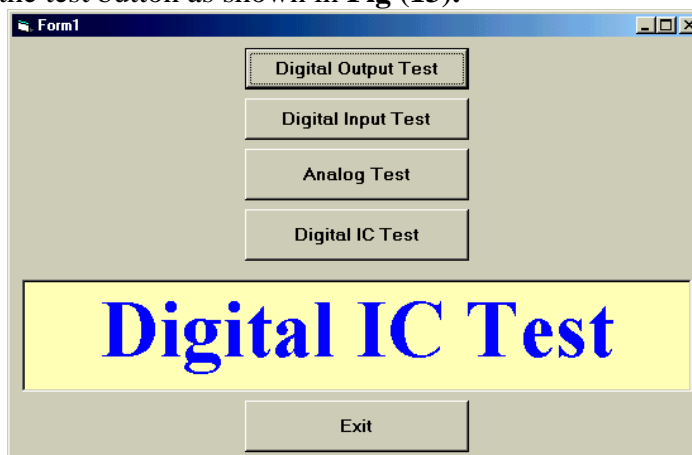


Fig 13. Selecting I.C. test

The operator will present with a new window that contains the type and number of I.C.s. He selects one of them for testing as shown in Figure (14).

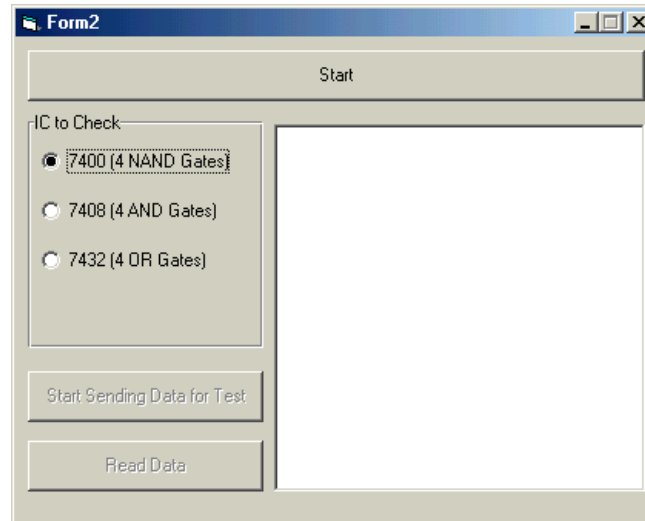


Fig14. Selecting I.C. under test

When the operator selects I.C. to be tested and then click start button the test starts and the result will be displayed, Figure (15), and Figure (16) shows the results obtained from testing two I.C.. One passed test and the other failed.

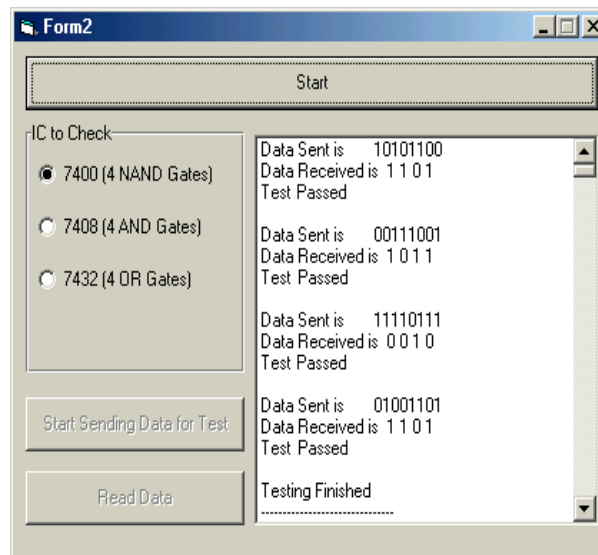


Fig 15. 7400 I.C. passing test result

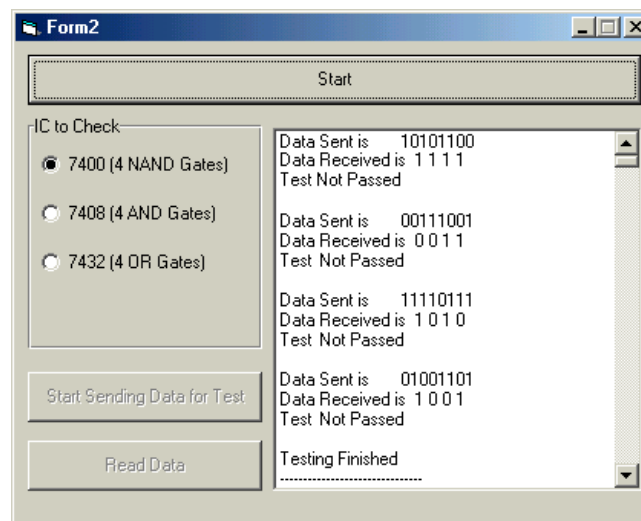


Fig16. 7400 I.C. Test is failed

After the test finished, a new window appears asking the operator to choose the next I.C. to be tested as shown in Figure (17).

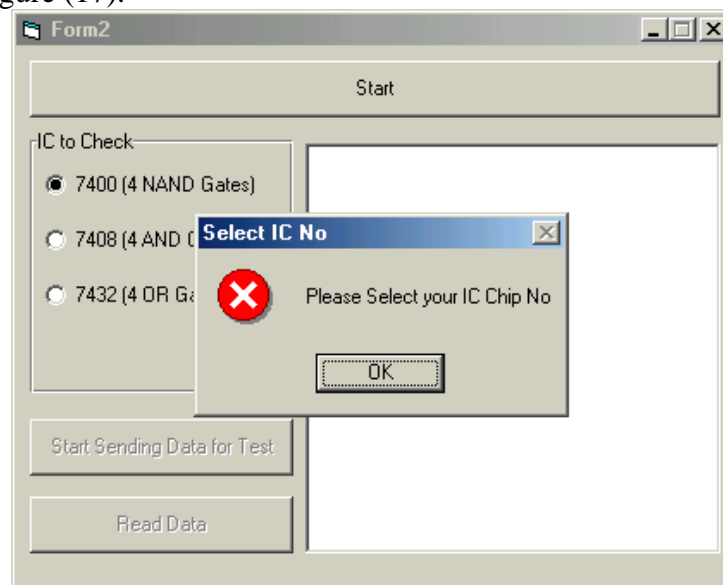


Fig 17. Selecting new I.C. to test

Analogue Test results

When the operator selects to test in analog mode. So at analog test message presents in text box, as shown in fig (18):

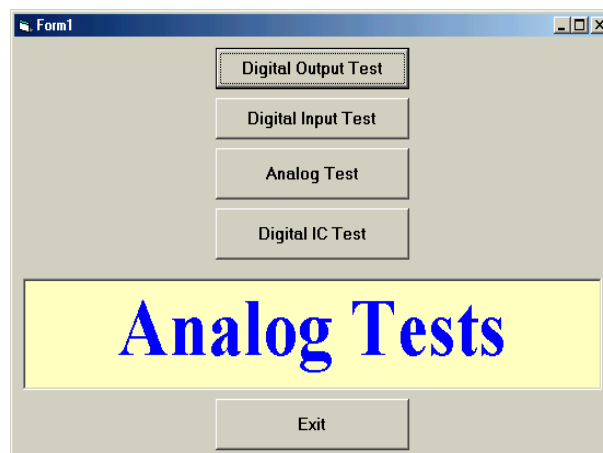


Fig18. Selecting Analog test mode

The operator after clicked the analog test button in Fig (18), a new window appears. Figure (19) then displays set of buttons each one of them indicates the type of test.

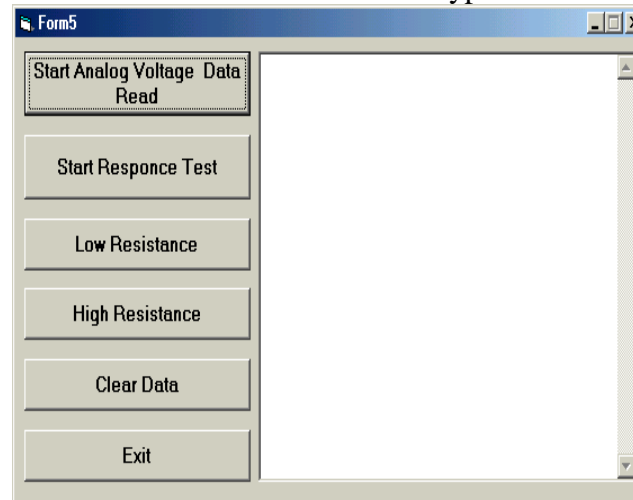


Fig 19. Analog test selection interface.

Analogue voltage results

This system displays the values of three different voltages and display the channel connected to it. Figure (20) displays two reading to the channels. In channel 6 there is different in the value because changing in the voltage.

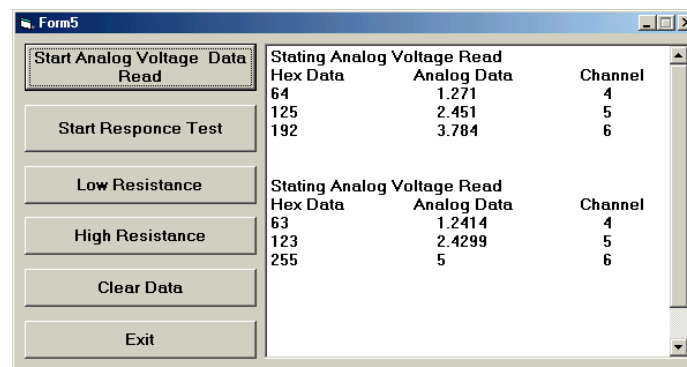
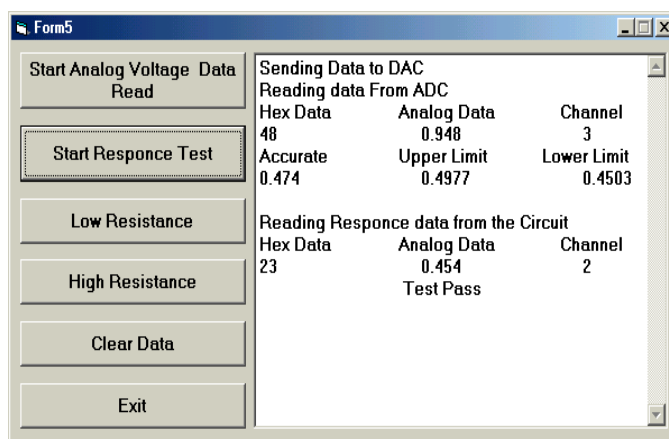


Fig 20. Analog voltage data read results

Response test results

The operator when clicks "Start Response Test" button the program presents a message showing to the operator the value of the voltage from DAC, also it shows the expected response of the attenuation circuit, and display the upper and lower acceptable limits. The program then displays the practical value of the response as read by the system and compare it with limits and finally displays the result as the circuit passed the test or failed. Figure (21).



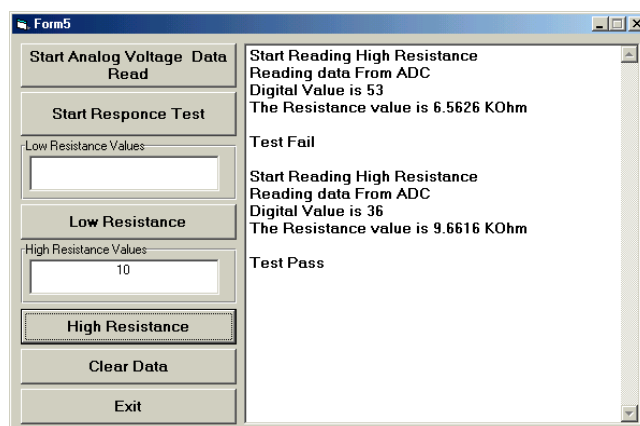
Hex Data	Analog Data	Channel
48	0.948	3
Accurate	Upper Limit	Lower Limit
0.474	0.4977	0.4503

Hex Data	Analog Data	Channel
23	0.454	2
Test Pass		

Fig 21. Circuit response result

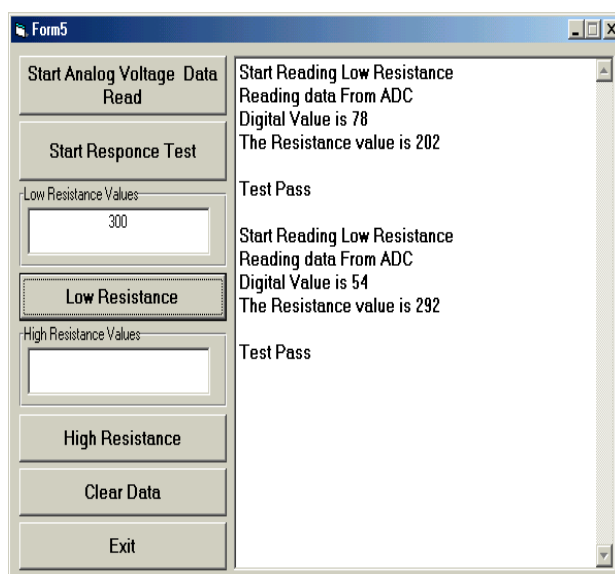
Resistor test circuit results

The operator must first set the value of resistor to be tested and starts the test. The program then sets the upper and lower acceptable limits. Read the value of the voltages, calculate the resistor value, compare it with the limits, and display the result where the test pass or not. Figures (22), and (23) for low range.



Digital Value	Resistance Value
53	6.5626 KOhm
Test Fail	
Digital Value	Resistance Value
36	9.6616 KOhm
Test Pass	

Fig22. High range results



Digital Value	Resistance Value
78	202
Test Pass	
Digital Value	Resistance Value
54	292
Test Pass	

Fig 23. Low range results

Sources of errors

-. Deviation from the amplifiers ideal characteristics

The op-amps used in test circuits is considered to be ideal, in fact there is no ideal op-amp due to various types of non-idealness of the circuit performance, such as finite input impedance which allows a voltage drop to exist between the inverting terminal and the guarding point. To minimize this voltage drop, an op-amp with very high input impedance (MOS or bipolar-field effect (BIFET)) should be used to minimize this voltage drop.

-. Errors in the ADC

The system uses an 8-bit ADC. The bit resolution is 0.019V which represents the basic error introduced by the ADC. This value of bit resolution will affect the accuracy of conversion especially for low values of DC voltages. The ADC error was taken into account when determining the upper and lower limits.

-. Conclusions

In previous chapters, the design, implementation, and testing of a flexible a PC-based test system has been carried out.

In this work, Automatic testing system has been designed and implemented which consists of two parts: the hardware circuits and software programs. The hardware structure consists of two parallel ports, Buffering circuits, resistor testing circuit, latching buffers. The First parallel port used to transfer the bi-directional data, while the second one used for controlling the I\O buffers and signaling the first parallel port to which mode to is set. The four I\O buffers used for isolation of the parallel port and to switch between types of I\O so can be called it as A\I, D\I, D\O, and D\I. To indicate to Analog or Digital input or output. The ADC chosen for the design of analog input section is Monolithic I.C. (ADC0816), which is appropriate for low speed input signals.

The software design of the system consists of two main parts: Selecting of the type of test, and the performing of the test. The selector parts is used to activate one of the four I\O buffers and indicates the first parallel port to change it's mode from writing to reading depends on the indications. The second parts is responsible of performing each type of test as reading the values, making the calculations; comparing the results with the limits, taking the decision as pass the test or not, and finally displays the results. The upper and lower limits can be adjusted to meet any modification introduced, by simply changing the reference values stored in the computer. The system software is implemented by using Visual Basic.6. The software structure of the Automatic test system algorithm is a general algorithm, which can be modified to achieve a specific function. The proposed system can be described as a prototype system which can be easily modified (by adding some function) to match the system under test.

References

Harold, T. McAleer, "A look at Automatic Testing", IEEE Spectrum report, IEEE Spectrum May 1971.

[http:// www.divsy.com/](http://www.divsy.com/)
"Test strategies"

Knowles, R., "Automatic Testing
System and Applications", McGraw Hill
Book, England, 1976.

Muslih, M.B.A., "Interfacing of
microcomputer produced by Electronics
Intellitech Corporation, " A
Methodology Guide for Board and
Module Testing Using IEEE 1149.1",
2000.

Schreiber, H.H., "A review of analog
automatic test generation", IEEE Int.



Automatic Test Conference

AUTOTESCON, 1978.

- . Bandler J.W. and A.E. Salama., " Fault Diagnosis of Analog circuits", IEEE (73) 8, 1985.
 - . AL-Qezweeny, M.S.A., "Design Implementation of Telephone and Tester". M.S.C. thesis. University of Baghdad. 1999.
 - AL-Haidari, W.M., "Data Acquisition System For Automated Test Equipment". M.S.C. thesis. University of AL-Nahreen. 2002.
- Carles, P.S., "Case Based Reasoning as an Extension of Fault Dictionary Methods for Linear Electronic Analog Circuits Diagnosis", M.S.C. thesis. University of Girona, 2004.
- . Takahashi, H., "A guide to low-cost in-circuit testers available in Japan" AEU, 1985.
 - . Tetsuro, T., "Functions required of an in-circuit board tester", AEU, 1985.
 - . Micaela Serra, "Digital IC Testing: An Introduction" University of Victoria, 1990.
 - . Shaahin Hessabi., " Digital Testing" Sharif University of Technology, 2004.

PASSWORD SECURITY VIA NEURAL NETWORKS

Ass. Lec. Mokhtar Mohammed Hasan

University of Baghdad/ College of Science for Women/ Department of Computer Science

ABSTRACT

Password security and protection are one of the important research topics in modern computer systems. Providing privacy, authenticity, integrity and limited access to data, encryption methods are proposed for password security schemes.

This paper proposes the use of neural network accessing the system, the system needs other information extracted from the user's password along with the password itself, these information is passed to two different neural networks to examine the authenticity of the user, and then decide whether the user is a legal user or an intruder.

The extracted information can be summarized by the time period between each two successive characters in the password and the strength of strike of the user when each character is typed at login time.

As a result is a powerful security scheme for password protection and the user has no worry about password being theft because the related password information can not be theft.

الخلاصة

حماية كلمة المرور و امنيتها هي احدى المواضيع المهمة في الانظمة الحاسوبية الحديثة, فمن اجل الحصول على الامنية, الموثوقية, و صحة المعلومات و جعل الوصول الى البيانات الموجودة في النظام يتم فقط من قبل اشخاص مخولين, للأسباب اعلاه نحتاج الى طرق حماية لمفتاح المرور.

الطريقة المقترحة هي باستعمال الشبكات العصبية من اجل الولوج الى النظام, حيث ان النظام المقترح يستعمل معلومات اخرى مستخلصة من كلمة المرور بالاضافة الى قيمة كلمة المرور, حيث ان هذا المعلومات يتم تمريرها على شبكتين عصبيتين مختلفتين من اجل التأكد من موثوقية المستخدم والسماح له بالدخول الى النظام او رفض هذا المستخدم.

المعلومات المستخلصة تمثل الفترة الزمنية بين حرف و اخر عند ادخال كلمة المرور و قوة الضغط لكل حرف مطبوع اثناء ادخال كلمة المرور, بالتالي هو بناء طريقة جيدة و كفوءة من اجل حماية كلمة المرور, وفي حالة تم اكتشاف كلمة المرور من قبل المتطفلين, فلا حاجة للقلق لان المعلومات المستخلصة من كلمة المرور لا يستطيعون اكتشافها

KEY WORD :

Security, Protection, Back Propagation Neural Network, Learning, Testing

INTRODUCTION

The mechanisms for security and protection of a computer system can be classified into three concentric circles ([8]):

- The innermost circle represents the memory of a computer—RAM and disk mechanisms such as base-bound registers, virtual memory mappings, and file access concern Trojan horses, processes entering supervisor state and gaining

supervisor privilege, and processes attaining super user privilege.

- The middle circle represents the security perimeter of a system: only authorized people are allowed to cross the perimeter and establish processes within; their processes are controlled by the mechanisms of the inner circle.
- The outer circle represents the network—all the other computers and people who want to interact with a given one. Here the concern becomes the ability to complete exchange transactions successfully (the central notion of commerce and collaboration). The biggest problem is authentication. Many of the vulnerabilities of networked systems arise from inadequate means authenticate users and machines. Sophisticated cryptographic protocols have been devised to assist with such aspects as secret communication, digital signatures, certificates, and money.

This paper reviews password security and protection, in a computer system and focuses on password protection using neural networks. Especially, a new method of password protection is invented.

There are many ways of password protection used in the current systems scaled from the easy methods such as encryption process of password for small and minor importance system to creating accounts for each user with a system list of password with some constraints for choosing the password itself using the access control list and access matrix found in the system that has a high importance.

THE PROPOSED SYSTEM

In order to prevent the password from being attacked by the penetrators, we have to design a good password features, these features represent the combinations of the characters in the password itself as well as the information that are taken from the password typing. The proposed system uses three different information for password protection:

- The value of the password itself
- The time period between each two successive password's characters (may be letters, or special characters and so on).
- The key strike of the characters

If we notice that, the password characteristics are difficult to achieve by the penetrators which are the strength of the key strike and the time period between each two successive characters, even if the penetrators can guess the password characters in some how, he can not for sure obtain the other password's characteristics which are the time period between each two successive characters and the strength of the key strike, because these information is supplied to the system at the login time by only the actual user who created the password and information is not saved in a system password file because we use neural networks for analyzing the correctness of such information, so, the password protection is achieved.

NEURAL NETWORKS FOR PASSWORD PROTECTION

The aim of a neural network is to recognize the other information extracted from the password at login time, let us rewrite these information again:

- The time period between each two successive characters in the password (PT as a shortcut for time period between password characters)
- The strength of the strike for each character in the password (ST as a shortcut for strike of characters in password)

As I mentioned, the extracted information is not saved in any system file to prevent accessing by other intruders, so the neural network will be used to recognize PT and ST information in order to check the user authenticity along with the password itself.

We used a neural network called Back Propagation Neural Network that is developed by Paul Werbos [1], this net used here for the following purposes:

- Very popular model in neural networks
- Easy to training Can estimate the behavior of the input patterns
- Supervised training algorithm

The estimation property means that, the user, for example, have one character password length, and PT = 300 milliseconds, the user want to login the system, he can not repeat the same operation with PT = 300 milliseconds every time he logs in the system, so the neural network manages this input with acceptable range of error.

The supervised property of this algorithm made it suitable for the proposed system because I have the input features represented by the PT and ST after formulating it to a suitable input codes, and these information should indicate exactly one user after matching with the value of the password itself, in other words, the system have the input features and the desired output user which is the supervised version of neural network is suitable for this purpose.

AN OVERVIEW FOR A BACK PROPAGATION NEURAL NETWORK

There are two stages in this network:

- The learning stage of the neural network

There are two phases in its learning cycle, one to propagate the input pattern and the other to adapt the output. It is the error signals those are backpropagated in the network operation to the hidden layer (s). It does not have feedback connection, but errors are backpropagated-during training, least mean squared error is used.

The input patterns represent by the PT and ST information as mentioned before, and the output represents the authenticity measure of that user.

This neural network composed of three different layers, the input layer which take the input pattern, and the hidden layer, and the output layer which represents the neural network response, a further point is that the network shown in Figure (5) is fully connected, which means that the output of every neuron in one layer is connected to an input of every neuron in the next layer, starting from the input layer and ending at the output layer. Not every multi-layered perception is connected in this way but this is the most common way of doing it.

Errors in the output determine measures of hidden layer output errors, which are used as a basis for adjustment of connection weights between the input and hidden layers. Adjusting the two sets of weights between the pairs of layers and recalculating the outputs is an iterative process that is carried on until the errors fall below a tolerance level. Learning rate parameters scale the adjustments to weights. A momentum parameter can also be used in scaling the adjustments from a previous iteration and adding to the adjustments in the current iteration.

- The testing stage of the neural network

Once training is completed, the weights are set and the network can be used to find output for new inputs. The dimension of inputs are limited by the number of neurons in the input layer, and the dimension of outputs are limited by the number of neurons in the output layer.

- Applying Neural Network in the System

The proposed system uses two different neural networks:

- 1) PTNN (Period Time Neural Network) : that is used for PT features
- 2) STNN (Strike Time Neural Network) : that is used for ST features

Both neural networks have the same general structure with same input, hidden and output neurons, the difference is with the type of the input information as an input pattern for each network, after the user start entering the password, the system collect the PT information and ST information, and when user finishes entering the password, the system search in system list of password in order to recognize the user as a first step, when matching is found, the system takes the user number that is assigned for each user inside the system, like user 1 has number =1, user 2 has number =2, and so on, this number taken and combined with PT and ST information to form two input vectors, PTNN input vector, STNN input vector, and use the corresponding neural network to recognize that vector pattern, if both of neural network responds for that user, the user will be allowed to enter the system, if one of them fails or both fails , the access is denied for that user.

PTNN

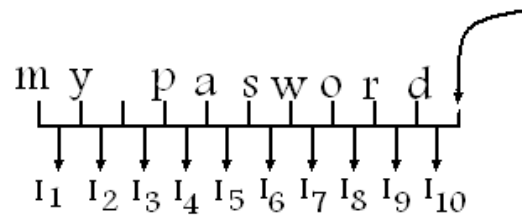
This neural network is used to recognize the PT feature of the current user, this network has 111 input nodes, 223 hidden nodes, and one output node, the input information here represented by the PT features as well as the user number to form the input vector for that neural network.

CALCULATING INPUT NEURONS

The longest password length in this system is 10 characters, and if we compute the numbers of pairs in this longest password we find 9 pairs with 9 elapsed times, and the time elapsed between the finish typing the last character in the password and pressing the login key, so we have 10 periods each of which represented by 10_bits, the time measure here in milliseconds by doubling the number; 50 milliseconds wait means 100 milliseconds; 500 milliseconds wait means 1000 milliseconds (1 second), so we have a maximum time of $2^{10} * 2 = 2048$ milliseconds = 2.048 seconds elapsed time between each two successive characters the user can range, so we have 10 different input information each of 10_bits = 100_bits = 100 neuron plus 10_bits for user number = 110_bits = 110 neurons, plus one for bias the total is 111 nodes.

Assume that the password was "my pasword", 10 characters, so there are 9 pairs of two successive characters in this password, and the tenth pair is between writing the last password character and pressing the login key:

Transferring and Pressing to Login Button



Where I=Information, so, each information takes:

$$10_bits = 10_information * 10_bits_for_each = 100_bits$$

We need extra 10_bits for user number, so, the total of:

$$100_bits + 10_bits_for_user_number = 110_bits = 110\ neurons$$

$$110 + 1\ for\ bias = 111\ neurons\ at\ the\ input\ layer$$

CALCULATING HIDDEN NEURONS

The number of hidden neurons are estimated, there is no ideal equation to compute the number of hidden neurons in back propagation neural network, so this number is depend on the experimental results and testing, some references emphasis on the following equation that we use it:

$$Hidden_neurons = Input_neurons * 2 + 1$$

Table (1) shows the different number of hidden neurons compared to the number of cycles need to learn the neural network assuming the system consists of 20 users, so we get the final number of hidden neurons.

Table (1) _ preliminary experiment results

Hidden number	Iterations number	Error
20	4000	0.3544
50	4000	0.3541
130	4000	0.0219
160	4000	0.0195
190	4000	0.0183
223	4000	0.0031

CALCULATING OUTPUT NEURONS

The number of output neurons used in this system are just one, after supplying the input vector features for the neural network, the output will be an authenticity measures that scaled between 0 and 1, as the output value goes to one, the user is more authenticate, as the output value goes to 0 the authenticity reduced, so we need a threshold to recognize between authentic users and no authentic users, this threshold decided to be 0.7, some errors are allowed here because it is difficult to the user to

supply the same exact PT and ST in each time which is one of the reasons of using back propagation neural network, figure (5) shows the layout of PTNN.

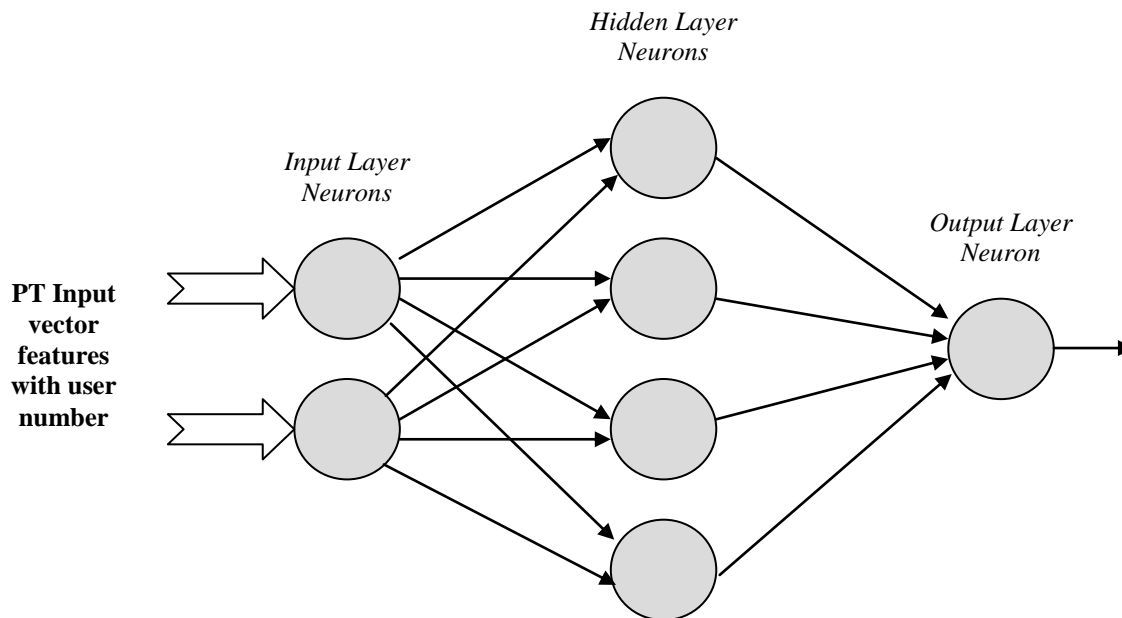


Fig (5) _ the layout of PTNN

STNN

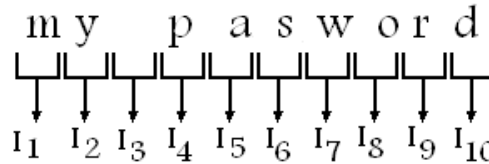
The design of this neural network is identical to this one that used in PTNN except that the codes in the input vector represents different kind of information, this network also has 111 input nodes, 223 hidden nodes, and one output node, the input information here represents the ST features a long with the user number to form the input vector for that neural network.

CALCULATING INPUT NEURONS

The longest password length in this system is 10 characters, each character has its own ST, so the system computes 10 different periods for ST, also each character has 10_bits representation which allows 2.048 seconds the ST of each character in the password.

The ST for each character is computed by computing the time elapsed between holding down the keyboard key and releasing up this key which represents the ST for that character, these 10 different periods as well as the user number are presented to the neural network in order to decide the authenticity of that user.

As an illustration example, assume that the password was "my pasword", 10 characters; the ST information will be computed from:



So, each information takes $10_bits = 10_information * 10_bits_for_each = 100_bits$
We need extra 10_bits for user number, so, the total of:

$100_bits + 10_bits_for_user_number = 110_bits = 110\ neurons\ in\ input\ layer$
 $110 + 1\ for\ bias = 111\ neurons$

Calculating Hidden Neurons

The number of hidden neurons are 221 in the same way computed in section (5.2.1.2).

CALCULATING OUTPUT NEURONS

There is one neuron used as an output neuron as illustrated in section (5.2.1.3), figure (6) shows the layout of the STNN.

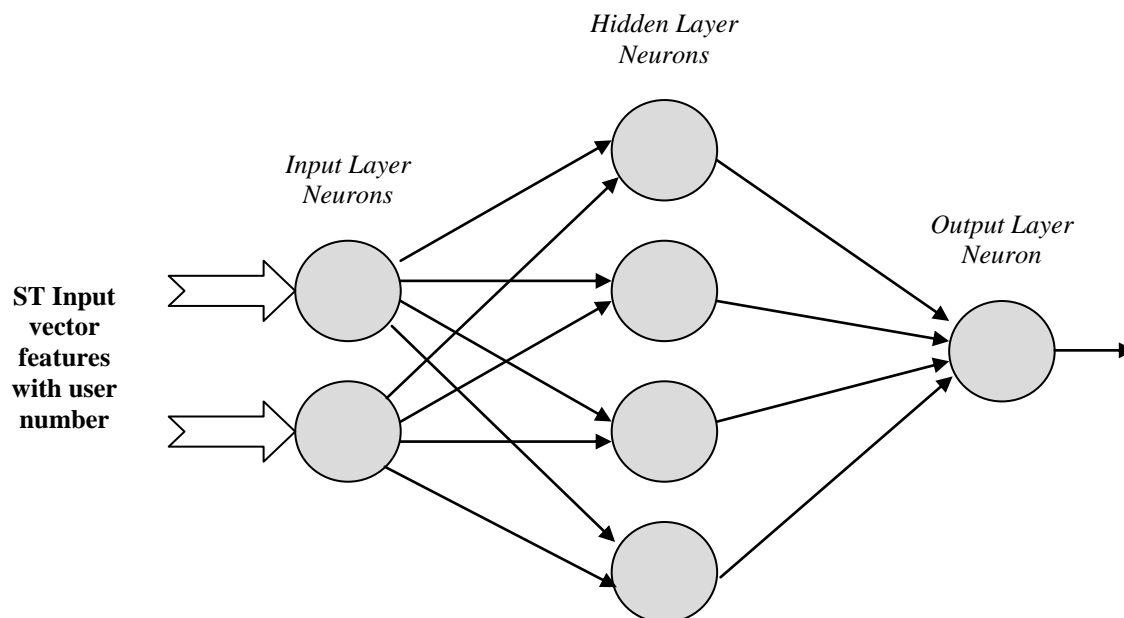


Fig (6) _ the layout of STNN

LEARNING STAGE OF THE PTNN AND STNN

Once the required system is installed on a target computer, the system needs now to learn the neural network to the available users in this system so the weights are saved.

Any new registered user in the system, his ID and Password will be taken as tradition, the system store the ID, password, user number that is generated by the system, and the extracted information from the password at the moment of typing the password will be used to learn the neural network, as a result, we can use the neural network at log in for registered users.

The Back-propagation network undergoes supervised training with a finite number of pattern pairs consisting of an input pattern and a desired or targets output pattern. An input pattern is presented at the input layer. The neurons here pass the pattern digits to the next layer neurons, which are in a hidden layer. The outputs of the hidden layer

neurons are obtained by using perhaps a bias, and also a threshold function with the activation determined by the weights and the inputs. These hidden layer outputs become inputs to the output neurons, which using possibly a bias and a threshold function with their activation to determine the final output from the network.

Learning Algorithm:

- Let $x_0(0)$, $x_0(1)$, $x_0(2)$, up to $x_0(111)$ be the input vector features to the input layer.
- Let $y_1(0)$, $y_1(1)$, $y_1(2)$ up to $y_1(223)$ be the input of the hidden layer, which is the output of the input layer.
- Let y_2 be the final output value.
- $w_1(i, j)$ is the weights connection between input node i and hidden node j
- $w_2(i)$ is the weights connection between hidden node i and output node
- $x_1(1)$, $x_1(2)$, up to $x_1(111)$ and x_2 is a temporary storage

As a first step, the system has to initialize all weights with a random number scaled between 0 and 1 and must be not equal to zero.

The system has to compute the hidden neurons which is:

$$x_1(j) = \sum_{i=0}^{111} w_1(i, j) * x_0(i) \quad \dots \text{Equation 1}$$

We need a derivative function to ensure that the output will fall in the range 0 to 1; the one that is most often used successfully in multilayered perceptrons is the sigmoid function, shown in Figure (7).

So, using the sigmoid function, the hidden layer inputs can be computed from the following equation:

$$y_1(i) = \frac{1}{(1 + e^{-x_1(i)})} \quad \dots \text{Equation 2}$$

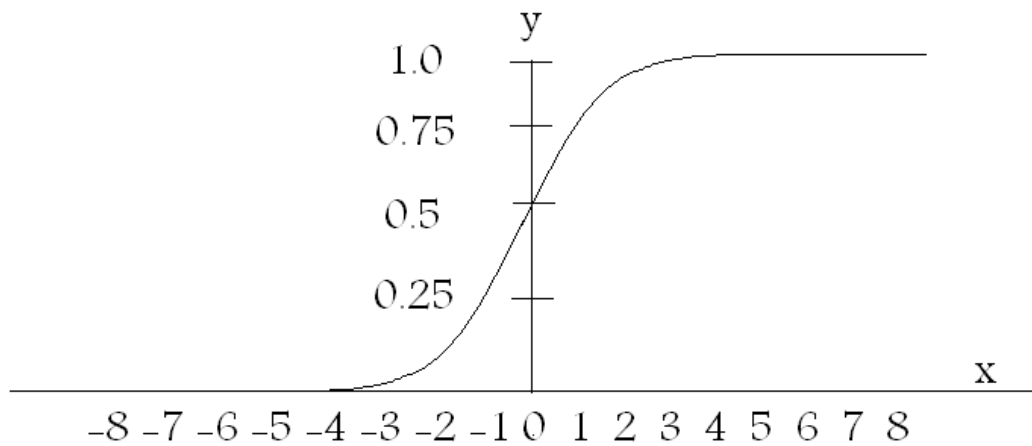


Fig (7) _ sigmoid function

For positive values of x, as x increases y approaches 1. Similarly, for negative values of x, as the magnitude of x increases y approaches 0. In addition, when $x = 0$, $y = 0.5$. So the output is continuous between 0 and 1 and is therefore differentiable.

The temporary output of the hidden layer is computed from the following equation:

$$x2 = \sum_{i=1}^{223} w2(i) * y1(i) \quad \dots \text{Equation 3}$$

Using the sigmoid function, the final output can be computed from the following equation:

$$y2 = \frac{1}{(1 + e^{-x2})} \quad \dots \text{Equation 4}$$

If the actual Neural Network output which is ($y2$) is far a way from the desired output, we have to go to the next step, which is Weight Adaptation..

Use a recursive algorithm starting at the output nodes and working back to the first hidden layer Adjust weight by:

$$w2_i(t+1) = w2_i(t) + \eta * \delta * y1_i \quad \dots \text{Equation 5}$$

Where

η : is a gain term

δ : is an error term for output node which can be computed from the following

equation:

$$\delta = y_2 * (1 - y_2) * (d - y_2) \quad \dots \text{Equation 6}$$

And similarly, d is the desired output of the output node which is 1.

The weight adaptation between input and hidden layer, Equation 5 is used by updating w_1 using y_2 , the equation of δ will be:

$$\delta_j = y_1 * (1 - y_1) * \sum_k \delta_k * w_{jk} \quad \dots \text{Equation 7}$$

Where k is the overall nodes in the layer above node j, internal node threshold are adapted in a similar manner by assuming they are connection weights on links from auxiliary constant valued inputs.

Convergence is sometimes faster if a momentum term is added and weight changes are smoothed by:

$$w_{ji}(t+1) = w_{ji}(t) + \eta * \delta_j * x_{0i} + \alpha * w_{ji}(t) - w_{ji}(t-1) \quad \dots \text{Equation 8}$$

Where $0 < \alpha < 1$

Note that the weights are updated after each pattern is presented and not after the whole training set is presented. The reason why this is done is because the training set is probably very large, so that the time taken to train becomes intolerable. This has not been shown to be equivalent to minimizing the mean squared error, but is widely adopted.

The above algorithm is repeated until the neural network is learned. Figure (8) shows the flowchart of the learning algorithm.

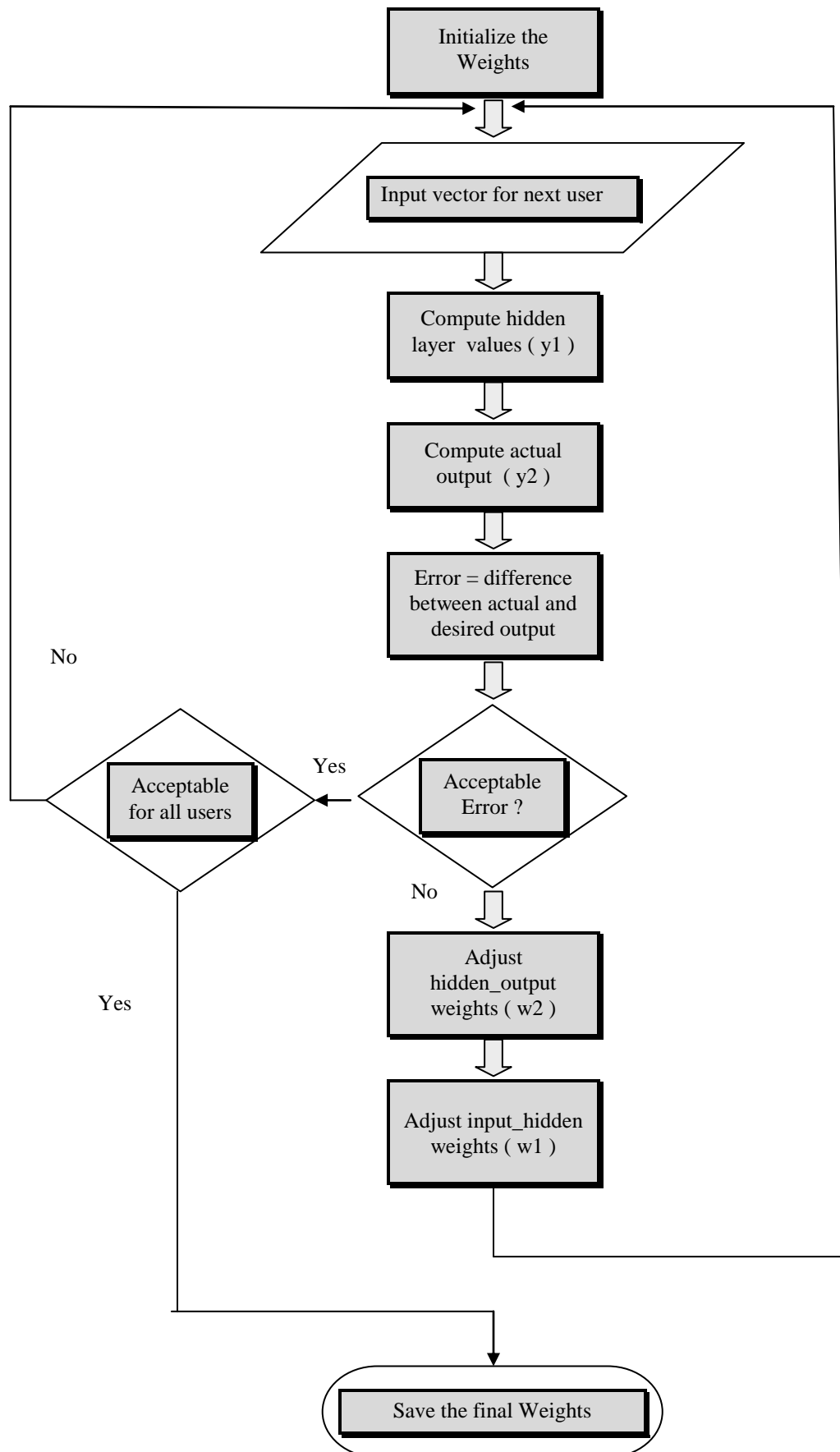


Fig (8) _ the learning process

Testing Algorithm:

- Let $x_0(0), x_0(1), x_0(2),$ up to $x_0(111)$ be the input vector features to the input layer.
- Let $y_1(0), y_1(1), y_1(2)$ up to $y_1(223)$ be the input of the hidden layer, which is the output of the input layer.
- Let y_2 be the final output value.
- $w_1(i, j)$ is the weights connection between input node i and hidden node j
- $w_2(i)$ is the weights connection between hidden node i and output node

The system has to compute the hidden neurons which is:

$$x_1(j) = \sum_{i=0}^{111} w_1(i, j) * x_0(i) \quad \dots \text{Equation 1}$$

Using the sigmoid function, the hidden layer inputs can be computed from the following equation:

$$y_1(i) = \frac{1}{(1 + e^{-x_1(i)})} \quad \dots \text{Equation 2}$$

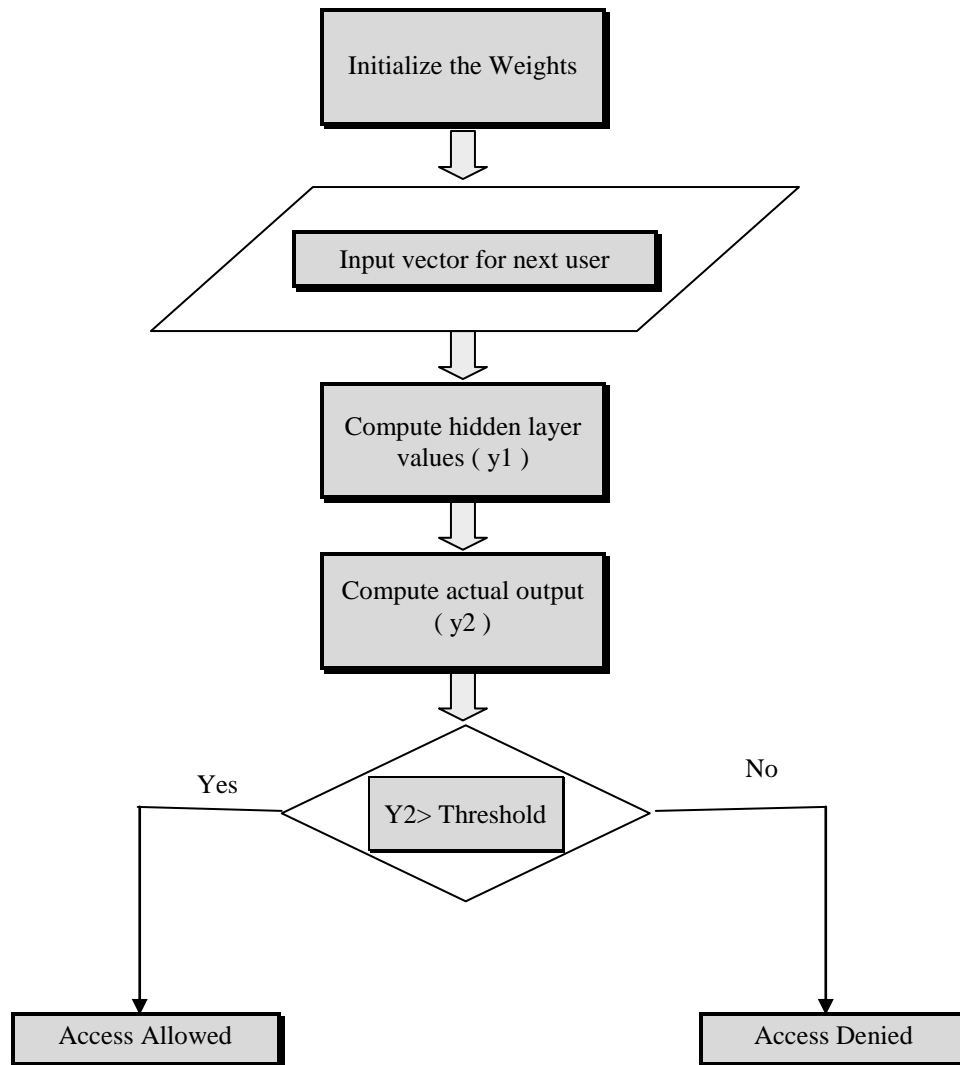
The temporary output of the hidden layer is computed from the following equation:

$$x_2 = \sum_{i=1}^{223} w_2(i, j) * y_1(i) \quad \dots \text{Equation 3}$$

Using the sigmoid function, the final output can be computed from the following equation:

$$y_2 = \frac{1}{(1 + e^{-x_2})} \quad \dots \text{Equation 4}$$

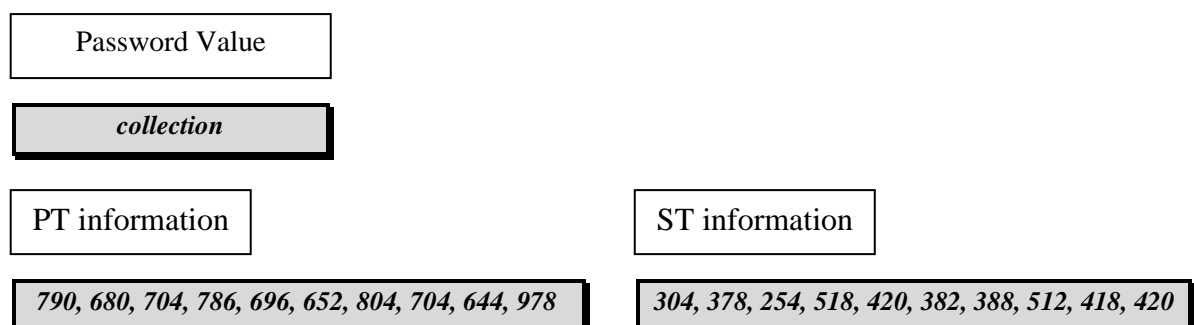
If the output (y_2) larger than the threshold value, then the user is allowed to access to the system, otherwise the user is denied access to the system. Figure (9) shows the flowchart of the testing algorithm.



Flowchart (9) _ testing process

EXPERIMENTAL RESULTS

I applied two examples on the suggested system, the first example is acceptable one, and the second example is rejected by the system, let us consider the user number 12 in the system, when the system create an account for that user and the user enters the user name and password for the first time, the system extracts these information from the password, these information after multiplying the PT and ST information by 2 as mentioned before is:



So that, the system will store the weights of the neural network after learning using the above information which will be used at login time.

ACCEPTABLE EXAMPLE

Assume that a user has the following information registered in the system:

User Name : beginner

Password : collection

The user number in the system was 12, so, at the login interface the user will type his user name and when switches to the password entering area and starts typing the first letter of the password which is letter 'c', the system starts to record two type of information which is PT and ST information, as mentioned before, according to the speed of that user that he decided using my proposed system, we get the following time periods in milliseconds and already multiplied by 2.

PT information

706,748, 766, 680, 758, 698, 736,682,664, 980

ST information

442, 464, 398, 424, 396, 462, 448, 388, 368, 378

User Number

12

The user number will be used for both PT and ST information.

The PTNN input vector features will be extracted from the above information as well as the STNN input vector features, Figure (10) and figure (11) shows the final PT and ST vectors that will be used as an input to both PTNN and STNN respectively.

PTNN input

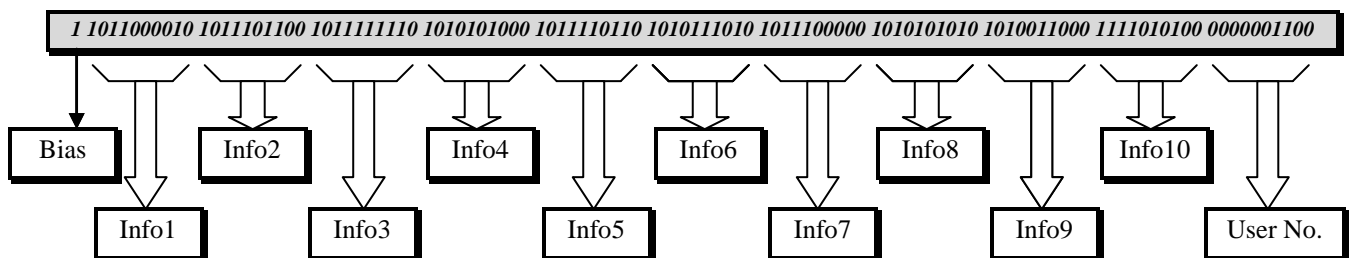


Fig (10) _ the input vector information for PTNN

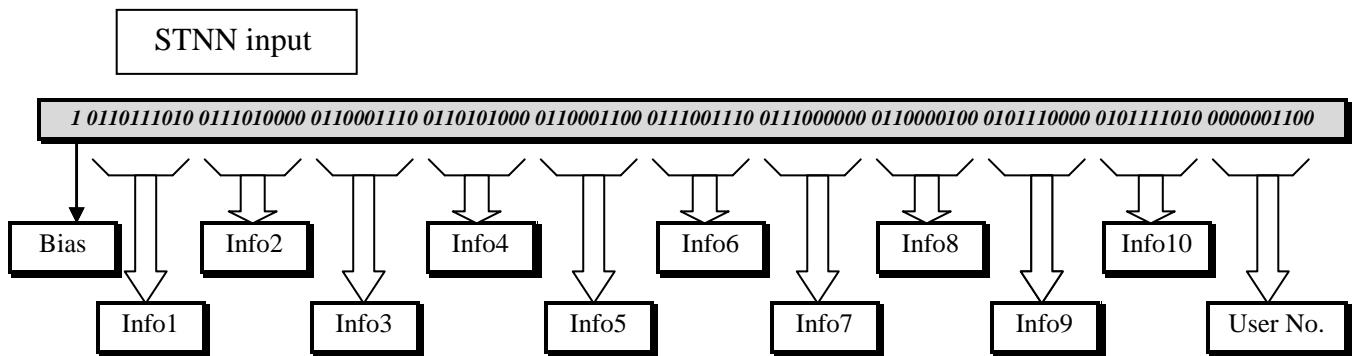


Fig (11) _ the input vector information for STNN

By applying each input vector to the corresponding neural network, i.e. by giving the PT vector features to the PTNN and ST vector feature to the STNN, we will obtain two different outputs each one from a network, these two outputs are:

PTNN output : 0.897 which is > 0.7

STNN output : 0.799 which is > 0.7

As noted above, the user is authenticated user, so this user is allowed to enter to the system.

REJECTED EXAMPLE

I applied the system on the same previous user:

User Name : beginner

Password : collection

The user number in the system was 12, so, the information that extracted from the user password at typing time is:

PT information

918,988, 834, 922, 812, 942, 898,864,890,968

ST information

788, 846, 738, 372, 358, 298, 324, 896, 842, 880

User Number

12

As you noticed, the PT and ST information is quiet different from the original user information, that is mean, the user is not authenticated that steals the password and tries to log into the system, let him do what he came for.

The PTNN input vector features will be extracted from the above information as well as the STNN input vector features. Figure (12) and figure (13) shows the final PT and ST vectors that will be used as an input to both PTNN and STNN respectively

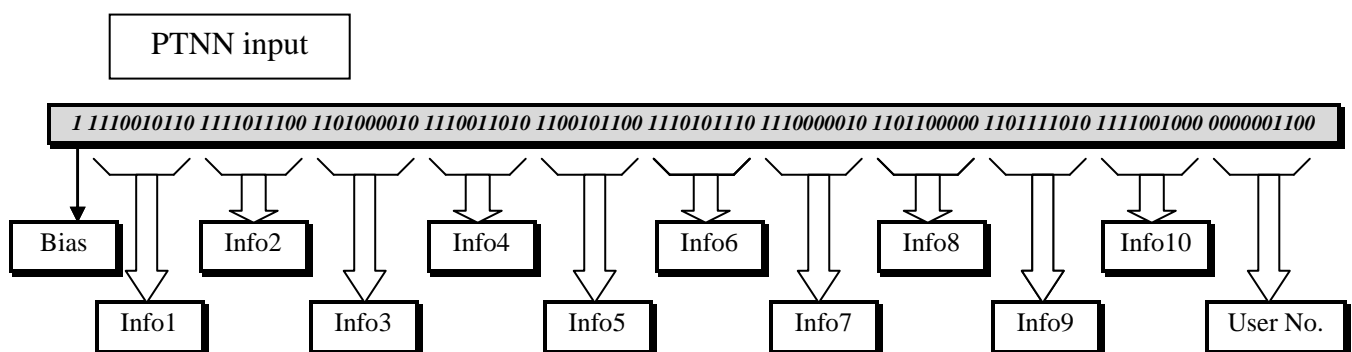


Fig (12) _ the input vector information for PTNN

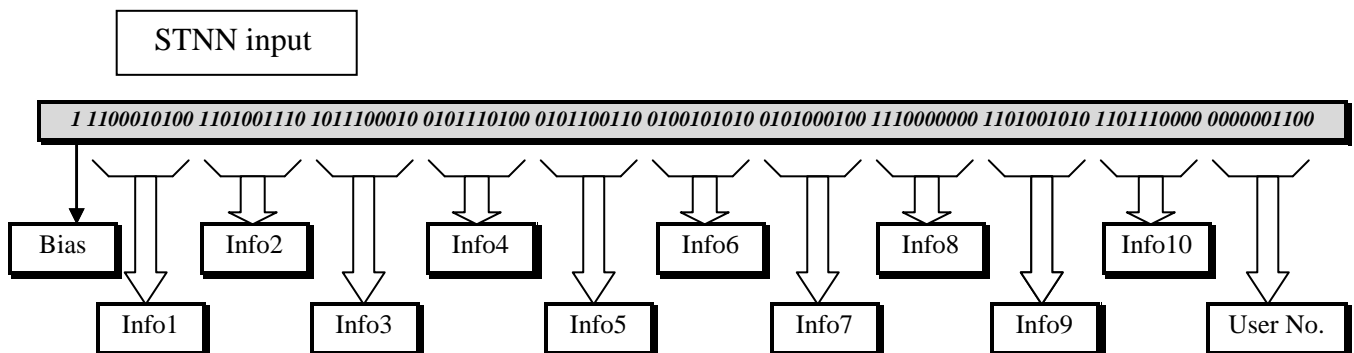


Fig (13) _ the input vector information for STNN

By applying each input vector to the corresponding neural network, i.e. by giving the PT vector features to the PTNN and ST vector feature to the STNN, we will obtain two different outputs each one from a network, these two outputs are:

PTNN output : 0.531 which is ≤ 0.7

STNN output : 0.242 which is ≤ 0.7



As noted above, the user is not authenticated user, so this user can not login into the system, which is the aim of this paper.

CONCLUSIONS

In this system, I built a strong enough security method for password because all the newer systems use the password as the live key for their users and the system is aware more than the user for the password security and provision new techniques for protection, this is a powerful method for protection, that uses the password value as well as the information extracted from the password itself which called PT and ST, if the penetrators can guess the password in some how, he can not guess the PT and ST information and I can say that it is impossible to guess these information, so, when the password is protected, the system is protected.

By using the Neural Network for password security, it has the main significant property which is the acceptable of input within a specific range of error, because the extracted information from the user's password at login time is not the same in each time the user logs in to the system and can not be so, there is a different in PT and ST because the time measured in milliseconds, so the neural network fits our demand in this case and it accepts the extracted user information at login time with a suitable error.

REFERENCES

- Werner Kinnebrock, "Neural Networks, Fundamentals, Applications, Examples", Technical University Rheinland-Pfalz, 2nd Revised Edition, 1995
- Kung S. Y., "Digital Neural Network", New Jersey, 1993
- Simon Haykin, "Neural Networks, A comprehensive Foundation", McMaster University, Hamilton, Ontario, Canada, 1994
- Richard P. Lippman, "An Introduction to Computing with Neural Nets", IEEE ASSP magazine, 1987
- Jacek M. Zurada, "Introduction to Artificial Neural Systems", 1996
- John R. Smith, "Feature Extraction for Neural Network", March 6, 1996, Internet Paper
- Wolfgang Banzhaf, Riccardo Poli, Marc Schoenauer and Terence C. Fogarty, "Lecture Notes in Computer Security", First European Workshop, Euro 99, Paris, France, April 1998.
- Henk C. A. Van Tilborg, "An Introduction to Cryptology", Kluwer Academic Publishers, 1988
- B. Schneier, "Applied Cryptography: Protocols, Algorithms, and Source Code", Second Edition, John Wiley & Sons Inc, 1997.
- Alan G. Konheim, "Cryptography: A Primer", John & Wily, 1992.



BIOSORPTION OF DISSOLVED Pb(II) IN DILUTE AQUEOUS SOLUTIONS BY USING AGRO-WASTE PRODUCTS

Dr. Mohammed Ali I. Al-Hashimi

Department of Building and Construction
University of Technology/ Baghdad- Iraq

Ban Ali Jabir

Environmental Engineering Department
University of Baghdad- Iraq

ABSTRACT

The potential to remove Pb(II) from aqueous solutions through biosorption using four raw dead plant biomasses (karab, bardie, rice hulls and corn-cobs) was investigated in batch tests and compared with that for the PAC. From tests, it was found that the four types of dead-plant biomasses had shown high removal efficiency with the descending order (karab, bardie, rice hulls and corn cobs). Their percent removal (% R) of Pb(II) were (98.76, 96.10, 95.16 and 94.70) respectively at pH 4 with 0.2 g of sorbent/100 ml of 10 ppm lead solution, while it was (99.8 %) for PAC. Generally through batch system at a laboratory scale, karab has proved to be an efficient biosorbent for the removal of Pb(II) from aqueous solutions with low initial ion concentration (1–10 mg Pb(II)/l) at pH (4 - 4.5). The EPA discharge limit (0.1 ppm) for lead was achieved. The biosorption rate is quite rapid and within 5 min of mixing more than 90 % of Pb(II) ions were removed by the karab biomass. Varying agitation speed has no influence on the rate of uptake and the Pb(II) uptake was not affected by karab particle size. The Freundlich and Langmuir isotherms described the data well. According to the evaluation using Langmuir equation, the maximum capacity q_{max} obtained from equilibrium biosorption isotherm test was 13.2 mg/l for pb (II). The ultimate sorption capacity K_F in the Frenldich model was 3.1.

الخلاصة

إزالة أيونات المعادن الثقيلة من المياه الملوثة بها وخاصة المياه الصناعية منها، تعتبر مشكلة بيئية رئيسية مما دفع العلماء والباحثين بإقامة دراسات كثيرة حول هذا الموضوع منذ الثمانينات وكان من أحد الحلول للمشكلة هو استعمال كتل عضوية ميتة حيوانية أو نباتية المصدر كوسائل لإنتزاع أيونات المعادن الثقيلة من الماء الملوث بها، ولتكون المعالجة البيئية اقتصادية يتطلب أن يكون مصدر الكتل العضوية من الطبيعة أو فضلات عضوية ناتجة من المصانع أو من النشاطات الزراعية وأن تكون متوفرة بكثرة و متجددة. إن المعالجة بطريقة فصل الأيونات من المياه بالكتل العضوية الميتة أخذت تجذب الكثير من العلماء والجهات المسؤولة عن حماية البيئة لأنها طريقة اقتصادية وكفوءة و يمكن لهذه التقنية أن تساهم في تحسين البيئة.

الغرض من هذا البحث هو دراسة إمكانية استخدام أجزاء نباتية ميتة ككتل عضوية لمعالجة المياه الحاوية على أيونات الرصاص الذائب وتخليصها منها ومدى كفاءة هذه المعالجة وخواصها و دراسة الشروط البيئية والتشغيلية لإزالة أفضل ولتحقيق الغرض الاقتصادي المطلوب في معالجة مشكلة تلوث البيئة.

أولاً، في هذا البحث تم اختيار أربع كتل عضوية ميتة ذات أصل نباتي وهي كرب النخيل و البردي وقشور الرز (السيوس) وعرائص الذرة حيث تعتبر مخلفات زراعية ما عدا البردي وتم اختبار قابليتها لإزالة أيون الرصاص ومقارنتها بالكربون المنشط المطحون (PAC) حيث تبين من التجارب بأن كفاءة الأنواع الأربعة من الكتل العضوية النباتية الميتة كانت عالية جداً وإن نسب الإزالة المئوية لها كانت كما يلي (98.76 % للكرب، 96.10 % للبردي، 95.16 % لقشور الرز وأخيراً 94.70 % لعرائص الذرة) بينما كانت 99.80 % للكربون المنشط المطحون (PAC). إن كفاءة الكرب في إزالة أيون الرصاص أعلى من الثلاث الأخريات و مقارنة لكفاءة ال PAC، لذلك تم التركيز على دراسة كرب النخيل في التجارب الأخرى.

نفذت التجارب مختبرياً باستخدام الدوارق الزجاجية و الخلاط المغناطيسي. الماء الملوث بأيونات الرصاص المذابة و المستخدم في المعالجة تم تحضيره مختبرياً بتركيز مخففة ومختلفة ضمن المدى (1- 100 ملغ رصاص/لتر). عموماً حصلنا بعد المعالجة على قيم تراكيز متبقية من أيون

الرصااص صغيرة جدا مساوية و حتى أقل بكثير من الحد الموصى به والمسموح به لأيون الرصاص في الماء الذي يتم تصريفه للأنهر حسب المواصفة العراقية و كذلك منظمة حماية البيئة العالمية (0.1ppm).

KEYWORDS

Heavy metal removal, wastewater treatment, sorption, isotherms, biosorption, agro-wastes, dead- plant biomass, agricultural by products.

INTRODUCTION:

The world suffers from chemical contamination of water supplies, largely due to uncontrolled industrial activity and so a water treatment technique which is able to deal with such pollutants in an effective way is very valuable.

The presence of heavy metal ions in surface and ground water supplies have been prioritized as major inorganic contaminants in the environment. It has been established that dissolved metals (particularly heavy metals) escaping into the environment pose a serious health hazard. They accumulate in living tissues throughout the food chain, which has humans at its top, multiplying the danger (Volesky, 1999). Besides, metal resources are non-renewable and natural reserves are becoming depleted. It is therefore imperative that those metals considered environmentally hazardous, or which are of technological importance, strategic significance or economic value, be removed/recovered at their source using appropriate treatment (Atkinson et al., 1998).

The biosorption appears to be a promising technology that could contribute to improving the environment. Biosorption technology, utilizing any natural form of biomass to passively sorb and immobilize solubilized heavy metals (Atkinson et al., 1998). Therefore, biosorption can be defined as the ability of certain types of inactive, dead biomass to binde and concentrate heavy metals from aqueous solutions (even very dilute ones) (Cordero et al., 2004; Ahalya et al., 2004). The use of non-living biomaterials as metal-binding compounds has been gaining advantage because high levels of contamination do not affect them. Moreover, they require minimum care and can be obtained more cheaply (Horsfall et al., 2003). Hence, the advantages of biosorption are the low cost, high efficiency of heavy metal removal from diluted aqueous solutions and environmentally friendly.

The economics of environmental remediation dictate that the biomass must come from nature, or even be a waste material (Vieiral and Volesky, 2000). Therefore, suitable biomass comes as a waste material or by-product from large-scale industrial operations (eg. Use of olive mill residues as heavy metal sorbent material) or certain waste from agricultural operations or biological materials that are available in large quantities (Nomanbhay and Palanisamy, 2005).

Several studies have shown that non-living plant biomass materials are effective for the removal of trace metals from contaminated waters (Horsfall et al., 2003). The unique ability of these plants (lignocellulosic biosorbents) to bind metals has been attributed to the presence of various chemical functional groups such as carboxyl, hydroxyl, amino, or phenolics, which can attract and sequester metal ions from their solutions (ABIA et al., 2002; Shin et al., 2003).

Research on biosorption is revealing that it is sometimes a complex phenomenon where the metallic species could be deposited in the solid biosorbent through various sorption processes, such as ion exchange, complexation, chelation, microprecipitation, etc. Due to the complexity of the



biomaterials used, it is possible that at least some of these mechanisms are acting simultaneously to varying degrees, depending on the biosorbent and the solution environment (Jeffers et al. 1991). The most probable mechanism may be ion exchange (Han et al., 2000).

Biosorption not only offers an innovative alternative to other remediation approaches, it also allows metals recovery. The metal ions can be readily desorbed from the biomass by use of a suitable eluting agent. It has been shown in certain cases, at least, that the biomass can be subjected to a number of loading and elution cycles without the biomass losing its sorption capacity (Schneider et al., 2001). Biosorption can be carried out as a batch process and/or a continuous process.

The goal for this research is to develop inexpensive, highly available, effective metal ion sorbent from agricultural by-products or agro-wastes as alternative to existing commercial adsorbents.

The work on this project include carrying out different equilibrium sorption tests for finding the optimum environmental and operating conditions and sorption isotherm experiments also performed using a synthetic single-solute aqueous solutions polluted with Pb(II).

MATERIALS AND METHODS:

Sorbate:

In the experimental works, the dissolved Pb(II) in aqueous solutions has been selected as the sorbate. The selection to this sorbate is based on the following reasons:

Lead is one of the oldest metals known to human and the most widely use of the toxic heavy metals (CWA, 1972). The hazard from lead is aggravated by its widespread distribution as the metal, inorganic and organometallic compounds (Manahan, 1999). In addition lead is non-biodegradable, persists in the environment and has a tendency for bioaccumulation (Reimann and De Caritat, 1998).

Lead is widely distributed in the environment of Iraq as a result of the use of tetraethyl lead in gasoline to control premature ignition (knocking), battery industrial factories, petrochemical industry, electroplating, metallurgy, paints, radiation protection equipment, pigments, stabilizer in plastic industries, ammunition, cable sheathing and in printing processes. Moreover, the absence of the direct control from environmental protection agencies on above industries has increased the size of this problem. Thus, it is existed in rain, runoff, soils, dust and industrial and municipal discharges.

The health hazards due to the presence of lead in water are of extreme concern to the public, government and industry. Lead is known to have a toxic effect on the neuronal system and on the function of brain cells (Baig et. al., 1999). The health hazards due to the toxicity of lead in waters have been reported in many journals and emphasize the need to identify effective lead sorption systems.

According to the U.S. EPA standards, the maximum concentration limit for Pb(II) for discharge into surface water is 0.1 mg/l and in drinking water is 0.05 mg/l (Nomanbhay and Palanisamy, 2005). This limit has been recommended for Iraqi water standards according to the Law No. 25, (1967) (Standard Iraqi Pollution Control Regulation for the Preservation of Water Resources from Contamination). While for lead in drinking water the maximum acceptable concentration (MAC) recommended by (WHO) is 0.01 mg/l (10 µg/l) (Reimann and De Caritat, 1998).

Biosorbents used:

- The old bases of leaves for date palm tree (karab),
- *Phragmites australis* (bardie) a large grass native to wetland sites.
- Rice hulls (or rice husks) and
- Maize cobs (corn cobs)

PREPARATION OF THE BIOMASS:

The palm Karab was collected from Baghdad, Khastawi type, sun dried and washed with tap water then rinsed with distilled deionized water several times and thereafter dried at a temperature of 105° C in an oven for 24 hours. Following cutting into small pieces then it was ground using a food processor (Blender) and screened through a sieve No.40 (ASTM E 11- 81). This was done to remove any large particles and to obtain particles of size less than (0.425 mm). This fine biomass was used in the batch experiments described below. For preservation, it was kept in plastic bags to minimize its contact with humidity. Same procedure was followed for preparing bardie, rice husk and corncobs.

PREPARATION OF SYNTHETIC POLLUTED WATER:

Firstly an aqueous stock solution (1000 mg/l) of Pb(II) ions was prepared using PbNO₃ salt according to (Standard Methods for the Examination of Water and Wastewater, 1971). Synthetic polluted water samples containing definite concentrations of Pb(II) were prepared by diluting stock (1000 ppm) solution with distilled water. Fresh dilutions were used for each study. The adjustment of lead solution pH at a desired value was done by adding drops of 0.1N HCl or NaOH.

ANALYTICAL MEASUREMENTS:

The polluted water sample and the samples resulted from each treatment were analyzed for Pb(II) using atomic absorption spectrometer (AAS).

BATCH TESTS:

A batch technique was used to perform biosorption experiments and to find the optimum environmental and operation parameters for biosorption of Pb(II) .

All experiments were carried out in 250 ml Erlenmyer flasks. In each experiment a solution of (100 ml) with known initial lead concentration adjusted to a desired pH value was mixed with a definite amount of biosorbent. After that the sample was mixed (stirred) for certain time by using a magnetic stirrer until reaching equilibrium condition. The suspension was then filtered with Whatman filter paper and the concentration of metal ion in the filtrate was measured by AAS. Then the final metal concentration can be recorded as a function of the initial metal concentration and the biomass loading.

Effects of various parameters such as pH, contact time, stirring speed, amount of biosorbent, initial metal concentration and effective biosorbent particle size were studied and details shown in Table 1. All experiments were carried out at room temperature (25 ± 2°C).



THE BIOREMOVAL EFFICIENCY:

The results were expressed also as the removal efficiency of the biosorbent on Pb(II), which was defined as follows (Aslam, M. M., et. al., 2004):

$$\text{Removal efficiency (\%)} = [(C_i - C_f)/C_i] \times 100$$

where C_i and C_f are the metal ion concentration in the sample solution before and after treatment, respectively.

CALCULATION OF METAL UPTAKE BY BIOMASS:

The amount of metal ion uptake by the biomass during the series of batch experiments, were determined using a mass balance equation which expressed as follows (Hussein et al., 2004):

$$q_e = \frac{(C_i - C_f) V}{S}$$

where q_e is the metal ion uptake capacity (mg of metal ion sorbed/g dry biomass) at equilibrium, C_f is the final metal ion concentration in solution (mg of metal ion/l) at equilibrium, C_i is the initial metal ion concentration in solution (mg of metal ion/l), V is the volume of initial metal ion solution used (l) and S is the mass (dry weight) of biomass used (g).

Table 1: Examined conditions of batch tests.

Test type	Test No.	Type of biosorbent	S (g of biomass/100ml)	Initial pH	C_o (mg/l)	Time of stirring (t)	Particle siz, d_p (mm)	Speed of stirring (rpm)
Effect of pH	1	PAC, Karab, Bardie, Rice hulls, Corncobs	0.2	(2, 3, 4, 5, 6, 7, 8.5) for each sorbent	10	1 h	< 0.425	120
	2			4				
Effect of biosorbent amount	1	Karab	(0.05 – 1.0)	4.5	10	1 h	< 0.425	120
	2		(0.05 - 1.5)		106.5			
Effect of contact time	1	Karab	0.2	4.5	10	(5 min- 4 h)	< 0.425	120
	2		1		106.5	(5 min- 4 h)		

Effect of initial Pb(II) concentration & biosorption isotherm (by changing Ci)	1	Karab	1	4.5	(1-100)	1h	< 0.425	120
Effect of stirring speed	1	Karab	1	4.5	37	1 h	< 0.425	(0-600)
Effect of particle size	1	Karab	0.2	4.5	10	(5 min- 60 min)	(< 0.426, 0.425 - 1.4, 2.0 - 2.36)	120

EQUILIBRIUM MODELING:

Biosorption has been studied as simplified sorption systems, usually containing one heavy metal. This is an appropriate simplification for effective experimentation. Langmuir and Freundlich are some of the simple sorption isotherm models that are most frequently applied. There is no critical reason to use a more-complex model if a two-parameter model (such as the Langmuir and Freundlich isotherm models) can fit the data reasonably well (Volesky, 2003).

The Langmuir equation has been extensively used for the evaluation and comparison of metal uptake capacities of biosorbents. The Langmuir isotherm is based on these assumptions (Muraleedharan et al., 1995):

1. Metal ions are chemically adsorbed at a fixed number of well defined sites;
2. Each site can hold only one ion;
3. All sites are energetically equivalent and;
4. There is no interaction between the ions.

The general form of the Langmuir relationship as follows (Ahalya et al., 2005):

$$q_e = \frac{q_{\max} b C_f}{1 + b C_f}$$

where q_e is milligrams of metal bound per gram of biosorbent at equilibrium, C_f is the metal residual concentration in solution at equilibrium (mg/l); q_{\max} is the maximum metal uptake corresponding to the site saturation (mg/g) and b is constant and is the ratio of adsorption and desorption rates .

The linearised Langmuir isotherm allows the calculation of adsorption capacities and the Langmuir costants and is equated by the following equation.

$$C_f/q_e = 1/q_{\max} \cdot b + C_f/q_{\max}$$

The Freundlich isotherm is represented by the equation (Watts, 1998):



$$q = K_F C_f^{1/n}$$

where C_f is the equilibrium concentration (mg/l), q is the amount adsorbed (mg/g) and K_F and n are constants incorporating all parameters affecting the adsorption capacity and intensity respectively.

The linearised forms of Freundlich adsorption isotherm was used to evaluate the sorption data and is represented as:

$$\ln q = \ln K_F + 1/n \ln C_f$$

Results and Discussions

Effect of pH:

Four types of dead plant biomass (karab, bardie, rice hulls and corncobs) were chosen to examine their ability to remove Pb(II) from aqueous solutions under different pH values. Also the PAC was used only in this test as a commercial sorbent for comparison. The comparison of the sorption performance of the different biosorbents was achieved under the same environmental and operating conditions.

The pH profile studies showed that the biosorption of Pb(II) is pH dependent. This effect in pH suggests that the binding mechanism for the metal investigated may be an ion-exchange type process. The protons of the acid functional groups in the biomass were exchanged with cationic Pb (II) at slightly acidic pH. Also, the Pb(II) uptake for the four types of agro-biomass is very low at a pH of 2.0, then increasing the pH of the solution from 2 to 4, leads to a rapid increase in the Pb(II) uptake. The optimum Pb(II) uptakes occur at pH value 4, with a further increase in pH to about 5 and more, the Pb(II) uptake by all of the four agro-biomass decreases due to the hydrolysis and precipitation of lead ions, as shown in Fig. 1. It is also noticed from the figure that the Pb(II) uptake of PAC is very high at a pH of 2.0. The increasing of the pH of the solution leads to a decrease in Pb(II) uptake. Steel and McGhee(1980) stated that the forces holding a molecule against the carbon surface may result from chemical bonding or Van der Waals attraction.

Adsorption is greatest at low pH since at low pH activated carbon is positively charged due to adsorption of hydrogen ion, while most colloids and all ionized polar groups on organic molecules are negatively charged.

The pH represents the negative logarithm of proton (H^+) concentration in aqueous solution, different levels of pH reflecting the hydrogen ion concentration, which affect the uptake of metal ions. Researchers reported that the decrease in metal uptake capacity for the biosorbents at lower pH values (≤ 2) can be attributed to the presence of H^+ ions in high concentration and compete with cations for the binding sites. While others stated that at the lower the pH value the higher the proton concentration in the solution and the surface of the sorbent would be closely associated with hydronium ions (H_3O^+) which hinder the access of heavy metal ions (i.e. cations), by repulsive forces, to the surface functional groups of biomass, consequently decreasing the percentage of metal removal conversely, the increase in biosorption as pH increases can be explained on the basis of a decrease in competition between protons and dissolved metal ions for the surface sites and by the decrease in positive surface charges which results in a lower coulombic repulsion of the cations (Tilaki and Ali, 2003; Cossich et al 2002).

From Figure 2, it can be seen that the high percent removal values were obtained at pH 4 by the four agro-biomasses used with the order as shown in bar chart. The karab has the higher ability followed by bardie, rice hulls and corncobs consequently. The removal efficiency with karab was (98.76 %) which gave the lower remaining concentration for Pb (II) in solution sample and it is comparable to that for the commercial sorbent PAC. Therefore, the karab biomass was selected as our objective biosorbent to study in more details. Besides, no further researches have been done on the use of Karab as agro-biomass sorbent for heavy metal ions removal.

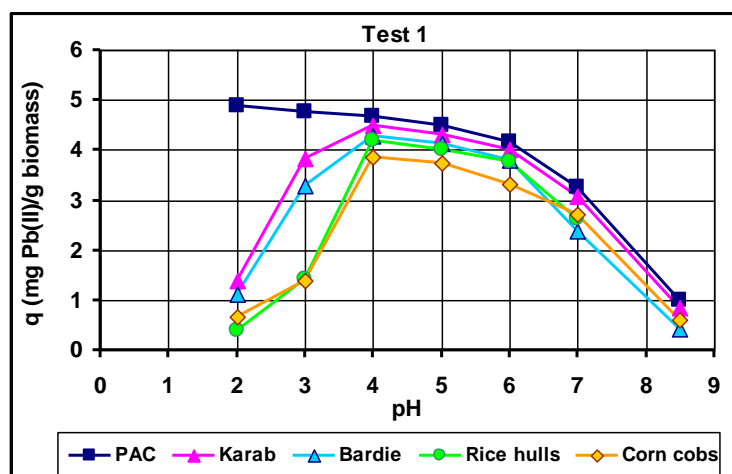


Fig 1 The pH profile for Pb(II) uptake for $C_i = 10$ ppm, by 2 g/l at 120 rpm with equilibrium time of 1 h.

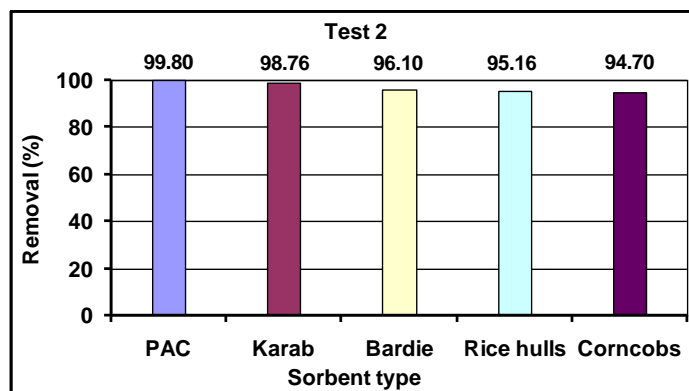


Fig 2 Effect of sorbent type on percent removal of lead ion.

Effect of biomass quantity on Pb(II) uptake by karab:

Effect of karab dosage on biosorption process was carefully studied through doing two tests with varied karab dosages, started with 0.05 to 1.5 g of karab/100 ml lead solution of two varied initial concentrations 10 and 106.5 ppm and keeping pH, agitation speed and contact time constant. The results have been plotted on arithmetic papers as shown in Figure 3 and 4 respectively.

It can be seen in Fig. 3 that the increase in the biomass concentration leads to decrease the metal ion uptake, this attributed to the responsibility of metal ion concentration shortage in solution.

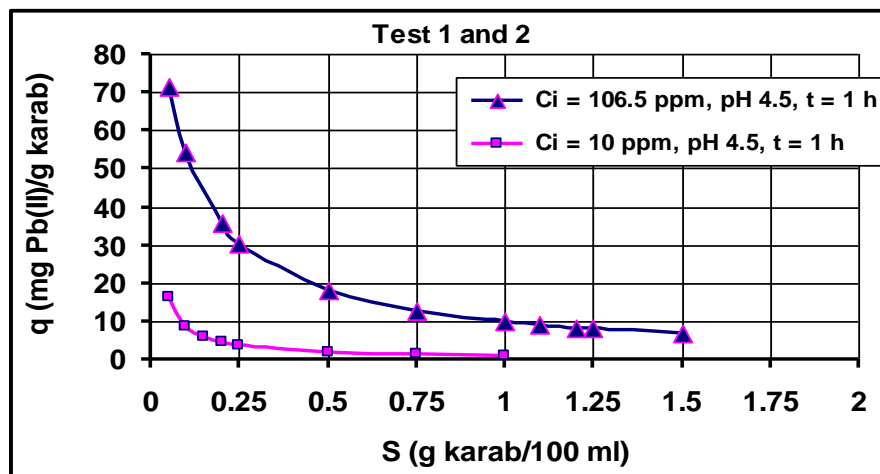


Fig3 Effect of karab dosage on Pb(II) uptake at various initial concentrations.

While, Figure 4 demonstrates that the metal bioremoval efficiency increases with increasing biosorbent dosage up to a certain value. Hence, the optimum sorbent amount required for cost-effective treatment can be well noticed from Fig. 4, where at 10 ppm the maximum percent removal for Pb(II) was about 96.63 % at the karab dosage of 0.2 g/100 ml. While at 106.5 ppm the maximum percent removal for Pb(II) was about 93.15 % at 1g/100 ml karab dosage.

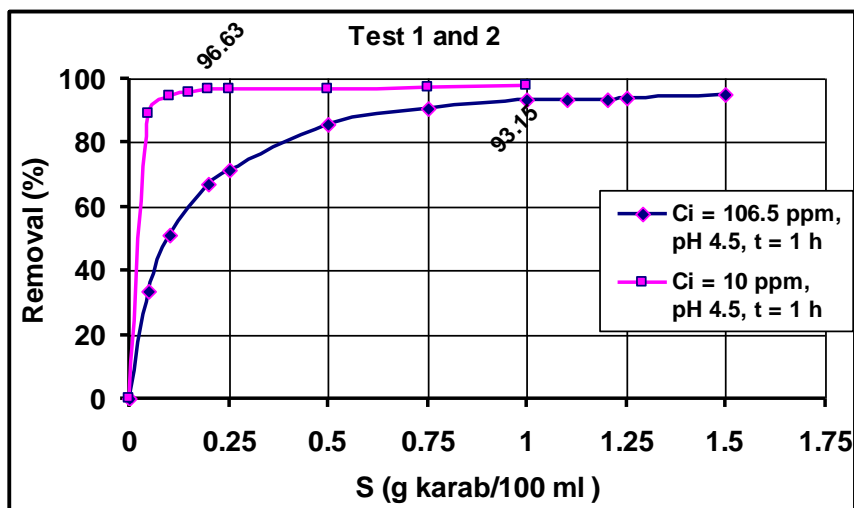


Fig4 Effect of karab dosage on lead percent removal from aqueous solutions of two different initial concentrations of Pb(II).

Biosorption kinetics:

The rate of Pb(II) uptake by karab biomass was investigated, in order to assess the required contact time between the biosorbent and the polluted water to reach an equilibrium state between the dissolved and solid-bound sorbate (lead ions).

From Figure 5 and 6, one can notice how rapidly the biosorption process happens; more than 90% of the equilibrium sorption has occurred within 5 minutes of exposure and remains relatively constant thereafter. This is explained by that, the initial rapid sorption of Pb(II) is due to ion exchange with surface cations on the biomass, while the later slow sorption of lead(II) represents a gradual uptake of cation exchange at the inner surface.

Generally, the equilibrium is attained at less than 30 min. After one hour Pb(II) concentration was found to be time invariant in all tests. Thus, one hour contact time was more sufficient to approach equilibrium. This result is important, as equilibrium time is one of the important parameters for an economical wastewater treatment system.

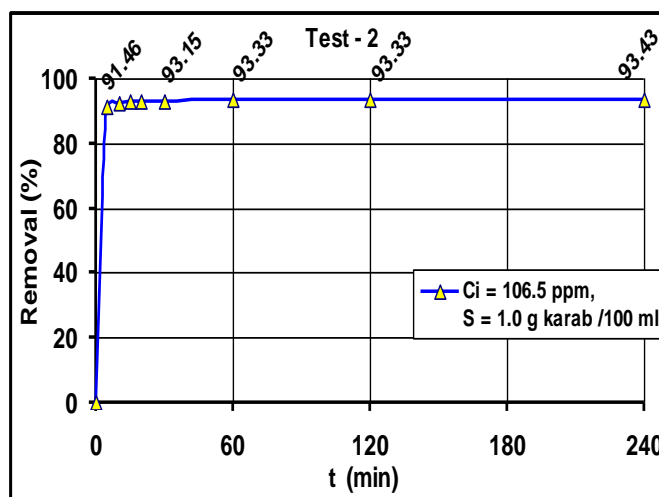
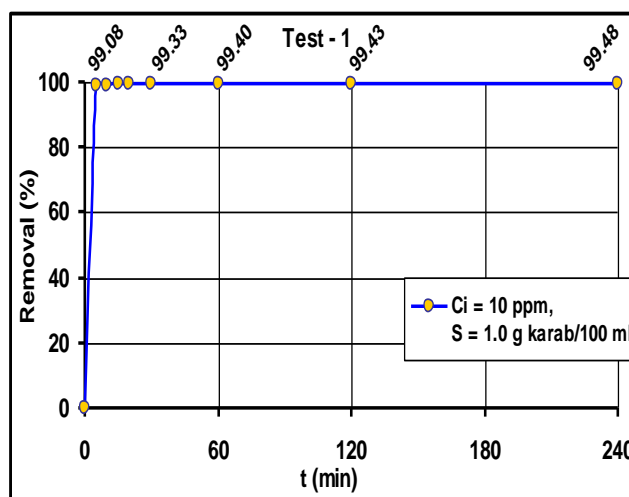


Fig 5 Rate of percent removal of Pb(II) by karab biomass for $[C_i = 10 \text{ ppm}]$. Figure 6 Rate of percent removal of Pb(II) by karab biomass for $[C_i = 106.5 \text{ ppm}]$.

Effect of initial concentration of Pb(II):

The initial concentration of the metal ion is a significant factor to be considered for effective biosorption.

The Pb(II) percent removal from solutions within the low concentration range (1-100 ppm) is shown in Fig. 7, the Pb(II) uptake percentage for 1 g karab biomass/100 ml is considered high and approximately in the range of (95 – 99 %).

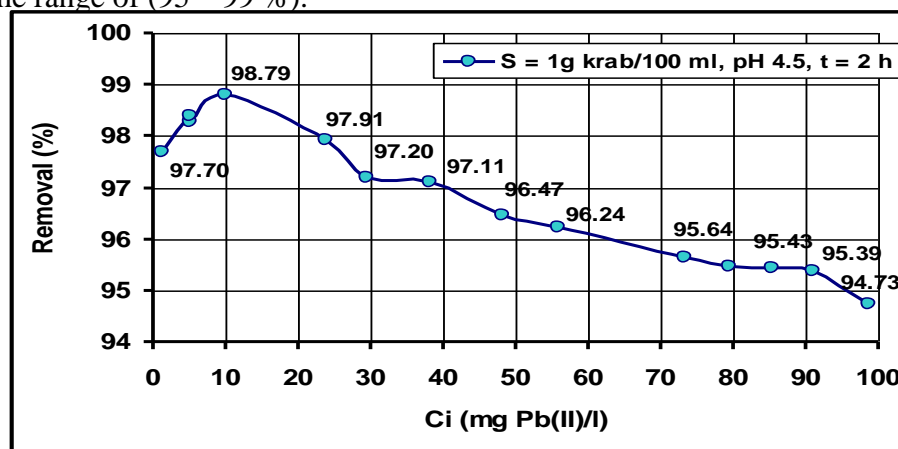


Fig 7 Percent removal of Pb(II) by karab biomass from solutions of various initial concentrations.

Also, it can be seen in Fig. 8, the final lead concentrations (C_f) for lower concentrations range (1-10 ppm) are within the allowable limit of wastewater discharge (0.1 ppm) for Pb(II). Moreover, some results are within the limit of drinking water (0.05 ppm) for Pb(II). Thus, results have encouraged us to continue the tests with column system.

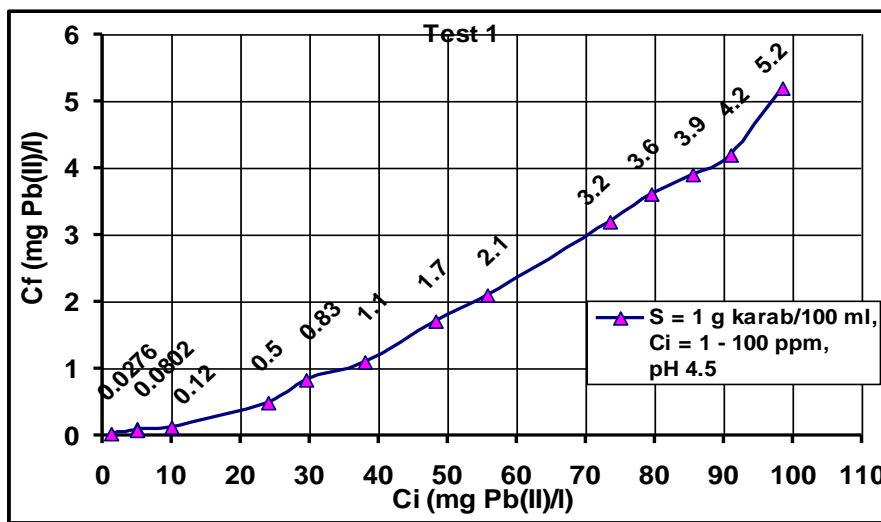


Fig 8 The final concentrations of Pb(II) at equilibrium.

- Effect of stirring (mixing) speed:

The effect of stirring (mixing) the biosorbent/sorbate system on Pb(II) removal efficiency by karab was studied by varying the speed of mixing from 0 (with no-mixing as a control for comparison) to 600 rpm, while keeping the dose of biosorbent, the contact time and optimum pH as constants.

It can be seen in Fig. 9, the Pb(II) bioremoval efficiency has increased with samples mixed at different speeds over the non-mixed samples of the karab/lead solution system. The Pb(II) removal efficiency increased from (21.62 %) for the sample without mixing to (96.5 %) for the sample mixed with 100 rpm. Then increasing the mixing speed from 100 rpm to 600 rpm there is no effect observed on Pb(II) removal efficiency and the biosorption capacity for karab remained constant with speed increase as shown in Fig. 10. Thus, results indicate that the contact between the karab biomass and lead solution is effective even at low mixing speed (100-120 rpm).

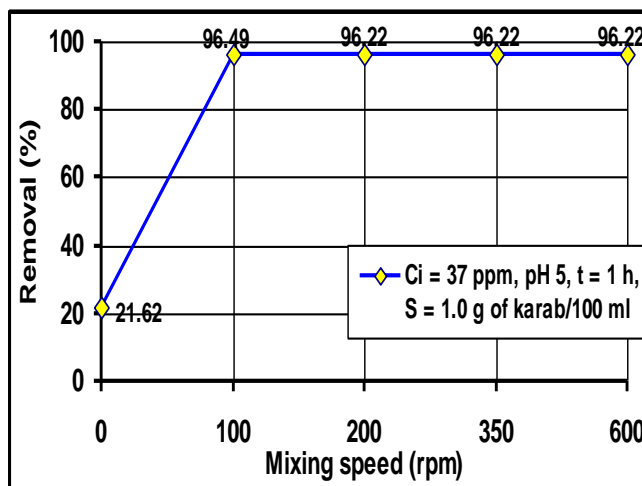


Fig 9 Effect of mixing speed on Pb(II) percent removal by karab.

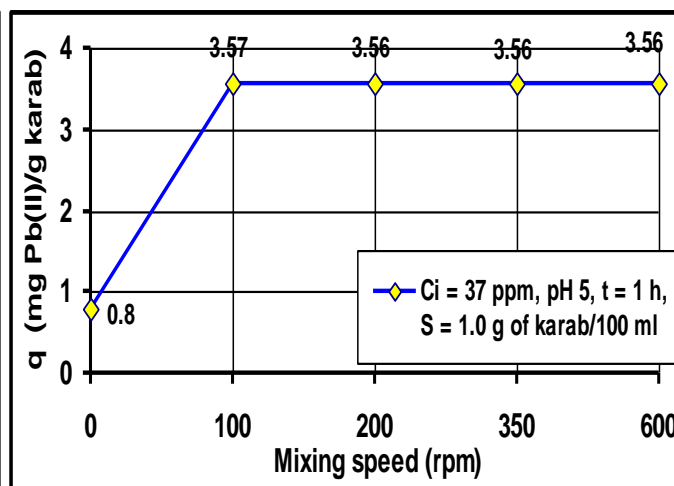
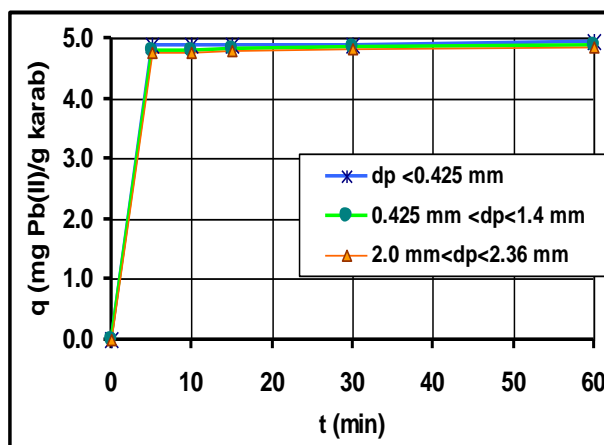


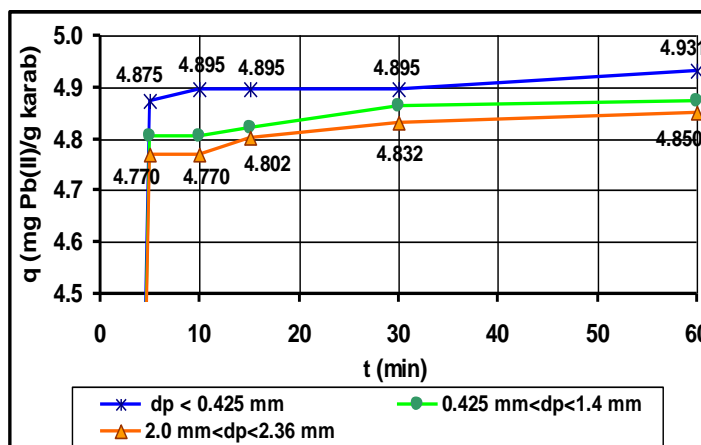
Fig 10 Effect of mixing speed on Pb(II) uptake for karab.

Influence of biosorbent particle size on lead biosorption:

From Figure 11(a), one can notice that the effect of karab particle size on Pb(II) uptake is negligible and can not be recognized easily. This small effect has been shown better in Fig. 11(b), after changing the scale of y-axis of Fig. 11(a). From this figure, it can be seen that the karab particle size has little influence on the capacity and rate of Pb(II) biosorption.



(a)



(b)

Fig 11 Pb(II) uptake related to time for various karab particle sizes.

Sorption equilibria studies:

The experimental results were analyzed in terms of two adsorption isotherm equations, the Langmuir and Freundlich isotherms. These two models were used to adjust (fit) the experimental data obtained for biosorption of Pb(II) from the synthetic lead solution by karab biomass. The parameters of

the two models, the ultimate sorption capacity (K_F) and the sorption intensity (n) in the Freundlich model as well as the maximum uptake capacity (q_{\max}) and the equilibrium constant (b) in the Langmuir model were calculated using the linear regression analysis of the experimental data. Also, the correlation coefficient (R^2) for each model and experiments was calculated. The Langmuir capacity (q_{\max}) is the maximum specific uptake corresponding to the site saturation. q_{\max} is used to compare the efficiency of the adsorbent (karab biomass) with other materials, which have been tested as biosorbent for Pb(II). The magnitude of K_F and n is used to compare easy separation of heavy metal ion from wastewater and high adsorption capacity of karab biomass with other materials.

K_F is the Freundlich capacity factor for various compounds is extremely wide. Because of the wide variation in the Freundlich capacity factor must be determined for each compound (Metcalf and eddy, 2003).

Table 2 Summary of Freundlich and Langmuir equilibrium biosorption isotherms results.

Exp. No.	pH	S (g of karab/100 ml lead solution)	t (h)	C_o (mg/l)	Linear Freundlich isotherm constants				Linear Langmuir isotherm parameters		
					K_F	$1/n$	n	R^2	q_{\max} (mg/g)	b (l/mg)	R^2
1	4	1.0	1	1 - 100	3.1	0.759	1.32	0.9732	13.2	0.4	0.9331

The correlation coefficient (R^2) of both models, were mostly greater than 0.9 (close to one). The values of correlation coefficients (R^2) indicated a strong positive relationship between the data and the linear equations of Langmuir and Freundlich as shown in Fig. 12 and 13 respectively. Also, that both models adequately describe the experimental data of the biosorption of these metals but Freundlich model fits experimental data better than Langmuir one as shown in Fig. 14.

According to Ahalya et al., (2005), n values between 1 and 10 represent beneficial adsorption. Hence, the value of n , which is related to the distribution of bonded ions on the sorbent surface, is found to be greater than unity for karab, indicating that adsorption of Pb(II) is favourable for karab biomass.

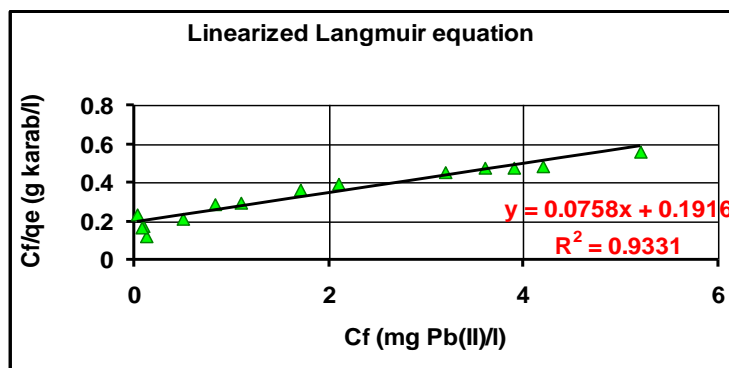


Fig 12 Langmuir adsorption isotherm for Pb(II) biosorption by karab, for $[C_i = 1-100\text{ppm}]$ and at optimum conditions.

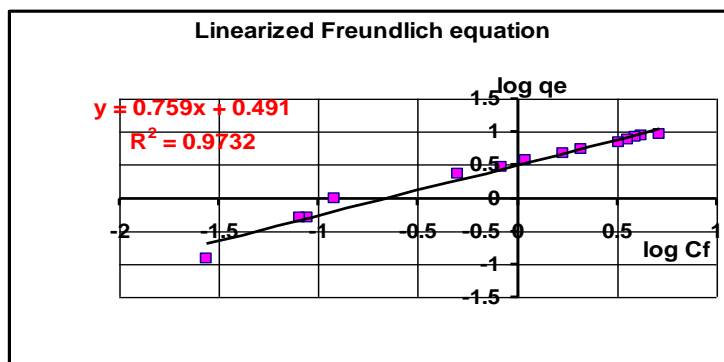


Fig 13 Freundlich adsorption isotherm for Pb(II) biosorption by karab, for $[C_i = 1-100 \text{ ppm}]$ and at optimum conditions.

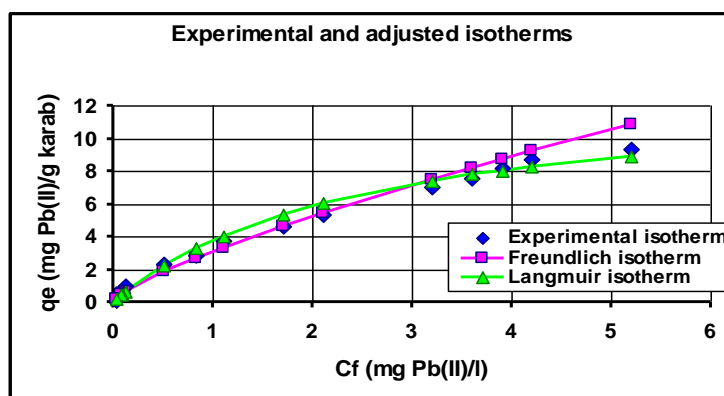


Fig14 Equilibrium biosorption isotherms for $C_i = 1-100 \text{ ppm}$.

Conclusion

Human populations need methods and technologies to clean waters and diminish the environmental dangers related to technological progress. Biosorption can be one such solution to clean up heavy metal contamination. The ability of the karab biomass to remove Pb(II) from synthetic aqueous solution with a single solute has been found higher than the ability for the other three biomasses “bardie, rice hulls and corncobs”, and as good as that for PAC. The karab biomass was used as an inactivated natural dead plant biomass. It is a lignocellulosic material. It is an agro-waste or agricultural by-product has negligible cost (cheap material) and has also proved to be an efficient biosorbent for the removal of Pb(II) ions from a synthetic aqueous solutions with low concentrations (1-100 mg of Pb(II)/L) in a laboratory scale. So its utilizing in industrial wastewater treatment plants would be convenient to provide economic metal decontamination of large amounts of wastewaters of low concentrations waste streams.



REFERENCES

- * ABIA, A. A, Horsfall, M. Jnr. and Didi, O., (2002), "Studies on the use of Agricultural By-Product for the Removal of Trace Metals from Aqueous Solutions", Journal of Applied Sciences & Environmental Management, Vol. 6, No. 2, pp. 89-95.
- *Ahalya, N., Ramachandra, T. V. and kanamadi, R. D., (2004) "Biosorption of Heavy Metals", Western Ghats Aquatic Biodiversity, Sahyadri E News, Issue 5.
- *Ahalya, N., Kanamadi, R. D. and Ramachandra, T. V., (2005), "Biosorption of Chromium (VI) from Aqueous Solutions by The Husk of Bengal Gram (*Cicer arietinum*)", Electronic Journal of Biotechnology, Vol. 8, No.3, pp. 258-264.
- *Aslam, M. M., Hassan, I. and Malik, M., (2004), "Sand as Adsorbent for Removal of Zinc from Industrial Effluents", Electronic Journal of Environmental, agricultural and Food Chemistry, Vol.3, No. 6.
- * Atkinson, B. W., Bux, F. and kasan, H. C., (1998), "Considerations for Application of Biosorption Technology to Remediate Metal-Contaminated Industrial Effluents", Journal of Water SA, Vol. 24, No. 2, pp. 129-135.
- * Baig, T. H., Gracia, K. J. and Gardea-Torresdey, J. L., (1999), "Adsorption of Heavy Metal Ions by the Biomass of *Solanum Elaeagnifolium* (Silverleaf Night Shade)", Proceedings of the 1999 Conference on Hazardous Waste Research, Dept. of Chemistry and Environmental Science and Engineering, University of Texas.
- * Cordero, B., Lodeiro, P., Herrero, R. and de Vicente, M. E. S., (2004), "Biosorption of Cadmium by *Fucus Spiralis*", Environ. Chem., Vol. 1, pp. 180-187.
- * Cossich, E.S., Tavarres, C.R.G. and ravagnani, T.M.K., 2003, "Biosorption Biomass", Electronic Journal of Biotechnology (EJB) vol.5, No.2.
- * CWA, (1972), "Clean Water Act", Full Text of the Law as Signed on October 1972.
www.esr.pdx.edu/pub/ESR622/metals.html
- * Han, J. S., Park, J. K. and Min, S. H., (2000), "Removal of Toxic Heavy Metal Ions in Runoffs by Modified Alfalfa and Juniper", 1st World Congress of the International Water Association, Paris, 3-7 July 2000.
- * Horsfall, M. Jnr., Abia, A. A. and Spiff, A. I., (2003), "Removal of Cu(II) and Zn(II) ions from wastewater by Cassava (*Manihot esculenta* Cranz) waste biomass", African Journal of Biotechnology, Vol. 2, No. 10, pp. 360-364.

- *Hussein, H., Ibrahim, S. F., Kandeel, K. and Moawad, H., (April 15th 2004), “Biosorption of Heavy Metals from Wastewater Using Pseudomonas sp.”, Electronic Journal Of Biotechnology ISSN: 0717-3458, Microbial Biotechnology, Vol.7, No. 1. www.ejbiotechnology.info/content/vol7/issue1/full/2
- * Jeffers, T. H., Ferguson, C. R. and Bennett, P. G., (1991), “Biosorption of Metal Contaminants Using Immobilized Biomass- A Laboratory Study”, U.S. Dept. of the Interior, Bureau of Mines, Report No. RI-9340.
- * Law No. 25, (1967), Standard Iraqi Pollution Control Regulation for the Preservation of Water Resources from Contamination.
- * Manahan, S. E., (1999), “INDUSTRIAL ECOLOGY: Environmental Chemistry and Hazardous Waste”, LEWIS PUBLISHERS, CRC Press LLC.
- * Metcalf and eddy ,2003 , "Wastewater Engineering , Treatment and Reuse", 4th ed., McGraw Hill Company.
- * Muraleedharan, T. R., Iyengar, L. and Venkobachar, C., (1995), “Screening of Tropical Wood-Rotting Mushrooms for Copper Biosorption”, American Society for Microbiology, Applied and Environmental Microbiology, Sept. 1995, Vol. 61, No. 9, pp. 3507-3508.
- * Nomanbhay, S. M. and Palanisamy, K., (2005), “Removal of Heavy Metal from Industrial Wastewater Using Chitosan Coated Oil Palm Shell Charcoal”, Electronic Journal Of Biotechnology ISSN:0717-3458, Environmental Biotechnology, Vol. 8, No. 1, April 15th . www.ejbiotechnology.info/content/vol8/issue1/full/7/reprint.html
- * Reimann, C. and de Caritat, P., (1998), “Chemical Elements in the Environment: Factsheets for the Geochemist and Environmental Scientist”, Copyright by Springer-Verlag Berlin, Heidelberg.
- * Schnider, I. A. H., Rubio, J. and Smith, R. W., (2001), “Biosorption of metals onto plant biomass: exchange adsorption or surface precipitation?”, Int. J. Miner. Process, Vol. 62, pp. 111-120.
- * Shin, E. W., Rowell, R. M., Peterson, J. O., Han, J. S. and Min, S. H., (2003), “Enhancement of Cadmium Ion Sorption Capacity of Lignocellulosic Bio-sorbent by Sulfonation”, American Institute of Chemical Engineering, Annual meeting, San Francisco, Nov. 17.
- * Standard Methods for the Examination of Water and Wastewater, 13th Edition, American Public Health Association, American Water Works Association, and Water Pollution Control Federation, 1971.
- * Steel, E. W. and McGhee T. J., 1980, “Water Supply and Sewerage”, 5th Edition, McGraw Hill Inc.
- * Tilki, D. and Ali, R., 2003, “Study on removal of cadmium from water environment by Adsorption on GAC, BAC and Biofilter”, Diffuse Pollution conference, Dublin, pp 8(35) – 8(39).
- * Vieiral, R. H. S. F. and Voleskey, B., (2000), “Biosorption: a solution to pollution?”. INTERNATL MICROBIOL, Vol. 3, pp 17- 24.



* Volesky, B., (2003), "Biosorption: Application Aspects- Process Simulation Tools", Dept. of Chemical Engineering, McGill University, Montreal, Canada,
<http://www.biosorption.mcgill.ca/publication/BVibs01.pdf>

* Volesky, B., (1999), "Biosorption for the Next Century", International Biohydrometallurgy Symposium, El Escorial, Spain.

* Watts, R. J., (1998), "Hazardous Wastes: Sources, Pathways, Receptors", John Wiley & Sons. INC.



COMPARISON STUDY BETWEEN DUBININ-RED USHKEVICH AND TEMKIN MODEL FOR ADSORPTION OF MERCURY ONTO ACTIVATED CARBON

Hayder Mohammed Abdul-Hameed

Lecturer / University of Baghdad / College of Engineering
Environmental Engineering Department

ABSTRACT:

Activated carbon has been used as an adsorbent in this work to remove mercury from aqueous solutions. The aim of the work is to test how best activated carbon can be used as an adsorbent for mercury. Equilibrium isotherms, both, Dubinin-Redushkevich, and Temkin have been test. The batch experiments were conducted at room temperature (30°C) and at the normal pH (7.0±0.1) of the solution. HYBRID fraction error function analysis shows that the best-fit for the adsorption equilibrium data is represented by (D-R) model rather than Temkin model. Its found that the correction factor (R^2) for (D-R) is 0.9928 while for Temkin model is 0.942, also the HYBRID fractional error was conducted for the both models and (D-R) model give minimum value of (0.0128) while it was (0.129) for Temkin.

الخلاصة :

يهدف البحث الى اجراء المقارنة لفاعلية موديلين رياضيين هما موديل Dubinin-Redushkevich وموديل Temkin لوصف عملية امتزاز الزئبق ضمن المحلول المائي باستخدام الكربون المنشط . وقد تم اجراء التجارب المتقطعة في درجة حرارة 30° وقيمة (pH=7) وقد وجد ان معامل التصحيح (R^2) للموديل الرياضي الاول يساوي (0.9928) بينما كانت القيمة للموديل الثاني تساوي (0.942) كذلك تم تطبيق معيار (HYBRID) الانحراف للخطأ ووجد ان قيمته للموديل الاول يساوي (0.0128) بينما للموديل الثاني (0.129) .

KEYWORDS

Adsorption, Mercury, Wastewater treatment, Isotherms, Kinetics.

INTRODUCTION:

Mercury has been chosen in this work for experimentation. Among several methods for the removal of heavy metal from solutions (precipitation, evaporation, electroplating, ion exchange and membrane separation). Adsorption onto activated carbon proves to be an efficient and cost effective method. In the present study, adsorption of mercury on AC has been studied at the normal pH (7.0±0.1) of the solution and at room temperature (30°C). Number of works on the removal of mercury using activated carbon had been reported(both Redad and Ruble),In addition to find the adsorption capacity of activated carbon for mercury,also to test the validity of batch experimental data to various two parameters adsorption isotherm models such as Dubinin-Redushkevich, and Temkin models.

Dubinin-Redushkevich (D-R) Model

This adsorption isotherm (Dubinin-Redushkevich) is given as:

$$q_e = q_m \exp(-Be^2) \quad \dots\dots (1)$$

Where q_m (mol/g) is the theoretical monolayer saturation capacity of the adsorbent and e (known as Polanyi potential) is given as:

$$e = RT \ln\left(1 + \frac{1}{C_e}\right) \quad \dots\dots (2)$$

The constant B (mol^2/J^2) given by the following equation, the mean free energy E (J/mol) of adsorption per molecule of adsorbate, when it is transferred to the surface of solid from infinity in the solution, is:

$$E = \frac{1}{\sqrt{2B}} \quad \dots\dots (3)$$

The linear form of D-R equation is:

$$\ln q_e = \ln q_m - Be^2 \quad \dots\dots (4)$$

Temkin Model:

The Temkin adsorption isotherm is expressed as:

$$q_e = \frac{RT}{b} \ln(K_T C_e) \quad \dots\dots (5)$$

The linearized form of the above equation is:

$$q_e = B_1 \ln K_T - B_1 \ln C_e \quad \dots\dots (6)$$

Where $B_1 = RT/b$; R is the universal gas constant (8.314 J/mol K) and T is the absolute temperature (K) (Temkin).

EXPERIMENTAL:**Materials and Methods**

The chemical used were mercury (II) chloride (Merck), and activated carbon (Merck). Specifications of activated carbon are given in table 1. The surface area of AC used is $1250 \text{ m}^2/\text{g}$ and the Hg(II) was determined by using spectrophotometer (HITACHI 2000).

Adsorption Experiments

100 mL solutions of 50 mg/L Hg(II) concentration each were treated with 20, 40, 60, 80, 100, 120, 140, 160, and 180 mg of AC, respectively, and equilibrated for a period of 24h at room temperature and at a pH of 7.0 ± 0.1 of the solution in an orbital flask shaker.



The solutions were then filtered and the residual Hg(II) concentrations determined spectrophotometrically.

Table 1: Specifications of activated carbon

Specifications	Value
Porosity	70-80%
Cation Exchange Capacity	0.71 meq/g
Surface Area	1250 m ² /g
Average Particle Size	250 µm
Particle Density	0.887 g/cm ³

RESULTS AND DISCUSSION

Experimental data (Table 2) on equilibrium studies for the adsorption of Hg(II) on AC were tested to fit the various two-parameter adsorption isotherm models.

Table 2: Batch experimental data for the Adsorption of Hg(II) on AC, at normal pH and at room temperature (30°C)

Equilibrium Studies	
Activated Carbon	
q _e (mg/g)	C _e (mg/L)
57.33	32.8
46.10	22.4
39.78	14.2
33.17	10.2
28.33	7.5
24.50	5.9
21.67	4.5
18.60	3.5
15.87	2.4
12.20	1.3

Linearized forms of the (D-R) and Temkin adsorption isotherms, the values of parameters involved and the correlation coefficients are given in Table 3.

Table 3: Two-parameters adsorption isotherm models and parameter values of the isotherms for the adsorption of Hg(II) on activated carbon at normal pH of the solution and at room temperature (30°C)

Model	Linearized Equation	Parameters values for the adsorption of Hg(II)
Dubinin-Resushkevich (D-R)	$\ln q_e = \ln q_m - B e^2$	$B = 4 \times 10^{-9}$; $q_m = 1.59 \times 10^{-3}$; $E = 11180$; $R^2 = 0.9928$
Temkin	$q_e = B_1 \ln K_T + B_1 \ln C_e$	$K_T = 1.23$; $B_1 = 13.951$; $R^2 = 0.942$

A plot of q_e versus e^2 should yield straight line. This plot for the present experimental data is shown in Fig. 1. the fits are good in the present study ($R^2 = 0.9955$ for AC).

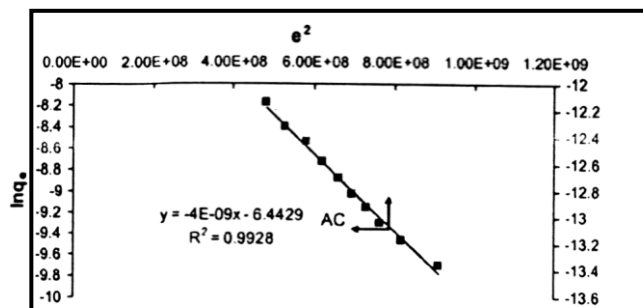


Fig (1): Dubinin-Redushkevich plots

Temkin isotherm takes in to account the adsorbing species-adsorbent interactions. A plot of q_e versus $\ln C_e$ yields a straight line (Fig. 2) from which the isotherm constants B_1 and K_T (L/mg) can be determined, K_T is the equilibrium binding constant corresponding to the maximum binding energy and constant B_1 is related to the heat of adsorption.

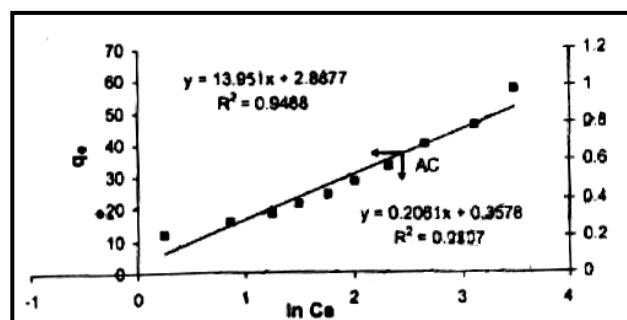


Fig (2): Temkin plots

BEST-FITTING ISOTHERM MODEL:

Both the isotherms studied in this work are in their linearized form. Due to the inherent bias resulting from linearization, to find of the best-fit isotherm model to the experimental equilibrium data, the hybrid fractional error function of non-linear regression is employed, as it compensates for low concentrations by balancing absolute deviation against fractional error and is more reliable than other error functions. The hybrid error is given as:

$$\text{HYBRID} = \frac{100}{N-p} \sum \left[\frac{q_{e,\text{exp}} - q_{e,\text{calc}}}{q_{e,\text{exp}}} \right]_i \dots (7)$$

Where N is the number of data points and p is the number of parameters in the isotherm model. The hybrid error is lowest for (D-R) model for adsorption on AC (0.0128) and for Temkin model was (0.129) and hence the best-fit is the (D-R) adsorption isotherm.

CONCLUSIONS:

The present study shows that activated carbon, follows the adsorption isotherm models tested; Dubinin-Redushkevich, and Temkin. However, the best-fit isotherm is the (D-R) model isotherm, as determined by hybrid fractional error analysis, also it clear that the values of R^2 for the (D-R) model are better for the Temkin model.

**REFERENCES:**

- M. M. Dubinin, L. V. Radushkevich, "Equation of the Characteristic Curve of Activated Charcoal", Proc. Acad. Sci. Phys. Chem. Sect. USSR 55 (1947), PP. 331-333.
- M. M. Dubinin, L. V. Radushkevich, "Evaluation of Microporous Materials with a new Isotherm", Doklady Akademii Nauk SSSR 55 (1966), PP. 331.
- M. J. Temkin, V. Pyzhev, "Recent Modifications of Langmuir Isotherms", Acta Physiochim USSR 12 (1940), PP. 217.
- W. D. Harkins, G. Jura, "Surface of Solids. XIII. Avapor adsorption Method for the Determination of the Area of a Solid without the Assumption of Molecular Area, and the Areas Occupied by Nitrogen and Other Molecules on the Surface of a Solid", J. Am. Chem. Soc. 66 (1944), PP. 1366-1377.
- W. D. Harkins, G. Jura, "An Adsorption Method for the determination of the Area of a Solid without the Assumption of Molecular Area, and the Areas Occupied by Nitrogen Molecules on the Surface of a Solids", J. Chem. Phys. 11 (1943), PP. 431-432.
- Y. S. Ho, G. McKay, "Sorption of dye from aqueous solution Peat", Chem. Eng. J. 70 (1998), PP. 115 – 124.
- Y. S. Ho, J. F. Porter, G. McKay, "Equilibrium Isotherm Studies for the Sorption of Divalent Metal Ions onto Peat: Copper Nickel and Lead Single Component Systems, Water, Air, Soil Pollut.", 141 (2002), PP. 1-33.
- Y. S. Ho, W. T. Chin, C. S. Hsu, C. I. Huang, "Sorption of Lead Ions from Aqueous Solution Using tree Fern as a Sorbent, Hydrometallurgy", 73 (2004), PP. 55-61.
- R. Jalali, H. Ghafourian, Y. Asef, S. J. Davarpanah, S. Sepehr, "Removal and Recovery of Lead Using Nonliving Biomass of Marine Algae", J. Hazard. Mater. B92 (2002), PP. 253-262.
- U. Kummar, M. Bandyopaphysy, "Sorption of Cadmium from Aqueous Solution Using Pretreated Rice Husk", Bioresour. Technol. 97 (2006), PP. 104-109.
- M. M. Nassar, "Equilibrium Studies on the Adsorption of Glycine on Resin", Adsorpt. Sci. Technol. 8 (1991), PP. 86-94.
- G. L. Rorrer, T. Y. Hsien, "Synthesis of Porous-Magnetic Beads for Removal of Cadmium", Chem. Eng. Res. 32 (1999), PP. 2170-2174.
- Metcalf & Eddy, "Wastewater Engineering: Treatment and Reuse", 4th ed., Tata McGraw-Hill, New Delhi, 1995.
- Z. Reddad, C. Gerente, Y. Andres, P. Le-Cloirec, "Adsorption of Several Metal Ions onto a Low-Cost Biosorbent: Kinetic and Equilibrium Studies", Environ. Sci. Technol. 36 (2002), PP. 2067-2073.
- C. L. Lasko, M. P. Hurst, "An Investigation in to the Use of Chitosan for Removal of Soluble Silver from Industrial Wastewater", Environ. Sci. Technol. 33 (1999), PP. 3622-3626.

- W. M. Antunes, A. S. Luna, C. A. Henriques, A. C. A. da Costa, "An Evaluation to Copper Biosorption by a Brown Seaweed under Optimized Conditions", Electron, J. Biotechnol. 6 (3) (2003) (ISSN: 0717-3458) This Paper is Available on Line at <http://www.ejbiotechnology.info/content/vol16/issue3/full/5>.
- N. Bektas, D. Soysal, "Kinetics of Phosphate Removal Using Surfactant Modified Clinoptilolite, Fresenius Environ. Bull. 13 (2004), PP. 366-369.
- V. M. Boddu, K. Abburi, J. L. Talbott, E. D. Smith, "Removal of Hexavalent Chromium from Wastewater Using a New Composite Chitosan Biosorbent, Environ. Sci. Technol. 37 (2003), PP. 4449-4456.
- A. Rubel, R. Andrews, R. Conzaes, J. Groppo, T. Robl, "Adsorption of Hg(II) and NO_x on Activated Carbon", Fuel 84 (2005), PP. 911-916

A STUDY OF INFLUENCE OF VERTICAL VIBRATION ON HEAT TRANSFER COEFFICIENT FROM HORIZONTAL CYLINDERS

Assist. Prof. Dr. Majid. H. M. Al-Shorafa'a
Al-Najaf Technical College
Foundation Of Technical Education

ABSTRACT

Electrically heated horizontal cylinders of diameters 2.15cm, 3cm, and 3.8cm were vibrated vertically in stagnant air at a frequency (10,15,20Hz) and amplitude range from (0.0005m) to (0.0076m). The effect of different parameters on the heat transfer ratio (h_v/h_o) was investigated from its outer surface. It is concluded that, heat transfer ratio increases at high frequency and small diameter. Vibration Reynolds number has good effects on heat transfer ratio. (Gr.Pr) has bad indication on heat transfer ratio at high temperature difference (high heat flow). The vibration intensity also has good influence on heat transfer.

الخلاصة

اسطوانات أفقية مسخنة كهربائياً باقطار 2.15 و 3.0 و 3.8 سم تهتز اهتزازاً عمودياً في هواء ساكن بتردد (10 و 15 و 20) هرتز و بسعة تتراوح بين (0.0005م) إلى (0.0076م). تم دراسة تأثير العوامل المختلفة على نسبة انتقال الحرارة (h_v/h_o) من سطحها الخارجي. وقد استنتج بان نسبة انتقال الحرارة تزداد مع التردد العالي والقطر الصغير. وعدد رينولد الاهتزازي له تأثير جيد على نسبة انتقال الحرارة في حين إن عدد (Gr.Pr) لهم تأثير ضعيف على نسبة انتقال الحرارة من الاسطوانات المهتزة عند فرق درجات الحرارة الواطئ (انتقال حرارة منخفض). كذلك وجد بان كثافة الاهتزاز لها تأثير جيد على انتقال الحرارة.

KEY WORDS

Influence of Vertical Vibration, Heat Transfer From Horizontal Cylinders, Heat Transfer Coefficient

INTRODUCTION

Heat transfer by free convection from engineering machineries can be increased by several methods. One of these methods is to create a relative motion between the heat surface and the surrounding fluid medium. This can be done by mechanical vibration, sound and fluid fluctuating methods.

One of the earliest investigations of the vibration effect on heat transfer was done by **(Martinelli and Boelter 1938)**. They studied the effect of vibrations upon the heat transfer from a horizontal tube immersed in the water. **(Penny and Jefferson 1966)**. Studied the heat transfer from an oscillating wire. The influence of vertical mechanical vibrations on a free convection heat transfer from a large horizontal cylinder has been studied by **(Fand and Keye 1971)**. **(Armarly and Madson 1973)** studied heat transfer from oscillating horizontal wire. **(Dawood and Mathotra 1980)** studied heat transfer from horizontal cylinders vibrated in air and they found that heat transfer is increased up to two and half times. Heat transfer from finned horizontal cylinders, that vibrated vertically was studied by **(Yacoab and Sabieh 1997)**. In this study the increase in vibration heat transfer coefficient to free heat transfer coefficient recorded to be about (1.16). **(Makki Al-Uboydi 2001)** in his thesis studied a wide range of vibration effects on the heat transfer from horizontal cylinders.

In this study the effects of vibration parameters on the heat transfer coefficient are investigated.

EXPERIMENTAL APPARATUS

The experimental apparatus consists of the following:-

- 1- Testing cylinder: which is used as a heated vibrated horizontal cylinder made of aluminum with outside diameters of (0.0215m, 0.03m, and 0.038m), with a heating length of 0.38m. This cylinder is heated by an electric heater passing through its core. The electric heater consists of resistance coil with voltage variance and current ammeter. Five thermocouples nodes are fixed on the cylinder outer surface to measure the temperatures at different places on the cylinder.
- 2- Rigid frame: The cylinder is fixed on a heavy rigid frame . this frame is fixed on a table with plastic fixtures to absorb the vibration from the frame.
- 3- Vibration instruments: The vibration instruments that used in the vibration generation and measurements are
 - a) Piezoelectric accelerometer
 - b) Vibration exciter
 - c) Power amplifier
 - d) Vibration meter with filter
 - e) Functional generator
 - f) Oscilloscope

The process of measuring is done as follows:

- 1- Heating the cylinder and measuring this value of heat flow by $Q = IV$. This quantity of heat generation due to electric current passage is equal to the heat transfer from the outer surface of the cylinder
- 2- When the study state was reached temperature is measured with no vibration.
- 3- The vibration exciter is operated with some frequency and amplitude values, to vibrate the cylinder.
- 4- When the steady state is reached the measurements are done and recorded from the instruments .



- 5- These previous four steps are repeated with different values of heat transfer, amplitudes, frequency and with different cylinder of different diameters.

THEORY

The heat generated electrically in the cylinder is transferred to the ambient by radiation and convection due to the temperature difference between the cylinder surface and the ambient.

$$Q = Q_r + Q_c \quad (1)$$

where Q=heat generated in the coil [W]

Q_r =heat transfer by radiation [W]

Q_c =heat transfer by convection [W]

The heat transfer by radiation can be calculated from the following equation

$$Q_r = A\varepsilon\sigma(T_s^4 - T_a^4) \quad (2)$$

Where A=surface area [m^2]

ε = the emissivity (taken as 0.9)

σ =Stefan Boltzmann constant= $5.67 \times 10^{-8} [W / m^2 K^4]$

T_s = surface temperature [K]

T_a = ambient area temperature [K]

Then;

$$Q_c = Q - Q_r \quad (3)$$

The value of heat transfer by convection can be calculated from eq.(3). The heat transfer by convection can be represented as:

$$Q_c = Ah(T_s - T_a) \quad (4)$$

hence

$$h = \frac{Q_c}{A(T_s - T_a)} \quad (5)$$

where h=coefficient of heat transfer by convection [$W/m^2.K$]

The dimensionless number Nu (Nussult Number) if function of coefficient of heat transfer by convection and is represented by:

$$Nu = \frac{hd}{k} \quad (6)$$

where d is the diameter of the cylinder in meter and k is the thermal conductivity of the fluid(air).

For free convection (with no vibration or any other effects on the heat flow) from the horizontal cylinder Nu is a function of (Gr.Pr).

$$Nu = f(Gr.Pr) \quad (7)$$

Where Gr = Grashof number and Pr =Prandtl number, and h in free convection can be denoted as h_o . For forced convection under the effect of vibration only the heat transfer coefficient is a function of many parameters as illustrated in following equation.

$$h_v = f(d, f, a, \mu, Cp, \rho, l, T_s, T_a, k) \quad (8)$$

Where f =frequency, a =amplitude, μ = viscosity, ρ =density, Cp =specific heat, and l = length.

From eq(8) the relation can be rewritten by dimensionless form that:

$$Nu_v = f(Re_v, Pr, \frac{al}{d^2}) \quad (9)$$

Where $Re_v = \frac{2\pi a f d \rho}{\mu}$

and the relation between the vibration heat transfer coefficient and the free heat transfer coefficient can be written as

$$\frac{h_v}{h_o} = \frac{Nu_v}{Nu} = \frac{f(Gr, Pr)}{f(Re_v, Pr, \frac{al}{d^2})} = f((Gr, Pr), Re_v, Pr, \frac{al}{d^2}) \quad (10)$$

RESULT AND DISCUSSION

The different parameters were taken in consideration to study its effect on heat transfer by convection from a horizontal vibrated cylinder in air.

a- Effect of vibration intensity

The vibration intensity is defined as the product of vibration amplitude by a frequency ($a.f$) with a unit of [m/sec].

Fig(1) to Fig(3) show the effect of the vibration intensity on the ratio of heat convection with vibration to the free convection (convection ratio= (h_v/h_o)) with different values of heat transfer (Q). The trend of the behavior of the increase in convection ratio is same, but its values affected by the frequency. The convection ratio increases with the increases of frequency. These figures show that as the heat transfer value is increased the convection ratio will decrease. This means that as the temperature difference is raised the free convection is increased and so the convection ratio decreases.

b- Effect of vibration Reynolds number

The effects of Re_v on the convection ratio for different heat transfer values (Q) and for different diameter and frequency values are illustrated in Figs (4(a,c,e)-6(a,c,e)). It is shown that with increase of Re_v , the convection ratio also increased. The frequency has the positive effect on the convection ratio. This effect increases with low heat transfer (low temperature difference), because at this case the effect of temperature difference is decreased so the increase in heat transfer is due to frequency.

c- Effects of ($Gr.Pr$)

To study the effect of the free convection terms ($Gr.Pr$) on the convection ratio, the relation between ($Gr.Pr$) and (h_v/h_o) was also drawn on Figs(5(b,d,f)-7(b,d,f)). It was shown from these figs that as heat transfer increases the term ($Gr.Pr$) is also increased and the convection ratio decreased and becomes about unity at high heat transfer. As the temperature difference is increased the buoyancy is increased and so the free convection term ($Gr.Pr$) effect is also increased.



The trend of the behavior is same for all values of (Q) with change in frequency and diameter.

d- Effect of the diameter of the shaft

It is shown from Fig(6(a,c,e)) that the effect of the diameter has indication on the convection ratio at high frequency, because at high frequency the free boundary layer may damaged and the heat transfer becomes in the region of turbulent force convection. These effects are inversely influence by the heat transfer by free convection as indicated with the ($Gr.Pr$) effects on the convection ratio, Figs(7(b,d,f)). It is shown at low frequency and large diameter, the convection ratio becomes high, Fig(7,a).

e- Effects of frequency

The effect of frequency on convection ratio is indicated in fig(8). The convection ratio is increases with increase of (Re_v), Fig(8,a,c,e). the convection ratio decreased with increasing of ($Gr.Pr$) and frequency, fig(8,b,d,f). The term (Re_v) indicates the inertia force effect, and this will increase the convection ratio. The term ($Gr.Pr$) indicates the buoyancy force effect, and this will decrease the convection ratio.

CONCLUSIONS

It is concluded that heat transfer has been affected by the vibration. The heat transfer increases greatly at high frequency and small diameter. The convection ratio is decreased with the increasing of the temperature difference(high heat transfer).

The vibration Reynolds number has good effects on the heat transfer from the cylinder. The free convection term ($Gr.Pr$) has bad effect on the vibration heat transfer.

This study can be expanded to include other shapes to study the vibration effects on the heat transfer from it.

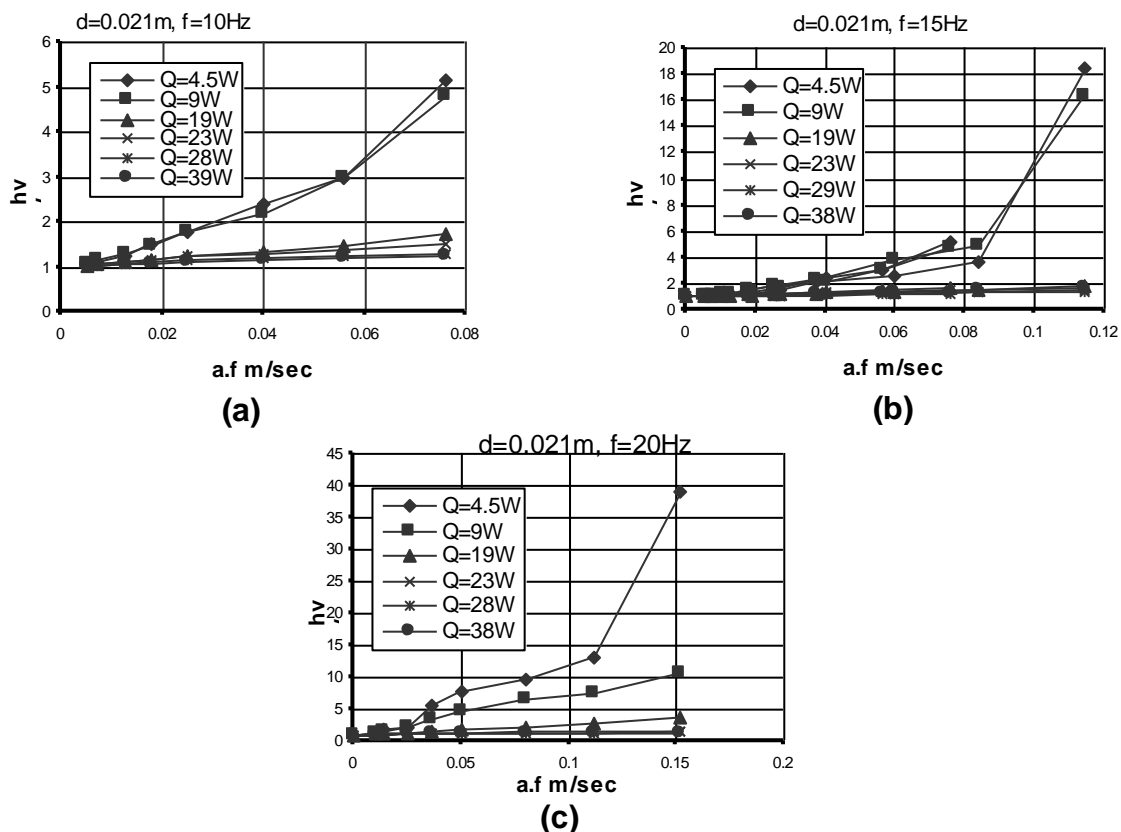
REFERENCES

- Al-Ubaydi M. H “ A Study of Influence of Vertical Vibration on Heat Transfer Coefficient By Free Convection From Cylinders” M.Sc. Thesis University of technology, 2001
- Armarly, B.F., and Madsen D. H., “Heat Transfer from an Oscillating Horizontal Wire”, J. Heat Transfer, Vol. 93C pp. 239-240, 1973
- Dawood A. S. Malhotra A, and Ali S. M. J “ The Effect of Vertical Vibration On Natural Convection Heat Transfer from Horizontal Cylinders” J. Heat and Mass Transfer, Vol. 24, pp. 491-496, 1980
- Fand, R. M. and Kaye, J. , “ The Influence of Vertical Vibration on Heat Transfer By Free Convection From a Horizontal Cylinder”, Int. Dev. In Heat Transfer, ASME, New York, pp. 490-498, 1971
- Martinelli, R. C. , and Boelter, L. M. K., “ The Effect of Vibration on Heat Transfer By Free Convection from a Horizontal Cylinder” Proc.5th Int. Conf. Appl. Mech. ,Pp 578-584, 1938
- Penney, W. R., and Jefforson, T. S., “ Heat Transfer from an Oscillating Horizontal Wire to Water and Ethylene Glycol” J. Heat Transfer, Vol.88C, pp. 359-366, 1966.

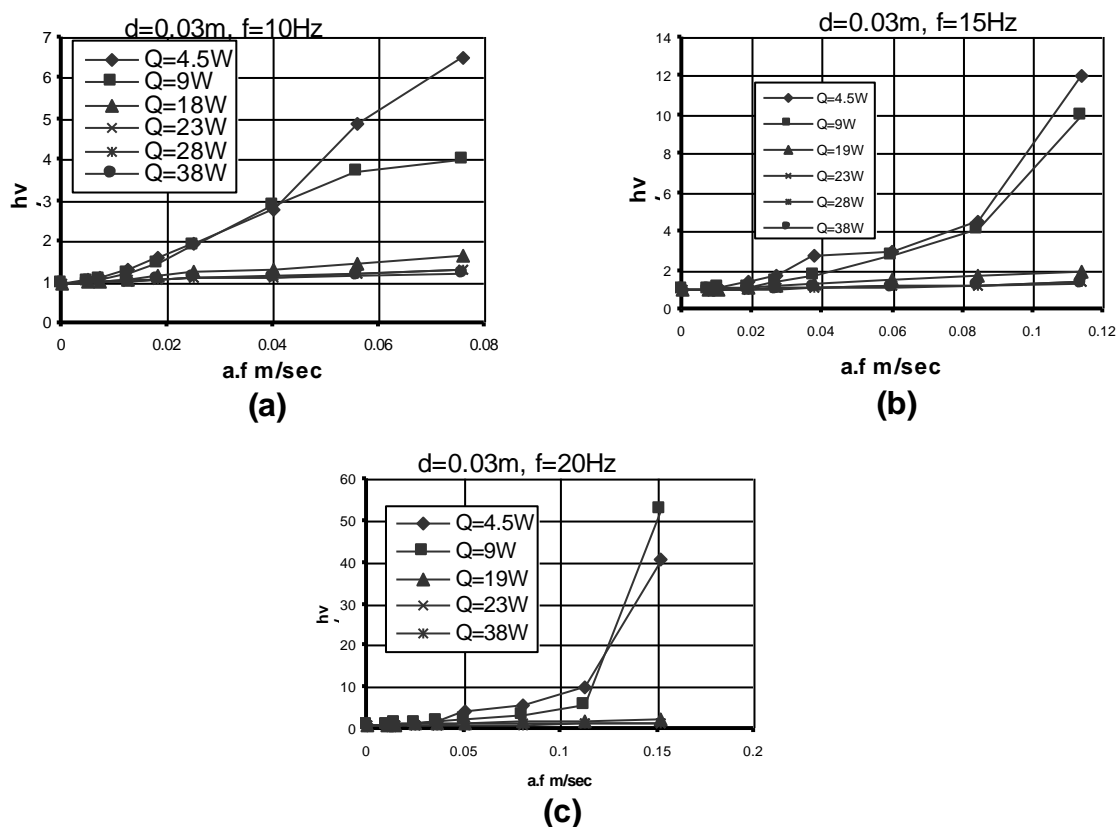
Yacoub K. Y, Sabieh A. J., and AL-Thaher M. A. " Heat Transfer From A vibrated Radial Fins Horizontal Cylinder in Air" J. Eng. Technology Vol. 16, pp. 424-435, 1997

LIST OF SYMBOLS:

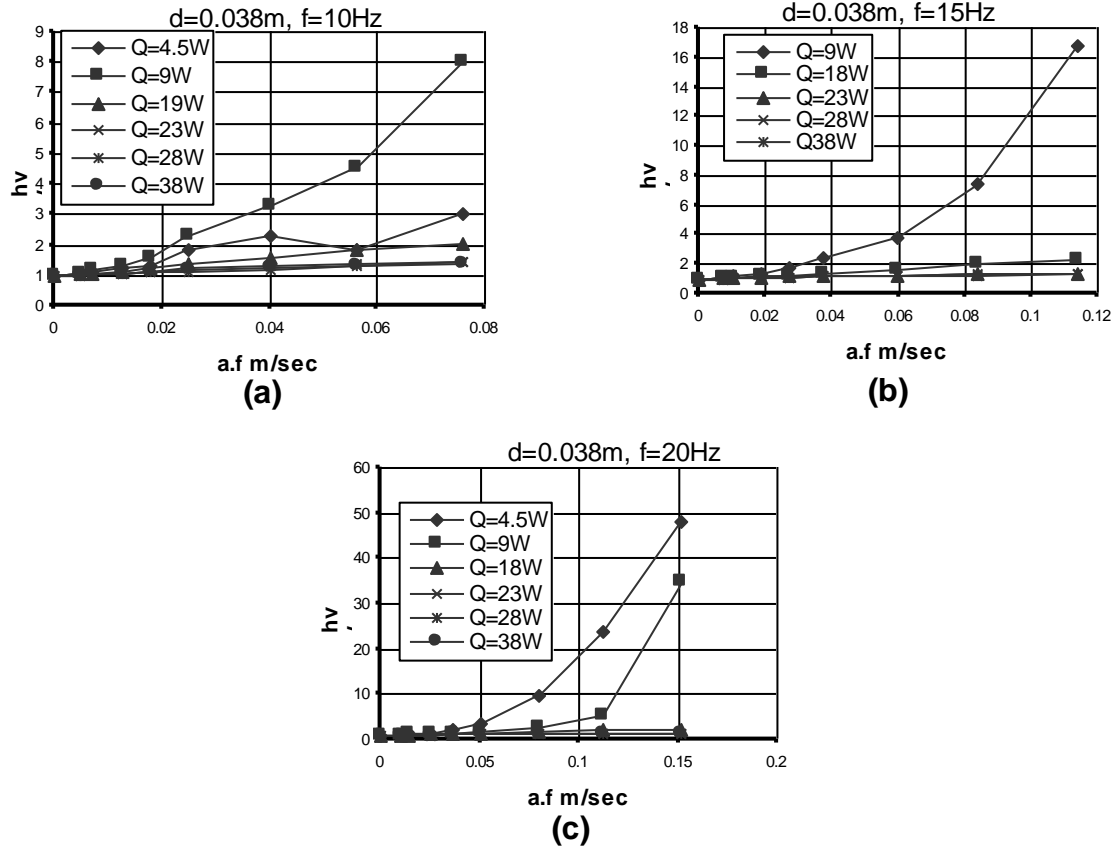
A	Area m^2	Nu_v	Vibration Nusslt number
a	Amplitude m	Pr	Prandtl number
Cp	Specific heat kJ/kgK	Q	Heat transfer W
d	Diameter of cylinder m	Q_c	Convection heat transfer W
f	Frequency Hz	Q_r	Radiation heat transfer W
Gr	Grashof number	Re	Reynolds number
h	Heat transfer coefficient $W/m^2.K$	Re_v	Vibration Reynolds number
h_o	Free heat transfer coefficient $W/m^2.K$	V	Voltage V
h_v	Vibration heat transfer coefficient $W/m^2.K$	ε	Emmisivity
I	Current am	ρ	Density m^3/sec
k	Thermal conductivity $W/m.K$	σ	Stefan-Boltzmann constant
l	Length of cylinder	μ	Viscosity kg(m.s)
Nu	Nussult number		



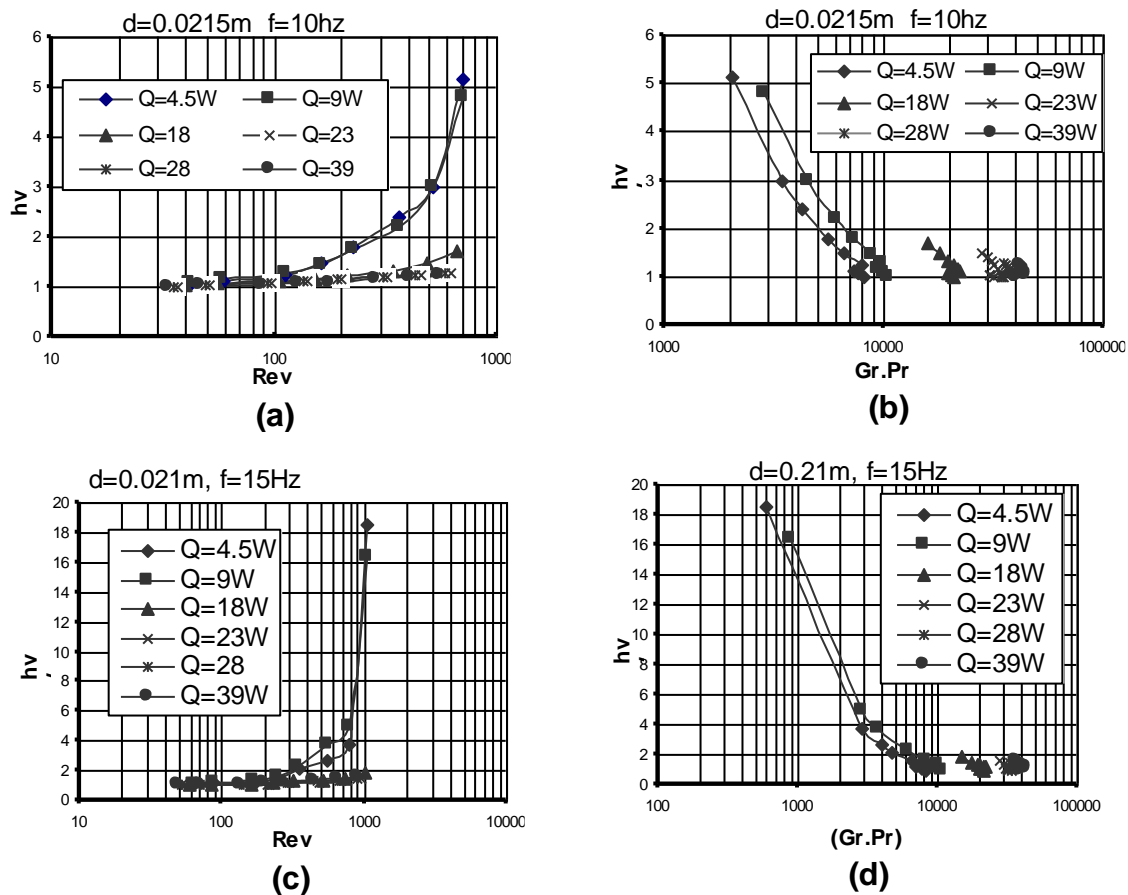
Fig(1) The Effect of Vibration density on Heat Transfer Coefficient for Different frequency and Heat Flux At $d=0.021m$

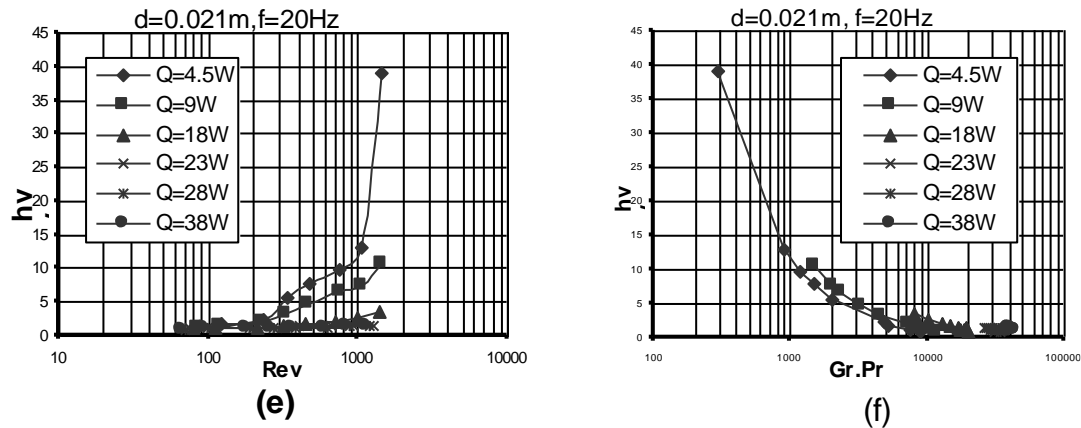


Fig(2) The Effect Of Vibration Density on heat Transfer Coefficient for Different Frequency And Heat Flux at $d=0.03m$

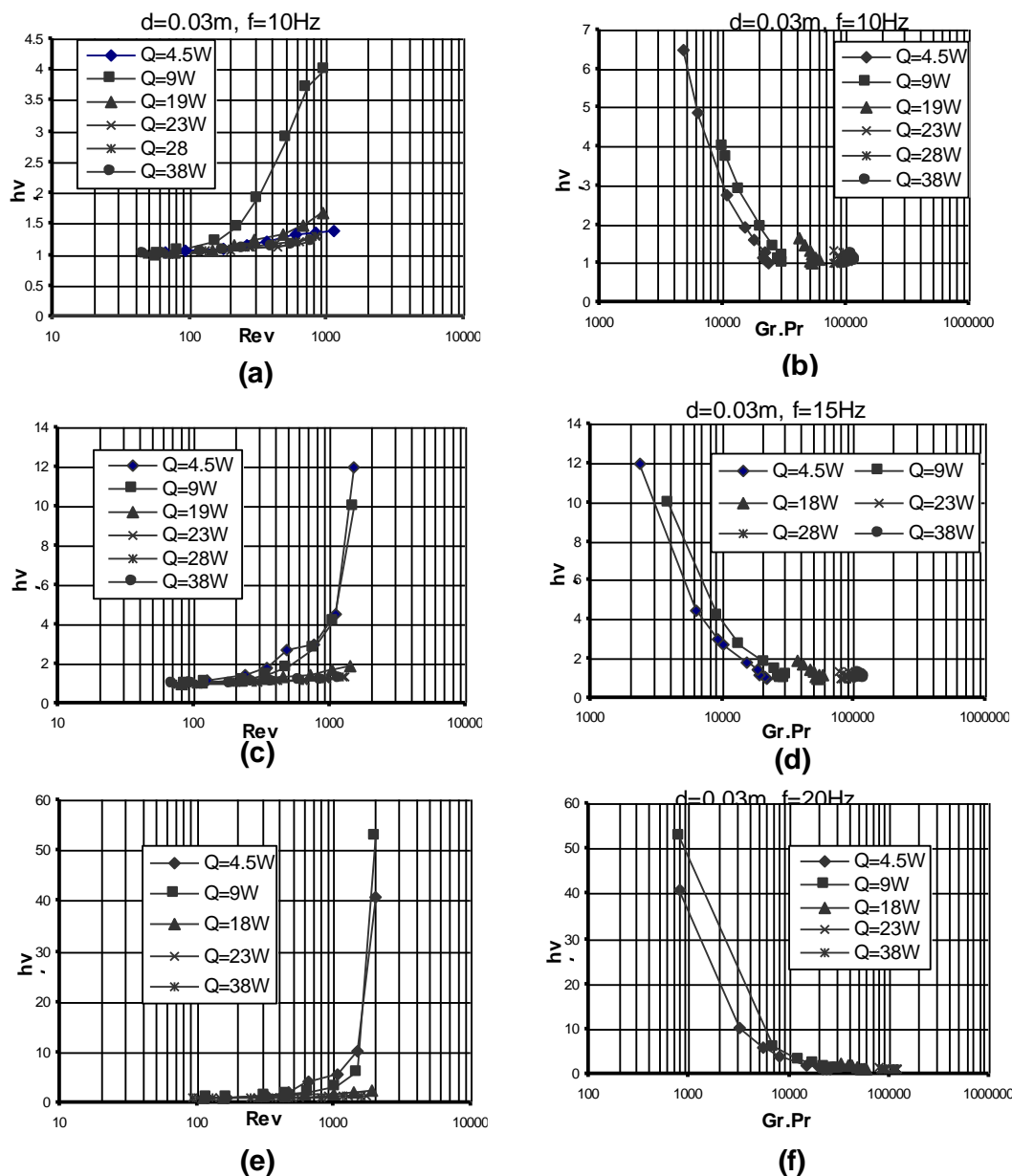


Fig(3)The effect Of Vibration Density on Heat Transfer Coefficient for Different Frequency and Heat Flux at d=0.038m

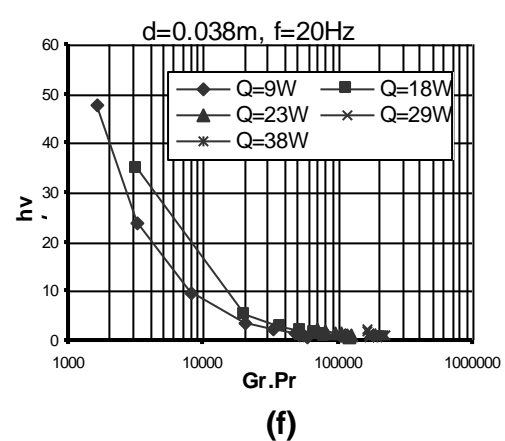
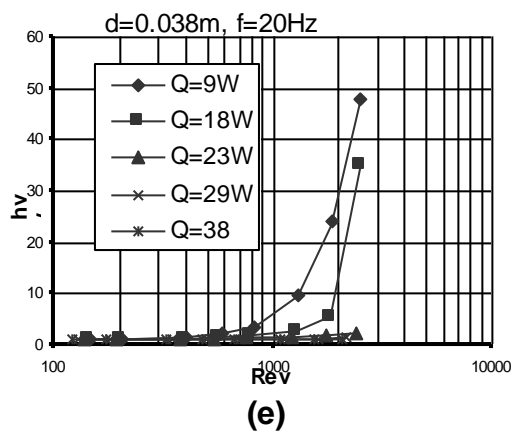
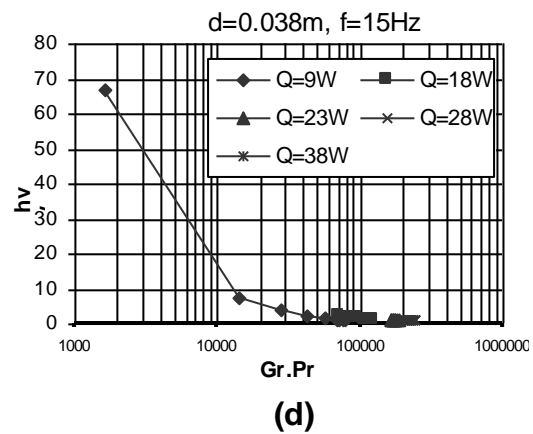
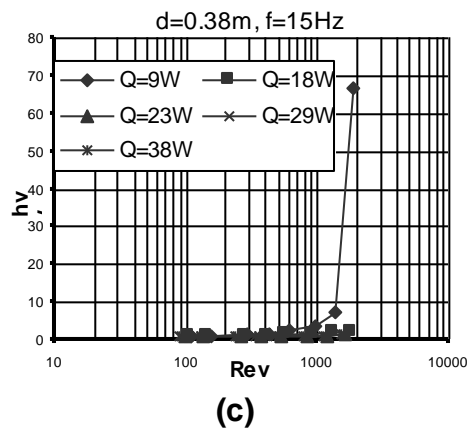
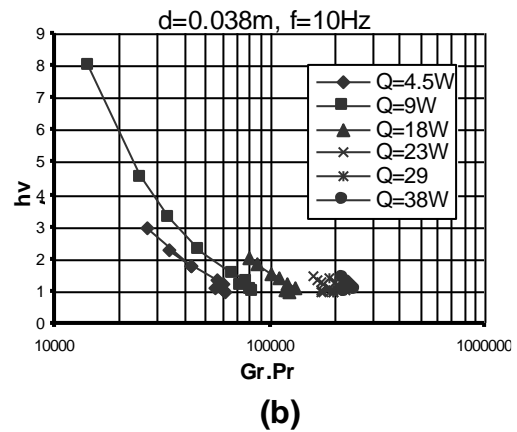
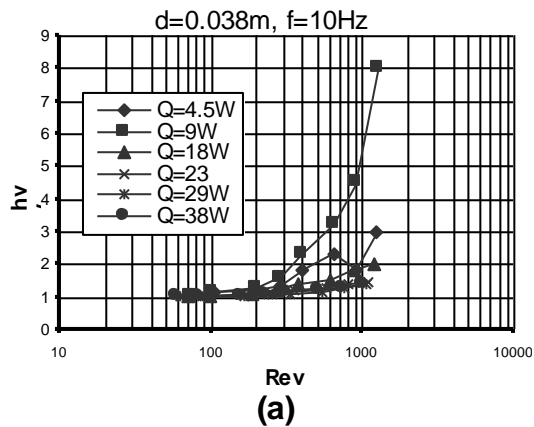




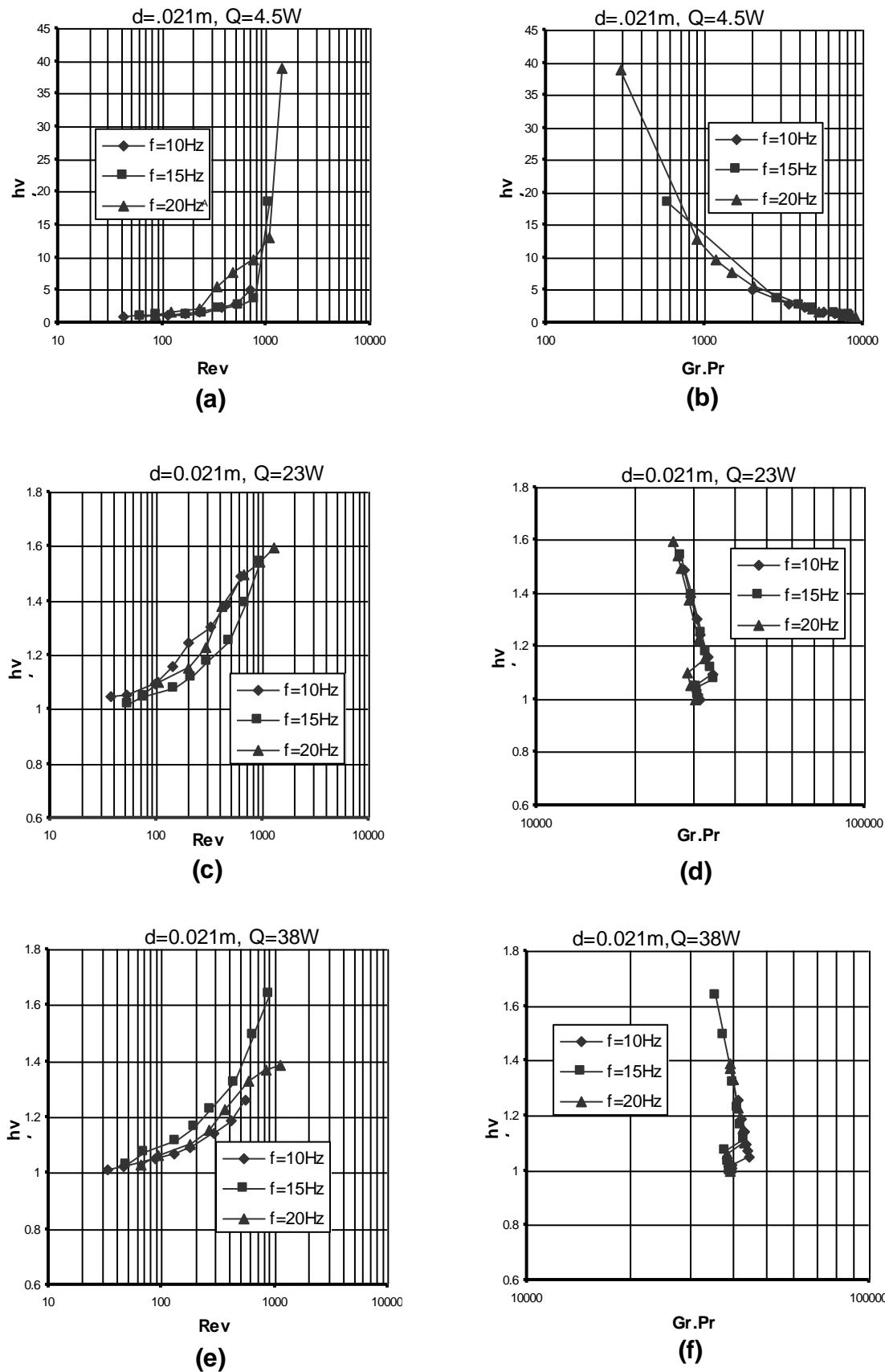
Fig(4) The Effect Of Re_v , and (Gr, Pr) on Vibration heat Transfer Coefficient at $d=0.021m$ for Different Frequency



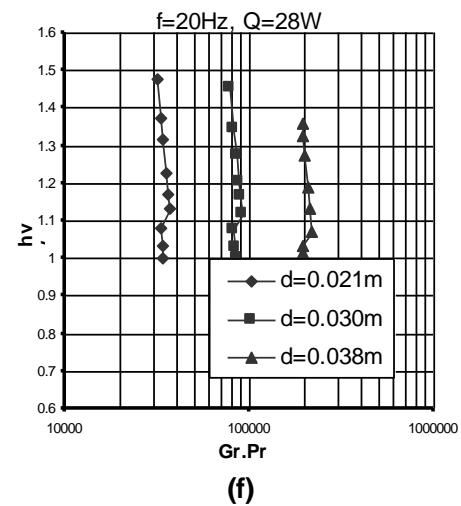
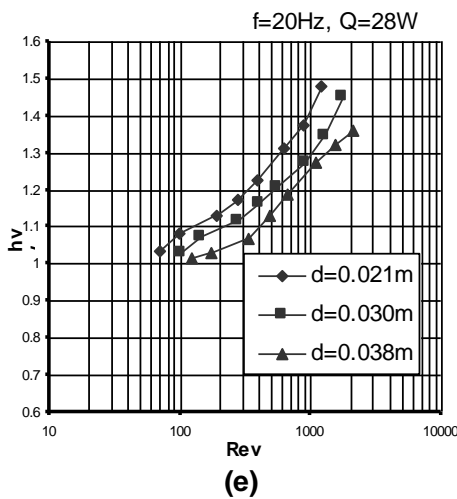
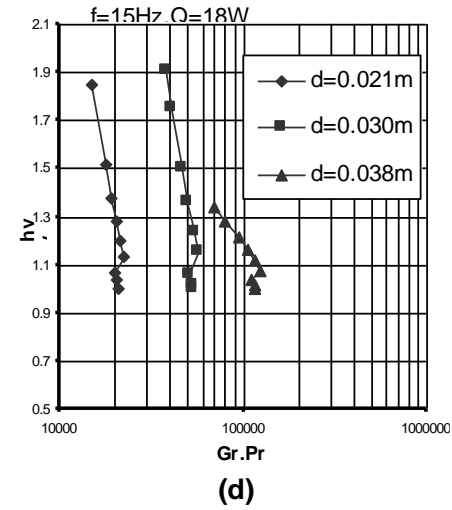
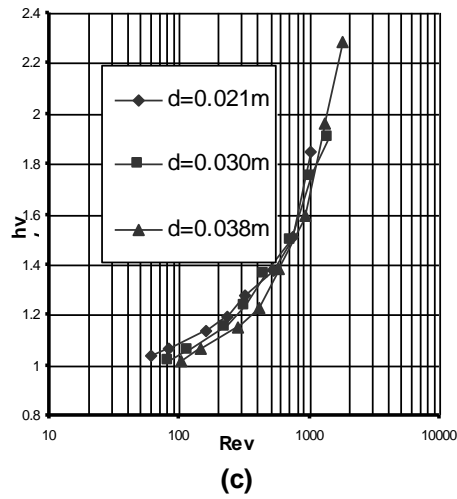
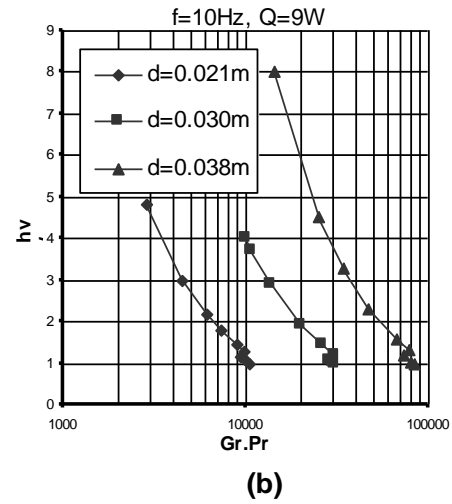
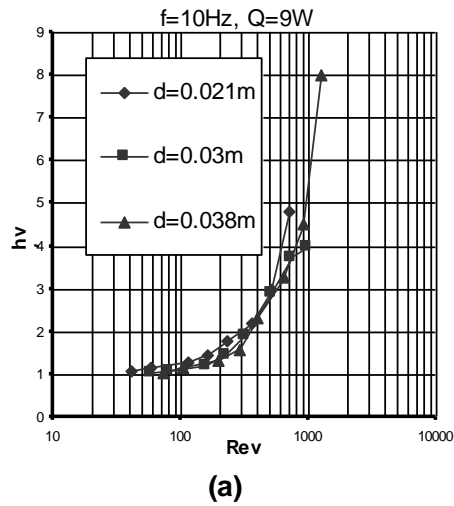
Fig(5) The Effect Of Re_v , and (Gr, Pr) on Vibration heat Transfer Coefficient at $d=0.030m$ for Different Frequency



Fig(6) The Effect Of Re_v , and (Gr, Pr) on Vibration heat Transfer Coefficient at $d=0.038\text{m}$ for Different Frequency



Fig(7) The Relation Between (Re_v), (Gr , Pr) and The (h_v/h_0) for Different Frequency at $d=0.021\text{m}$ for different Heat Transfer



Fig(8) The Relation Between (Re_v), (Gr, Pr) and The (h_v/h_0) for Different Diameters at Different Frequency and Heat Transfer

THE AXISYMMETRIC DYNAMICS OF ISOTROPIC CIRCULAR PLATES WITH VARIABLE THICKNESS UNDER THE EFFECT OF LARGE AMPLITUDES

Dr. Ahmed A. Al-Rajihy
College of Eng., University of Kerbalaa

ABSTRACT

This paper presents a study of the geometrically non-linear vibrations of clamped circular plates with variable thickness by taking the effect of large amplitude motion. The maximum thickness is considered to be at the plate center and it is taken to be twice the value of thickness at the edge. The problem is solved by the numerical iteration procedure to obtain the results of vibration amplitudes up to twice the maximum plate thickness. The results are presented for the first two modes of vibration. The obtained results indicate that increasing the ratio of thickness has the effect of increasing the nonlinear frequency and modify the corresponding mode shape.

الخلاصة

في هذه البحث تمت دراسة الإهتزازات اللا خطية لصفحة دائرية محكمة الإسناد على المحيط ، ذات سمك متغير وذلك بأخذ تأثير السعة العالية على الأهتزاز . لقد تم إعتبار أقصى سمك عند مركز الصفحة ومساويا لضعف السمك عند الحافة . لقد تم إستخدام طريقة التكرار العددي للحصول على النتائج وذلك بأعتبار أن الأراحة مسوية لضعف السمك الأقصى ، وأخذت النتائج للنسقين الأوليين فقط . لقد بينت النتائج أن زيادة نسبة السمك (أقصى سمك الى السمك عند الحافة) يزيد من قيمة الذبذبة اللاخطية ويؤثر على شكل الموجة التابعة للنسق .

KEYWORDS: Non-Linear Vibration, Circular Plate, Variable Thickness, Large Amplitudes

INTRODUCTION

Thin plates are used in various modern engineering problems and they are often subjected to severe dynamic loading. In some cases this may result in large amplitudes vibration which leads to a behavior different from that predicted by the classical linear theory. Thus it is necessary to include the geometrical non-linearity. In the literature, the Von Ka'rma'n relations is the most widely used. The governing equations are coupled non-linear partial differential equations of motion. Also no general and symmetric approach to nonlinear problems is available which allows all or most of the various non-linear effects to be described in a unified manner (**Benamar 1990**).

In the study of geometrically non-linear axi-symmetric vibrations of clamped circular plates, the common approach has been to use an assumed space or time mode. The different methods of solution used in the literature related to the subject of interest

have been presented in (Benamar 1991). In the very recent works, the finite element method has been applied to study the nonlinear vibrations of hinged orthotropic circular plates with a concentric rigid mass using Von Ka'rma'n equations (Huang 1998) and geometrically nonlinear free vibrations of polar orthotropic circular plates with various boundary conditions, using the three-dimensional elasticity theory with all of the non-linear terms retained in the strain expressions (liu 1996). If the single mode approach is used, this approach is not completely useful for studying the geometrically non-linear vibration of thin structures, therefore multimode analyses are used.

In the present paper the nonlinear vibration of a clamped circular plate with linearly varied thickness is studied taking both the in-plane and the transverse motions into account. The method of solution depends on the explicit approach. This approach is based on the linearization of the set of algebraic equations in the neighbourhood of each resonance.

MATHEMATICAL ANALYSIS

The plate is considered to have a radius R and variable thickness h clamped along its edge. The variation of the plate thickness is assumed as linear. The origin of the coordinate system is taken at the center of the plate, as shown in Fig. 1.

The plate is assumed to be elastic with homogeneous isotropic mechanical properties. For circular plate having large amplitude vibrations, the strains are given by the following equation (Hung, 1971) :

$$\begin{aligned}\varepsilon_r &= \frac{\partial U}{\partial r} + \frac{1}{2} \left(\frac{\partial W}{\partial r} \right)^2 - z \frac{\partial^2 W}{\partial r^2} \\ \varepsilon_\theta &= \frac{U}{r} - \frac{z}{r} \frac{\partial W}{\partial r}\end{aligned}\quad (1)$$

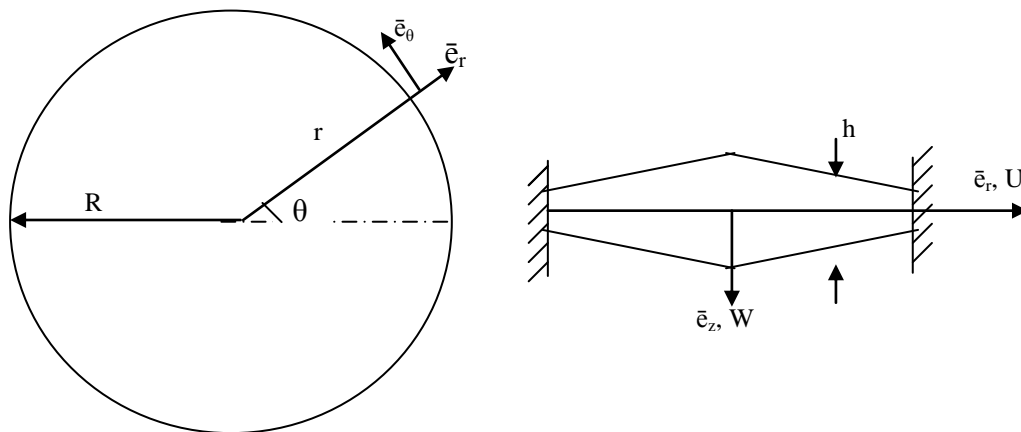


Fig. 1: Plate and Coordinate Notation

In large amplitude vibration, the strain energy is the sum of strain energy due to bending and the strain energy due to membrane, that is:

$$V = V_b + V_m \quad (2)$$

the bending strain energy of the clamped circular plate with axi-symmetric vibrations is **(Haterbouch 2003)** :

$$V_b = \pi D \int_0^a \left\{ \frac{\partial^2 W}{\partial r^2} + \frac{1}{r^2} \left(\frac{\partial W}{\partial r} \right)^2 \right\} r dr \quad (3)$$

where, $D = Eh^3 / 12(1-\nu^2)$. The membrane strain energy of the circular plate is given by **(Timoshenko 1959)** :

$$V_m = \frac{12\pi D}{h^2} \int_0^a \left\{ \left(\frac{\partial U}{\partial r} \right)^2 + \frac{U^2}{r^2} + 2\nu \frac{U}{r} \frac{\partial U}{\partial r} + \left(\frac{\partial W}{\partial r} \right)^2 \frac{\partial U}{\partial r} + \frac{1}{4} \left(\frac{\partial W}{\partial r} \right)^4 + \nu \frac{U}{r} \left(\frac{\partial W}{\partial r} \right)^2 \right\} r dr \quad (4)$$

Now the total strain energy is:

$$V = \pi D \int_0^a \left\{ \frac{\partial^2 W}{\partial r^2} + \frac{1}{r^2} \left(\frac{\partial W}{\partial r} \right)^2 \right\} r dr + \frac{12\pi D}{h^2} \int_0^a \left\{ \left(\frac{\partial U}{\partial r} \right)^2 + \frac{U^2}{r^2} + 2\nu \frac{U}{r} \frac{\partial U}{\partial r} + \left(\frac{\partial W}{\partial r} \right)^2 \frac{\partial U}{\partial r} + \frac{1}{4} \left(\frac{\partial W}{\partial r} \right)^4 + \nu \frac{U}{r} \left(\frac{\partial W}{\partial r} \right)^2 \right\} r dr \dots \dots \dots (5)$$

The kinetic energy of the circular plate with neglecting the rotary inertia is:

$$T = \pi \rho h \int_0^a \left\{ \left(\frac{\partial W}{\partial t} \right)^2 + \left(\frac{\partial U}{\partial t} \right)^2 \right\} r dr \quad (6)$$

The most common approach in seeking an approximate solution of geometrically non-linear vibration is by separation of space and time functions. The transverse displacement function is:

$$W(r, t) = w(r) \cos(\omega t) \quad (7)$$

and the in-plane radial displacement is given by **(Haterbouch 2004)** :

$$U(r, t) = u(r) \cos^2(\omega t) \quad (8)$$

The spatial functions $u(r)$ and $w(r)$ are expanded in the form of finite series of p_i and p_o in-plane $u_i(r)$ and transverse motion $w_i(r)$ basic functions, respectively as:

$$\begin{aligned} w(r) &= a_i w_i(r), \\ u(r) &= b_i u_i(r) \end{aligned} \quad (9)$$

Now the discretized forms for the total strain and kinetic energies are:

$$V = \frac{1}{2} a_i a_j k_{ij}^1 \cos^2(\omega t) + \frac{1}{2} [a_i a_j a_k b^1_{ijkl} + a_i b_j k^2_{ij}] \cos^4(\omega t) \quad (10)$$

$$T = \frac{1}{2} \omega^2 [a_i a_j m_{ij}^1 \sin^2(\omega t) + b_j b_j m_{ij}^2 \sin^2(2\omega t)] \quad (11)$$

where, m_{ij}^1 , m_{ij}^2 , k_{ij}^1 , k_{ij}^2 are the mass and stiffness tensors associated with W and U respectively, and b_{ijkl} & c_{ijk} are fourth order and third order non-linearity tensors respectively. These tensors are:

$$m_{ij}^1 = 2\pi\rho h \int_0^a w_i w_j r dr \dots\dots\dots (12a)$$

$$m_{ij}^2 = 2\pi\rho h \int_0^a u_i u_j r dr \dots\dots\dots (12b)$$

$$k_{ij}^1 = 2\pi\rho h \int_0^a \left(\frac{d^2 w_i}{dr^2} \frac{d^2 w_j}{dr^2} + \frac{1}{r^2} \frac{dw_i}{dr} \frac{dw_j}{dr} \right) r dr \dots\dots\dots (12c)$$

$$k_{ij}^2 = \frac{24\pi D}{h^2} \int_0^a \left(\frac{du_i}{dr} \frac{du_j}{dr} + \frac{1}{r^2} u_i u_j + \frac{\nu}{r} \frac{d_i}{dr} u_j + \frac{\nu}{r} u_i \frac{du_j}{dr} \right) r dr \dots\dots\dots (12d)$$

$$c_{ijk} = \frac{24\pi D}{h^2} \int_0^a \left(\frac{dw_i}{dr} \frac{dw_j}{dr} \frac{du_k}{dr} + \frac{\nu}{r} \frac{dw_i}{dr} \frac{dw_j}{dr} u_k \right) r dr \dots\dots\dots (12e)$$

$$b_{ijkl}^1 = \frac{6\pi D}{h^2} \int_0^a \left(\frac{dw_i}{dr} \frac{dw_j}{dr} \frac{dw_k}{dr} \frac{dw_l}{dr} \right) r dr \dots\dots\dots (12f)$$

Hamilton's principle is powerful to govern the dynamics of structures, which is written in its general symbolic form as:

$$\delta \int_0^{2\pi} (V - T) dt = 0 \quad (13)$$

Substituting **Eq. (5)** and **(6)** into **Eq. (13)** and after integrating the time functions and differentiating with respect to a_i 's & b_i 's results the following set of non-linear algebraic equations:

$$2a_i k_{ir}^1 + 3a_i a_j a_k b_{ijk}^1 + \frac{3}{2} a_i b_k c_{irk} - 2\omega^2 a_i m_{ir}^1 = 0, \dots\dots r = 1, \dots, p_o \quad (14a)$$

$$\frac{3}{4} (a_i a_j c_{ijs} + 2b_i k_{is}^2) - 2\omega^2 b_i m_{is}^2 = 0, \dots\dots s = 1, \dots, p_i \quad (14b)$$

In order to generalize the analysis, the following non-dimensional displacements may be used;

$$r^* = \frac{r}{R}, \dots, w_i^*(r^*) = \frac{w_i(r)}{h_0}, \dots, u_i^*(r^*) = \frac{u_i(r)}{\lambda h_0} \quad (15)$$

where, $\lambda = \frac{h_o}{R}$

Now **Eq. (14)** may be written to take the form:

$$2a_i k_{ij}^{1*} + 3a_i a_j a_k b_{ijk}^{1*} + \frac{3}{2} a_i b_k c_{irk}^* - 2\omega^{*2} a_i m_{ir}^{1*} = 0, \dots, r = 1, \dots, p_o \quad (16)$$

$$\frac{3}{4} (a_i a_j c_{ijs}^* + 2b_i k_{is}^{2*}) - 2\lambda^2 \omega^{*2} b_i m_{is}^{2*} = 0, \dots, s = 1, \dots, p_i$$

where ω^* is the non-dimensional non-linear frequency, which is defined by:

$$\omega^{*2} = \frac{\rho h_o R^4 \omega^2}{D} \quad (17)$$

The dimensional terms in (12) may be written in non-dimensional forms as:

$$m_{ij}^{1*}, m_{ij}^{2*} = \frac{1}{2\pi \rho R^2 h_o^3} (m_{ij}^1, m_{ij}^2 l \lambda^2), \quad (18)$$

$$(k_{ij}^{1*}, k_{ij}^{2*}, c_{ijk}^*, b_{ijkl}^{1*}) = \frac{R^2}{2\pi D h_o^2} (k_{ij}^1, k_{ij}^2, c_{ijk}, b_{ijkl}^1)$$

These non-dimensional terms are given by:

$$m_{ij}^{1*} = \int_0^1 w_i^* w_j^* r^* dr^* \dots \dots \dots (19a)$$

$$m_{ij}^{2*} = \int_0^1 u_i^* u_j^* r^* dr^* \dots \dots \dots (19b)$$

$$k_{ij}^{1*} = \int_0^1 \left(\frac{d^2 w_i^*}{dr^{*2}} \frac{d^2 w_j^*}{dr^{*2}} + \frac{1}{r^{*2}} \frac{dw_i^*}{dr^*} \frac{dw_j^*}{dr^*} \right) dr^* \dots \dots \dots (19c)$$

$$k_{ij}^{2*} = 12 \int_0^1 \left(\frac{du_i^*}{dr^*} \frac{du_j^*}{dr^*} + \frac{1}{r^{*2}} u_i^* u_j^* + \frac{\nu}{r^*} \frac{du_j^*}{dr^*} u_i^* + \frac{\nu}{r^*} u_i^* \frac{du_j^*}{dr^*} \right) r^* dr^* \dots \dots \dots (19d)$$

$$c_{ijk}^* = 12 \int_0^1 \left(\frac{dw_i^*}{dr^*} \frac{dw_j^*}{dr^*} \frac{du_k^*}{dr^*} u_j^* + \frac{\nu}{r^*} \frac{dw_i^*}{dr^*} \frac{dw_j^*}{dr^*} u_k^* \right) r^* dr^* \dots \dots \dots (19e)$$

$$b_{ijkl}^{1*} = 3 \int_0^1 \left(\frac{dw_i^*}{dr^*} \frac{dw_j^*}{dr^*} \frac{dw_k^*}{dr^*} \frac{dw_l^*}{dr^*} \right) r^* dr^* \dots \dots \dots (19f)$$

The transverse functions $w_i^*(r^*)$ for the clamped axisymmetric circular plate are written as (**Hatrbouch 2003**) :

$$w_i^*(r^*) = A_i \left[J_o(\beta_i r^*) - \frac{J_o(\beta_i)}{I_o(\beta_i)} I_o(\beta_i r^*) \right] \quad (20)$$

where, β_i 's are the real positive roots of:

$$J_1(\beta_i)I_o(\beta_i) + J_1(\beta_i)I_o(\beta_i) = 0 \quad (21)$$

In this equation J_n , I_n are the Bessel and the modified Bessel functions of the first kind of order n . The parameter β_i related to $(\omega^*)_i$ by;

$$\beta_i^2 = (\omega^*)_i \quad (22)$$

The values of β can be found from **Eq. (21)**.

The in-plane basic functions $u_i^*(r^*)$ for the immovable axisymmetric circular plate are (**Lee 1971**) :

$$u_i^*(r^*) = \beta_i J_1(\alpha_i r^*) \quad (23)$$

where, α_i is the i th real root of ;

$$J_1(\alpha) = 0 \quad (24)$$

The functions $w_i^*(r)$ and $u_i^*(r)$ should be normalized as:

$$m_{ij}^{1*} = \int_0^1 w_i^* w_j^* r^* dr^* = \delta_{ij} \quad (25)$$

$$m_{ij}^{2*} = \int_0^1 u_i^* u_j^* r^* dr^* = \delta_{ij}$$

The values of k_{ij}^{1*} , k_{ij}^{2*} , c_{ijk}^* and b_{ijkl}^{1*} given by **Eq. (19)** were computed by Simpson's rule. The set of nonlinear algebraic equations (16), which called the amplitude equation, can be written in matrix form as:

$$([K^{1*}] + [K_{nl}^*])\{A\} - \omega^{*2}[M^{1*}]\{A\} = \{0\} \quad (26)$$

where, $[K^{1*}]$, $[M^{1*}]$ and $[K_{nl}^*]$ are respectively the non-dimensional linear stiffness, mass and non-linear geometrical stiffness matrices. The terms of the matrix $[K_{nl}^*]$ are; $(K_{nl}^*)_{ij} = (3/2)a_k a_l b_{ijkl}^*$. Neglecting the term $[K_{nl}^*]$ from **Eq. (26)** gives the classical eigenvalue problem;

$$[K^{1*}]\{A\} = \omega^{*2}[M^{1*}]\{A\} \quad (27)$$

In this equation each eigenvalue have a corresponding eigenvector while the nonlinear **Eq. (26)** lead to a set of amplitude-dependent eigenvectors with their amplitude-dependent associated eigenvalues.

The single mode assumption, which neglects all of the coordinates except the single resonant coordinate, has been used widely in the geometrical non-linearities due to the great simplifications it introduces (**Azrar, 1999**). Also this approach does not give any information about the amplitude dependence between the deflection shape and distribution of stresses (**El Kadiri 2002**). Therefore the explicit method of solution is used because it remedies this insufficiency of the single mode approach.

If the effect of λ in **Eq. (16)** is neglected due to its very small values, it can be rewritten according to this approach as:

$$a_i k_{ir}^{1*} + \frac{3}{2} a_i^3 b_{111r}^3 - \omega^{*2} a_i m_{ir}^{1*} - 0, \dots, r = 1, \dots, p_o \quad (28)$$

For $r=1$, we have,

$$\omega^{*2} = \frac{k_{11}^{1*}}{m_{11}^{1*}} + \frac{3}{2} \frac{b_{1111}^{1*}}{m_{11}^{1*}} a_1^2 \quad (29)$$

The (p_o-1) remaining equations are:

$$(k_{rr}^{1*} - \omega^{*2} m_{rr}^{1*}) \varepsilon_r = \frac{-3}{2} a_1^3 b_{111r}^3, \dots, r = 2, \dots, p_o \quad (30)$$

where, ε_r is the contribution coefficient of the non-resonant modes which is given by:

$$\varepsilon_r = -\frac{3a_1^3 b_{111r}^3}{2(k_{rr}^{1*} + \omega^{*2} m_{rr}^{1*})}, \dots, r = 2, \dots, p_o \quad (31)$$

substituting **Eq. (29)** into **(31)** gives:

$$\varepsilon_r = -\frac{3a_1^3 b_{111r}^3}{2\left(k_{11}^{1*} + \frac{3}{2} a_1^2 b_{1111}^3 - k_{rr}^{1*}\right)}, \dots, r = 2, \dots, p_o \quad (32)$$

Eq.(32) is an explicit formula, allowing direct calculation of higher order contribution corresponding to the first mode shape. Thus the first non-linear amplitude dependent clamped circular plate mode shape, $w_{n1}^*(r^*, a)$ can be defined in a series form as:

$$w_{n1}^*(r^*, a_1) = a_1 w_{11}^*(r^*) + \sum_{r=2}^{p_o} \frac{3a_1^3 b_{111r}^3}{2(k_{11}^{1*} + \frac{3}{2} a_1^2 b_{1111}^3 - k_{rr}^{1*})} w_r^*(r^*) \quad (33)$$

In this equation the predominant term in which proportional to the first linear mode shape is $a_1 w_{11}^*(r^*)$ and the others which corresponding to the higher linear mode shapes $w_2^*(r^*), \dots, w_{p_o}^*(r^*)$ are corrections due to the non-linearity.

In order to determine the distribution of membrane stresses, the in-plane displacement coefficients b_i should be determined. As mentioned above, because of the very small values of λ , **Eq. (16)** gives:

$$b_i = a_j a_l d_{jli}^*, \dots, i = 1, \dots, p_i \quad (34)$$

where, $d_{ijk}^* = -\frac{1}{2} k_{kl}^{2*} c_{ijl}^{1*}$, is a third order terms expressing the coupling between the transverse and in-plane motions, the tensor k_{ij}^{2*} .

If the first and second order terms in the expression $a_i a_j d_{ijk}^*$ are neglected, the in-plane contribution coefficients are simply given by:

$$b_i = a_1^2 d_{11i}^*, i=1, \dots, p_i \quad (35)$$

Thus the in-plane shape function is given by:

$$u^*(r^*) = a_1^2 d_{1li}^* u_i^*(r^*) \quad (36)$$

If the first order term $a_1 \varepsilon_1 d_{1li}^*$ is added, the in-plane basic function contribution coefficients, **Eq. (35)**, are given by:

$$b_i = a_1^2 d_{1li}^* + \sum_{l=2}^{p_o} a_1 \varepsilon_l d_{1li}^* \quad , \quad i=1, \dots, p_l \quad (37)$$

now the in-plane function is:

$$u^*(r^*) = a_1^2 [d_{1li}^* + \sum_{r=2}^{p_o} \frac{3a_1^2 b_{11lr}^* d_{1ri}^*}{(2k_{11}^{1*} + 3d_{111l}^* b_{111l}^* - 2k_{rr}^{1r})}] w_i^*(r^*) \quad (38)$$

This equation improves significantly the membrane stress estimates for amplitudes higher than those permitted by expression (35).

RESULTS AND DISCUSSIONS

The dependence of the non-linear frequency on the amplitude of vibration is shown in **Fig. (2)** for thickness ratios of 1, 1.5 and 2. This figure is plotted for the first two axisymmetric mode shapes. The ratio of thickness (h_i/h_o) has the effect of magnifying the frequency ratio (ω_{nl}^*/ω_1^*). Also it is seen that a spring hardening effect is present and this effect increased with increasing the amplitude ratio. The plot also shows that the first mode shape exhibits less change in frequency with the vibration amplitude than does the second non-linear mode shape. This is because that the deflection shape associated with the first mode shape produces less induced tensile forces than does that associated with the second mode shape for the same maximum displacement amplitudes. This figure shows that the nonlinear frequency increased with increasing the ratio of thickness. This is because of the bending effect arise due to the geometry of the plate. This effect increased with increasing the ratio of thickness.

Figs. (3a) and (3b) show the effect of thickness ratio on the non-linear mode shape. The non-linear mode shapes are plotted for the first two axisymmetric modes. The effect of amplitude ratio is presented in (**Haterbouch 2003 & Haterbouch 2004**), therefore it is not presented here. The values of thickness ratio has the effect of keeping away the mode shape in the direction of the plate edge. Also it can be seen that the mode shapes become more flatening near to the centre of the circular plate with the increase of vibration amplitude. But here it is shown that the effect of thickness ratio is more pronounced than the amplitude ratio.

The effect of amplitude of vibration and thickness ratio on the normalized in-plane displacement shape functions is shown in **Figs. (4a) and (4b)** respectively for the first two modes. Increasing the ratio of thickness has the effect of pulling the in-plane mode shape in the direction of plate centre. This effect because that the inertia force near the centre of plate is higher than that near the edge.

Fig. (5) shows that the normalized amplitude is affected by the ratio of thickness in which increasing this ratio cause a shift to higher values at dimensionless radius values between 0.2 and 0.8. This trend is due to the high inertial values which cause higher values of deflection.



Conclusions

From the presented results the following two conclusions can be drawn;

- 1- It is shown that both of the amplitude of vibration and thickness nonuniformity have a clear effect on the nonlinear frequency and the corresponding mode shape.
- 2- Increasing these two parameters cause an increase in the nonlinear frequency and change the mode shape.

References

C.F. Liu, G.T. Chen, "Geometrically nonlinear Axisymmetric Vibrations of Polar Orthotropic Circular Plates", *International Journal of Mechanical Science*, 38, 3, 1996, pp. 1715-1726.

C.F. Liu, G.T. Chen, "Geometrically nonlinear Axisymmetric Vibrations of Polar Orthotropic Circular Plates", *International Journal of Mechanical Science*, 38, 3, 1996, pp. 1715-1726.

C.L.D. Huang, I.M. Al-Khattat, "Finite Amplitude Vibrations of a Circular Plate", *International Journal of nonlinear Mechanics*, 12, 1977, pp. 297-306.

L. Azrar, R. Benamar, R.G. White, "A Semi-Analytical Approach to the nonlinear Dynamic Response Problem of S-S C-C Beams at Large Vibration Amplitudes. Part I: General Theory and Application to the Single Mode Approach to free and Forced Vibration Analysis", *Journal of Sound &Vibration*, 224, 2, 1999, pp. 183-207.

L.C. Wellford, G.M. Dib, W. Mindle, "Free and Steady-State Vibration of nonlinear Structures using a Finite Element nonlinear Eigenvalue Technique", *Earthquake Engineering and Structural Dynamics*, 8, 1980, pp. 97-115.

M. El Kadiri, R. Benamar, R.G. White, "Improvement of the Semi-Analytical Method for Determining the Geometrically non-linear Response of Thin Straight Structures. Part I: Application to Clamped-Clamped and Simply Supported_ Clamped Beams", *Journal of Sound &Vibration*, 249, 2002, pp. 263-205.

M. Haterbouch, R. Benamar, "The Effects of Large Vibration Amplitudes on the Axisymmetric Mode Shapes and Natural Frequencies of Clamped Thin Isotropic Circular Plates. Part I: Iterative and Explicit Analytical Solution for nonlinear Transverse Vibrations", *Journal of Sound &Vibration*, 265, 2003, pp. 123-154.

M. Haterbouch, R. Benamar, "The Effects of Large Vibration Amplitudes on the Axisymmetric Mode Shapes and Natural Frequencies of Clamped Thin Isotropic Circular Plates. Part II: Iterative and Explicit Analytical Solution for nonlinear Transverse Vibrations", *Journal of Sound &Vibration*, 277, 2004, pp. 1-30.

R. Benamar, "Non-linear Dynamic Behaviour of Fully Clamped Beams and Rectangular isotropic Laminated Plates", Ph.D. Thesis, Institute of Sound and Vibration Research, 1990.

R. Benamar, M.M.K. Bennouna, R.G. White, "The effects of Large Vibration Amplitudes on the Mode Shapes and Natural Frequencies of Thin Elastic Structures. Part I: Simply Supported and Clamped-Clamped Beams", Journal of Sound &Vibration, 194, 1991, pp. 179-195.

S. Huang, "Nonlinear Vibration of a Hinged Orthotropic Circular Plate with a Concentric Rigid Mass", Journal of Sound &Vibration, 241, 5, 1998, 873-883.

S. Timoshenko, S. Woinowsky-Krieger, "Theory of Plates and Shells", 2nd Edd., Mcgraw-Hill, New York, 1959.

T.W. Lee, P.T. Blotter, D.H.Y. Yen, "On the nonlinear Vibrations of a Clamped Circular Plate" Developments in Mechanics, 6, 1971, pp. 907-921.

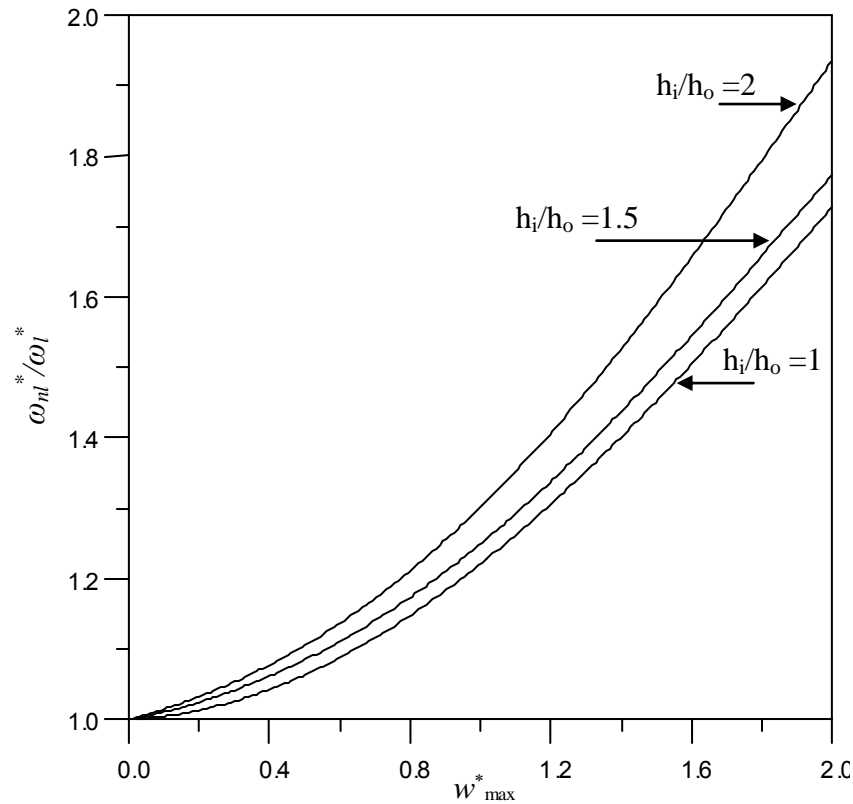


Fig. 2: Effect of Thickness Ratio and Maximum Vibration Amplitude on the nonlinear Frequency.

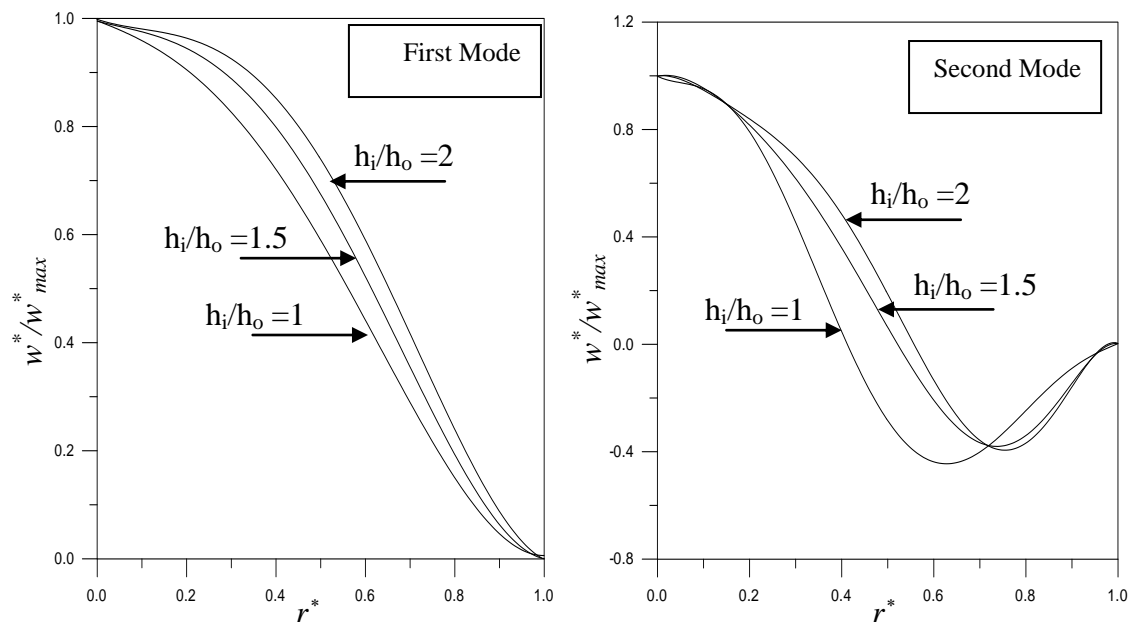


Fig. 3: Effect of Thickness Ratio on the normalized mode shape of the first two nonlinear Axisymmetric modes of the clamped circular plate, $w_{max}^* = 2$.

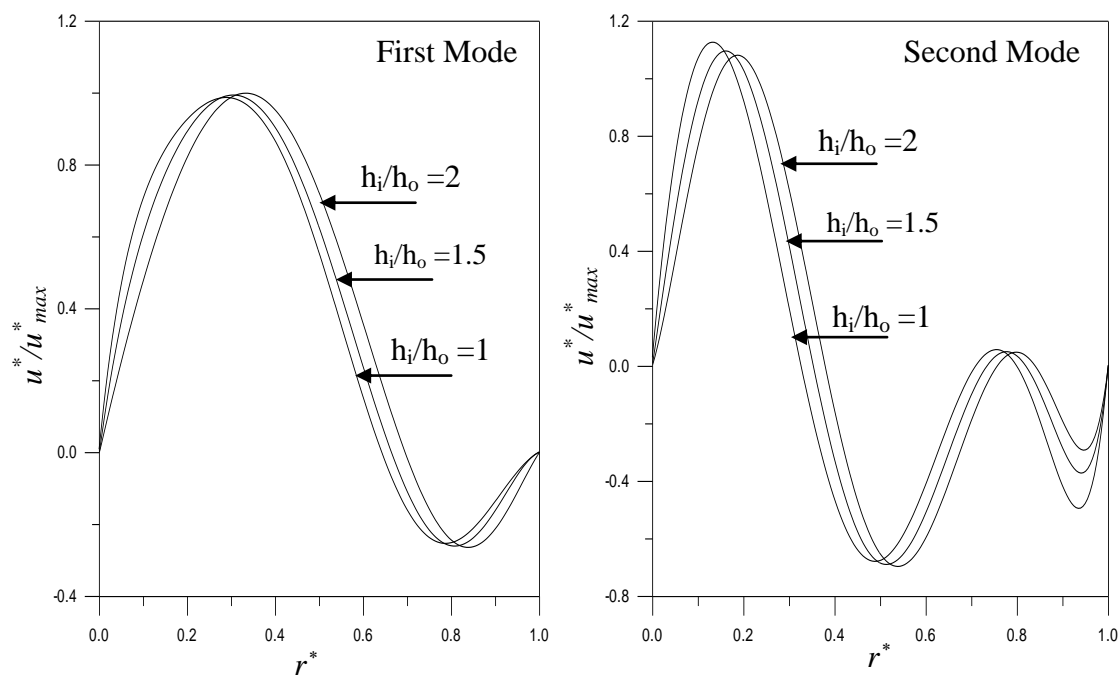


Fig.4: Effect of Thickness Ratio the Normalized in-Plane Shape Functions of the nonlinear Axisymmetric Modes of a Clamped Circular Plate, $w_{max}^* = 2$

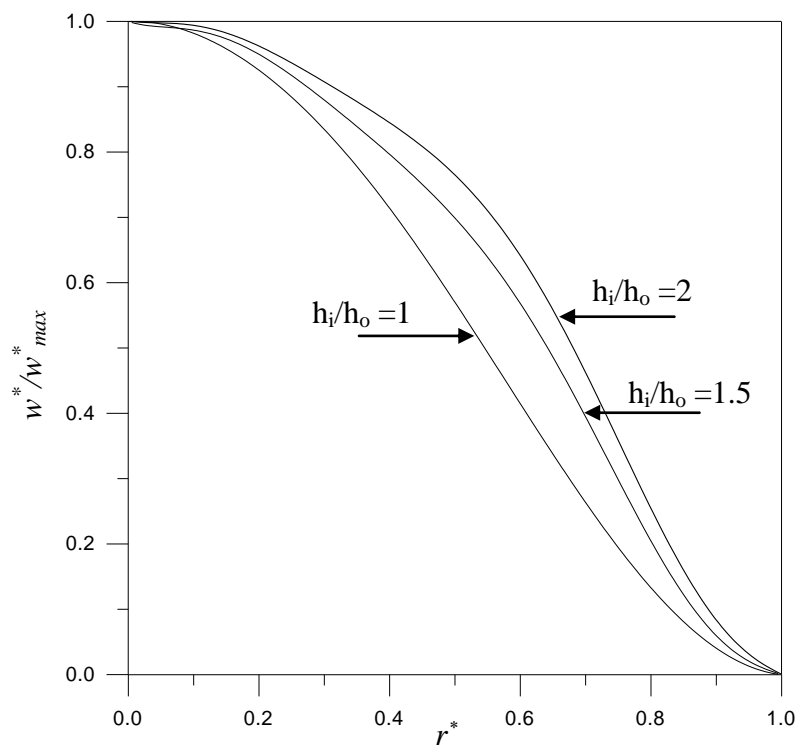


Fig. 5: Effect of Thickness Ratio on the First Mode Shape from Model with w and u , $w_{max}^* = 2$.

EFFECT OF THE OUTLET NOZZLE DIAMETER ON THE PERFORMANCE OF DIVERGENT VORTEX TUBE

Dr. Asaad T. Al-Omran
Technical College
Baghdad

Dr. Ramzi R. Ibrahim
Ins. Of Technology
Baghdad

Dr. H. N. Al-Rawi
Unv. Mamoon College
Baghdad

ABSTRACT

The aim of the present work is to study the effect of different outlet nozzle diameters, by using one or two nozzles on the performance of divergent vortex tube and also to determine the effects of various parameters on the vortex tube cooling performance such as: refrigeration capacity, coefficient of performance, isentropic efficiency. The experimental investigation was carried out on a divergent vortex tube rig manufactured for the present study covering all tests. The effect of different outlet nozzle diameters ($d_n = 4$ mm, $d_n = 5$ mm, and $d_n = 6.5$ mm) on the performance of the vortex tube is described by using one nozzle or two nozzles by varying the pressure of the inlet air and cold air mass ratio (μ_c) within the ranges ($P_{i\ abs} = 2 - 7$ bar) and ($\mu_c = 0 - 1$). The outlet nozzle diameter, ($d_n = 5$ mm), and the outlet cold diameter ($d_c = 10$ mm), when using two nozzles, give high temperature separation and may considered to be the optimum for different pressures of the inlet air regarding all the size tube diameter. The experimental study predicts two empirical results between the outlet nozzle diameter (d_n), number of nozzles (N), inside vortex tube diameter (D), and length of vortex tube (L) as:

$$\frac{Nd_n^2}{D^2} = 0.105 \quad \text{for (} N=1 \text{) and;}$$

$$\frac{Nd_n^2}{D^2} = 0.211 \quad \text{for (} N=2 \text{)}$$

الخلاصة

الهدف من البحث الحالي هو دراسة تأثير القطر الداخلي للمنافث باستخدام منفث واحد ، ومنفتان على أداء الأنبوب الدوامي المنفرج ، وكذلك دراسة مختلف العوامل التي تؤثر على الأداء التبريدي مثل سعة التبريد ، معامل الأداء ، الكفاءة الايزنتروبية. أنجزت التجارب من خلال بناء جهاز متكامل للأنابيب الدوامة المنفرجة ، صمم

وصنع خصيصاً لهذا البحث، حيث غطى جميع التجارب. تمت دراسة تأثير تغير القطر الداخلي للمنفث ($d_n = 4 \text{ mm}, 5 \text{ mm}, 6.5 \text{ mm}$) على أداء الأنبوب الدوامي المنفرج، مع تغير الضغط المطلق للهواء الداخل ونسبة كتل الهواء البارد الى الهواء الداخل (μ_c) ضمن المدايات ($2-7 \text{ bar}$) و ($\mu = 0 - 1$) على التوالي. عند استخدام فتحة المنفث ($d_n = 5 \text{ mm}$) وفتحة البارد الخارج ($d_c = 10 \text{ mm}$) وباستخدام منفثان تعطي اعلى فصل في درجة الحرارة ويمكن اعتبارها الامثل لضغوط المختلفة الداخلة الى الانبوب الدوامي. تم الحصول على علاقتين تجريبية تربط قطر المنفثات، عدد المنفث، القطر الداخل للأنبوب (D)، طول الأنبوب (L) بحيث تعطي افضل تصميم للأنبوب الدوامي المنفرج ذو طاقة فصل عالية، كالتالي:

$$\frac{Nd_n^2}{D^2} = 0.105 \quad N=1$$

$$\frac{Nd_n^2}{D^2} = 0.211 \quad N=2$$

KEY WORDS

Counter Flow Vortex Tube , Thermal / temperature Separation , Design

Parameters

INTRODUCTION

A vortex tube uses compressed air as a power source, has no moving parts and produces hot air from one end and cold air from the other, as shown in **Fig.1**.

There is one widely accepted explanation of the phenomenon: (**Prasad 1963 , vortex tube theory 2000**). Compressed air is supplied to the vortex tube and passes through nozzles that are tangent to the internal counterbore. These nozzles set the air in a vortex motion. The spinning stream of air turns and passes down the hot tube in the-form of a spinning shell, similar to a tornado. A valve at one end of the tube allows some of the warmed air to escape. What does not escape, heads back down the tube as a second vortex inside the low-pressure area of the larger vortex. The inner vortex losses heat and exhausts through the other end as

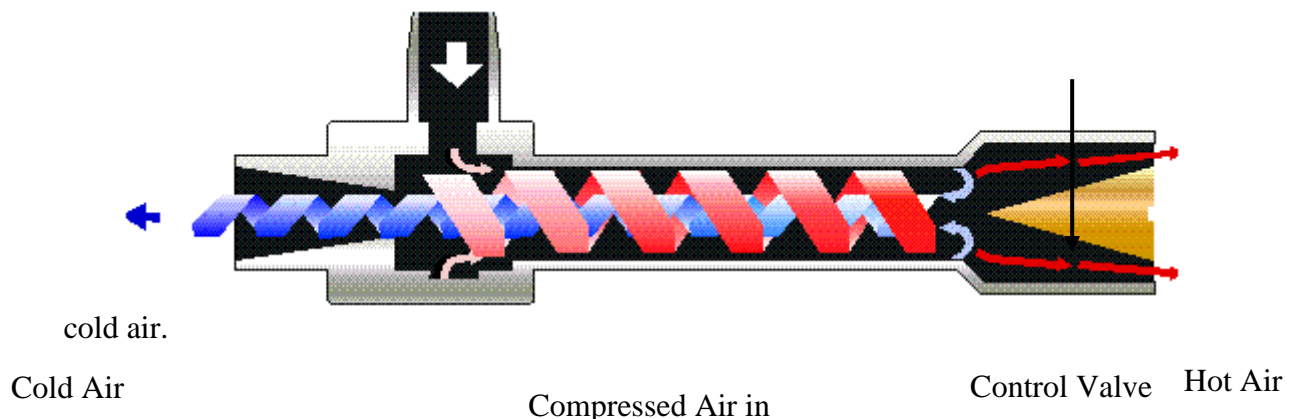


Fig.1: Diagrammatic view of the pattern in a counter-flow tube .

While one air stream moves up the tube and the other down it, both rotate in the same direction at the same angular velocity. Due to the principle of conservation of angular momentum the speed of the inner vortex remains the same. Angular momentum has been lost from the inner vortex. The energy lost shows up as heat in the out vortex. Thus the outer vortex becomes warm, and the inner vortex is cooled.

A number of researches mention the effects of tapering the vortex tube, with conflicting results. (**Martynovskii and Alekseev 1957**), find a contracting hot tube to be preferable and get optimum performance for $(40 < L/D < 50)$ which is comparable to (**Hilsch's 1947**) comment that (L/D) should be around (50) for good temperature separation.

(**Raiskii and Tunkel 1974**) investigated the influence of the vortex tube configuration (cylinder, diffuser and step), on the vortex-temperature gas-separation process. Results show that long cylindrical tubes are most effective in a broad range of variations of structural and modal parameters, noting that the majority of the energy transfer appears to occur within the first five diameters of the tube.

(**Soni and Thomson 1975**) employed a systematic method of experimental design to determine the optimum performance of a vortex tube as a function of the pertinent design parameters, especially the individual experiments were stipulated according to the simplex modification of the method of evolutionary operations, (**EVOP 1962**).

The results indicate the following optimum design parameters for maximum (ΔT_c) and maximum isentropic efficiency (η_{ise}) .

A_N (Nozzle / tube area) = 0.11 ± 0.01 (0.08 ± 0.001)

A_ϕ (Orifice area / tube area) = 0.08 ± 0.01 (0.145 ± 0.035)

(**Takahama and Yakosawa 1981**) investigated the measurements of the swirling flows inside the divergent chambers. The results show that the shorter divergent chambers ($L=900$ mm) have a higher angular velocity near the center of the back flow and the swirl intensity increases in divergent chambers in the direction of flow with relatively large divergent angles.

(**Mitushen and Mohammed 1992**), part I, designed “ Laser Doppler Velocimeter” that provides three velocity components of the flow inside the counter flow vortex tube. Results indicate a reverse flow from the axial velocity profiles in the central region ($r < 4 - 5$) mm of the vortex tube and the maximum axial velocity was is to the tube wall.

(**AL-Abriy 1997**) carried out an experimental study on the effect of tangential nozzles number on the performance of vortex tube by varying the number of tangential nozzles to become between (1-8) nozzles under inlet pressure of (3-7) bar at cold air mass fractions of ($\mu_c = 0-1$).

A laboratory device, “Hilton Co. Manufacture” and rig employed by (**Al-Jielawe 1994**) were used to carry out the experiments studying.

Results show that there is an optimum value of number of nozzles ($N = 8$ and $d_c = 0.8$ mm) to get high performance.

(**AL-Barwari 2004**) studied the experimental study on the thermodynamic properties of vortex tubes with a divergent chamber. The experimental investigation was carried on a divergent vortex tube rig especially designed for the present study covering all tests. The effect of different cold outlet diameters ($d_c=10$ mm, $d_c=12$ mm, and $d_c=14$ mm) on the performance of the vortex tube is described .The results show a pronounced influence of divergent vortex tube ($\theta^\circ = 1.72$, $L= 460$ mm), on the energy separation performance.

REFRIGERATION PERFORMANCE

Performance of simple refrigeration plant is usually characterized by means of the Coefficient of Performance (C.O.P) defined for the cyclic work-absorbing device **Fig.2** as (**vortec corporation catalogue 1992**).

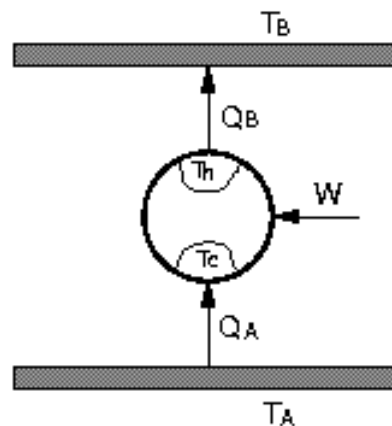


Fig (2) cyclic work absorbing device.

$$\text{COP} = \frac{Q_A}{W_{\text{act}}} \quad (1)$$

The process of ideal compression of the inlet air mass from the atmospheric pressure (P_a) to high pressure (P_i) is represented by the line ($T_i - T_f$) in **Fig.3** and the actual compression is represented by the line ($T_i - T_f'$). [13]

The COP of the vortex tube is defined as the ratio of the actual cooling effect to the work input to the air-compressor.

The compressed air has to be cooled at constant pressure in a cooler to the initial temperature (T_i) before being sent to the vortex tube. The refrigeration capacity (actual cooling) of the vortex tube is simply equal to Q_r .

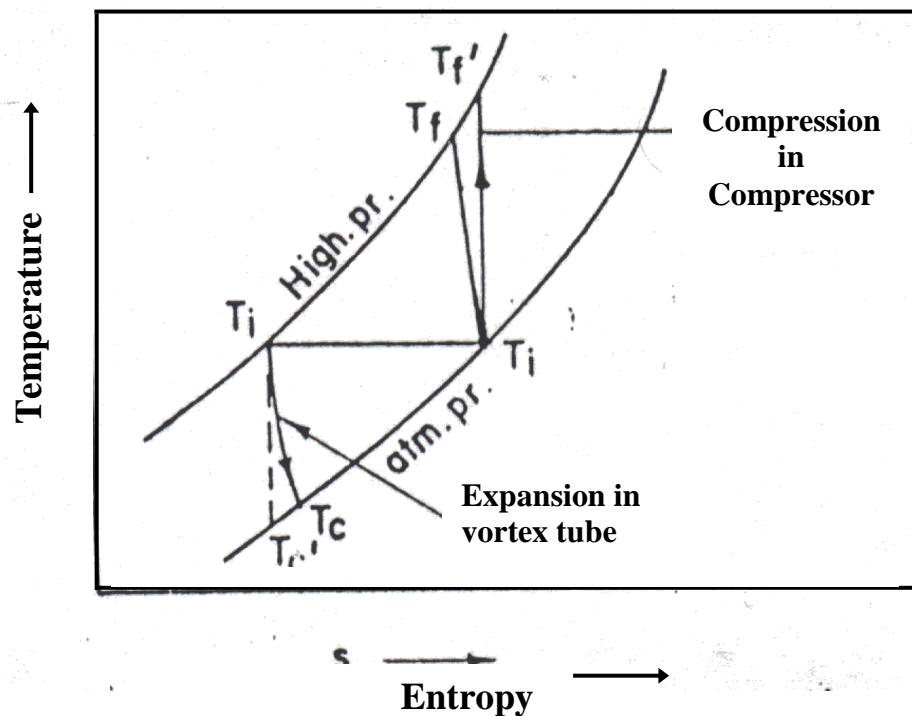


Fig.3:

Compression and expansion

process in a vortex tube

$$Q_r = m_c C_p (T_i - T_c) \quad (2)$$

Thus:

$$COP = \frac{m_c C_p \Delta T_c \eta_{comp}}{m_i C_p T_i \left[\left(\frac{P_i}{P_a} \right)^{\frac{\gamma-1}{\gamma}} - 1 \right]} \quad (3)$$

If the process undergoes an isentropic expansion from the inlet pressure (P_i) to atmospheric pressure (P_a) at the cold end then the static temperature drop due to expansion is given by:

$$\Delta T_{c'} = T_i - T_{c'} = T_i \left[1 - \left(\frac{P_a}{P_i} \right)^{\frac{\gamma-1}{\gamma}} \right] \quad (4)$$

The actual temperature drop due to expansion occurred in vortex tube is ΔT_c the ratio of ΔT_c to $\Delta T_{c'}$ is called “Relative Temperature Drop”.

$$R.T.D = \frac{\Delta T_c}{\Delta T_{c'}} \quad (5)$$

The adiabatic (isentropic) efficiency of the vortex tube is defined as:

$$\eta_{ise} = \frac{\text{Actual Cooling effect obtained in the vortex tube}}{\text{Ideal cooling effect possible with adiabatic expansion}}$$

$$\eta_{ise} = \mu_c \frac{\Delta T_c}{\Delta T_{c'}} \quad (6)$$

Sub. Eq. (4) in (6) one gets:

$$COP = \mu_c \left(\frac{\Delta T_c}{\Delta T_{c'}} \right) \eta_{comp} \left(\frac{P_a}{P_i} \right)^{\frac{\gamma-1}{\gamma}} \quad (7)$$

By substituting the value of $\left(\mu_c \frac{\Delta T_c}{\Delta T_{c'}} \right)$ from Eq.(6), in Eq.(7), one gets:

$$COP = \eta_{ise} \eta_{comp} \left(\frac{P_a}{P_i} \right)^{\frac{\gamma-1}{\gamma}} \quad (8)$$

EXPERIMENTAL APPARATUS AND RIG LAYOUT

The test rig is designed and manufactured to fulfill the requirements of the test system for different divergent vortex tube. The main rig, and the apparatus of the system illustrated in Figs. 4 and 5 and photograph (1).

RESULTS AND DISCUSSION

Effect of cold air mass ratio (μ_c) on the temperature difference ($\Delta T_h, \Delta T_c$), isentropic efficiency (η_{ise}) coefficient of performance (COP), and refrigeration capacity (Qr), for the inlet air pressure change and outlet nozzle diameter (d_n), are investigated.

Fig.6 at ($P_{i abs} = 7$ bar), number of nozzle = 1, and, ($\mu_c = 0.408$), shows, that the best energy separation, i.e highest temperature separation is for the outlet nozzle diameter ($d_n = 6.5$ mm), and ($d_c = 10$ mm), in respect with all selected outlet nozzle diameters, which give the minimum values of the cold air temperature differences (ΔT_c), as shown in **Table (1)**

Table (1): Results of One Nozzle

Number of nozzles = 1, D= 20 mm, L/D = 23, L = 460, ($\theta^\circ = 1.72$), $T_{in} = 30^\circ\text{C}$ $d_c = 10$ mm					
$d_n = 4$ mm		$d_n = 5$ mm		$d_n = 6.5$ mm	
Minimum $T_c (^\circ\text{C})$	Maximum $T_h (^\circ\text{C})$	Minimum $T_c (^\circ\text{C})$	Maximum $T_h (^\circ\text{C})$	Minimum $T_c (^\circ\text{C})$	Maximum $T_h (^\circ\text{C})$
1.2	55.2	-14.5	71.2	-20	72.3

Fig.7, at ($P_{i abs} = 7$ bar), (number of nozzles = 2), ($\mu_c = 0.409$). shows clearly, that the best performance is for the outlet nozzle diameter ($d_n = 5$ mm), and ($d_c = 10$ mm), which gives the minimum values of the cold air temperature i.e maximum temperature differences (ΔT_c), and the maximum value of the hot temperature, i.e the highest value of the hot temperature, as shown in **Table (2)**:

Table (2): Results of Two Nozzle

Number of nozzles = 2, D = 20 mm, L/D = 23, L = 460, ($\theta^\circ = 1.72$), $T_{in} = 30^\circ\text{C}$ $d_c = 10$ mm					
$d_n = 4$ mm		$d_n = 5$ mm		$d_n = 6.5$ mm	
Minimum $T_c (^\circ\text{C})$	Maximum $T_h (^\circ\text{C})$	Minimum $T_c (^\circ\text{C})$	Maximum $T_h (^\circ\text{C})$	Minimum $T_c (^\circ\text{C})$	Maximum $T_h (^\circ\text{C})$
-20.2	70.5	-35.5	81.2	-34.1	77.5

In **Figs. 8, 9** and **10** samples are selected to illustrate the effect of outlet nozzle diameter on isentropic efficiency with two nozzles at outlet cold diameter ($d_c = 10$ mm) as illustrated in **Table (3)** for different outlet nozzles diameters.

Table (3): Isentropic Efficiency Results

One nozzle				Two nozzles			
$d_c = 10$ mm				$d_c = 10$ mm			
	$d_n = 4$ mm	$d_n = 5$ mm	$d_n = 6.5$ mm	$d_n = 4$ mm	$d_n = 5$ mm	$d_n = 6.5$ mm	$P_{i abs}$



η_{ise}	10.58	18.25	22	22.9	28.2	27.9	2
%							
μ_c	0.601	0.718	0.706	0.714	0.703	0.714	7
η_{ise}	6.22	13.38	18.1	18.8	20.6	21.8	
%							
μ_c	0.607	0.617	0.707	0.715	0.702	0.713	

In **Figs. 11, 12 and 13** samples are selected to show the effect of changing (μ_c) on (COP) of vortex tube ($\theta^\circ = 1.72$), at ($L/D = 23$) for different pressure ranges between (2-7) bar, with two nozzles at outlet cold diameter ($d_c = 10$ mm).

The best values were acquired for the above mentioned outlet nozzle diameters, as illustrated in **Table (4)**:

Table (4): Effect of Cold Air Ratio Optimum Results of COP

One nozzle				Two nozzles			
$d_c = 10$ mm				$d_c = 10$ mm			
	$d_n = 4$ mm	$d_n = 5$ mm	$d_n = 6.5$ mm	$d_n = 4$ mm	$d_n = 5$ mm	$d_n = 6.5$ mm	$P_{i abs}$
COP	0.05	0.094	0.126	0.127	0.180	0.159	2
μ_c	0.701	0.616	0.606	0.714	0.712	0.604	
COP	0.035	0.079	0.09	0.094	0.125	0.108	7
μ_c	0.702	0.612	0.605	0.712	0.711	0.603	

Figs. 14, 15 and 16, show the effect of changing (μ_c) on the refrigeration capacity for vortex tube ($\theta^\circ = 1.72$) at ($L/D = 23$) for the pressure range between ($P_{i abs} = 2-7$) bar, with two nozzles at outlet cold diameter ($d_c = 10$ mm).

The best values acquired for the above mentioned outlet nozzle diameters at highest pressure ($P_{i abs} = 7$ bar) and minimum at pressure ($P_{i abs} = 2$ bar), are shown in **Table (5)**:

Table (5): Effect of Cold Air Ratio Optimum Results of Qr

One nozzle				Two nozzles			
$d_c = 10$ mm				$d_c = 10$ mm			
	$d_n = 4$ mm	$d_n = 5$ mm	$d_n = 6.5$ mm	$d_n = 4$ mm	$d_n = 5$ mm	$d_n = 6.5$ mm	$P_{i abs}$
Qr, watt	15.7	33.25	60.03	54.81	150.5	149.51	2
μ_c	0.601	0.616	0.706	0.718	0.714	0.714	
Qr, watt	308	610	1180	1284	1875.8	1866	7
μ_c	0.611	0.617	0.712	0.716	0.713	0.714	

CONCLUSIONS

- The outlet nozzle diameter ($d_n = 6.5$ mm), and the outlet cold diameter, ($d_c = 10$), when using **one nozzle** give a high temperature separation and may considered to be the optimum for different pressures of the inlet air regarding the size of tube diameter.
- The outlet nozzle diameter, ($d_n = 5$ mm), and the outlet cold diameter ($d_c = 10$ mm), when using **two nozzles**, give high temperature separation and may considered to be the optimum for different pressures of the inlet air regarding all the size tube diameter.
- The isentropic efficiency of the divergent vortex tube ($\theta^\circ = 1.72$), ($L/D = 23$), ($L = 460$ mm), ($d_c = 10$ mm), ($d_n = 6.5$ mm), when using one nozzle and two nozzles, increase with cold air mass ratio (μ_c) and reaches the highest value at ($\mu_c = 0.6-0.72$). On the other hand they decrease with the inlet air pressure increase. Divergent vortex tube ($\theta^\circ = 1.72$) has a highest isentropic efficiency attain: ($\eta_{ise} = 27.9$ %) at ($\mu_c = 0.714$), when using **two nozzles**.
- The coefficient of performance (COP) of the divergent vortex tube ($\theta^\circ = 1.72$), ($L/D = 23$), ($L = 460$ mm), ($d_c = 10$ mm), ($d_n = 6.5$ mm), when using one nozzle and two nozzles, increase with cold air mass ratio (μ_c) and reaches the highest value at ($\mu_c = 0.6-0.72$). On the other hand they decrease with the inlet air pressure increase. Divergent vortex tube ($\theta^\circ = 1.72$) has a highest coefficient of performance attain: ($COP = 0.159$ %) at ($\mu_c = 0.604$), when using **two nozzles**.
- The refrigeration capacity of the divergent vortex tube ($\theta^\circ = 1.72$) when using one nozzle and two nozzles is increased with cold air mass ratio (μ_c) till reaching the highest value at ($\mu_c = 0.6 - 0.72$). They increase with the inlet air pressure increase and has a higher refrigeration capacity attain: ($Q_r = 1866$ Watt) at ($\mu_c = 0.714$), when use **two nozzles**.

REFERENCES

- AL-Abriy, Z. T. "Effect of tangential nozzles number on the Performance of the vortex tube". Master's Thesis, University of Technology, Mech. Eng. Dep. Baghdad, Iraq, December 1995.
- AL-Jielawe, A. F. "Effect of divergent angle on the Performance of Vortex tube". Master's Thesis, University of Technology, Mech. Eng. Dep. Baghdad, Iraq, September 1994.
- AL- Barwari, R. R. I., "Experimental Study on The Thermodynamic Properties of Vortex Tubes With a Divergent Chamber". Ph. D. thesis, University of Technology, Mech. Eng. Dep., Baghdad Iraq, February 2004.
- Hilsch, R. "The use of the expansion of gases in a centrifugal field as a cooling process". *The Review of Scientific Instruments*, vol.18, No. 2, pp. 108-113, Feb. 1947.
- Mitushen, A.I and Mohammed, A. K. Part I: "Design and construction of Laser Doppler Velocimeter", Part II: "Visualization of the spiral flow inside the vortex tube by using laser". *Soviet researches, The library Of gas and Oil Institute*, Vol. 10, and 11 Moscow, 1992.



Martynovskii, V. S., and Alekseev, V. P. "Investigation of the vortex thermal separation effect for gases and vapors." *Technical physics*, vol.26, No. 2, pp. 2233-2243, 1957.

Prasad, M. "*Refrigeration and Air-conditioning*." 5th. Ed., July, pp. 174-179, 1996.
Raiskii, Y. D., and Tunkel, L. E. "Influence of vortex tube configuration and length on the process of energetic gas separation." *Journal of engineering physics*, vol.27, No. 6, pp. 1578-1581, December 1974.

Soni, Y. and Thompson, W. J. "Optimal design of the Ranque-Hilsch Vortex tube". Transaction of the ASME, *Journal of Heat Transfer*, pp. 316-317, May 1975.

Spendley, W., Hext, W., and Himsvarth, F. R. "Sequential application of simplex design in optimization and Evolutionary operation". *Technometrics*, vol.4, pp. 441-461, 1962.

Takahama, H. and Yokosawa, H. "Energy separation in vortex tubes with a divergent Chamber". *Transactions of the ASME, Journal of Heat Transfer*, vol.103, pp. 196-203, May 1981

Vortex tube theory. <http://www.free-serve.co.uk/rhvtmati/explan.htm>, 2000.
Vortec Corporation Catalogue. Company Catalogue, 10125 Carver Road, Cincinnati, Ohio, USA, 1992. UK Distributor: MEECH VORTEC, Burford House, 15 Thorney, Leys Business Park, Witney, Oxford, OX87GE

NOMENCLATURE

A_c, A_h	Cross sectional area of the cold end orifice and hot end of the outlet air	m^2
A_i	Cross sectional area of inlet pipe	m^2
COP	Coefficient of performance	-
C_p	Specific heat at constant pressure	J/kg. K
D	Inner diameter of vortex tube	mm
d_c	Diameter of cold end orifice	mm
d_h	Diameter of hot end outlet	mm
d_n	Diameter of nozzle outlet	mm
h_i	Specific enthalpy of the inlet air	J/kg
L	Length of vortex tube	mm
L/D	(Length / inner diameter) of the vortex tube	-
\dot{m}	Mass flow rate per nozzle	kg/s
$\dot{m}_i, \dot{m}_c, \dot{m}_h$	Mass flow of inlet air, cold air and hot air	kg/s
P_a	Ambient pressure	bar
P_i, P_c, P_h	Pressure of the inlet air, cold air and hot air	bar
Q_r	Refrigeration capacity	Watt
Q	Heat exchanged between the system and its surrounding	Watt
T_a	Ambient temperature	$^{\circ}\text{C}$
T_i, T_c, T_h	Temperature of the inlet air, cold air and hot air	$^{\circ}\text{C}$
T_o	Temperature at the nozzle outlet	$^{\circ}\text{C}$

ΔT_c	Temperature difference of cold air = $T_c - T_i$	$^{\circ}\text{C}$
$\Delta T_{c'}$	Isentropic (maximum) temperature difference	$^{\circ}\text{C}$
ΔT_h	Temperature difference of the hot air = $T_h - T_i$	$^{\circ}\text{C}$
η_{comp}	The isentropic efficiency of the compressor	%
η_{ise}	Isentropic efficiency of the vortex tube	%
θ	Angle of divergence	degree
μ_c	$\frac{m_c}{m_i}$ Cold air mass ratio = $\frac{m_c}{m_i}$	-
ρ	Density of the air	kg/m^3
c, h, i	Subscripts refer to cold, hot and inlet air	-

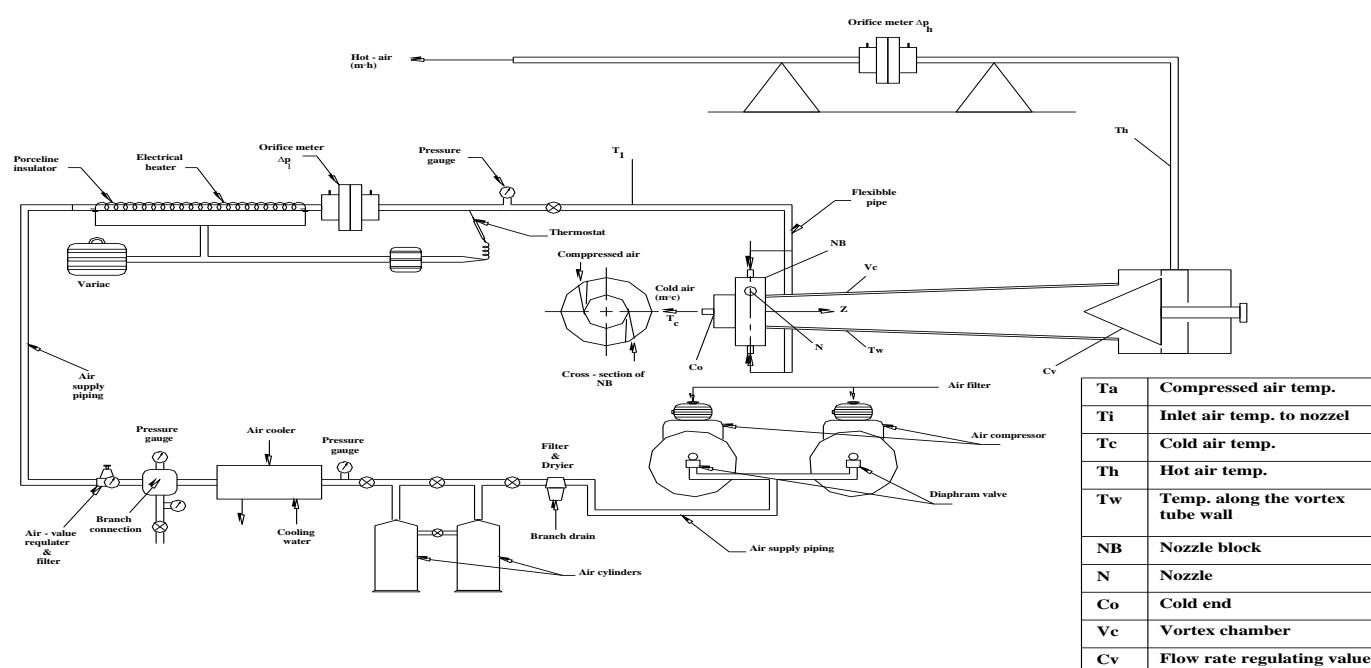


Fig. (4) Schematic diagram of the experimental rig.

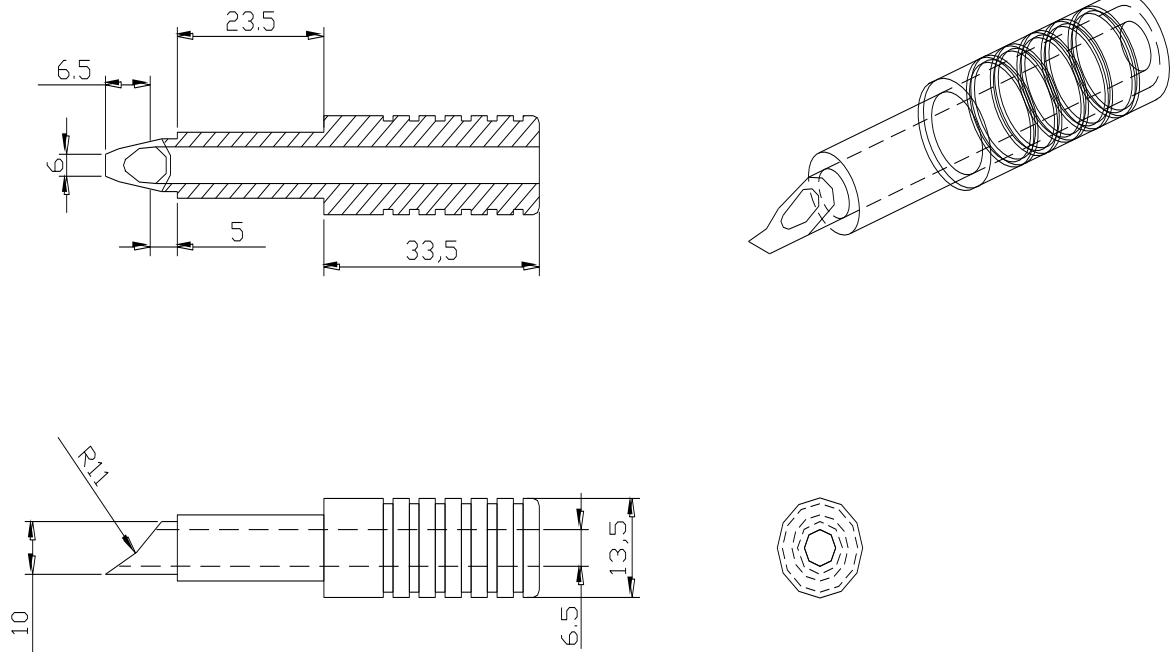


Fig. (5) Nozzle

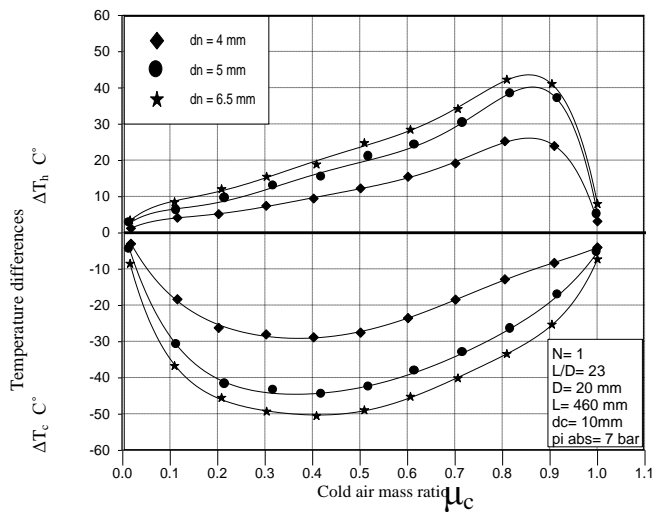


Fig. (6) Variation of temp. differences ΔT_c & ΔT_h with the mass ratio (μ_c) for vortex tube ($\theta=1.72$), with outlet diameter (d_n) of the vortex tube as a parameter.

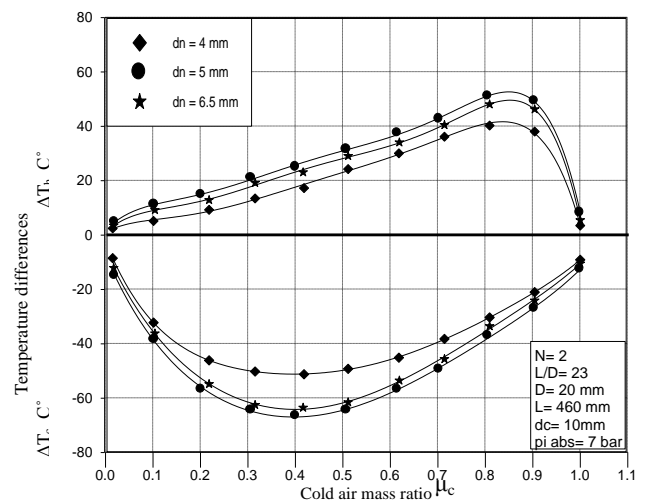


Fig. (7) Variation of temp. differences ΔT_c & ΔT_h with the cold air mass ratio (μ_c) for vortex tube ($\theta=1.72$), with outlet nozzle diameter (d_n) of the vortex tube as a parameter.

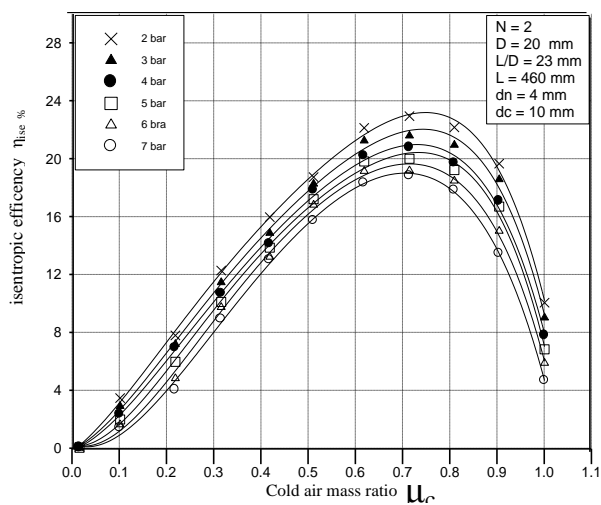


Fig. (8) The relation between isentropic efficiency (η_{ise}) and cold air mass ratio (μ_c) for vortex tube ($\theta=1.72$), with the absolute pressure (p_i) of the inlet air as parameter.

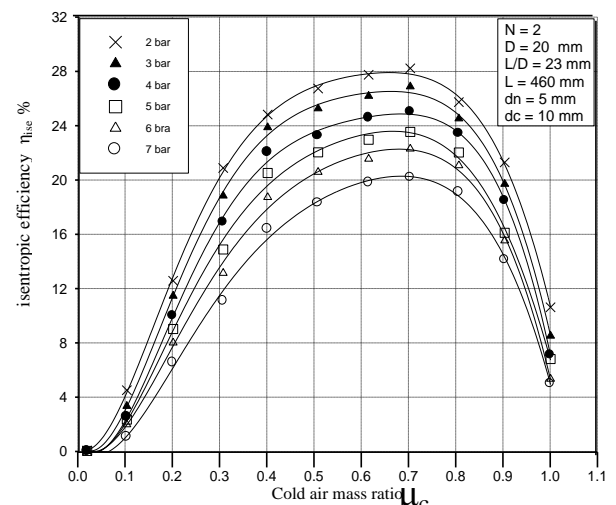


Fig. (9) The relation between isentropic efficiency (η_{ise}) and cold air mass ratio (μ_c) for vortex tube ($\theta=1.72$), with the absolute pressure (p_i) of the inlet air as parameter.

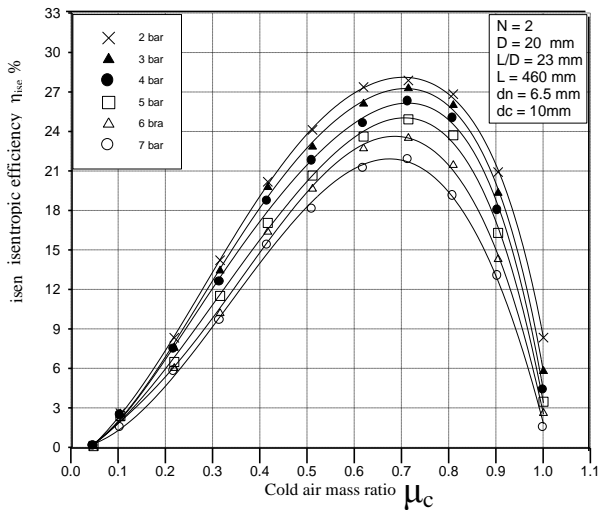


Fig. (10) The relation between isentropic efficiency (η_{isen}) and cold air mass ratio (μ_c) for vortex tube ($\theta^\circ = 1.72$), with the absolute pressure (p_i) of the inlet air as parameter.

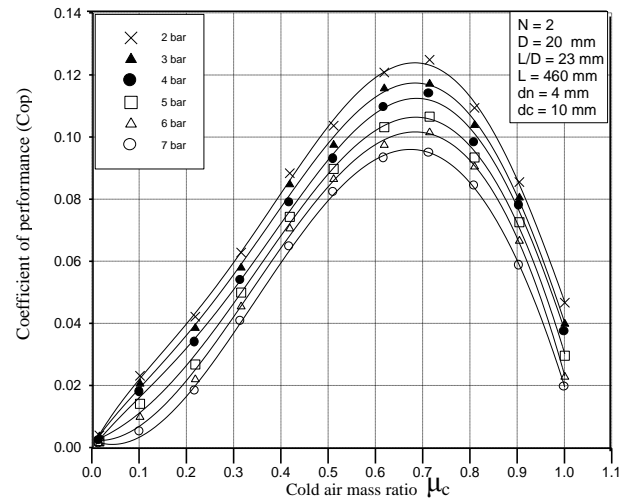


Fig. (11) The relation between coefficient of performance (COP) and cold air mass ratio (μ_c) for vortex tube ($\theta^\circ = 1.72$), with the absolute pressure (p_i) of the inlet air as a parameter

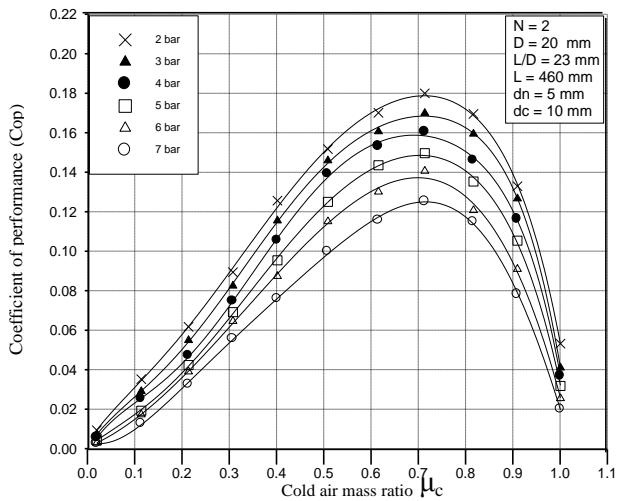


Fig. (12) The relation between coefficient of performance (COP) and cold air mass ratio (μ_c) for vortex tube ($\theta^\circ = 1.72$), with the absolute pressure (p_i) of the inlet air as a parameter

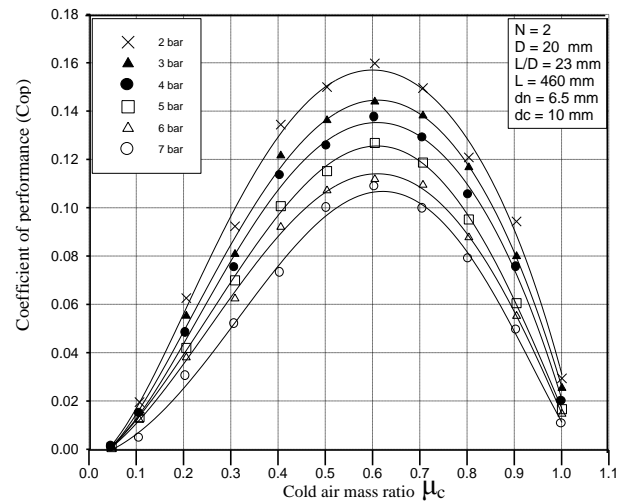


Fig. (13) The relation between coefficient of performance (COP) and cold air mass ratio (μ_c) for vortex tube No.2 ($\theta^\circ = 1.72$), with the absolute pressure (p_i) of the inlet air as a parameter

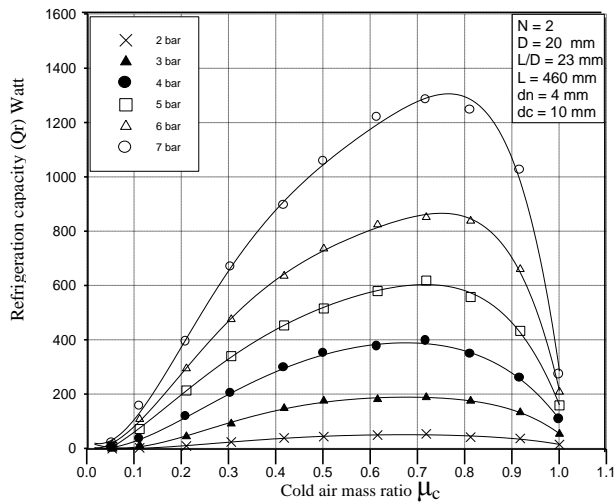


Fig. (14) The relation between Refrigeration capacity (Q_r) and cold air mass ratio (μ_c) for vortex tube ($\theta^\circ = 1.72$), with the absolute pressure (p_i) of the inlet air as a parameter.

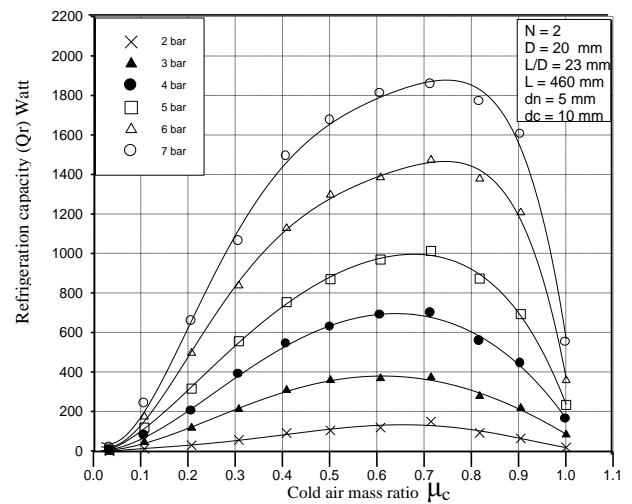


Fig. (15) The relation between Refrigeration capacity (Q_r) and cold air mass ratio (μ_c) for vortex tube ($\theta^\circ = 1.72$), with the absolute pressure (p_i) of the inlet air as a parameter.

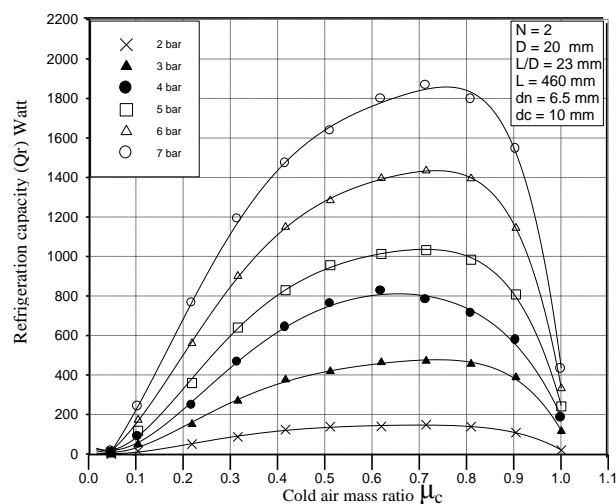


Fig. (16) The relation between Refrigeration capacity (Q_r) and cold air mass ratio (μ_c) for vortex tube ($\theta^\circ = 1.72$), with the absolute pressure (p_i) of the inlet air as a parameter.



INVESTIGATION OF THE THERMAL PERFORMANCE OF A CROSS-FLOW WATER COOLING TOWER WITH DIFFERENT PACKINGS

Dr. A. N. S. Kassim and Basim A. Rasheed
University of Baghdad – College of Engineering
Mechanical Engineering Department

ABSTRACT

The present research involves experimental and theoretical work to study the performance of three kinds of packing (PVC, corrugated and flat plate asbestos) in a cross-flow water cooling tower under different atmospheric conditions and then comparing the performance of them with each other. The experimental work included the design, constructions and installation of a cross-flow cooling tower test rig suitable for measuring the individual coefficients (k_{Ga}) and ($k'a$). The experimental results were found by varying the inlet air flow rate and inlet water flow rate which are used as an input data to the computer program for finding the available performance coefficient (NTU) using the method of Webb with some modifications. Least square method was then used to correlate the experimental results of (NTU) in terms of water to air ratio (L/G).

الخلاصة

يتضمن البحث الحالي دراسة نظرية وعملية لاداء ثلاث انواع من الحشوات (بلاستيكية PVC ، الواح اسبست متموجة و مستوية) في برج تبريد متعامد الجريان تحت ظروف جوية متغيرة و ظروف تشغيلية مختلفة، ثم مقارنة اداء هذه الحشوات مع بعضها. و قد تطلب العمل تهيئة منظومة برج التبريد و حساب معامل انتقال المادة و الحرارة للبرج بتحليل القياسات العملية. و قد تم في التجارب تغيير كمية الهواء و الماء الداخل و التي اصبحت بيانات دخول الى برنامج حسابي للحصول على معامل الاداء باستعمال طريقة الباحث (Webb) مع اجراء بعض التحويلات. و قد استعملت طريقة المربعات الصغرى للحصول على علاقات بين معامل الاداء و نسبة معدل جريان الماء الى الهواء.

Key words: Cooling Tower, Cross-Flow, Thermal Performance, Different Packings

INTRODUCTION

Probably the most important device utilizing direct contact between water and atmospheric air is the cooling tower. The objective of cooling tower is not the processing of the air, but cooling of the spray water. Cooling towers may be used thermally to reclaim circulating water for re-use in refrigerant condensers, power plant condensers and other heat exchangers.

There are two basic cooling tower heat transfer packing or fill arrangements, namely, counter-flow and cross-flow. In the counter-flow cooling towers, the air is directed to flow vertically upwards against the descending flow of water. In the cross-flow arrangement, the air flow is directed in a perpendicular direction to the flow of water, as shown in **Fig (1)**. For both packing configuration, drift eliminators are placed beyond the packing to prevent loss of water droplets into the leaving air stream.

The advantages and disadvantages of the counter-flow cooling towers:

Advantages:

1. It has the most efficient means for heat transfer, since the coolest water contacts the coolest air.
2. Close control of cold water temperature.
3. Small ground area in which it can be operated.
4. Close approach and long cooling range possible.

Disadvantages:

1. Restricted louver area at the base with high velocity of inlet air increases the fan horsepower.
2. Resistance of upward air travel against the falling water, results in higher static pressure loss and a greater fan horsepower than with air/ water flow in cross-flow towers.
3. Uneven distribution of air velocities through the packing with very little movement near the walls and center of the tower.
4. High pumping head necessary because of the tower height and nozzle pressure require the packing to be placed high up in the tower because the intakes at the base must be unobstructed.
5. The hot water system is inaccessible for ready maintenance, because the water spray system is sandwiched between the top of the fill and the drift eliminators.

The advantages and disadvantages of the cross-flow cooling towers:

Advantages:

1. Low pumping head.
2. Low static pressure drop at the air side.
3. Low fan horsepower.
4. Convenient arrangement of the distribution system requiring only (6-8in) depth of water over the top of the tower.
5. It is possible to clean the distribution system while the tower is in operation.
6. Higher water loadings are possible for a given height.

Disadvantages:

1. A substantial cross-flow correction factor needs to be applied to the driving force, particularly where long range and close approach performance are required.
2. A cross-flow tower may need more ground area and more packing or fill material to transfer the same amount of heat, because the performance calculated has a greater NTU and this has been interpreted to indicate the cross-flow tower will have a larger required coefficient so must be physically larger to meet this condition.
3. In a cross-flow cooling tower the water temperature decreases vertically while the air enthalpy increases horizontally, requiring a double integration.

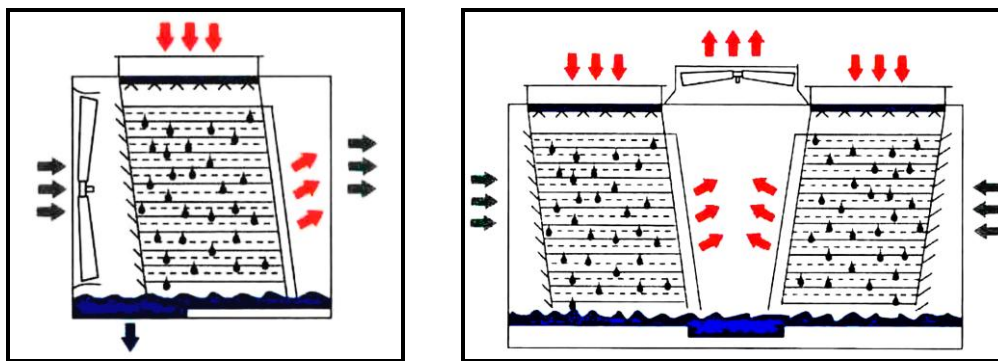


Fig (1) : Cross-Flow Cooling Tower

Merkel developed the first practical use of the differential equations in 1925. He combined the equations for heat and water vapor transfer and used enthalpy as the driving

force to allow for both sensible and latent heat transfers. Heat is removed from the water by a transfer of sensible heat due to a difference in temperature levels and by the latent heat equivalent of the mass transfer resulting from the evaporation of a portion of the circulating water. Merkel's method has been the basis of most cooling tower analysis. His analysis is based on the assumptions that the water evaporation loss in the energy balance equation is negligible and that the Lewis number for air/ water vapor system is unity.

(**Molyneux 1967**) theoretical and experimental work to determine the difference between counter-flow and cross-flow cooling towers. He concluded that for the large industrial units with relatively small ranges, an approach of less than (15°F) and operating with large flows of cooled water at (L/G) ratios greater than (1), the double induced draught cross-flow cooling tower can give economic advantages and the capital cost need to be no higher than that of the counter-flow tower having the same duty, but there can be significant saving in air and water pumping cost.

(**Sutherland 1983**) covered a wide range of air conditioning applications of cooling tower and should be of real value for design purposes. The accurate thermodynamic predictions apply generally and not to one particular tower and packings. His analysis did not utilize the assumptions of Merkel.

(**Webb and Villacres 1984**) presented algorithms for the performance simulation of evaporative cooling equipments. The algorithm performs a rating calculation for a given cooling tower fluid cooler or evaporative condenser. The most common rating calculation seeks the heat duty of the evaporative heat-exchanger for a specified operating condition (fluid flow rates, inlet process conditions and ambient air wet-bulb temperature).

Two types of packings were used in the experimental research work. The first is made of PVC sheets which are compressed thermally and having corrugations and extensions to increase the wetted surface area and to increase the spraying of the water. The second type is manufactured from asbestos cement, either as a flat plate or corrugated sheets.

CROSS-FLOW COOLING TOWER THEORY

The present analysis is based on the theory proposed by (**Baker and Shryock 1961**), which is an extension and development of the original theory of cooling tower by (**Merkel 1925**).

Both mass transfer (water evaporating from the droplets falling through the tower) and heat transfer (cooling of the water due to evaporation) are incorporated in the single coefficient ($K'aV/L$). The driving force for both is represented by the enthalpy potential difference between the air at the local wet-bulb temperature (h_a) and air at the local water temperature (h').

As shown in **Fig (2)**, water falls through the tower and is cooled by sensible heat loss and latent heat loss due to evaporation. The air is drawn across the tower by the fan, picking up sensible heat and water vapor in the process. Starting at the top left corner where the water temperature and air enthalpy are known, calculating the air enthalpy horizontally and water temperature vertically, as represented by the equations:

$$K'aV / L = \int_{t_1}^{t_2} C_{pw} \frac{dt}{h' - h_a} \quad (1)$$

and

$$K'aV / G = \int_{h_{a1}}^{h_{a2}} \frac{dh_a}{h' - h_a} \quad (2)$$

Numerically, the tower volume is divided into incremental volumes each of which accomplishes an identical fraction of the total transfer duty. The typical increment framed in **Fig (2)** and **Fig (3)**. The air enters at the left of the increment, its enthalpy increases as water vapor is added, and it exits to the right. The water is cooled from (t_1) to (t_2) due to the evaporation. After all increments have been traversed ($M=10$ is the number of increments), the calculation is terminated by averaging the temperature of the water leaving the bottom group of increments to yield the water outlet temperature.

A computer program was prepared based on Webb's method with some modifications to calculate the required conditions such as, temperatures and enthalpies for the bulk water, bulk air and interface for all the increments of the tower.

The algorithm for performance simulations of cross-flow cooling tower in the computer program consists of two iterations (inner and outer), starting from integrating **eq. (2)**, which gives:

$$K'aV / G = \frac{\Delta h_a}{h' - h_a} = (NTU)_G \quad (3)$$

The above equation is applied to each incremental unit volume. The inlet and outlet water and air properties in the incremental volume are symbolized as shown in Fig (3). The enthalpy of air entering to each increment of the first column is ($h_w = h_a$) and the temperature of water entering to each increment of the first row is ($t_N = t_1$). At the bottom of grid we found the water outlet temperature of the last vertical increment (M) and for each of the horizontal increments ($i = 1, 2, 3, \dots, M$) or $t_2(M, i)$ from the equation :

$$t_2 = \frac{1}{M} \sum_{i=1}^M t(M, i) \quad (4)$$

The outer iteration was developed for comparing the water outlet temperature (t_2) with a specified water outlet temperature, and if they are not in agreement a new value of $(NTU)_G$ is assumed until the difference between them meet a specified value. The enthalpy for the outlet air is then computed from the following equation:

$$h_{a_2} = \frac{1}{M} \sum_{j=1}^M h(j, M) \quad (5)$$

Then we can find $(NTU)_L$ from the following equation:

$$(NTU)_L = (NTU)_G \times \frac{G}{L} \quad (6)$$

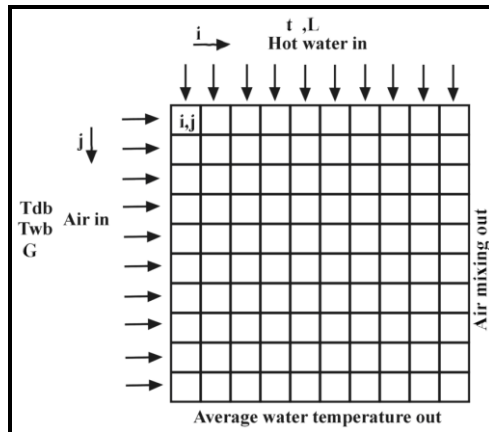


Fig (2): Cross-flow cooling tower
Incremental volume

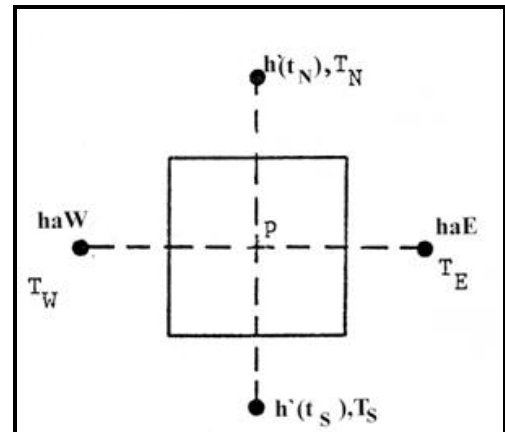


Fig (3): Incremental unit volume

RESULTS AND DISCUSSIONS

Results:

Results of this study are shown in **Figs. (4 to 7)**.

**Discussions:**

On comparing the performance of the three packings with each other it appears from **Fig.4** that the performance of the PVC packing is higher than the other two by about (98%) because its wetted surface area per unit volume is higher than the other two packing. In addition to that the ascending water spray down as small droplets, because of the packing corrugation and slots which increase the period of contact between air and water. This figure also shows that the performance of the corrugated asbestos packing is slightly higher than the flat plate asbestos packing by about (10%) because the wetted surface area per unit volume for the corrugated asbestos packing is higher than corresponding value for the flat plate asbestos packing.

As a practical application, the correlation equation for each of the three packing used in the tower (PVC, flat plate asbestos and corrugated asbestos packing) had been obtained for the range of air flow rates (1.3964 kg/s.m²) to (0.6991 kg/s.m²). The correlation equations are:

$$NTU = 0.2660 (L/G)^{-0.9144} \text{ (For flat plate asbestos packing)}$$

$$NTU = 0.4581 (L/G)^{-0.7171} \text{ (For PVC packing)}$$

$$NTU = 0.2567 (L/G)^{-0.5815} \text{ (For corrugated asbestos sheets spaced 15mm)}$$

$$NTU = 0.2438 (L/G)^{-0.5141} \text{ (For corrugated asbestos sheets spaced 25mm)}$$

The volumetric mass transfer coefficient ($K'a$) for the PVC packing is higher than ($K'a$) for the other two types as shown from the same **Fig.5**. This figure also show that the volumetric mass transfer coefficient ($K'a$) for the corrugated asbestos sheets with (S=15mm) is higher than ($K'a$) of the flat plate asbestos packing with (S=25mm).

The correlation of each line is represented in the following relation:

$$K'a = cG^bL^d, \text{ where: } c, b \text{ and } d \text{ are constant}$$

From the above relation, the volumetric mass transfer coefficients equations which had been obtained for the range of air flow rates (1.3964 to 0.6991kg/s.m²) are:

$$K'a = 1.5976 G^{0.9144} L^{0.0856} \quad (\text{Flat plate asbestos packing})$$

$$K'a = 2.7513 G^{0.7171} L^{0.2829} \quad (\text{PVC Packing})$$

$$K'a = 1.5413 G^{0.5815} L^{0.4185} \quad (\text{Corrugated asbestos sheets spaced 15mm})$$

$$K'a = 1.4643 G^{0.5141} L^{0.4859} \quad (\text{Corrugated asbestos sheets spaced 25mm})$$

The volumetric heat transfer coefficient (K_Ga) is highly increased with (G), but slightly increased with (L) as shown in **Fig.6**. Also it can be seen from this figure that the volumetric heat transfer coefficient (K_Ga) is higher for PVC packing than for the flat plate and corrugated asbestos packings. The volumetric heat transfer coefficient (K_Ga) for the corrugated asbestos packing is also higher than the corresponding value for the flat plate asbestos packing.

The above influences, the volumetric heat transfer coefficient (K_Ga) as with the volumetric mass transfer coefficient ($K'a$), because of the Lewis relation which relates them:

$$\frac{K_Ga}{k'a \times c_{pm}} = Le \quad (7)$$

This relation is considered unity.

Fig.7 is a plot of volumetric rate of mass transfer coefficient ($K'a$) in (kg/s.m^3) versus air flow rate (G) in (kg/s.m^2) for the results of Molyneux^[3] using fiber glass packing and for the three packing used in this experimental work and for a constant water flow rate of (1.358kg/s.m^2). This Figure shows a good matching with the results of Molyneux, especially for the corrugated asbestos packing ($S=25\text{mm}$).

The reason for the differences in the slope of these lines is because of the differences in types of packing.

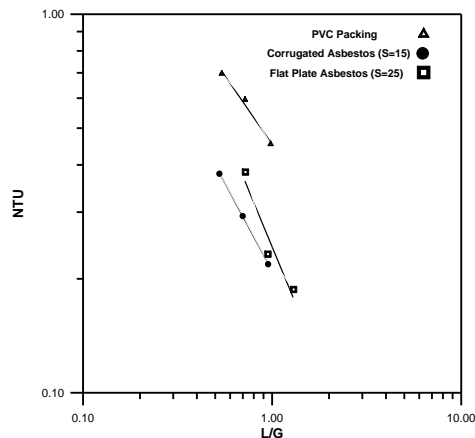


Fig (4) The (NTU) Vs (L/G) For Flat Asbestos Corrugated Asbestos And PVC Packings For Air Flow Rate About (0.775kg/S)

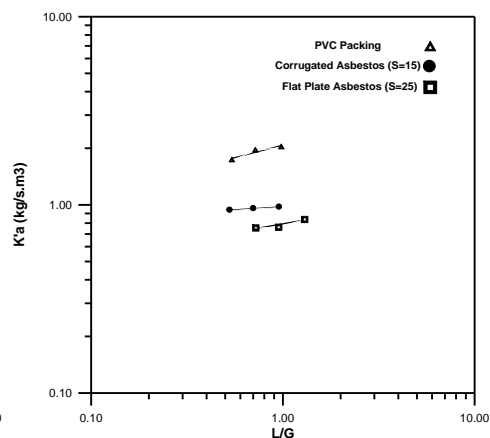


Fig (5) Volumetric Mass Transfer Coefficient Vs. L/G For Different Packings At Air Flow Rate About (0.775kg/S)

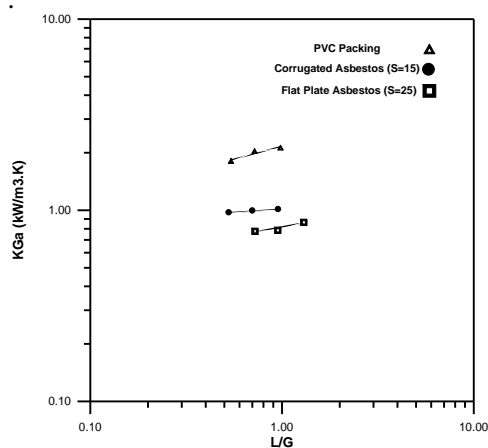


Fig (6) Volumetric Heat Transfer Coefficient Vs. L/G For Different Packing At Air Flow Rate About (0.775kg/S)

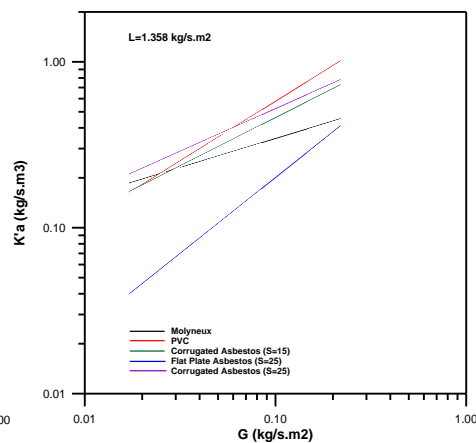


Fig (7) K'A Vs. G For Molyneux (1967) Data Compared With The Present Work

CONCLUSIONS

1. The performance of a given volume of tower packing is affected mainly by the ratio of water flow rate to the air flow rate. This means that the maximum performance can be obtained with minimum water and air flow ratio (L/G).
2. The mass and heat transfer coefficients ($K'a$) and (K_Ga) are mainly affected by the air flow rates and slightly by the water flow rates.
3. For a given volume of packing, air flow rates and water flow rates, the performance of PVC packing exceeds that of the two types of the asbestos packings by about (45%-50%). Also the performance of the corrugated asbestos sheets is more than the corresponding performance of the flat plate asbestos by about (6.5%-7%).
4. We found that in the case of using PVC packing, substantial decrease in volume of the cooling tower is obtained compared to using the other two kinds of asbestos packings to achieve the same operating conditions due to the performance of PVC packing being higher than the corresponding value of the other types.

REFERENCES

- Baker, D.R. and Shryock, M.A, Aug. 1961, "A Comprehensive Approach to the Analysis of Cooling Tower Performance."Trans. ASME Series C83: 339-45.
- Merkel, F., 1925, "Verdunstungshuhlung", V.D.I, Forschungs-Arbeiten, No.275.
- Molyneux, F., "Counter and Cross-flow Cooling Towers" Chemical and Process Eng., Vol.48, No.8, pp. 56-60, May 1967.
- Sutherland, J.W., "Analysis of Mechanical Draft Counter-flow Air/Water Cooling Tower", Trans. Of ASME, Journal of heat Transfer, Vol.105, pp. 576-583, Aug. 1983.
- Webb, R.L. and Villacres, A., "Algorithms for Performance Simulation of Cooling Towers, Evaporative Condensers and Fluid Coolers", ASHRAE Transactions, 1984.

**NOMENCLATURE**

A	<i>Area of water surface per unit volume</i>	K'	<i>Unit conductance, mass transfer, interface to main air stream</i>
C_{pw}	<i>Specific heat of water assumed, 4.19</i>	L	<i>Inlet water mass flow rate</i>
G	<i>Inlet air mass flow rate (dry air)</i>	M	<i>Number of horizontal and vertical increments</i>
h_a	<i>Enthalpy of moist air, h_{a1} entering, h_{a2} leaving (dry air)</i>	NTU	<i>Number of transfer units</i>
H'	<i>Saturated enthalpy of moist air at bulk water temperature</i>	V	<i>Cooling volume</i>

PLOUGHING OF WORK-HARDENING ASPERITIES BY A HEMISPHERICAL SLIDER

AHMED ABDUL HUSSAIM ALI

UNIVERSITY OF BAGHDAD / COLLEGE OF ENGINEERING

MECHANICAL DEPARTMENT

ABSTRACT

A theoretical description is given for the ploughing of a work-hardening inclined surface by a hemispherical slider. As the indenture is moving horizontally, the grooving force and the depth of penetration are expressed for conditions that correspond to the climbing and descending asperities. Assuming a constant vertical load on the slider, the friction coefficient due to ploughing, F_p , is shown to be affected by surface inclination moreover, the limiting value of F_p when the vertical load on slider is made infinitely small is shown to be independent upon the asperity angle and the shape of the slider. The treatment has some use in predicting the extent of surface damage in contact profilometry, especially for soft materials in particular, the depth of penetration is shown to be different when climbing or descending a surface whose inclination is θ .

الخلاصة:

تم اجراء توصيف نظري لعملية حرث سطح مائل مصلد بالتشغيل بواسطة منزلق نصف كروي . عندما يتحرك المنزلق الخارق أفقياً، فإن قوى الحرث وكذلك عمق الخرق تم التعبير عنها لحالة التسلق والانحدار للنتؤ. بأفتراض وجود حمل عمودي ثابت على المنزلق فإن معامل الاحتكاك نتيجة الحرث F_p تبين بأنه يتأثر بميلان السطح بالإضافة الى أنه القيم الحديه ل F_p عندما الحمل العمودي على المنزلق يصل الى قيم متناهيه في الصغر أثبت أنه يعتمد على زاوية النتؤ وشكل المنزلق. هذه المعالجه لها بعض الاستخدامات في التنبؤ بمدى تشوه السطح في تلامس البروفيلوميتر (profilometry) خاصه للمعادن اللينه.

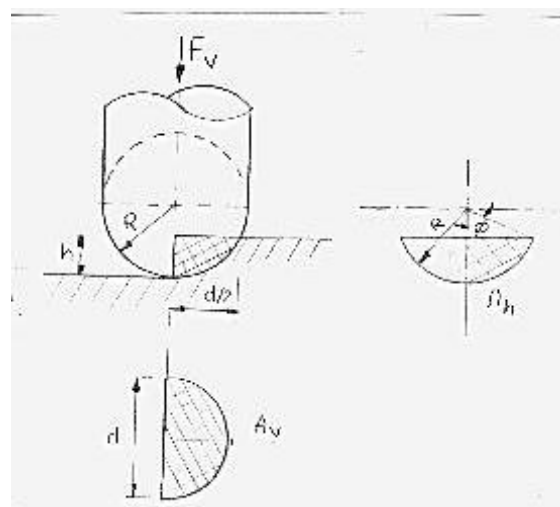
على وجه الخصوص، عمق الخرق أثبت أنه يختلف عند التسلق أو الأنحدار من سطح ميلانه θ .

INTRODUCTION:

When a rigid indenter slides over a work-hardening surface, the resistance to motion is generally due to two different factors: the elastoplastic deformation of metal, or ploughing, and the adhesion at the interface of the components. This physical phenomenon is treated in text books on tribology [Moore. D.F. 1975] and a number of experiments which have been performed to establish the validity of some mathematical models or to analyze the wear mechanism in this study, an extension to classical demonstration about the ploughing component of friction are presented. One of the aims to model how surface damage is done in contact profilometry when a slider or a tiny rigid stylus travels on a surface showing an irregular profile for the proposed mathematical models, the shape of asperities is simplified as to be represented by straight inclined surface . Therefore, relative to the primary direction of motion, the slider has to climb or descend surfaces inclined at an angle θ , as shown in fig. (1). Note that in this work, and contrary to the usual terminology, the word `asperity` is associated with the surface that is being deformed and not with the slider.



Fig.(1) Representation of a Slider Moving on Horizontal, then Inclined Surface .



Fig(2) Hemispherical Slider Moving on Horizontal surface

PLOUGHING OF A HORIZONTAL SURFACE:

The ploughing component of friction is often modeled assuming that a slider of simple geometry moves parallel to an ideally flat surface and grooves its path into it. Fig.(2) represent such situation with a hemispherical slider of radius R deforming plastically a softer, yielding material in the following development the following assumption are made.

- Material pile-up surrounding the slider is neglected.
- Effects of slider speed (inertial forces) and heat generation (modification of material properties) are not considered.

A static analysis of force balance gives a relation ship between the vertical load , F_v , and the extent of surface damage in terms of groove width, d , or groove depth, h , and yield pressure P_y , as in fig.(2) .

$$F_v = P_y \times A_v = P_y (\pi d^2 / 8) = P_y \lambda \pi R h / 2$$

From [J.Halling 1975] Halling found λ to be

$$\lambda = 2 - n^{0.5}$$

$$F_v = \frac{1}{2} P_y (2 - n^{0.5}) \pi R h$$

$$h = R - (R^2 - (d/2)^2)^{0.5}$$

$$F_v = P_y (\pi / 2) (2 - n^{0.5}) R^2 (1 - (1 - (d/2R)^2)^{0.5}) \text{-----}(1)$$

The horizontal force opposing motion is derived similarly and yields

$$F_h = P_y A_h \lambda / 2 = P_y \lambda R^2 (\Phi - d/2R (1 - (d/2R)^2)^{0.5}) / 2$$

Where $\Phi = \sin^{-1}(d/2R)$; $\lambda = 2 - n^{0.5}$

n : work hardening index (0) for plastic (1) for elastic

$$F_h = P_y (2 - n^{0.5}) R^2 / 2 (\sin^{-1}(d/2R) - d/2R (1 - (d/2R)^2)^{0.5}) \text{-----}(2)$$

We can now write the expression for the coefficient of friction due to ploughing. It is the ratio of the horizontal and vertical forces:

$$F_p = F_h / F_v = A_h / A_v \text{-----}(3)$$

Eqs.(1and2) are given independently as a function of d, h, n and R since those parameters are of more practical importance than Φ . The width can be estimated by observing a grooved surface under the microscope. The depth of penetration may be useful in interpreting data related to surface profilometry.

In the same way , other basic slider shapes have been investigated, namely the cylinder, cone and pyramid[Nam P. 1970, Hisakado T. 1970 , Sin H.G.1979].

PLOUGHING WHILE CLIMBING OR DESCENDING AT θ :

We now consider a hemispherical slider that climbs fig.(3) or descends fig.(4) a surface having an inclination θ .

The load on the slider, F_v , is assumed to be remain constant and vertical Eq.(1) still applied and , in non dimensional terms we define .

$$F_v^* = \frac{F_v}{P_y(\pi R^2/2)} = \frac{A_v}{\pi R^2/2} \text{-----(4)}$$

In the present analysis the contact is restricted to the lower hemisphere that is for

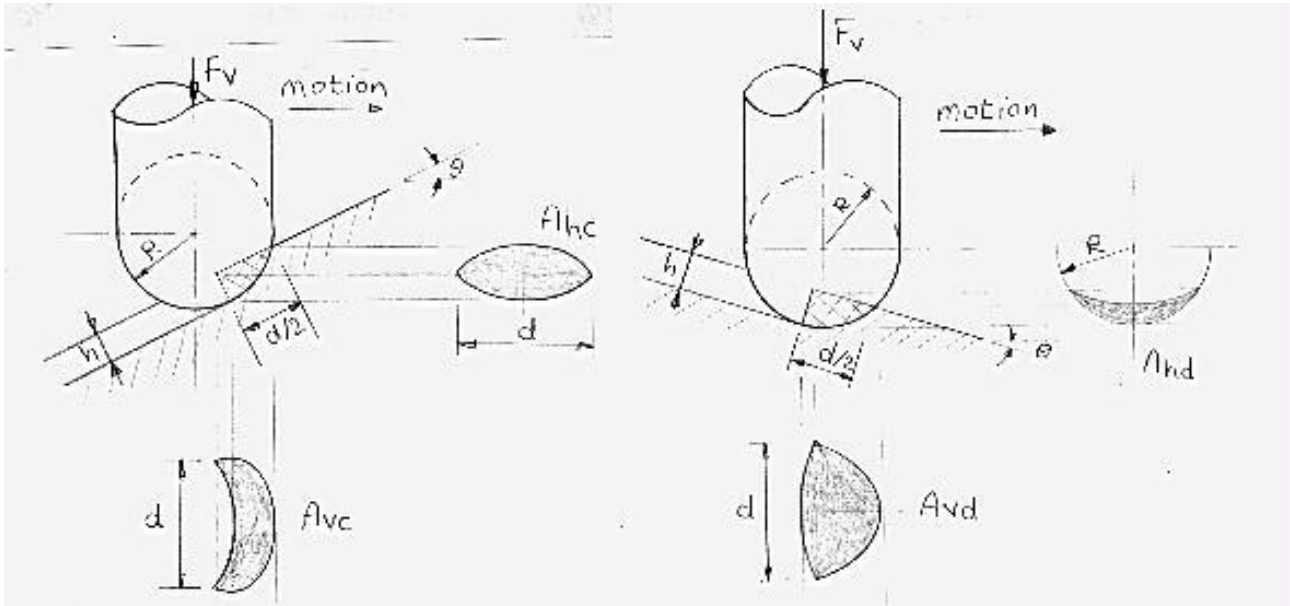
$$\theta \leq \cos^{-1}(d/2R) = \theta_{\max} \text{-----(5)}$$

WIDTH OF GROOVING:

The projected areas A_{vc} and A_{vd} (fig.3 and fig.4) are composed of elliptical and circular segments subtracting or adding with each other. With proper geometrical considerations, one obtain the following equations

$$F_v^* = \frac{A_{vc}}{\pi R^2/2} = \frac{(\pi/2)(2-n^{0.5})R^2\{1-(1-(d/2R)^2)^{0.5}\}\cos\theta}{\pi R^2/2} - \frac{0.5(2-n^{0.5})R^2\{\sin^{-1}(d/2R)-(d/2R)(1-(d/2R)^2)^{0.5}\}\sin\theta}{\pi R^2/2}$$

$$F_v^* = (2-n^{0.5})\{1-(1-(d/2R)^2)^{0.5}\}\cos\theta - \frac{(2-n^{0.5})}{\pi}\{\sin^{-1}(d/2R) - (d/2R)(1-(d/2R)^2)^{0.5}\}\sin\theta \text{-----(6)}$$



Fig(3) Hemispherical Slider Climbing an Inclined Surface at θ

Fig.(4) Hemispherical Slider Descending an Inclined Surface at θ

$$F_v^* = \frac{A_{vd}}{\pi R^2 / 2} = (2 - n^{0.5}) \{1 - (1 - (d/2R)^2)^{0.5}\} \cos \theta + \frac{(2 - n^{0.5})}{\pi} \{ \sin^{-1}(d/2R) - (d/2R)(1 - (d/2R)^2)^{0.5} \} \sin \theta \quad \text{-----}(7)$$

By substituting eq.(4) into eq.(6) and eq(7) it is possible to calculate the width of the grooving at various angles and work-hardening index for any test parameter values.

Results are given in fig.s(5.1,2,3,4) for a climbing trajectory and in fig.s(6.1,2,3,4) for a decent. To maintain vertical force equilibrium (for given values of R and P_Y), the groove width has to increase in a non-linear fashion with increasing θ and with the increasing of the work-hardening index n.

By comparing the graphs one can see that for a given F_v^* the width of grooving is always when descending than climbing at the same θ and n (i.e. $A_{vd} > A_{vc}$). The difference also becomes larger as the angle gets steeper. Mathematically, this is explained by the facts that the second right-hand term of eq.(6) and eq.(7) is always small in comparison with the other.

Figures 5 and 6 could be used to predict the groove width when a stylus is used for surface measurements of hard and soft surfaces. By knowing the geometry of the stylus, the depth of indentation could also be determined.

FRICTION COEFFICIENT:

The friction coefficient due to ploughing is calculated using generalized form of eq(3) as the ratio of the horizontal and the vertical projected areas.

For climbing an asperity, and referring again to fig.(3) the horizontal projected areas is:

$$\frac{A_{hc}}{\pi R^2 / 2} = (2 - n^{0.5}) \{1 - (1 - (d/2R)^2)^{0.5}\} \sin \theta + \frac{(2 - n^{0.5})}{\pi} \{ \sin^{-1}(d/2R) - (d/2R)(1 - (d/2R)^2)^{0.5} \} \cos \theta \quad \text{-----}(8)$$

One can now obtain the analytical expression for the friction coefficient F_p by dividing eq.(6). The result is shown graphically in fig.s(7.1,2,3,4) as a function of the non dimensional load F_v^* while F_p never exceeds 1.0 in the more conventional case of ploughing a horizontal surface, it may theoretically increases in sever climbing conditions.

For descending an asperity, and referring to fig.4 the horizontal projected areas is:

$$\begin{aligned} \frac{A_{hd}}{\pi R^2 / 2} &= \frac{(2 - n^{0.5}) / 2}{\pi R^2 / 2} \left\{ R^2 \phi - \frac{R \sin 2\phi}{2} - \frac{R^2 \pi}{2} [(d/2R) - \tan \theta (1 - (d/2R)^2)^{0.5}] \sin \theta \sin \phi \right\} \\ &= \frac{2 - n^{0.5}}{2} \left\{ 2\phi / \pi - \sin 2\phi / \pi - \frac{d \sin \theta \sin \phi}{2R} + (1 - (d/2R)^2)^{0.5} \tan \theta \sin \theta \sin \phi \right\} \quad \text{-----}(9) \end{aligned}$$

$$\text{Where } \phi = \cos^{-1} \frac{(1 - (d/2R))^{0.5}}{\cos \theta}$$

In this analysis the specific angle at which no resistance to motion occurs when descending an asperity can be expressed mathematically by:

$$\theta = \tan^{-1} \frac{(d/2R)}{(1 - (d/2R)^2)^{0.5}} = \sin^{-1}(d/2R)$$

The friction coefficient that applies in a descend is obtained by dividing eq(9) by eq(7) and a graphical representation of it appears in fig.s(8.1,2,3,4) as a function of the non dimensional load F_V^* .

Figs.7 and 8 show that the friction coefficient due to ploughing increases and the slope of the asperity increases during climbing the asperity, on the contrary decreases when the slider descends [Ishizuka 1985] has found that the friction coefficient between a hard conical projection and soft rubbing surface having the projection of triangular prism increases with increasing the half angle of the prism which is well represented by the present model for descending a surface whose inclination is θ .

CONCLUSIONS:

Essentially the extent of ploughing can be the depth of penetration of a soft material by a hard slider. This factor is a function of the shape and size of the indenter, the load applied on it, the work-hardening index and the yield pressure of the material that under goes grooving.

Taking into account only ploughing component of friction, it was demonstrated that a simple model can be extended to predict damage on rough surfaces.

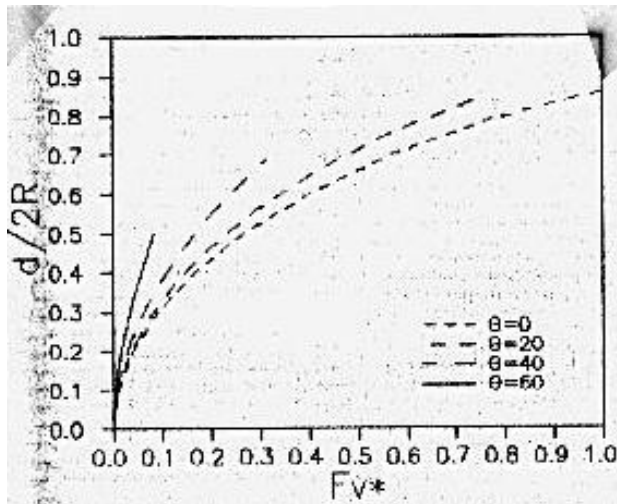
In the case of a hemispherical slider climbing and descending asperities that are represented by inclined surfaces, the groove width was shown to be dependent upon the inclination θ .

REFERENCES:

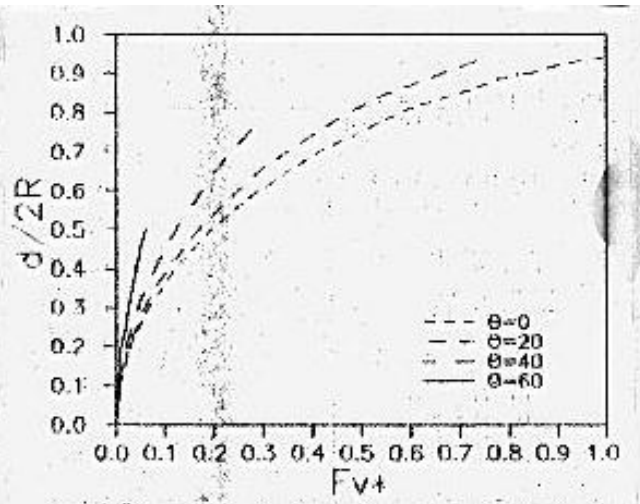
- * Hisakado T. "On the mechanism of contact between solid surfaces " Bull. of the JSME,13,1970.
- * Ishizuka S. "Fundamental studies on dry friction" proc. of the JSLE, Int Tribology conf. 1985, p135-139
- * J.Halling and K.A.Nuri "Contact of rough surfaces of work hardening materials " Proceedings of the symposium of the international union of theoretical and applied mechanics. 1975
- * Moore D.F. "Principles and applications of tribology" 1975.
- * Nam P. Suh." Elements of the mechanical behavior of solids."

* Sin H.C. , Saka N. and Suh H.P. "abrasive wear mechanisms and the grit size effect" Wear ,55,1979

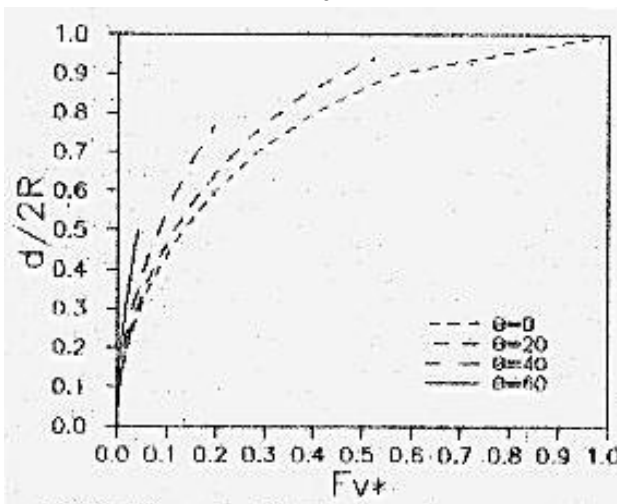
* S.M.H. Benabdallah and J.P.Chalifoux "Ploughing of soft asperities by a hemispherical slider tribology international" Vol.22, No.6, 1989.



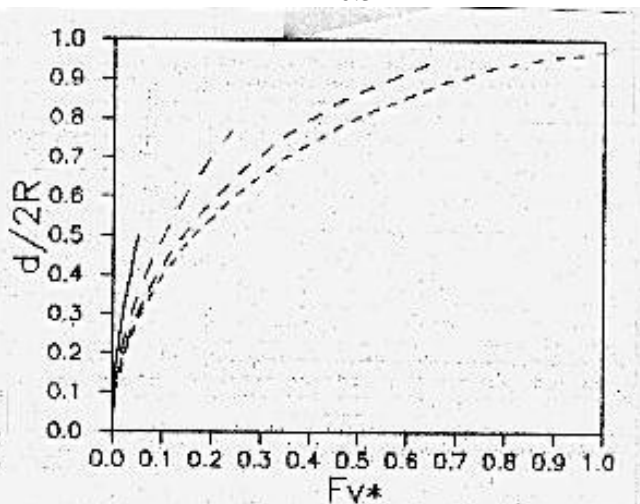
Fig(5.1) Graf of Width of Grooving versus vertical force For Various θ in a Climbing Situation , For $n=0$



Fig(5.2) Graf of Width of Grooving versus vertical force For Various θ in a Climbing Situation , For $n=0.3$



Fig(5.4) Graf of Width of Grooving versus vertical force For Various θ in a Climbing Situation , For $n=1$



Fig(5.3) Graf of Width of Grooving versus vertical force For Various θ in a Climbing Situation , For $n=0.6$

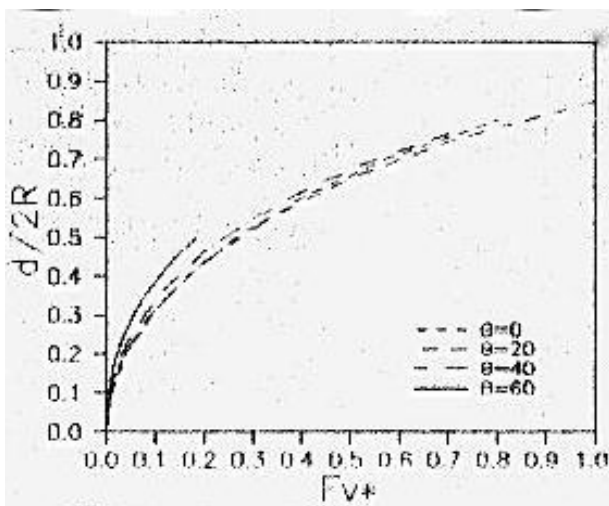


Fig.(6.1) Graf of Width of Grooving Versus vertical Force for Various θ in a Descending Situation for $n=0$

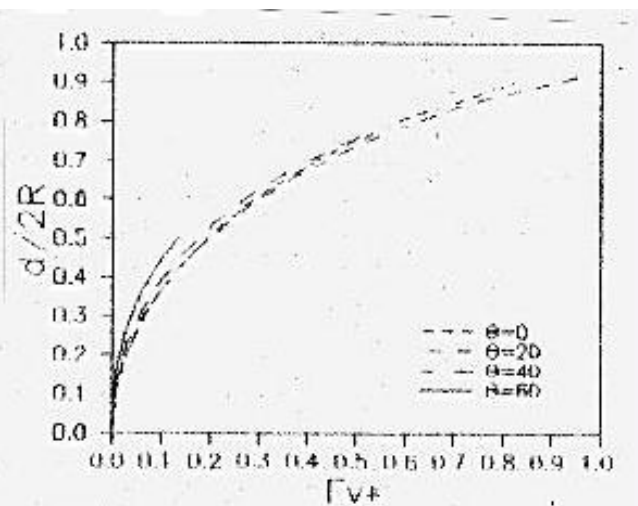


Fig.(6.2) Graf of Width of Grooving Versus vertical Force for Various θ in a Descending Situation for $n=0.3$

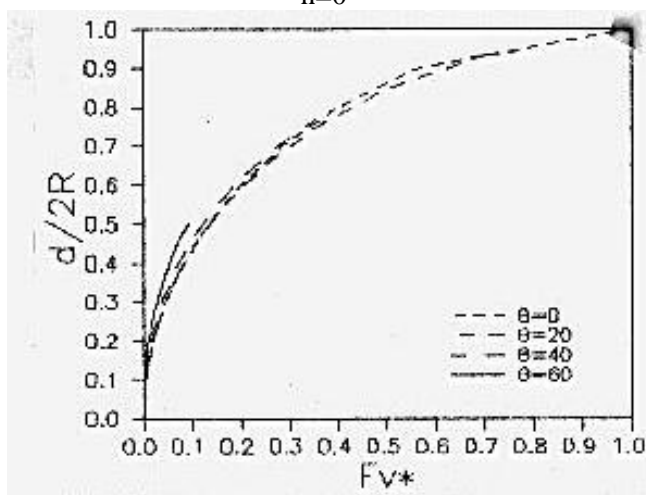


Fig.(6.4) Graf of Width of Grooving Versus vertical Force for Various θ in a Descending Situation for $n=1$

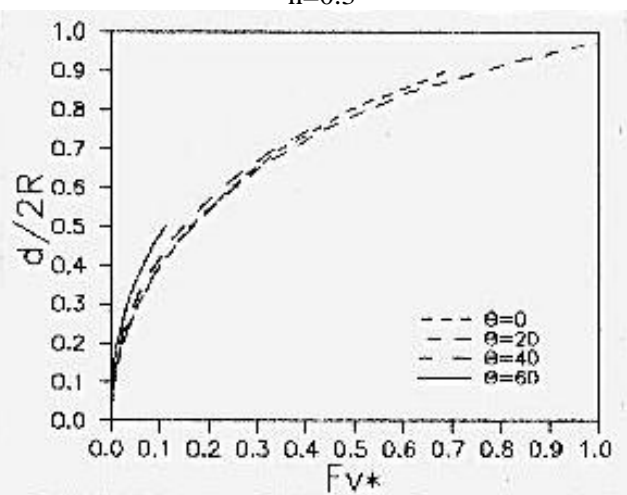


Fig.(6.3) Graf of Width of Grooving Versus vertical Force for Various θ in a Descending Situation for $n=0.6$

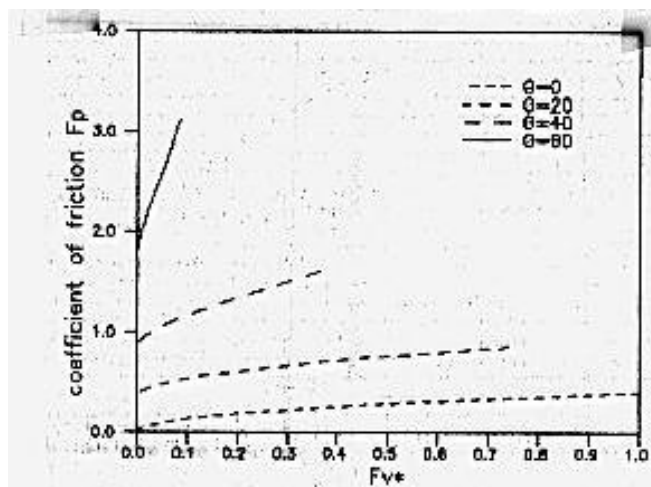


Fig.(7.1) Graf of Friction Coefficient Versus Vertical Force For Various θ in Climbing Situation For $n=0$

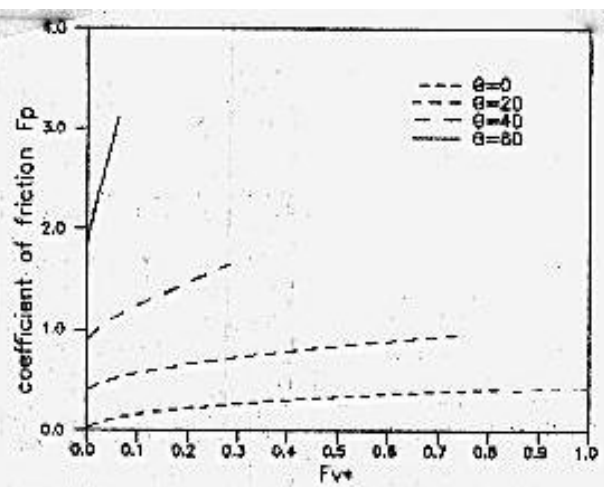


Fig.(7.2) Graf of Friction Coefficient Versus Vertical Force For Various θ in Climbing Situation For $n=0.3$

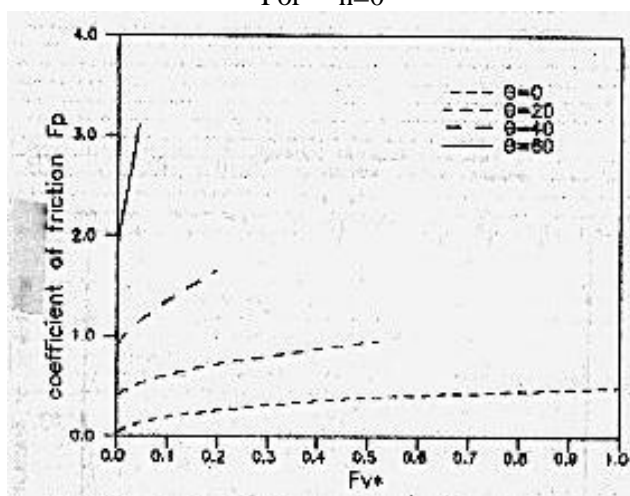


Fig.(7.4) Graf of Friction Coefficient Versus Vertical Force For Various θ in Climbing Situation For $n=1$

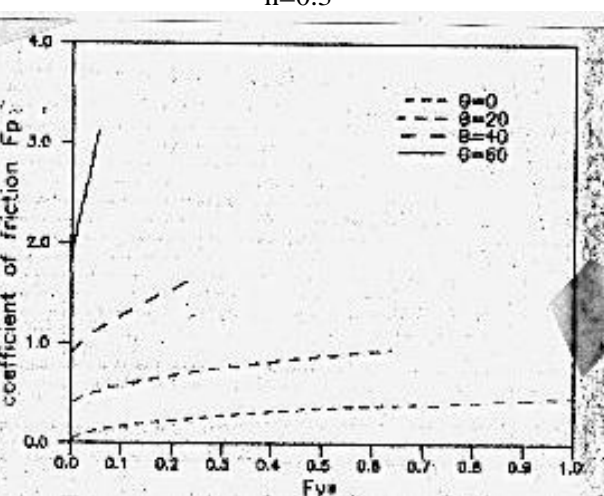


Fig.(7.3) Graf of Friction Coefficient Versus Vertical Force For Various θ in Climbing Situation For $n=0.6$

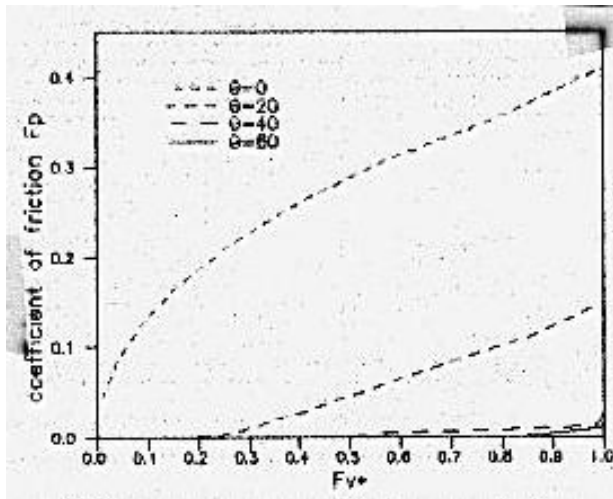


Fig.(8.1) Graph of Friction Versus Vertical Force For Various θ in a Descending Situation For $n=0$

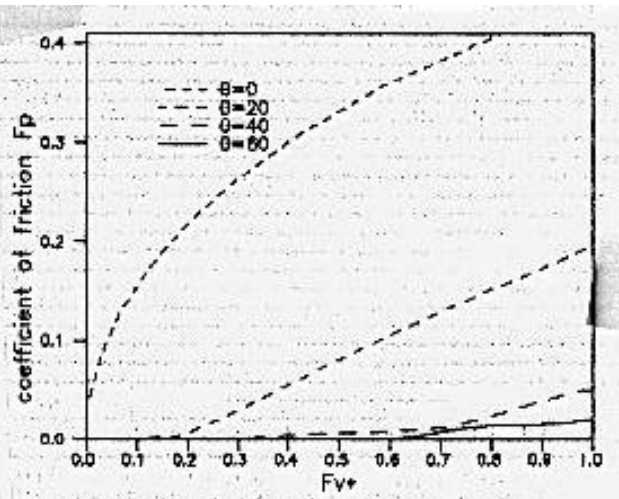


Fig.(8.2) Graph of Friction Versus Vertical Force For Various θ in a Descending Situation For $n=0.3$

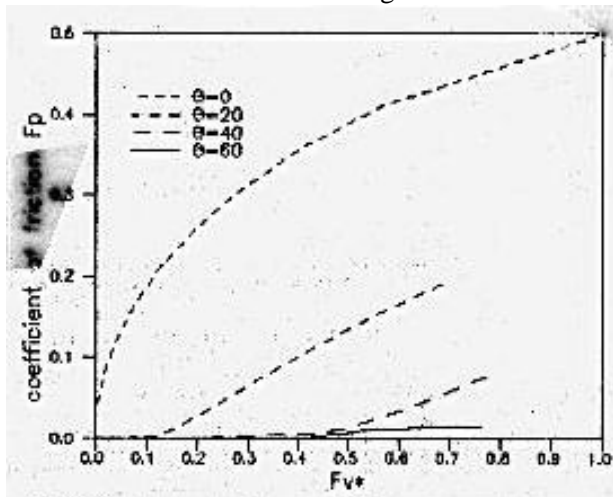


Fig.(8.4) Graph of Friction Versus Vertical Force For Various θ in a Descending Situation For $n=1$

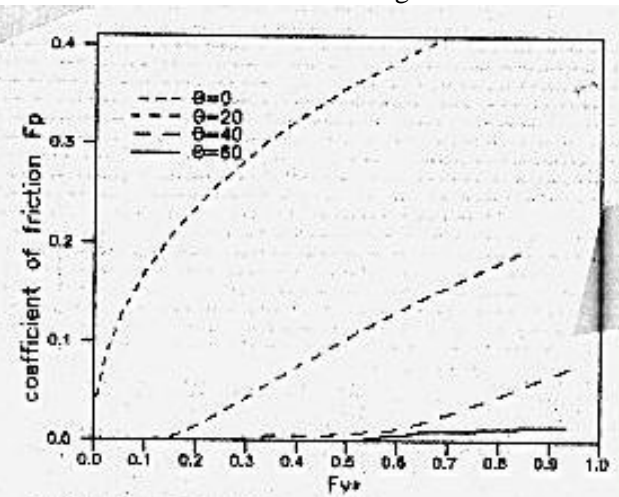


Fig.(8.3) Graph of Friction Versus Vertical Force For Various θ in a Descending Situation For $n=0.6$

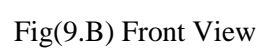
APPENDIX:

Here are the details for derivation of eq(9) to calculate A_{hd} as shown in fig(4). Fig (9) gives an outlines of fig(4) and is used in the following equations.

$$\text{area } OB''B'O = I = R \cos \phi R \sin \phi = \frac{R^2 \sin 2\phi}{2}$$

$$\begin{aligned} \text{area } B''BB'CB'' &= II = 2(\pi/4)(BC \times BB') \\ &= (\pi/2)\{(d/2R) - \tan \theta(1 - (d/2R)^2)^{0.5}\} R \sin \theta R \sin \phi \end{aligned}$$

$$\begin{aligned} \text{area } B''CB'FB'' &= III = R^2 \phi - I - II \\ &= R^2 \phi - \frac{R^2 \sin 2\theta}{2} - \frac{R^2 \pi}{2} \{(d/2R) - \tan \theta(1 - (d/2R)^2)^{0.5}\} \sin \theta \sin \phi \end{aligned}$$



SOLVING PROBLEMS OF UNSTEADY – CONFINED FLOW TO PUMPED WELLS BY COMPUTER

By: Abdulhadi A. A. Al-Delewy

Prof.; Department of Civil Engineering; College of Engineering; University of Babylon

ABSTRACT

In this research, a procedure to solve problems of unsteady flow to wells in confined aquifers by the computer is developed. The solution is based on the [THEIS:1935] procedure to solve such problems. The developed procedure is applied to (14) different sets of well – test data, including a predicted ideal one. The respective problems are solved completely by the computer without the need to construct or to refer to tables or nomographs; this, accordingly, deletes the role of personal judgment and the need to a high skill.

The applications indicate that the developed solution procedure is simple, easy to use, elaborate, superiorly fast in giving the required results, and comparatively accurate.

Despite that the developed solution procedure has been set for the case of a pumped well in an ideal confined aquifer, it is basically general; the computer program can be easily modified to fit the solution of problems of the other cases of groundwater flow to wells after introducing the additions that consider the respective boundary conditions.

KEYWORDS:

Wells hydraulics; Unsteady confined flow; Theis equation; Solution by computer.

الخلاصة

تمّ بهذا البحث تطوير طريقة لحل مسائل الجريان غير الثابت الى الآبار في الحشارج المحصورة وذلك باستعمال الحاسوب، واستند الحل على طريقة [ثايس:1935] في حل مثل هذه المسائل. جرى تطبيق الطريقة المطوّرة على (14) مجموعة مختلفة لرصودات فحص الآبار، منها مجموعة مثالية مستنبطة. لقد تمّ حل المسائل ذات العلاقة كلياً بواسطة الحاسوب دون الحاجة الى إعداد أو الرجوع الى جداول أو رسوم بيانية، وهذا بالنتيجة ألغى دور الاجتهاد الشخصي والحاجة الى الخبرة العالية. لقد بينت التطبيقات ان طريقة الحل المطوّرة هي بسيطة وسهلة الاستعمال ومُتقنة وفائقة السرعة في إعطاء النتائج المطلوبة ودقيقة نسبياً.

ورغم ان طريقة الحل المطوّرة وُضعت لحالة بنر ضخّ في حشرج محصور مثالي، فإنها بشكل أساس عامة إذ بالإمكان تعديل برنامج الحاسوب بسهولة ليوائم حل مسائل الحالات الأخرى لجريان الماء الجوفي الى الآبار وذلك بعد تضمين برنامج الحاسوب الإضافات التي تأخذ بعين الاعتبار الأوضاع التُخميّة ذات العلاقة.

INTRODUCTION

Groundwater represents a major water resource – if not the only one – in too many localities all over the world. Beside its relatively good quality, in general, the attainable quantity of the world's groundwater (at depths less than 760 m) has been estimated at (3, 853, 213 km³) [UNESCO:1978], which is more than (33) times of the estimated total quantity of fresh water in all rivers, reservoirs, and lakes.

Groundwater is extracted mainly by means of pumped wells. The flow to a well is in fact unsteady. However, a steady state may be practically assumed after a continuous pumping from a well at a constant rate for a considerably long time. The pumped aquifers may be unconfined, semi – confined (leaky), or confined; the basic hydraulic principles for the aforementioned flow cases are essentially the same.

Practical problems of most concern in the field of groundwater hydrology and hydraulics fall in one of the following categories :

- (1). Estimating the average values of the aquifer characteristics, namely, the transmissivity (T) and storativity (S).
- (2). Determining the safe yield of a well (or an aquifer, or even a basin) for known (T) and (S).
- (3). Predicting the drawdown (z) at the pumped well or in an observation well at a distance (r) from the pumped well at any time (t) since the start of pumping, provided that aquifer's (T) and (S) are known.

Pumping tests are the major tool for establishing the field data which are necessary for the solution of the aforementioned problems. Results of pumping tests are usually recorded in the form of tables giving the depth of water (d) in the considered observation well (measured from the ground surface) versus the respective time elapsed since the start of pumping, (t). The water surface in a well represents the instantaneous level of the piezometric surface in the confined aquifer (or that of the water table in an unconfined aquifer).

As it is discussed later, solution of any problem related to the discussed subject necessitates the reference to some pre – established tables. Besides, the available procedures for solving problems of category (1) are graphical (in which human judgment plays a major role).

Realizing that the basic principles behind the Theis equation and Theis procedure of solution (mentioned hereafter) are unquestionable, this research aims at developing a simple and accurate methodology to solve problems of any of the three aforementioned categories. The solution is to be performed completely by computer and, consequently, there will be no further reference to tables, nomographs, or graphical solution for which high personal skill and experience are prerequisites. An ideal confined aquifer will be considered in establishing the methodology. The validation of the methodology is checked through application to some selected case studies.

THE GOVERNING EQUATION

Actual groundwater flow is three – dimensional and unsteady, with the storage characteristics of the aquifer playing a major role. Thus, an actual soil – water system is so complex that the solution of any problem concerning it, no matter how simple is, cannot be performed straightforward and accurately; wells hydraulics is one such example. Consequently, accompanying simplifying assumptions are always indispensable.

For an assumed laminar groundwater – flow, the general governing differential equation is developed by combining Darcy's equation and the continuity (mass balance) equation. The resulting equation can be written as [MCWHORTER and SUNADA:1977] :

$$\frac{\partial}{\partial x} \left(Kx \frac{\partial h}{\partial x} \right) + \frac{\partial}{\partial y} \left(Ky \frac{\partial h}{\partial y} \right) + \frac{\partial}{\partial z} \left(Kz \frac{\partial h}{\partial z} \right) = S_s \frac{\partial h}{\partial t} \quad [1]$$

where, for a confined aquifer, the specific storage (S_s) is a measure of compressibility of the aquifer and water.

The solutions of Eq. (1) give the time and space distributions of the piezometric head (h) in heterogeneous, anisotropic, confined aquifers, in the usual three Cartesian coordinates (x, y, z).

To overcome the big difficulty and the complexity involved in solving Eq. (1), some practical simplifying assumptions, beside the assumption of laminar flow, are usually introduced. Such assumption involve **[CHOW:1964]** :

1. The aquifer is homogeneous, isotropic, of infinite areal extent, bounded by impermeable (confining) strata above and below, and has constant coefficients of transmissivity and storage in all directions at all times.
2. The discharging well is of infinitesimal diameter and completely penetrates the aquifer.
3. Pumping is maintained at a constant rate (Q).
4. Water is released instantaneously with decline in head.

It is to be noted, however, that for an assumed horizontal confined aquifer of a relatively uniform thickness (b) and an extensive areal extent, when average values of the effective soil characteristics, namely, the hydraulic conductivity (K) and the specific storage (S_s), are considered then the assumptions of homogeneity and isotropy are implicitly justified.

Thus, under the aforementioned assumptions, Eq. (1) reduces to :

$$\frac{\partial^2 h}{\partial x^2} = \frac{S_s}{K} \frac{\partial h}{\partial t} \quad [2]$$

where : K = overall average hydraulic conductivity of the aquifer.

For a radial flow towards a well, Eq. (2), written in polar coordinates, becomes :

$$\frac{\partial^2 h}{\partial r^2} + \frac{1}{r} \frac{\partial h}{\partial r} = \frac{S_s}{K} \frac{\partial h}{\partial t} \quad [3]$$

With the assumption that the aquifer is of a uniform thickness (b), and defining the aquifer's storativity (S) and transmissivity (T) as :

$$S = S_s \cdot b \quad [4]$$

$$T = K \cdot b \quad [5]$$

then Eq. (3) could be written as :

$$\frac{\partial^2 h}{\partial r^2} + \frac{1}{r} \frac{\partial h}{\partial r} = \frac{S}{T} \frac{\partial h}{\partial t} \quad [6]$$

which is the governing equation for the groundwater flow described hereinbefore.

SOLVING THE GOVERNING EQUATION

The difficulty in solving Eq. (6) led C.V. Theis to present a formula based on heat – conduction analogy, accounting for the effects of the storage characteristics of the aquifer and the time. For the conditions of $(h = h_0)$ at $(t = 0)$ and $(h \rightarrow h_0)$ as $(r \rightarrow \infty)$ for $(t \geq 0)$, the equation was [THEIS:1935] :

$$h_0 - h_r = z_r = \frac{Q}{4\pi T} \int_u^\infty \frac{e^{-y}}{y} dy \quad [7]$$

which is the nonequilibrium or Theis equation. The parameters (h_0) , (h_r) , and (z_r) are as shown in Fig. (1). The dimensionless parameter (u) is given by :

$$u = r^2 S / 4 T t \quad [8]$$

In groundwater literature, the integral in Eq. (7), known in mathematics as the exponential integral, is commonly denoted by $[W(u)]$ and called "the well function of (u) "; the log – log plot of $[W(u)]$ versus $[u]$ or $[1/u]$ is called the type curve. Thus, Eq. (7) is commonly written as :

$$z_r = \frac{Q}{4\pi T} W(u) \quad [9]$$

No analytic solution is available for $[W(u)]$ but a numerical representation by the infinite series :

$$W(u) = -0.5772 - \ln u - \sum_{n=1}^{\infty} \frac{(-)^n u^n}{n.n!} \quad [10]$$

Based on that, [WENZEL:1942] prepared a table for the values of $[W(u)]$ versus values of $[u]$, available for the range $(1 \times 10^{-15} \leq u \leq 10)$. The solution of any problem in this respect necessitates the reference to Wenzel's table.

There is only one equation, the governing equation, which is available for solving the faced problems. Problems of categories (2) and (3) involve one unknown only and, therefore, can be solved directly, of course with the aid of Wenzel's table. However, the case is not so for a problem of category (1) because it involves two unknowns, namely, (T) and (S) . For this [THEIS:1935] proposed his well – known graphical solution. Later, [COOPER and JACOB:1946] proposed a modified graphical procedure to solve problems of this category, provided that (u) has a small value. [CHOW:1952] developed a method that avoids the curve fitting of the Theis method and not being restricted to small values of (u) . Nevertheless, the method is also graphical and necessitates the use of a second table for a new function (Fu) , beside Wenzel's table.

In an extensive study to solve some subsurface flow problems by the use of a computer, [AL-ASSAF:1976], supported by some hypothetical and real examples, established the respective computer programs. One such a program is to estimate the aquifer characteristics directly from well test data through an iterative approach and in two stages. The first stage involves approximating the Theis equation and solving the approximated version for the considered data. The second stage uses the approximate results obtained in the first stage to solve the exact Theis equation and thus, obtaining the exact results aimed at.

PRACTICAL CONSIDERATIONS

To keep the computer work within some reasonable limits, the following practical considerations would be helpful. However, the developed solution procedure, in general, and the computer work, in particular, are by no means limited to these considerations as they are only indicative.

[A] Values of (u)

Theoretically, the dimensionless parameter (u), as defined in Eq. (8), may take any value in the range ($0 < u < \infty$). However, in real practice, the following may be considered.

(1): Values of (r)

With a specified constant pumping rate (Q), the value of the radial distance (r) from the pumped well depends mainly on the characteristics of the aquifer. Values of (r) of (5 – 100 m) are common in practical use. Reasonable values of (10 – 50 m) will be considered in the following analysis.

(2): Values of (S)

Values of the aquifer storativity (S) in the range ($1 \times 10^{-6} - 5 \times 10^{-3}$) have been recorded. Values of (1×10^{-4}) and (1×10^{-3}) will be used in the following analysis.

(3): Values of (T)

The hydraulic conductivity (K) of a natural soil is the most variable soil characteristic; it ranges from as low as (1×10^{-7} m/day) for clay to as high as (10^3 m/day) or even more for gravel [CHOW:1964]. However, establishing a pumped – wells scheme in an aquifer of low permeability is not a feasible practice. Consequently, practical values of (2 – 20 m/day) seem reasonable for the purposes of this research.

The average thickness (b) of the source confined aquifer could be from few meters to several hundreds of meters. For the purposes of this research, values in the range (20 – 100 m) shall be considered.

Based on the considered values of (K) and (b) hereinbefore, the extreme values of (T), as defined by Eq. (5) would be (40 – 2000 m²/day).

(4): Values of (t)

Duration of pumping, (t), in a pumping test, i.e., the time of continuous pumping from its start until stoppage, depends on the characteristics of the aquifer and the degree of accuracy of results aimed at. Values of (t) in the range (0.5 – 2 day) are practically reasonable.

On considering the extreme values of (r), (S), (T), and (t) mentioned hereinbefore, the respective values of (u) would be in the range ($6.25 \times 10^{-7} - 3.125 \times 10^{-2}$). Consequently, the practical range of (u) for the purposes of this research will be considered as ($1 \times 10^{-7} - 0.1$).

[B] Values of (Q)

The pumping rate (Q) should be high enough to produce measurable drawdowns in the respective observation wells. Values of ($5 \text{ l/s} \leq Q \leq 40 \text{ l/s}$) shall be considered when needed in this research.

THE DEVELOPED PROCEDURE OF SOLUTION

The type curve, {the $\log - \log$ plot of [$W(u)$] vs. [u]}, resembles the theoretically – expected trend of the observed data of a pumping test when drawn as [(z) vs. (r^2 / t)] on a $\log - \log$ paper of the same scale as that of the type curve. Two basic assumptions in the derivation of Eq. (9) are that (Q) is constant throughout the test, and water is released instantaneously with decline of head. Practically, these two assumptions are commonly not well met during the first few observations. Consequently, less weight is usually given to the data of such observations.

With the progress of the pumping, the plot of the pumping – test data, $[(z)$ on an arithmetic scale versus (t) on a logarithmic scale], will be close to a straight line, the longer (t) is the more the closeness will be. For such a straight line, the data could be represented by :

$$z = C + m \log(t) \quad [11]$$

where : (C) is the logarithmic intercept; (m) is the slope of the line, calculated between any two points, $[(t_a, z_a)$ and (t_b, z_b) ; $(t_b > t_a)$] as :

$$m = \frac{z_b - z_a}{\log(t_b) - \log(t_a)} = \frac{\Delta z}{\log(t_b / t_a)} \quad [12]$$

If the two points were chosen such that they cover a complete logarithmic time cycle, i. e., $(t_b = 10 t_a)$, then $[\log(t_b / t_a) = 1]$ and Eq. (12) reduces to $(m = \Delta z)$.

Each observation shall be denoted by (R) with a subscript to denote its serial number. Thus, an observation will be $[(R_i); i = 0, 1, \dots, N; N = \text{the serial number of the last observation}]$. Consequently, and if the available data permit, the analysis will consider (J) observations [from (R_a) or (R_{N-J+1}) to (R_N)] that cover the last complete time logarithmic – cycle [that is from (t_a) to (t_N) , where $(t_a = t_N / 10)$]. If (t_a) is not the time of an existing observation then an existing observation $(R_{a'})$ is to be considered such that the time $(t_{a'})$ is just preceding (t_a) .

The developed solution procedure is summarized in the following steps :

[A] Verification of the observed data :

- (1): Imagine that all data points have been located on a semi – log plot, (z) on the vertical arithmetic scale versus (t) on the horizontal logarithmic scale. After deciding on the (J) data points to be considered in the analysis (as mentioned hereinbefore), imagine that each two consecutive data points of the chosen ones are connected by a chord.
- (2): Use Eq. (12) to calculate the slope of the established chords, $(m_j; j = 1, 2, \dots, J-1)$. Of course, (m_j) as calculated would never be (–ve); otherwise, a point creating a (–ve) (m_j) should be considered as an outlier and, consequently, discarded.

It is to be noted that whenever an observation is discarded from the analysis, the number of involved observations (J) is decreased by one for the following calculations.

- (3): For the considered data points to form a single, reasonably – acceptable straight line [outlined by the established $(J-1)$ chords], the computed values of (m_j) should be insignificantly different.

[B] For the (J) observations still under consideration, the best – fit straight line is found by the least squares method.

Denoting $[\log(t)]$ as (X) and (z) as (Y) , then Eq. (11) becomes :

$$Y = C + m X \quad [13]$$

According to the least – squares fitting [MONTGOMERY et al.:1998] :

$$C = \frac{(\sum Y)(\sum X^2) - (\sum X)(\sum XY)}{J(\sum X^2) - (\sum X)^2} \quad [14]$$

$$m = \frac{J(\sum XY) - (\sum X)(\sum Y)}{J(\sum X^2) - (\sum X)^2} \quad [15]$$

and the respective regression coefficient (R) is computed as :

$$R = \sqrt{\frac{\text{Explained variation}}{\text{Total variation}}} \quad [16]$$

which, for linear regression, could be set in a form simpler for calculation as :

$$R = \frac{J(\sum XY) - (\sum X)(\sum Y)}{\sqrt{[J(\sum X^2) - (\sum X)^2][J(\sum Y^2) - (\sum Y)^2]}} \quad [17]$$

[C] The function (Fu) of [CHOW:1952]

To connect the observed data with the type curve, [CHOW:1952] defined a function (Fu) such that :

In relation to the considered observed data :

$$Fu = z_i / m \quad [18]$$

where (z_i) is the drawdown of an observation (R_i) chosen arbitrarily from the considered set of observations.

In relation to the type curve :

$$Fu = \frac{1}{\ln 10} W(u) \cdot e^u \quad [19]$$

where (Fu), [$W(u)$], and (u) are all evaluated at (R_i).

The value of (Fu) is calculated by Eq. (18). Then, the solution of Eq. (19) would give unique values of (u) and [$W(u)$] evaluated at (R_i). This would enable solving Eq. (9) for (T) and then solving Eq. (8) for (S).

[D] Solving for [$W(u)$] and (u)

What is mentioned in item [C] hereinbefore sounds attractive. However, it involves an obstacle in that, despite of that [$W(u)$] being a function of (u) (and vice versa), Eq. (19) could not be solved explicitly, neither for (u) nor for [$W(u)$].

To overcome the involved dilemma, [CHOW:1952] prepared a table (and also a *log – log* nomograph) for values of (Fu) corresponding to a range of values of [$W(u)$] and their respective values of (u).

For a solution to be performed completely by a computer, the reference to tables or nomographs should be avoided. Accordingly, the case under consideration could be tackled by a computer through a trial – and – error solution. Such a solution would involve assuming a reasonable value for (u), computing the respective value of [$W(u)$] by Eq. (10), computing the respective value of (Fu) by Eq. (19), and comparing this value with that computed by Eq. (18); the two values should be insignificantly different (within a pre-specified tolerance limit). If the two values were not so, the calculations are repeated for modified values of (u) until the aimed goal is achieved. However, this would be a cumbersome and tedious task. An elaborate alternative is to provide the necessary explicit mathematical relationships between each two of the three

involved parameters, namely, (Fu) , $[W(u)]$, and (u) . This implies the establishment of the following functional relationships : $\{W(u) = f_1[u]\}$, $\{u = f_2[W(u)]\}$, and $\{u = f_3[Fu]\}$ or $\{W(u) = f_4[Fu]\}$.

Taking into consideration the practical range of values of (u) of $(1 \times 10^{-7} - 0.1)$ mentioned before, the following has been deduced in this respect.

(1): $\{W(u) = f_1[u]\}$

Such a relationship is already given by Eq. (10). However, it is logical and more practical that for small values of (u) , the series may be truncated after the second term. Thus, Eq. (10) becomes :

$$W(u) = -0.5772 - \ln u = \ln (1 / 1.781 u) \quad [20]$$

To check the validity of such an approximation, consider values of (u) of (0.001), (0.01), and (0.1). Moreover, and for illustrative purposes and based on the practical considerations outlined before, consider average practical values of the involved parameters, say $[Q = 10 \text{ l/s}; T = 400 \text{ m}^2/\text{d}]$. The drawdowns calculated for the aforementioned cases are summarized in **Table (1)**. For drawdowns calculated to the nearest millimeter, the results show that the approximation of $[W(u)]$ for the considered values of (u) will yield a relative percent decrease (D_1) in the computed drawdowns of (0.0), (0.29), and (5.35), respectively. The relative percent decrease (D_2) would be (0.0), (0.0), and (3.23), respectively, if the drawdowns were calculated to the nearest centimeter. This indicates that the use of Eq. (20) is well justified, at least for the purposes of this research, for $(u < 0.01)$.

(2): $\{u = f_2[W(u)]\}$

(i): Since Eq. (20) was found satisfactorily accurate for $(u < 0.01)$ [for which $W(u) > 4.0379$], then the inverse functional relationship will be valid too. That is :
For $[W(u) > 4.0379]$:

$$u = 1 / \{1.781 \exp. [W(u)]\} \quad [21]$$

(ii): For $[4.0379 \geq W(u) \geq 1.8229]$, [that is $0.01 \leq u \leq 0.1$] :

For purposes other than this research, the researcher solved Eq. (10) up to $(n = 34)$ (which was the limit of the capacity of the used computer) and prepared a table similar to Wenzel's table and for the same values of (u) involved therein. The respective type curve is then divided into several overlapping hypothetical sectors. The data of each sector were regressed, $[W(u)$ on (u) and vice versa]; the sectors were shortened or elongated until the best regression, i. e., the highest regression coefficient (R) , was obtained.

For the aforementioned relationship, the obtained one was :

$$u = \text{Exp. } \{- [1.04 W(u) + 0.41]\}; \{R = 1.0\} \quad [22]$$

(3): $\{W(u) = f_4[Fu]\}$

(43) values of (u) , covering the range $(1 \times 10^{-7} \leq u \leq 0.1)$ were selected. The respective values of $[W(u)]$ were calculated by Eq. (10) or Eq. (20), as the case indicated. Then, Eq. (19) is used to calculate the corresponding values of (Fu) .

The software GRAPHER was used to perform the regression of $[W(u)]$ on (Fu) . Of the various styles the software offers, the best functional relationship obtained in this respect was a third – degree polynomial which, after modification, came as :

$$a_0 = -0.34; a_1 = 2.55; a_2 = -0.0567; a_3 = 0.004124; \{R = 1.0\} \quad [23]$$

With known (Q) , (r) , and $[W(u)]$ in respect to the chosen observation (R_i) with known (t) and (z) , the solution for (T) and (S) would be systematic and straightforward and as follows :

(1):Solve Eq. (5) for (T) .

(2):Solve Eq. (22) [or Eq. (21) as the case may be] for (u) ; then, solve Eq. (4) for (S) .

It is known in statistics that when a set of data points $\{X, Y\}$ is fitted linearly, a point (\bar{X}, \bar{Y}) , whether real or predicted, would locate on the fitted straight line. Consequently, it was thought that such a point would be an appropriate choice for (R_i) . Thus, the established computer program has been set accordingly; it computes (\bar{t}, \bar{z}) of the considered (J) data points and uses the respective values to represent the chosen observation (R_i) .

APPLICATION

The researcher was hoping to apply the developed solution procedure to some recent, dependable well – test data, Iraqi in particular. However, he was almost unfortunate in this respect. Nevertheless, (14) different data sets were used to form the application cases. The information regarding these sets are outlined hereinafter.

[1] For a rigid check of the applicability of the developed procedure, an ideal hypothetical data set has been fabricated as follows :

(a) (24) values of (u) representing the practically – common range of $(2.5E-1 \geq u \geq 4E-5)$ have been selected. The respective values of $[W(u)]$ were calculated by Eq. (10) [for $(u \geq 0.01)$] or by Eq. (20) [for $(u < 0.01)$].

(b) For assumed reasonable values of $(Q = 20 \text{ l/s} = 1728 \text{ m}^3/\text{d})$, $(r = 25 \text{ m})$, $(T = 400 \text{ m}^2/\text{d})$, and $(S = 2.5E-4)$, the values of (z) [by Eq. (9)] corresponding to the calculated values of $[W(u)]$ and then the values of (t) [by Eq. (8)] corresponding to the chosen values of (u) , were calculated.

(c) The resulting (24) (t, z) data points formed the application set [1] for the present research.

[2] To illustrate his developed graphical approach, [CHOW:1952] used the well - test data shown in his Fig. (3). The values of (22) data points (t, z) abstracted from the aforementioned figure formed the application set [2].

[3] Test data for well (1) at Gridley, Illinois is used as an illustrating example in [WALTON:1970], (P 229). The data of the example formed the application set [3].

[4] Data constituting (29) observations are given in Problem (4-1), P 283 in [WALTON:1970]. He indicated the solution to be $(T = 358000 \text{ gpd/ft})$; $S = 4.7E-4$) without mentioning the procedure of solution. This data formed the application set [4].

[5]; [6]; [7]: Data from the pumping test Qude Korendjik are given in [KRUSEMAN and DE RIDDER:1970], (P 53). Observations were made in three piezometers, (P1), (P2), and (P3), located at radial distances from the pumped well of (30 m), (90 m), and (215 m), respectively. The basic assumptions mentioned before were closely satisfied in the test.

[KRUSEMAN and DE RIDDER:1970] used the aforementioned data to estimate (T) and (S) . The procedures of solution used were as follows :

(a)[THEIS:1935] procedure applied to the data of the three piezometers collectively.

(b)[COOPER and JACOB:1946] procedure. This was used in three approaches :

(i): The traditional approach, that is : $[(z) \text{ vs. } (t)]$ for constant (r) , for each piezometer separately.

(ii): $[(z) \text{ vs. } (r)]$ for constant (t) ; solved for $(t = 140 \text{ min.})$.

(iii): $[(z) \text{ vs. } (t/r^2)]$ for the data of the three piezometers collectively.

(c) [CHOW:1952] procedure applied to the data of (P1).

The data of (P1), (P2), and (P3) have been considered as the application sets [5], [6], and [7], respectively.

[8]; [9]; [10]: [LOHMAN:1972] used data observed at three observation wells ($N-1$), ($N-2$), and ($N-3$) in a solution by the Theis procedure. These data have been considered as the application sets [8], [9], and [10], respectively.

[11]: [LINSLEY et al.:1988] present an illustrative example on (P 179). They solved for (T) and (S) by the Theis and the Jacob procedures. The data of the example have been considered as the application set [11].

[12]; [13]; [14]: [ABDULLA:2001] used data sets observed at seven observation wells in the Jolak Basin (Al-Ta'miem Governate, Iraq), each corresponds to a certain pumped well. Those corresponding to the wells Yarimja, Kurzi, and Nabi Awah have been considered as the application sets [12], [13], and [14], respectively, for the purposes of the present research.

RESULTS AND ANALYSIS

The basic results of applying the developed solution procedure to the considered (14) data sets are summarized in **Table (2)**. In this respect, the following is worth mentioning :

[A] No data point has been found to be as an outlier.

[B] The respective values of the regression coefficient (R) were high enough to indicate excellent linear fittings.

[C] Values of (T) and (S) estimated by the solution procedure developed in this research are designated as (CT) and (CS), respectively. The corresponding reference values are designated (RT) and (RS), respectively; those concerning data set [1] are the assumed values; those concerning the other data sets are the values estimated by the respective researchers; the abbreviations (TH), (JA), and (CH) denote that the respective values have been estimated by the [THEIS:1935], [COOPER and JACOB:1946], and [CHOW:1952] procedures, respectively.

[D] Values of (T) and (S) could be described as exact only when they are obtained by a purely – theoretical solution (without any added assumptions other than those accompany the derivation of the governing equation) and for ideal well – test data. This is virtually the case of (RT) and (RS) of application case [1].

The values (CT) and (CS) obtained by the solution procedure developed in this research and for the same data set [1] were identical to the reference values. This clearly proves the elaborateness and accuracy of the developed procedure.

[E] The developed procedure solves the involved problem completely by the computer without the need neither to construct nor to refer to any table or graph. In fact, when the computer program is ready in the computer, the time to obtain the results is just that time for inputting the data and pressing the "run" button.

[F] Recalling that the keystone in the solution of the considered problems is the Theis equation. However, actual field conditions are never ideal; the percent deviation between the two could be anywhere between the two extreme limits, (0) and (100). The error in the results due to ignoring such a deviation may be exaggerated when using different data sets for the same aquifer, using

different approximate procedures of solution, or when the solutions are performed by different persons and by procedures in which the personal skill and judgment play a significant role. Consequently, the comparison of different mere results for the same data would be indicative only.

All the known procedures of solution in this respect are issued from the same theoretical basis. The differences between them are basically the additional assumptions, simplifications, and approximations to facilitate and accelerate the solution process while keeping the results closely comparable to some references ones, usually taken as those of the Theis procedure of solution. Accordingly, one can pronounce that no other solution procedure may be more accurate than the one developed in this research since it adds no further assumptions or conditions, except that the well test should last long enough to make the plot $[(z) \text{ vs. } (\log t)]$ closely approximates the expected straight line (which is, in fact, a general prerequisite to any well test). Moreover, the procedure involves no approximations other than those required to give the highest reasonable computation accuracy the computer provides. Yet, the fully – computerized solution by the developed procedure leaves no role to personal judgment or the necessity to highly – skilled personnel.

Keeping in mind the aforementioned merits of the developed solution procedure, the obtained values (*CT*) and (*CS*) for the application cases [2] through [14], given in **Table (2)**, indicate that they were :

- ◆ Close to (*RT*) and (*RS*) for [2] by (*CH*).
- ◆ Identical to (*RT*) and (*RS*) for [3] by (*TH*).
- ◆ Somehow comparable to (*RT*) and (*RS*) for [4] (for which the reference do not mention his procedure of solution).
- ◆ Somehow different from (*RT*) and (*RS*) for [5] as obtained by all the five applied procedures.
- ◆ Somehow comparable to (*RT*) and (*RS*) for [6] as obtained by all the five applied procedures.
- ◆ Identical to (*RT*) and (*RS*) for [7] by (*JA*–1).
- ◆ Different from the average (*RT*) and (*RS*) obtained for [8], [9], and [10] collectively, by (*TH*).
- ◆ Very closely comparable to those obtained for [11] by both (*TH*) and (*JA*).
- ◆ Ditto, for [12].
- ◆ (*CT*) was identical to (*RT*) for [13] obtained by both (*TH*) and (*JA*). However, (*CS*) was identical to (*RS*) by (*TH*) but different from that by (*JA*) {unless there is a misprint}.
- ◆ Almost identical to (*RT*) and (*RS*) for [14] by (*TH*) and closely comparable to those by (*JA*).

CONCLUSIONS

In summary, the following conclusions could be stated :

1. The fully – computerized procedure developed in this research for solving problems of unsteady flow to wells in confined aquifers is simple, elaborate, superiorly fast in giving the required results, and without the need of graphics or the reference to tables or nomographs. Moreover, on considering the results obtained by the available solution procedures for the same data, the accuracy of the results of the developed procedure are comparatively unquestionable.
2. The procedure is basically general; it is equally applicable to the different problems encountered in wells hydraulics (such as those for data of water – level recovery, for unconfined or semi – confined aquifers, or when accretion is present) after introducing the additions that count for the relevant boundary conditions.

Table (2) : Summary of results [The cases and symbols are explained in the text]

Item	Parameter	Units	Case Number						
			(1)	(2)	(3)	(4)	(5)	(6)	(7)
1	Q	M ³ /d	1728	4088	1200	8176	788	788	788
2	r	m	25	245	251.2	91.44	30	90	215
3	N	---	24	22	22	29	34	35	9
4	J	---	9	16	13	11	11	15	9
5	C	m	0.4763	-0.8848	-1.2823	0.2346	0.4169	0.0256	-0.1679
6	m	---	0.7914	0.6519	1.6993	0.2890	0.2297	0.2390	0.1450
7	R	---	1.0000	0.9984	0.9988	0.9982	0.9977	0.9991	0.9948
8	\bar{t}	min.	1524.41	166.79	142.45	503.09	281.53	274.88	274.44
9	\bar{Z}	m	2.995	0.564	2.377	1.015	0.982	0.608	0.186
10	ΔZ	m	0.792	0.652	1.699	0.289	0.230	0.239	0.145
11	F(u)	---	3.782	0.865	1.399	3.512	4.270	2.544	1.283
12	W(u)	---	8.7084	1.8260	3.1278	8.0867	9.8320	5.8578	2.8470
13	u	---	9.28E-5	9.94E-2	2.57E-2	1.73E-4	3.02E-5	1.60E-3	3.44E-2
14	CT	M ² /d	399.8	1053.1	125.6	5183.2	627.8	604.1	959.7
15	CS	---	2.51E-4	8.08E-4	2.00E-5	1.50E-4	1.60E-5	9.10E-5	5.44E-4
16a	RT	M ² /d	(TH) 400	(CH) 1008.1	(TH) 125.24	(?) 4439.2	(TH) 418		
17a	RS	---	2.50E-4	8.83E-4	2.00E-5	4.70E-4	1.7E-4		
16b	RT	M ² /d					(JA-1) 401	480	960
17b	RS	---					1.7E-4	1.8E-4	5.8E-4
16c	RT	M ² /d					(JA-2) 355		
17c	RS	---					4.5E-4		
16d	RT	M ² /d					(JA-3) 438		
17d	RS	---					1.7E-4		
16e	RT	M ² /d					(CH) 375		
17e	RS	---					2.2E-4		

**Table (2) :** [Continued]

Item	Parameter	Units	Case Number						
			(8)	(9)	(10)	(11)	(12)	(13)	(14)
1	Q	M ³ /d	2718.4	2718.4	2718.4	3672	3120	691.2	907.2
2	r	m	61	122	244	30	50	30	30
3	N	---	25	25	25	11	17	20	25
4	J	---	12	12	12	10	15	17	19
5	C	m	0.5382	-0.2137	-0.8924	-5.3440	-0.5443	-0.1741	-0.1632
6	m	---	1.3184	1.3003	1.2545	2.6451	0.6516	1.1292	0.4103
7	R	---	0.9999	0.9998	0.9994	0.9829	0.9961	0.9991	0.9987
8	\bar{t}	min.	83.38	83.38	83.38	422.34	69.53	249.59	453.64
9	\bar{Z}	m	3.071	2.284	1.518	1.601	0.656	2.533	0.927
10	ΔZ	m	1.318	1.300	1.255	2.645	0.652	1.130	0.411
11	F(u)	---	2.330	1.757	1.210	0.605	1.006	2.242	2.255
12	W(u)	---	5.3650	4.0456	2.6698	1.1829	2.1721	5.1624	5.1923
13	u	---	2.63E-3	9.83E-3	4.13E-2	1.94E-1	6.93E-2	3.22E-3	3.12E-3
14	CT	M ² /d	377.9	383.1	380.4	215.9	822.0	112.1	404.3
15	CS	---	6.2E-5	5.9E-5	6.1E-5	5.46E-2	4.40E-3	2.78E-4	1.78E-3
16a	RT	M ² /d	(TH) 1267.0			(TH) 196.7	(TH) 856.2	(TH) 114.6	(TH) 424.7
17a	RS	---	1.98E-4			6.4E-2	4.8E-3	2.8E-4	1.7E-3
16b	RT	M ² /d				(JA) 200.8	(JA) 878.9	(JA) 110.0	(JA) 437.2
17b	RS	---				5.6E-2	4.9E-3	1.53E-3	4.3E-3

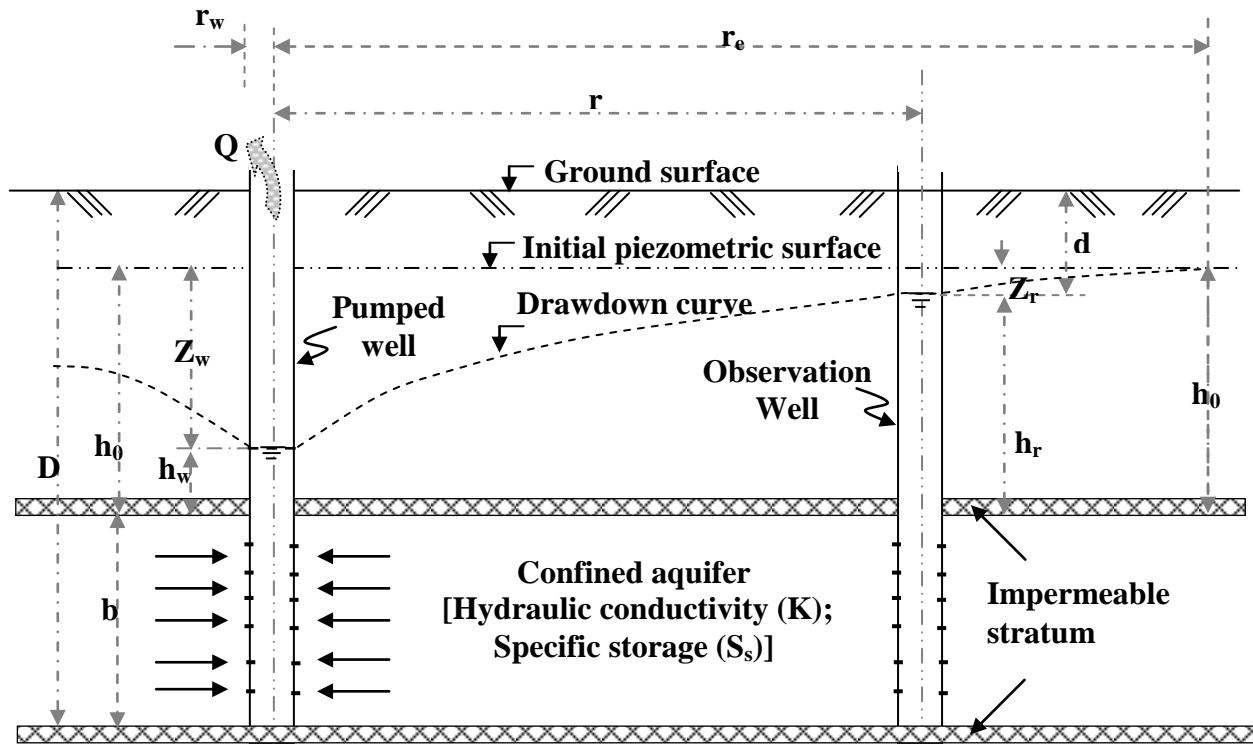


Fig. (1) : Definition sketch for a confined flow to a pumped well.

Table (1) : Results by approximating $W(u)$. [$Q = 10 \text{ l/s}$; $T = 400 \text{ m}^2/\text{d}$]

Parameter	Units	Values of (u)		
		0.001	0.01	0.1
$W(u)$ { Eq. (10) }	----	6.3315	4.0379	1.8229
Z_1 { Eq. (9) }	m	1.088	0.694	0.313
$W(u)$ { Eq. (15) }	----	6.3306	4.0280	1.7255
Z_2 { Eq. (9) }	m	1.088	0.692	0.297
$D_1^{(*)}$	%	0	0.29	5.35
$D_2^{(*)}$	%	0	0	3.23

(*) $D = \frac{Z_1 - Z_2}{Z_1} \times 100$; (D_1) and (D_2) are calculated for values of (Z) computed to the nearest millimeter and centimeter, respectively.

REFERENCES

- ⌘ **ABDULLA, H. H. [2001]:** "Quantitative and qualitative evaluation of groundwater resources in the Jolak Basin". M. Sc. thesis; University of Baghdad.
- ⌘ **AL-ASSAF, S. A.-H. [1976]:** "Application of computer techniques to ground-water flow problems". Ph. D. Dissertation; University College, London.
- ⌘ **CHOW, V. T. [1952]:** "On the determination of transmissibility and storage coefficients from pumping test data". Am. Geophys. Union Trans.; Vol. (33), pp. (397 – 404).
- ⌘ **CHOW, V. T. {Editor-in-Chief} [1964]:** "Handbook of applied hydrology". McGraw-Hill, U.S.A.
- ⌘ **COOPER, H. H. and JACOB, C. E. [1946]:** "A generalized graphical method for evaluating formation constants and summarizing well field history". Am. Geophys. Union Trans.; Vol. (27), PP. (526-534).
- ⌘ **LINSLEY, R. K. (Jr.), KOHLER, M. A., and PAULHUS, J. L. H. [1988]:** "Hydrology for engineers", (SI Metric Edition). McGraw-Hill, Singapore.
- ⌘ **LOHMAN, S. W. [1972]:** "Ground-water hydraulics". Geological Survey Professional Paper 708; U.S. Government Printing Office; Washington.
- ⌘ **KRUSEMAN, G. P. and DE RIDDER, N. A. [1970]:** "Analysis and evaluation of pumping test data". International Institute for Land Reclamation and Improvement; Wageningen, The Netherlands.
- ⌘ **MCWHORTER, D. B. and SUNADA D. K. [1977]:** "Groundwater hydrology and hydraulics". Water Resources Publications; Fort Collins, Colorado, U.S.A.
- ⌘ **MONTGOMERY, D. C., RUNGER, G. C., and HUBELE, N. F. [1998]:** "Engineering statistics". John Wiley; U.S.A.
- ⌘ **THEIS, C. V. [1935]:** "The relation between the lowering of the piezometric surface and the rate and duration of discharge of a well using groundwater storage". Am. Geophys. Union Trans.; Vol. (16), PP. (519-524).
- ⌘ **UNESCO [1978]:** "World water balance and water resources of the earth". Studies and Reports in Hydrology -25; UNISCO.
- ⌘ **WALTON, W.C.[1970]:** "Groundwater resource evaluation". McGraw-Hill Kogakusha; Tokyo.
- ⌘ **WENZEL, L.K.[1942]:** "Methods for determining permeability of water-bearing material, with special reference to discharging – well methods". U.S. Geol. Survey; Water Supply Paper 887; U.S.A.

SPOT WELDING RESIDUAL STRESSES ASSESSMENT USING NONLINEAR NUMERICAL TECHNIQUE

Dr. Nabeel K. Alsahib
University of Baghdad
AL-Khwarizmi college of Eng.

Dr. Somer M. Nacy
University of Baghdad
AL-Khwarizmi college of Eng.

Dr. Faiz F. Mustafa
University of Baghdad
AL-Khwarizmi college of Eng

ABSTRACT

A description is given of the resistance spot welding process in terms of internal behavior of the weld as welding takes place. Heat input due to spot welding of steel sheet plate causes temperature gradient in the parent metal. After cooling, residual stresses appear around the welding zone reducing the strength. Residual stresses are a result of the temperature gradient and the dependency of material properties on the temperature, such as yield strength, elasticity modulus, and thermal expansion coefficient. Nonlinear transient heat transfer analysis performed in order to obtain the temperature distribution in the welded part. A nonlinear thermo-plastic stress analysis is then performed to predict the stress and strain fields during and after welding. The material properties such as yield strength, elasticity modulus, convection coefficient, conduction, specific heat, and thermal expansion coefficient are used as a function of temperature. The heat transfer results are compared with experimental results performed within the scope of work of this study. On the other hand, the residual stress results are compared with experimental result obtained from literature. The comparison shows good agreement between numerical and experimental results.

الخلاصة:

يقدم البحث وصف دقيق لعملية اللحام النقطي على اساس التغيرات الداخلية الحاصلة في المعدن أثناء وبعد عملية اللحام، حيث اعتمدت طريقة رقمية لاختية معتمدة على العناصر المحددة يمكن من خلالها تعيين درجات الحرارة الناجمة عن عملية اللحام النقطي وتغييرها مع المسافة والزمن ((انتقال الحرارة للاختي والمعتمد على التغيير مع الزمن)) ومن ثم يمكن بأستخدام طريقة العناصر المحددة للاختية ((الدونة الحرارية)) لتعيين الأجهادات المتبقية في الجزء الملحوم وما حوله بعد عملية التبريد. ان الاجهادات المتبقية تظهر نتيجة لتغير درجات الحرارة وما يصاحبها من تغير في خواص المعدن مثل مقاومة الخضوع، حد المرونة، معامل التمدد الحراري ومعامل التوصيل والحمل مع التغير في درجات الحرارة، ولقد تم اجراء تجارب لقياس درجات الحرارة للجزء الملحوم أثناء وبعد عملية اللحام في اجزاء وأزمنة مختلفة لمقارنتها بالنتائج الرقمية ، وتم الأعتداد على تجارب لقياس الأجهادات المتبقية أجريت في أبحاث أخرى للمقارنة حيث ظهر صلاحية الطرق الرقمية بكفاءة عالية وخاصة لتعيين درجات الحرارة وذلك نتيجة دقة التمثيل الرقمي في وصف وتغيرها مع الحرارة ووصف الظروف المحيطة سواء التمثيل الحراري أو الأجهادات.

KEYWORDS

Heat transfer, Residual stress, Finite element, Spot weld, Stainless steel.

INTRODUCTION

Residual stress distribution and distortion in welded plates are strongly affected by many parameters and by their interaction. In particular, there are structural, material and welding factors. The structural parameters include geometry of the plates, thickness and width and joint type. Among the material parameters mechanical and physical properties. Welding variables such as current, force, and weld time. As a consequence of the non-uniform temperature distribution, parts of material close to the weld is subjected to different rates of expansion and contraction developing a three-dimensional complex residual stress state, (**Sarkani and Lutes, 1988**). To understand the formation of residual stress, node temperature history during the welding process must be calculated. During the weld thermal cycle material mechanical properties change—drastically, especially when material approaches melting temperature. Therefore, due to the temperature dependence of material properties and the large deformation in welding, material and geometrical non-linearity have to be taken into account. The initial expansion of material due to the temperature increase is constrained by material placed away from the heat source. Therefore generating compressive stress. At a temperature higher than material critical temperature, the material starts exhibiting thermal softening where heating results in decrease of flow stress. As phase change occurs deviatoric stress become zero and considerable plastic deformation occurs in the weld metal and the base metal near the weld. As temperature decreases during the cooling phase, the stress in the solidifying material increases, and become tensile due to the positive temperature gradient. The region placed away from the welding area, will therefore, be in compression since the resultant force and the resultant moment induced by residual stress evaluated in the center spot plane section must satisfy translation and rotational equilibrium. Plate stiffness affects strongly magnitude and distribution of residual stress. In some cases, residual stress may or exceed the yield stress of the parent plate material, (**Tall, 1964**), (**Sun and Dong, 2000**). The plastic strains resulting from heating induce stress, which in turn produce internal forces that may cause bending and rotation. The displacements are in general called distortion. The residual stress combined with distortion and degradation of the material mechanical properties influence the buckling strength and fatigue life of welded structure.

FINITE ELEMENT MODELING PROCEDURE

Spot welding is a material joining technology using electrical resistance heat of metallic and it is a complicated phenomena. The FE analysis was carried out in two steps (coupled-field analysis that coupling between two or more fields of engineering). A non-linear transient thermal analysis was conducted first to obtain the global temperature history generated during the welding process. A stress analysis was then developed with the temperatures obtained from the thermal analysis used as loading to the stress model, M. Meo and R. Vignjevic. In this analysis, the left and bottom edge of **Fig. 1**, are symmetry axes so only one quadrant of the weld nugget (upper right corner) is shown, ANSYS (8) package was used with an axisymmetric 2D model; solid 8-node element.

The accuracy of the FE method depends upon the density of the mesh used in the analysis. Both the stress and thermal analysis have identical meshes. The weld nuggets temperature is higher than the melting point of the material, and it drops sharply in regions away from the weld nugget. Therefore in order to obtain the correct temperature field in the region of high temperature gradients it was necessary to have a more refined mesh close to the weld nugget. While in regions located away from weld-nugget a more coarse mesh was used. Sensitivity

analysis of mesh density was performed and a satisfactory mesh was adopted for further studies, the higher is the heat input the higher is the number of nodes necessary to accurately interpolate high temperature gradient, H. Huh and Kang, 1997. A stainless steel (304) material property was used for FE model. The chemical composition, mechanical properties of the specimens at room temperature are given in **Table 1&2**, respectively, William, and spot welding condition described in **Table 3**, Roy and Norman, 1976.

NON-LINEAR TRANSIENT HEAT TRANSFER NUMERICAL MODEL

One of the fundamental problems in the analysis of heat flow during welding is how to take into account physical material changes due to temperature changes during the welding process. If the material properties are treated as temperature dependent the **eq. (1)** of heat –flow become non-linear, Cosmos, 2000.

$$\rho \frac{\partial c_p T}{\partial t} = Q + \frac{\partial(k \times \frac{\partial T}{\partial X})}{\partial X} + \frac{\partial(k_y \frac{\partial T}{\partial y})}{\partial y} + \frac{\partial(k_z \frac{\partial T}{\partial Z})}{\partial Z} \quad (1)$$

Where c_p is the specific heat, K thermal conductivity, T temperature, Q is the volumetric heat generation and t is time .If the material properties are considered temperature independent the equation (specific heat, thermal conductivity do not change with temperature) is reduced to a linear differential **eq. (2)**.

$$\rho c_p \frac{\partial T}{\partial t} = Q + K \left(\frac{\partial(\frac{\partial T}{\partial X})}{\partial X} + \frac{\partial(\frac{\partial T}{\partial y})}{\partial y} + \frac{\partial(\frac{\partial T}{\partial Z})}{\partial Z} \right) \quad (2)$$

In the current analysis temperature-dependent thermal properties were assumed, therefore non-linear equations were obtained and solved. **Fig. 2**, shows the thermal specific heat (CP), conductivity ($K=K_x=K_y=K_z$), and convection coefficient relationship with temperature, Ajinomoto, 2001. The material density is approximately considered constant (7850 kg/m^3). To determine temperature and other thermal quantities that vary over time there was the need to perform a transient thermal analysis. Implicit method of time discrimination was employed which allows for larger time steps .It is important not to forget that time step size is not a problem with respect to calculation stability but it determines the accuracy of the solution. Using the FE analysis the thermal and stress analysis are uncoupled while in reality thermal effect and mechanical deformation occur at the same time .The de-coupled line of the analysis becomes acceptable if one assumes that dimensional change (mechanical deformation) during welding process are negligible because thermal energy change is predominant over mechanical work done during welding, and the internal energy dissipation effect on the temperature distribution is negligible. Therefore to evaluate distortion and residual stress distribution the thermal analysis was performed first in order to find nodal temperature as a function of time. Once defined temperature history for each node, temperature loads were applied to the structural model. Temperature history can be shown in **Fig. 3**. The heat within a spot weld is generated totally by resistance to the high electric current passing through the joint and consequently the points of greatest heat generation are the points of greatest resistance (faying surface) .The plate absorbs a part of the heat generated. There are losses from the surfaces in the form of convection. Therefore, to evaluate the amount of heat absorbed by the plates as a portion of the total heat generated the following formula was used, (**Milner and Apps, 1968**).

$$Q = I^2 R t \quad (3)$$

Where I is the welding current, R is the faying surface resistance and t the time of welding.

The assumptions made are:

- Thermal properties, i.e. conductivity, specific heat and convection are temperature dependent.
- Effects arising from phase change are taken in to account, enthalpy change during the phase change.
- Heat losses by transfer to the ambient medium by radiation are negligible.

Convection losses are evaluated using the eq. (4)

$$Q_i = hA_i(T_i - T_o) \quad (4)$$

Where h is the convection heat transfer coefficient (for free convection in air, h has maximum of $(9W/m^2 - C^\circ)$), (Chapman, 1987). Q_i denotes the heat loss on surface i with area A_i , T_i is the temperature on surface A_i , and T_o is the ambient temperature.

During the welding process phase change occurred, to account the effect of latent heat, i.e. heat energy which, is released or stored by the material during a phase change enthalpy was specified. The concept that could be readily adopted by the finite element was formulated on the basic of integrating the heat capacity of the material over a small region of phase changes (see eq. (5)), (Tekriwal and Mazumunder, 1988).

$$H_{(T)} = \int \rho C_p(T) dT \quad (5)$$

EXPERIMENTAL RESULTS FOR HEAT TRANSFER PROBLEM

The experimental temperature of melting pool zone could not be measured with simple technique such as thermocouples, but in the region away from weld nugget, peak temperature was measured using a thermocouple located at five different positions A, B, C, D and E from the center of spot as shown in Fig. 4. The temperature measured from the experiment and the temperature result from the numerical analysis can be shown in Fig. 5. The nodal numerical results temperature distribution for the (0.6mm) plate at different time steps during welding and cooling are shown in the Fig. 6, and Table 4, gives the maximum temperature measured compared with temperature calculated and its discrepancy.

NON-LINEAR NUMERICAL MODEL FOR RESIDUAL STRESS

An important problem in the analysis of residual stress during welding is how stress develops in region near the welding nugget when structural members are joined by spot welding the material of the plates has to be heated to its melting point and then cooled again rapidly under restraint conditions imposed by the geometry of the joint. As a result of this severe thermal cycle the original microstructure and properties of the metal in a region close to the weld are change. This part of the metal, or zone, is usually referred to as heat-affected zone (HAZ). The change in the HAZ dependent upon the thermal and mechanical history of the metal. Therefore, after the welding

process there will be different zones with different mechanical properties. In particular, there is a softening of the material in the HAZ, and decrease mechanical properties, i.e. Yield strength, ultimate strength, but elastic modulus remains unaffected by the welding process, (Mansubuchi, 1980).

After calculation the temperature distribution in time, the next step was to find distortion and residual stress distribution. The residual stress distribution calculation was based on the following assumptions:

- Parent plate metal and welded zone metal have the same mechanical properties, i.e. softening of material was neglected.
- Deformation process was rate independent, and a elastic – plastic constitutive model with isotropic hardening was assumed for the material.
- Mechanical properties depend on temperature as shown in **Fig. 7**.

The analysis was performed for the time period between the start of welding and the end of cooling phase. Within each time increment, the solution of elastic–plastic problem was found by linearizing the non-linear stress–strain curved. The analysis was performed and stresses and displacements were calculated by Newton–Raphson iterative process. The iterations were repeated until convergence is achieved. Boundary conditions were imposed to prevent any rigid body motion of the plate. Additional symmetry boundary conditions were imposed since only half of the plate was analyses.

RESULTS AND DISCUSSIONS

It is found that magnitude and distribution of residual stress is strongly affected by:

- Temperature gradient and distribution through the thickness and width of the plates.
- Thermal expansion coefficients of the materials.
- Mechanical properties of material at elevated temperature

The longitudinal residual stress distribution is shown in **Fig. 8**, evaluated at middle cross-section, bottom surface of spot. The positive stress (tension) in x direction peak of (317 MPa) is at the weld area, while away from the weld center the stress is negative (compression) and the maximum is (21 MPa). The shape of longitudinal stress distribution dose not change but the stress amplitude decreases towards the top surface when the maximum longitudinal stress is (91 MPa) seeing **Fig. 9, 10**. This was due to the assumption that heat generation was coming through the bottom weld surface. The Von Misses stress distribution over the entire plate is shown in **Fig. 11**. The peak stress is (321 MPa) close to the material yield strength. The out-of-plane displacement is shown in **Fig. 12**, and the maximum displacement amplitude was 0.0074mm, this means that the out-of-plane displacement was 1.23% of plate thickness. The displacement is very important for the buckling behavior of welded panel. The other displacement UX, (see **Fig. 13**) are negligible compared to the UY. For a similar plate with same geometry, same boundary condition with higher thickness, residual stress would be higher but distribution would become smaller due to the increased in stiffness of the plate, Meo and Vignjevic. The residual stress results are verified with experimental measurements obtained from literature, where the longitudinal stress reach a maximum of (301 MPa) in tension and (17 MPa) in compression. Such a discrepancy between the numerical and experimental values for welding residual stress may be attributed to the difference between the condition of the numerical analysis and the experiment. The nugget metal was actually pressed out by the electrode force and thermal expansion. However, such actual welding condition and various thermal and physical properties were neglected in the process of the FEA. Also, the releases of residual stress when cutting off the plate with wet machining were not considered in the FE analysis.

CONCLUSION

The residual stress and distortion for the 304 stainless steel plate were calculated. De-coupled thermal and structural analyses were performed. Good correlation between experimental results and analytical calculation was achieved. In particular, an error of 6.12% between calculated temperature profile and experimental measurement was found. Residual stress distribution agrees with the experimental result obtained with an error of 5% for the tension–stress and 19% for the compression.

REFERENCES

- Ajinomoto .T Bldg “Nippon Yakin Kogyo co.” Material Property Data.
- Chapman, A. J., “Fundamentals of Heat Transfer”, Macmillan, New York. 1987.
- Cosmos / M finite Element Software, Advanced Modules Theoretical Manual SRAC, Los Angeles, California, USA, 2000.
- D.R. Milner and R.L. Apps “Introduction to Welding and Brazing” Library of Congress Catalog. 1968.
- Faiz F. Mustafa, "Static and Dynamic Analysis of Plates with Spot Welded Stiffeners", Ph.D. thesis, University of Baghdad, College of Engineering, Mech. Dept., October 2006.
- H. Huh and W.J Kang “Electro thermal Analysis of Electric Resistance Spot Welding processes by a 3-D finite Element Method” Journal of Materials processing Technology, 63, PP. 672-677, 1997.
- Mansubuchi K. “Analysis of welded structure”. Pergaman Press. Oxford , 1980.
- M. Meo and R.Vignjevic “welding Simulation Using FEA” College of Aeronautics, Canfield University, Bedford, UK, MK43 OAL.
- Roy. A. Linderg and Norman R. Braton "welding and other Joining Processes 1976.
- Sarkani, S.S. and Lutes, L.D., “Residual Stress Effect in Fatigue of Welded Joints”, Journal of Structural Engineering, Vol, 114 No.2, PP. 462-474, Feb.1988.
- Tall L., “Recent Developments in the Study of Column Behaviour”. Four. Inst. Engrs., pp. 319-333, Aust., Dec. 1964.
- Tekriwal P., Mazumunder J., “Finite Element Analysis of Three Dimensional Transient Heat Transfer in GMA”, Welding Journal, 1988.
- William H. Cubberly," Metals Handbook "Ninth Edition, American Society for Metals.
- X.Sun and P.Dong, “Analysis of Aluminum Resistance Spot welding Processes using Coupled finite Element Procedures”, Welding research supplement, PP. 215s-221s, August, 2000.

SYMBOLS

- A Area (mm^2)
- Cp Specific heat ($w.sec/kg.c^\circ$)
- H Enthalpy ($w.sec.c^\circ/mm^3$)
- h Convection heat transfer ($w/mm^2.c^\circ$)



I	Welding current (<i>Amp</i>)
K	Thermal conduction (<i>w/mm.c°</i>)
Q	Heat generation (<i>w.sec/mm³</i>)
Qi	Heat losses (<i>w.sec</i>)
R	Surface resistance
T	Temperature (<i>c°</i>)
t	Time (<i>sec</i>)

Table 1 - Chemical composition of stainless steel (304), William.

	C	Cr	Fe	Mn	N	Ni	P	S	Si
Stainless steel (304)	0.08	18-20	71	2	0.1	8-11	0.045	0.03	1

Table 2 – Mechanical properties of stainless steel (304), William.

	Tensile strength (MPa)	Yield strength (MPa)	Modulus of Elasticity (GPa)	Elongation %
Stainless steel (304)	572	290	200	50

Table 3 – Welding condition of stainless steel (304), Roy and Norman.

	Electrode force (N)	Welding current (A)	Welding time (cycles)	Tip diameter (mm)
Welding condition	2300	4000	12	0.5

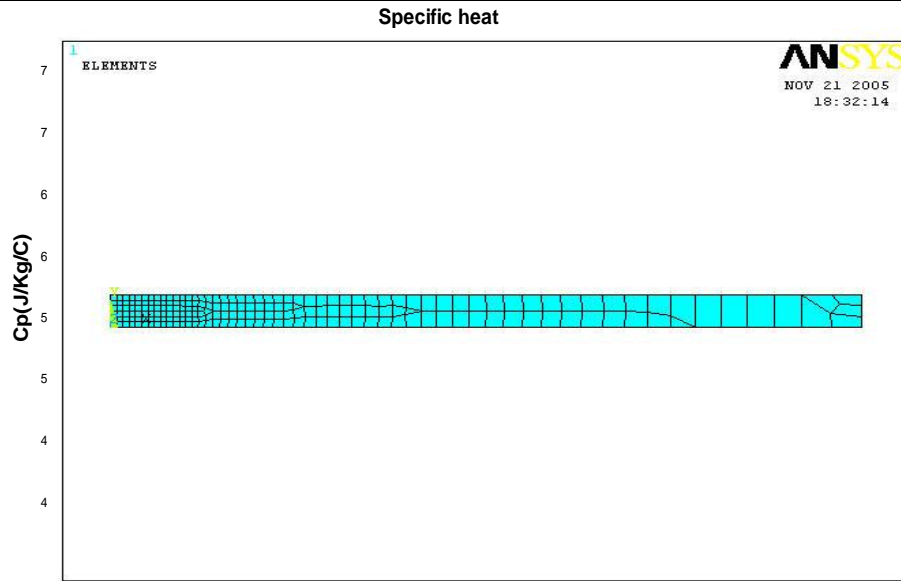


Fig. 1. Finite Element Model and Mesh

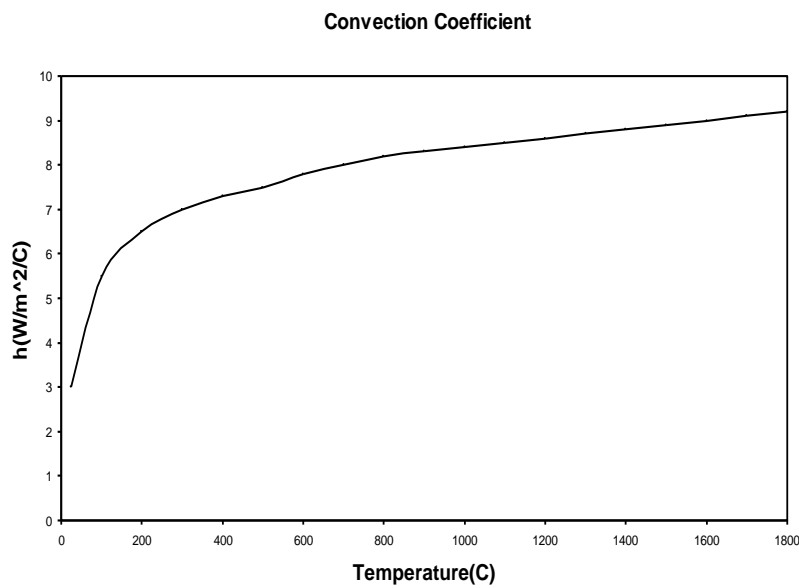
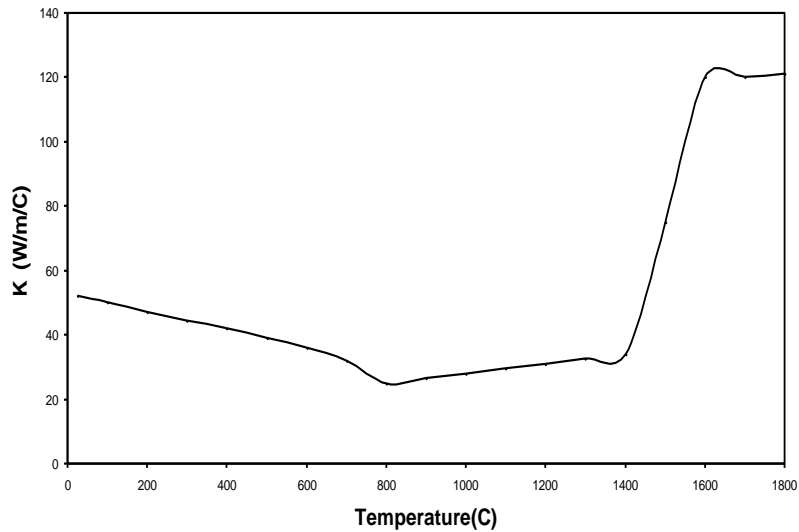


Fig. 2. Variation of Heat Transfer Parameters with temperature, Ajinomoto,
Available online @ 1asj.net 2209

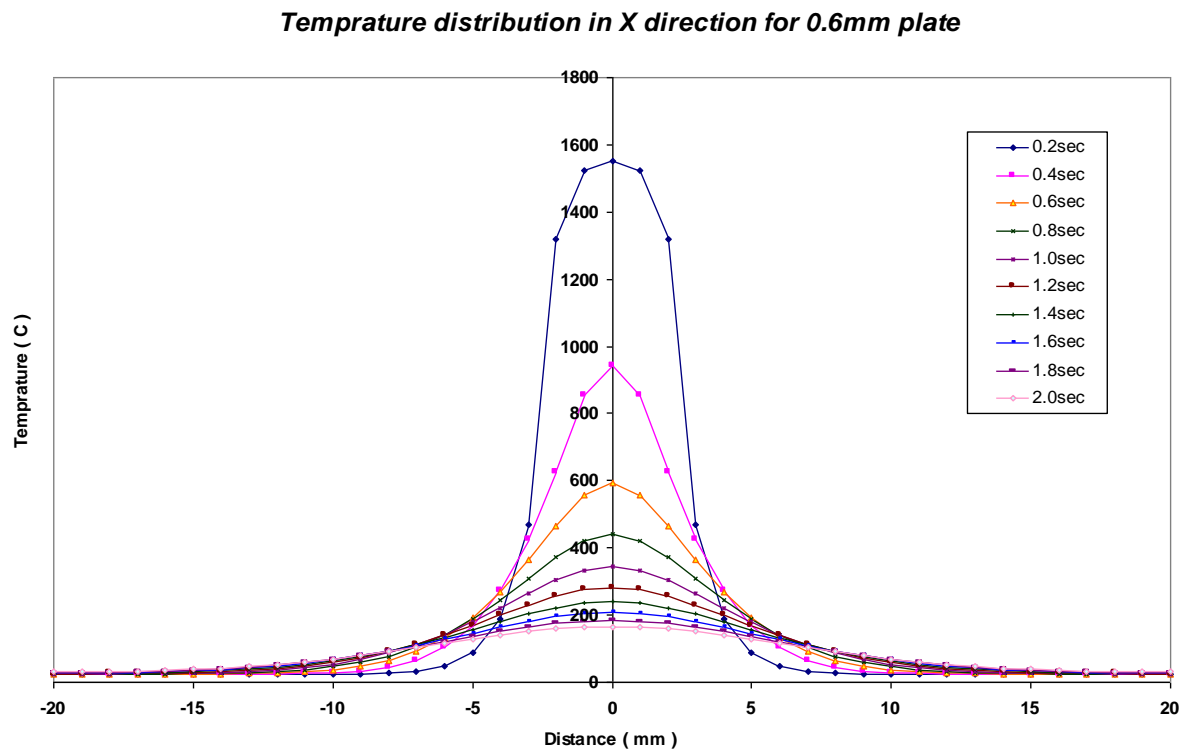


Fig. 3. Temperature distribution in X direction for 0.6mm plate

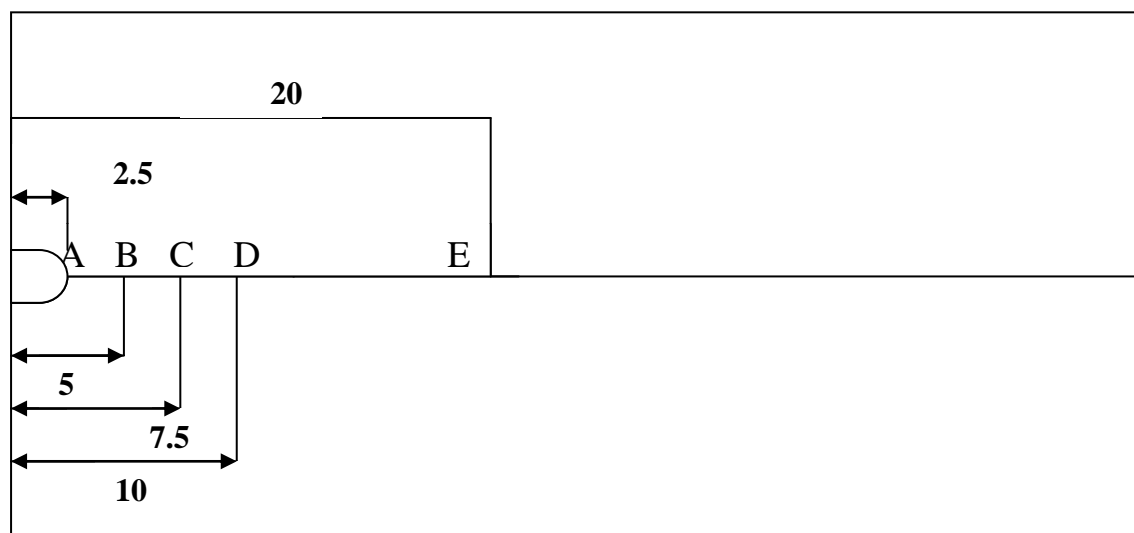


Fig. 4. Holes Positions of Thermocouples (mm).

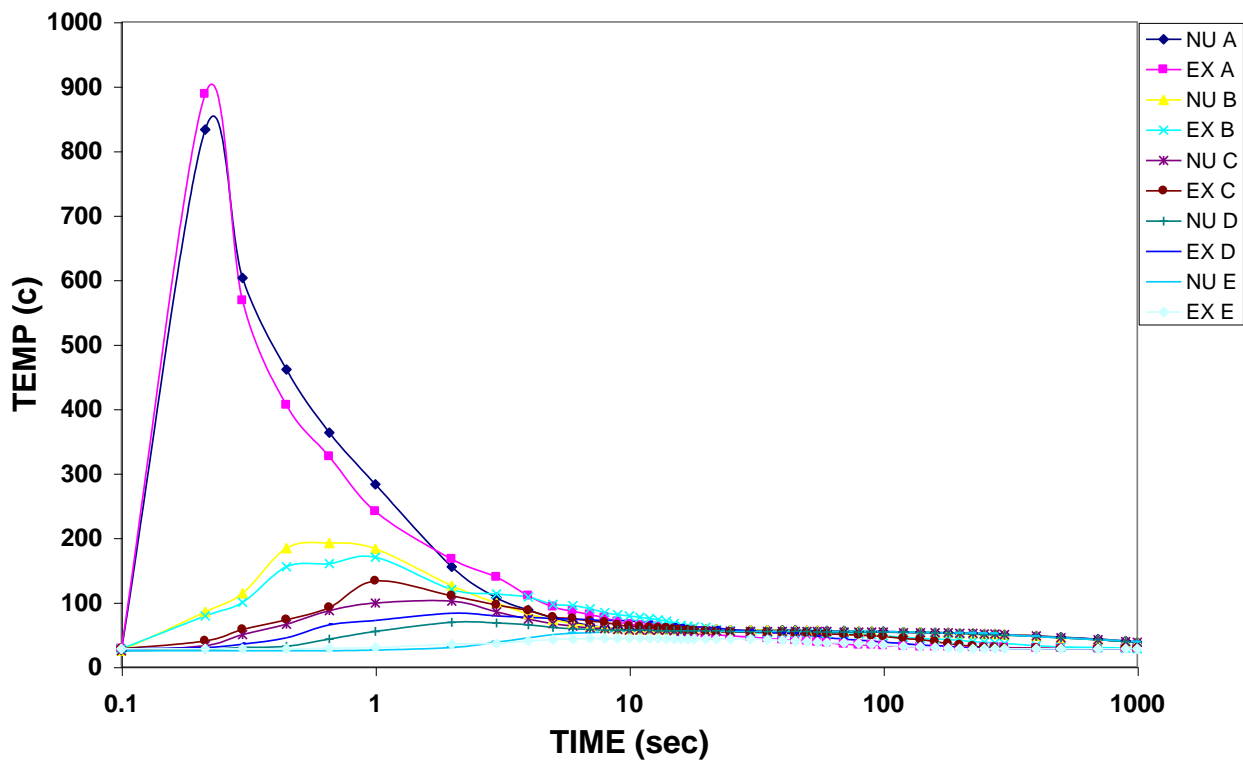
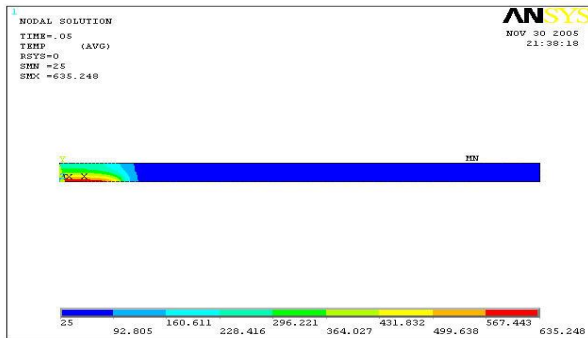


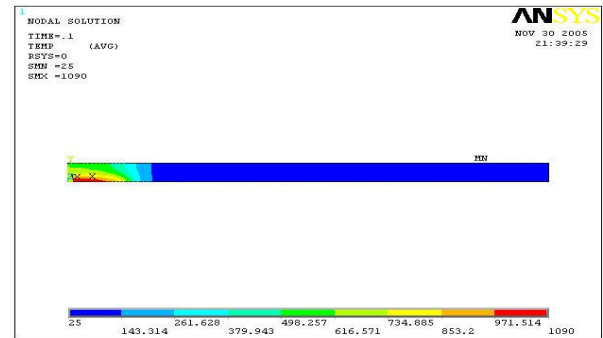
Fig. 5. Computed and measured temperature for 0.6mm plate

Table 4 - Maximum Numerical and Experimental Temperature.

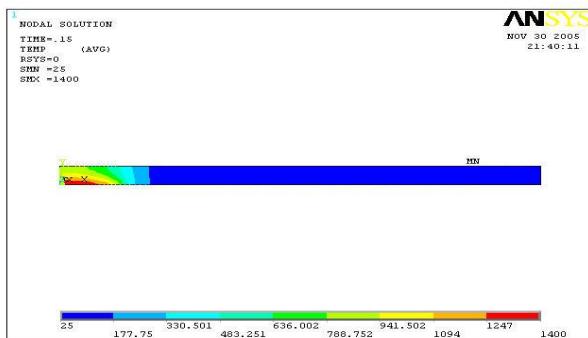
Measured Point	Maximum Numerical Temperature	Maximum Experimental Temperature	Discrepancy %
A	833	888	+6.2
B	192	179	-7.2
C	102	112	+8.9
D	73	79	+7.6
E	55	51	-7.8



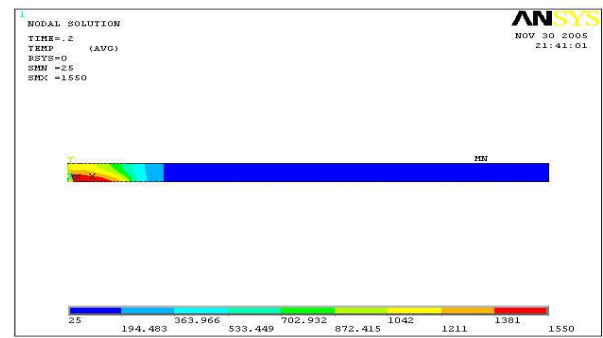
a. Time = 0.05 sec



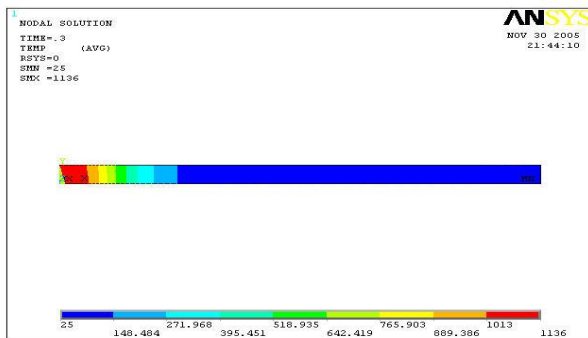
b. Time =0.1sec



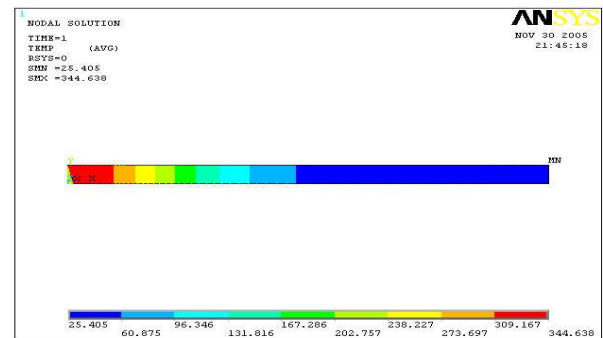
c. Time =0.15 sec



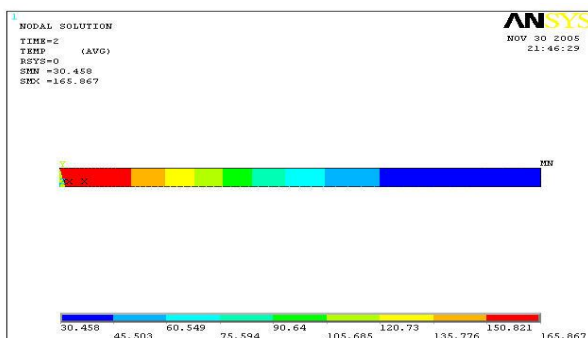
d. Time = 0.2 sec



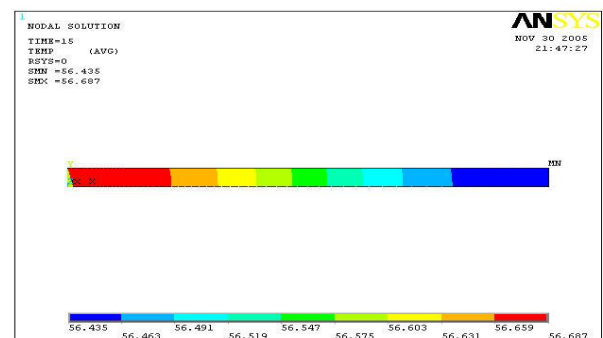
e. Time = 0.3 sec



f. Time = 1sec



g. Time = 2sec



h. Time = 15sec

Fig. 6. Temperature distribution at different time for 0.6mm plate

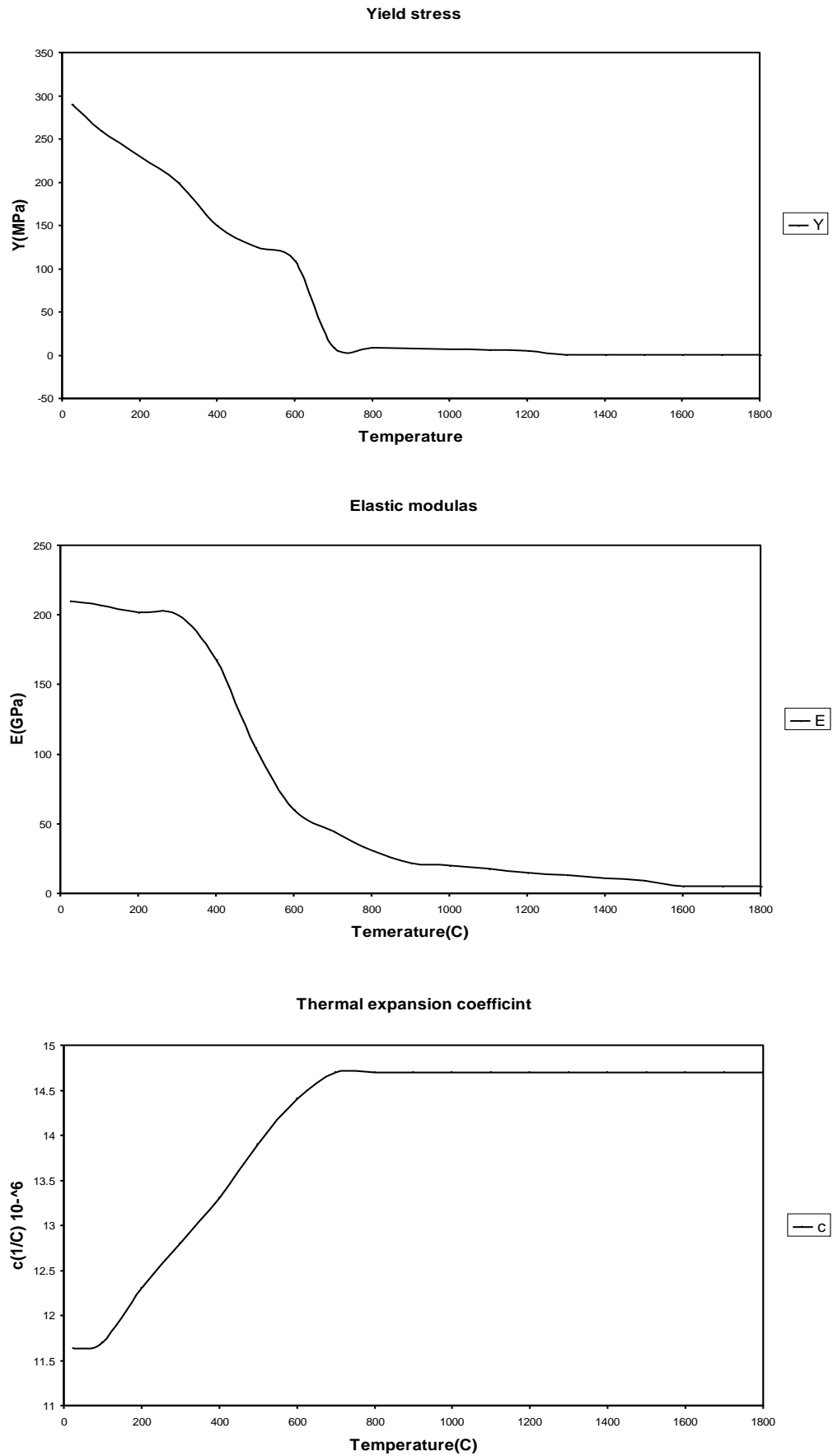


Fig. 7. Variation of Mechanical properties with temperature, Ajinomoto, 2001

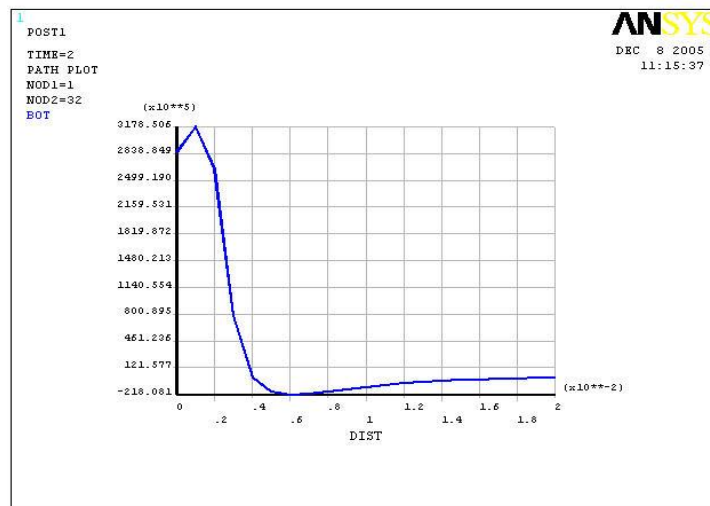


Fig. 8. Longitudinal Stress evaluated at middle Cross-Section – Bottom Surface through the Thickness

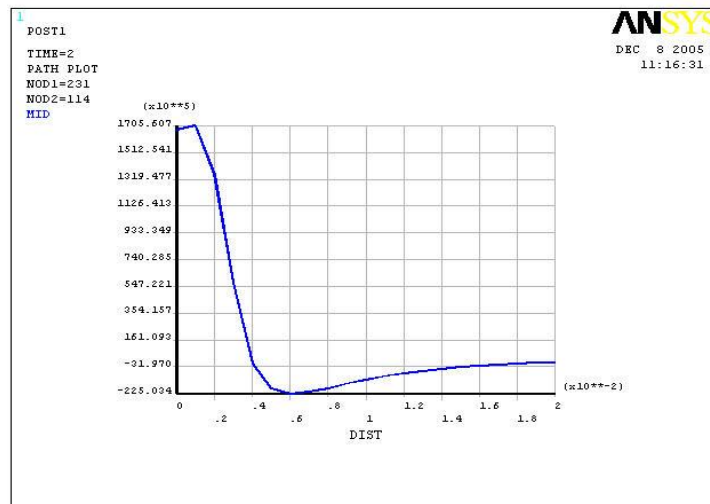


Fig. 9. Longitudinal Stress evaluated at middle Cross-Section – Mid Surface through the Thickness

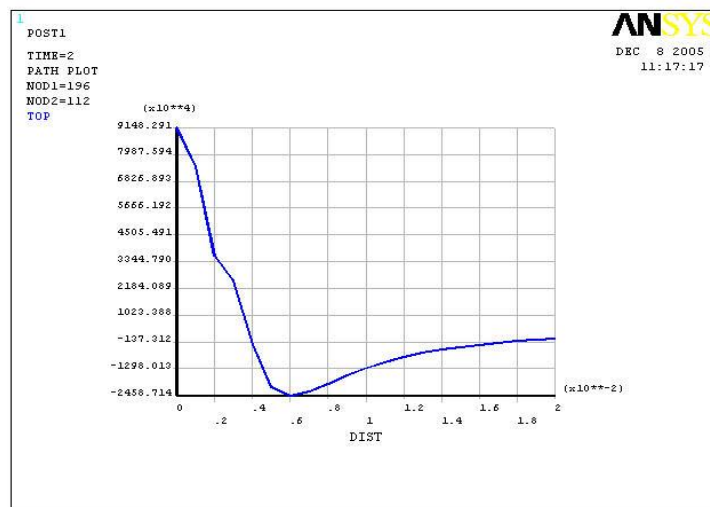


Fig. 10. Longitudinal Stress evaluated at middle Cross-Section – Top Surface through the Thickness

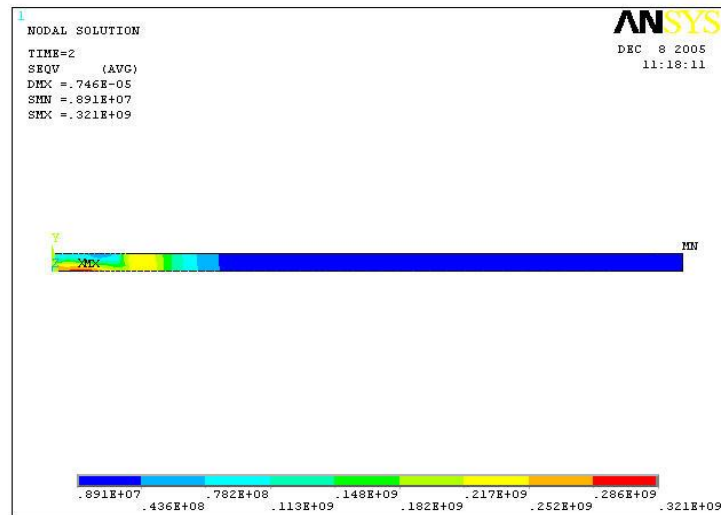


Fig. 11. Von Misses Stress Distribution

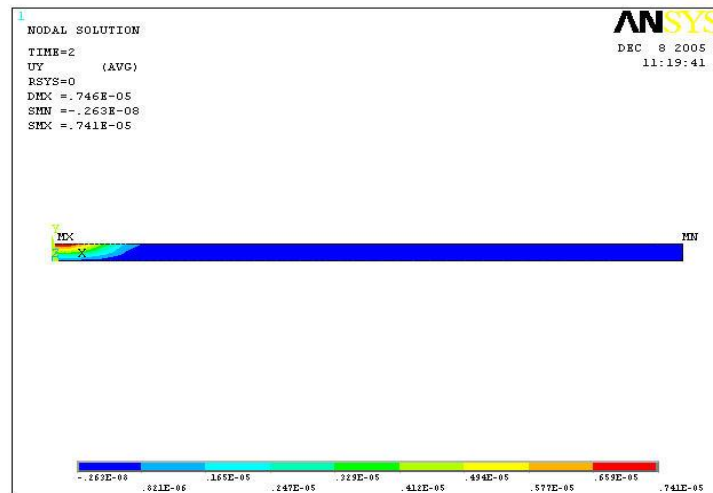


Fig. 12. Out – OF – Plane Displacement, UY

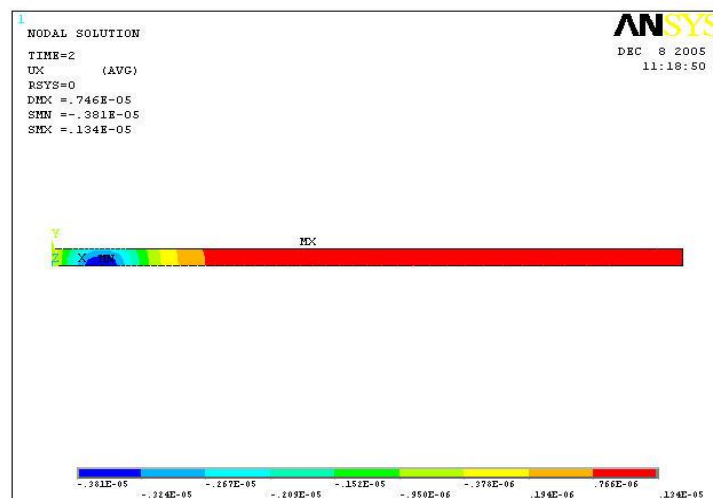


Fig. 13. UX Displacement